NSF Grant ATM-9015485
National Science Foundation

# Cloud-to-Ground Lightning in Tropical Mesoscale Convective Systems

by
Walter Petersen

Department of Atmospheric Science
Colorado State University
Fort Collins, Colorado

Steven A. Rutledge, P.I.

Colorado State University

Department of Atmospheric Science

Paper No. 503

# CLOUD-TO-GROUND LIGHTNING

# IN

# TROPICAL MESOSCALE CONVECTIVE SYSTEMS

by

**Walter Petersen**

Department of Atmospheric Science

Colorado State University

Fort Collins, CO 80523

**Research Supported by**

**National Science Foundation**

under Grant ATM-9015485

June 5, 1992

Atmospheric Science Paper No. 503

## ABSTRACT

## CLOUD-TO-GROUND LIGHTNING IN TROPICAL MESOSCALE CONVECTIVE SYSTEMS

This study presents observations of the cloud-to-ground lightning associated with seven tropical mesoscale convective systems (MCSs) observed during the Down Under Doppler and Electricity Experiment (DUNDEE). Similar to recent studies of the cloud-to-ground lightning (CG) in middle-latitude MCSs, radar and lightning location network data indicated a preference for negative (positive) CGs to occur in the convective lines (trailing stratiform regions) of the tropical MCSs examined. Further, in break period MCSs it was found that positive peak current maxima tended to occur in the trailing stratiform region while positive peak current minima were generally situated in convective precipitation. This pattern was also observed in two middle-latitude MCSs that occurred on 3-4 June and 10-11 June 1985. The magnitude of the positive peak current maxima in the tropical and the middle-latitude MCSs increased coincidentally in time with the growth of the stratiform regions, and reached peak values when the stratiform regions were most intense. This implies that stratiform microphysics associated with the development of a mesoscale updraft may be responsible for the electrification and subsequent cloud-to-ground lightning observed in the stratiform regions of MCSs. Further analysis of the tropical stratiform regions with radar, wind profiler, and electric field data coupled with the results of a simple one-dimensional model to test for the presence of supercooled water seems to positively correlate stronger

mixed phase regions to the number of cloud-to-ground flashes observed in the stratiform regions. From this study, further support is offered for a non-inductive charging mechanism being responsible for the electrical charging and subsequent lightning observed in the trailing stratiform regions of MCSs.

The conclusion of this study presents peak current statistics and distributions compiled for approximately 5000 cloud-to-ground flashes observed during the DUNDEE. Statistical analysis of the lightning data produced an average peak current (independent of polarity) of 39 kA. When considered with the average cloud-top heights of the tropical MCSs examined herein, the 39 kA peak current average appears to be in general agreement with Orville's (1990) hypothesis of latitudinal variation in peak current.

Walter A. Petersen
Department of Atmospheric Science
Colorado State University
Fort Collins, CO 80523
Summer 1992

## ACKNOWLEDGEMENTS

I would like to thank my advisor Dr. Steve Rutledge for the opportunities, support, encouragement, and friendship he has shown me over the past two years. Secondly, I would like to thank Dr. Graeme Stephens and Dr. Raymond Robinson for being on my graduate committee. To my wife Kara and my children LuAnn, Sheralyn and Daniel: Thank you for being there for me, this never would have been possible without you. My office mates and friends Terry Schuur, Nick Powell, Rob Cifelli, Charlotte Demott, Rita Roberts, Kevin Manning, Scott Randell and Tom Rickenbach are all gratefully acknowledged for providing insightful discussions pertaining to my research (and other topics of course). Bill Hiscox at LLP in Tucson, AZ. is acknowledged for helping me to better understand the lightning location network data. I am also gratefull to Professor Earl Williams for providing me with LLP and electric field data, Dr. Eric Rasmussen for supplying much of the software used for my research (and time spent helping me to use it), and Doug Burks for helping me to unravel the mysteries of Plotgks. This research was supported by the National Science Foundation, by the grant ATM-9015485 from the Physical Meteorology and Mesoscale Dynamics programs. Most importantly I would like to thank God for allowing me to pursue a dream.

TABLE OF CONTENTS

## LIST OF TABLES

## LIST OF FIGURES

# CHAPTER 1

# INTRODUCTION

During the Southern Hemisphere summers of 1988-89 and 1989-90 the DUNDEE (Down Under Doppler and Electricity Experiment) was conducted in tropical north central Australia, centered on Darwin (12.4° S, 130.9° E). The experiment was designed to study the electrical and dynamical characteristics of tropical mesoscale convective systems. The research presented in this thesis uses data collected during the DUNDEE to investigate the electrification mechanisms and cloud-to-ground lightning characteristics of tropical mesoscale convective systems (MCSs) observed in the Darwin area.

## 1.1 Background and motivation for the research

With the exception of the DUNDEE, observations and studies of cloud-to-ground lightning associated with tropical MCSs, particularly the trailing stratiform regions of these storms, are rare. However, studies of cloud-to-ground lightning (CG) associated with middle-latitude MCSs and attendant stratiform regions are comparitively numerous and have produced specific hypotheses to explain the mechanisms responsible for the electrification and subsequent lightning produced in stratiform regions. These hypotheses (e.g., Orville et al. 1988; Rutledge and MacGorman 1988; Engholm et al. 1990; Rutledge et al. 1990; Schuur et al. 1990) cannot be completely accepted or

rejected until they are tested with equivalent data sets and observations from other regions of the globe, specifically the tropics.

For example, several studies of the cloud-to-ground lightning (CG) associated with middle-latitude MCSs (e.g., Rutledge and MacGorman 1988; Engholm et al. 1990; Rutledge et al. 1990), have indicated that CGs of positive polarity (i.e., transfer of positive charge to ground by the flash) may be more frequent than CGs of negative polarity (i.e., transfer of negative charge to ground) in the stratiform regions. Conversely, the majority of the CGs associated with the convective line tend to be negative in polarity. Herein we describe this type of flash pattern (positive CGs associated predominantly with stratiform precipitation, negative CGs with convective precipitation) as "bipolar" (Orville et al. 1988), even though the patterns are not those of a "true" bipole which implies a *complete* separation between the locations of positive and negative CGs in an MCS (Fig. 1.1).

The observations of bipolar CG patterns (e.g., Orville et al. 1988; Rutledge and MacGorman 1988), highly sheared flow in middle-latitude MCSs (Smull and Houze 1987; Rutledge et al. 1988), and the tripole model of a thunderstorm (i.e., a main positive charge center located in the upper portions of the cloud overlying negative charge centered near the -10° to -20° C levels with a weak positive charge center near the 0° to -10° C levels; Krehbiel 1986; Williams 1989), led some researchers to suggest that positive charge situated on ice particles was being advected large distances (i.e., >50-100 km) rearward (Fig. 1.2) from the convective line into the stratiform region (e.g., Rutledge and MacGorman 1988; Hill 1988). This would presumably lead to the accumulation of positive charge in the stratiform region and hence, positive CGs. A similar argument, and possibly the mechanism behind shorter bipoles (i.e., length ≤ 20-

30 km), was made by Brook et al. (1982). Based on observations of the cloud-to-ground lightning associated with thunderstorms in Japan, Brook et al. (1982) suggested that the shear actually "tilted" the dipole down shear of the storm allowing the upper positively charged anvil easier access to ground, causing positive CGs to occur away from the convective line.

Based on a one-dimensional modeling study, Rutledge et al. (1990) suggested that CGs occurring in the stratiform region were associated with the electrification of the stratiform region by an in-situ (internal to the stratiform cloud), non-inductive charging mechanism (Takahashi 1978; Jayaratne et al. 1983; Keith and Saunders 1989; Saunders et al. 1991). Their simple one dimensional model of a middle-latitude stratiform region, based on the laboratory hydrometeor charging experiments of Takahashi (1978), produced ample charge for lightning in the stratiform region through the collisions of ice particles in the presence of small amounts of supercooled liquid water. The charge produced was situated in the stratiform region as an inverted dipole (negative overlying positive charge), which may be due in part to the positive charging of ice hydrometeors growing in a depositional state above the melting level (Takahashi 1978; Williams et al. 1991; Caranti et al. 1991). This places the positive charge region closer to ground which would presumably result in a higher number of positive cloud-to-ground flashes (Williams,1989).

While the charge advection and non-inductive charging mechanisms suggested above both seem to explain observations in the middle-latitudes of positive CGs in the stratiform region, several questions remain. Indeed, recent in-situ measurements of the electric field in several middle-latitude MCSs and associated stratiform regions reveal a complex electrical structure in the vertical (e.g., Schuur et al. 1991; Marshall and Rust

1991). Marshall and Rust (1991) inferred four to ten charge layers of differing sign, thickness, and magnitude obtained from electric field measurements made in middle-latitude MCSs. One example of the many charge layers observed in an MCS stratiform region by Marshall and Rust (1991) is shown in Fig. 1.3. This figure shows the vertical electric field as a function of altitude (as measured by a balloon-borne electric field meter similar to that described by Winn et al. 1978). Each of the ten boxes (representing a charge layer) on the right side of Fig. 1.3 contains a layer's charge density (derived from the vertical gradient of the electric field), thickness in meters, and average temperature (°C). Note that observations of this type are in direct conflict with simple tripole models of thunderstorms (e.g., Krehbiel 1986; Williams 1989) and are not uniquely explained by either the charge advection or in-situ mechanisms mentioned above.

It is apparent that more observations and analysis will be required to resolve the problem of lightning in the trailing stratiform regions of MCSs. In addition, it is equally apparent that the electrification processes of *tropical* stratiform regions should be examined and compared with other similar middle-latitude data sets. This might enable the formulation of more globally valid hypotheses to explain MCS and associated stratiform region electrification, while providing an increased statistical data base for tropical cloud-to-ground lightning in general.

Indeed, general statistical information for cloud-to-ground lightning in the tropics such as the average peak current of first return strokes, flash rates, and polarity percentages are important to our understanding of lightning and its relation to the global electrical circuit (e.g., C.T.R. Wilson 1920; Kasemir 1979). For example, Orville (1990) hypothesized the existence of a latitudinal variation in the average peak current of

the first return stroke in a cloud-to-ground flash. This hypothesis states that an inverse relationship exists between the average peak current of a cloud-to-ground flash and the latitude of the flash position. Orville's (1990) suggestion is based on observations of peak current magnitudes in the Eastern United States. Unfortunately, Orville could not completely verify the hypothesis since no similar cloud-to-ground lightning data sets for the tropics were available. If in fact Orville's (1990) hypothesis is valid, it might be possible to redefine calculations of the total earth-ionosphere supply current as a function of latitude, thus refining the present estimates (see Kasemir 1979) provided by gross scaling considerations.

## 1.2 An overview of the data presented

In this thesis, data relating the positions, polarities and peak currents of cloud-to-ground flashes to the radar reflectivity patterns of several tropical MCSs are presented. Also, electric field data will be analyzed to infer the sign of charge in stratiform clouds as they passed over the observation site. Such data will allow statements to be made regarding the charging processes operating within the stratiform clouds. Further, we correlate kinematic properties of the observed tropical stratiform regions such as the vertical shear of the horizontal wind and strength of the mesoscale updraft (estimated from vertically-pointing profiler data), with recorded CG flash rates. These data will then be compared to similar middle-latitude observations (e.g., Rutledge and MacGorman 1988; Rutledge et al. 1990; Engholm et al. 1990). Specific comparisons will be made between the positions of positive peak current extrema observed in the DUNDEE MCSs presented herein and the positions of positive peak current extrema in two middle-latitude MCSs (3-4 June 1985, and 10-11 June 1985) observed during

PRE-STORM (Preliminary Regional Experiment for Stormscale Operational Research Meteorology; see Cunning 1986 for a description of PRE-STORM).

We also present the results of a simple one-dimensional model that uses the observed magnitudes of the mesoscale updraft present above the melting level for two of the stratiform regions studied herein, together with the observed saturated specific humidities to assess the probability of supercooled liquid water existing above the melting level (a prerequisite for non-inductive charging to take place; Takahashi 1978; Jayaratne et al. 1983; Keith and Saunders 1989). Based on the results of the modeling study and analysis of the data presented above, we offer further evidence for the existence of an in-situ, non-inductive charging mechanism in the trailing stratiform regions of tropical MCSs as an explanation for the generation of cloud-to-ground lightning therein, particularly positive flashes (e.g., Engholm et al. 1990; Rutledge et al. 1990).

To conclude the data analysis we present general statistical information compiled from approximately 5000 cloud-to-ground flashes recorded during the DUNDEE. The statistics presented include the average and extrema of peak currents associated with the first return stroke of a cloud-to-ground flash, percentage of the total number of CGs that were positive, and average CG flash rates. Further, we use the average peak current data to assess the hypothesis of latitudinal variation in peak currents made by Orville (1990).

## 1.3 Scientific objectives and organization of the thesis

The scientific objectives of this research are:

1) to provide new insights into the electrification of tropical MCS stratiform regions;

2) to identify similarities or differences between the electrification of middle-latitude MCS stratiform regions and those in the tropics;

3) and to supplement the existing statistical data base of parameters describing tropical cloud-to-ground lightning.

To accomplish these objectives we present data collected during the 1989-90 season of the DUNDEE.

This thesis contains seven chapters. Following the introductory chapter, Chapter 2 contains a brief description of the DUNDEE. Chapter 3 presents a synopsis of previous studies of the microphysical and electrical properties of stratiform clouds associated with MCSs. Chapter 4 is an overview of the DUNDEE MCS cases selected for study in this thesis together with the analysis method employed. Chapter 5 contains a detailed analysis of the data. Chapter 6 presents conclusions and recommendations for future research. Appendix A contains descriptive statistics for 5000 cloud-to-ground flashes observed during the DUNDEE

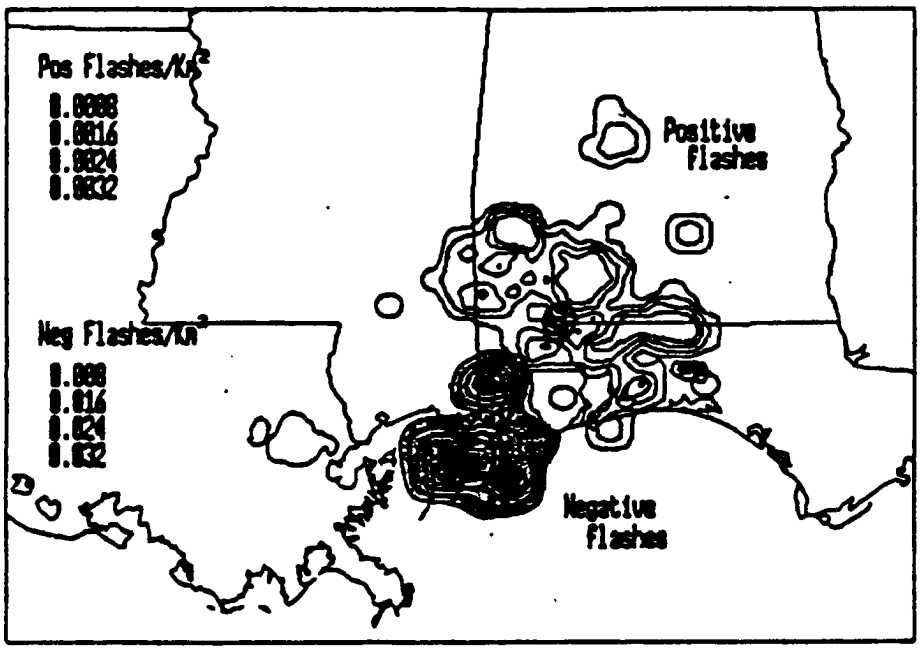


Figure 1.1 Example of a bipolar cloud-to-ground lightning pattern (adapted from Orville et al. 1987). Negative cloud-to-ground flash densities (shaded area) and positive cloud-to-ground flash densities (unshaded area) are contoured in units of flashes $km^{-2}$.

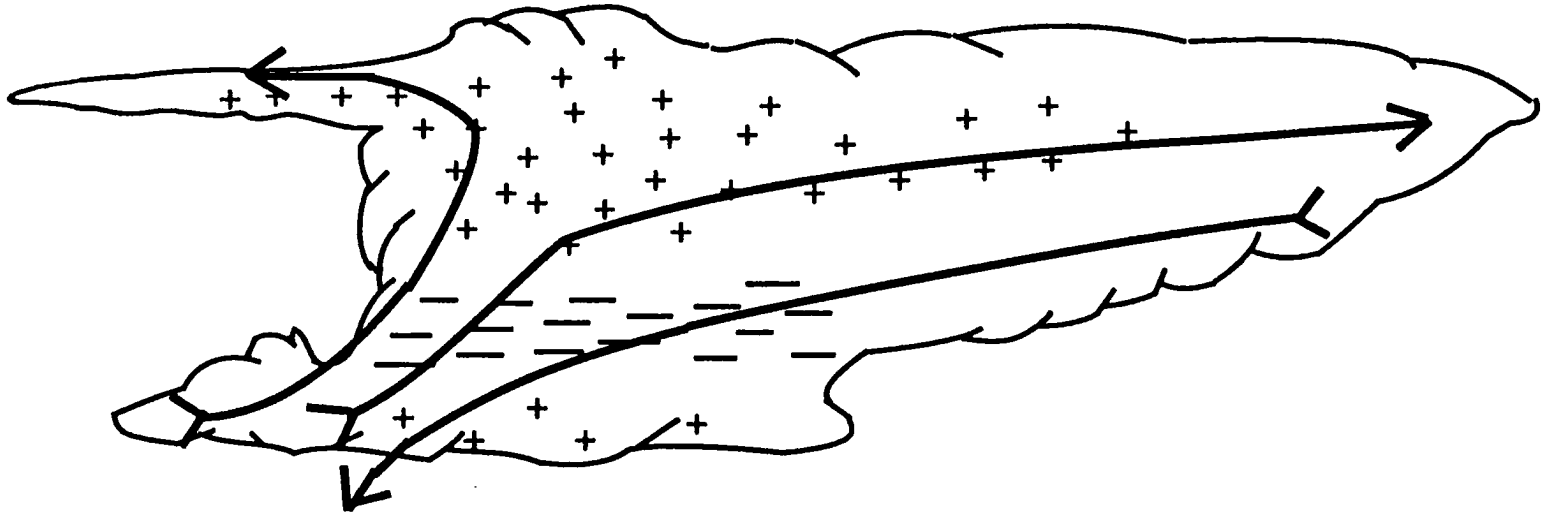

Figure 1.2 Positive dipole model of a thunderstorm illustrating charge advection by the mean storm relative flow (indicated by arrows). Positive charge is represented with a (+), negative charge with a (-).

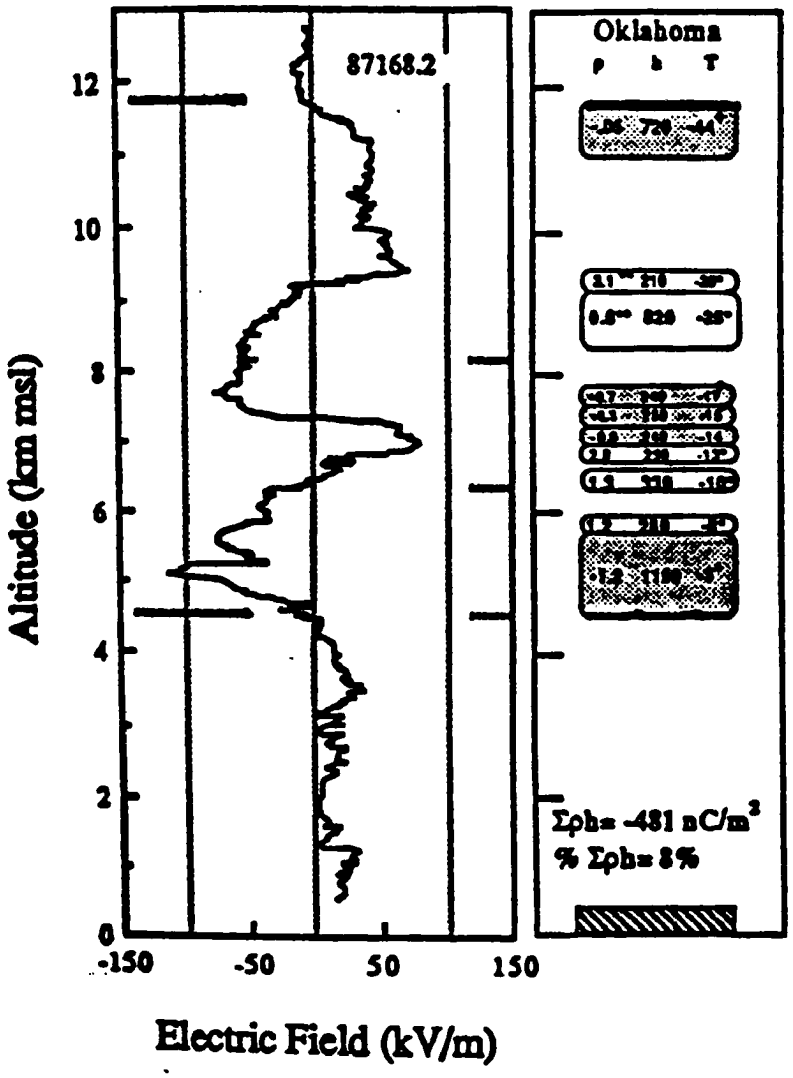


Figure 1.3 16 June 1987 vertical electric field sounding taken in the stratiform region of an Oklahoma MCS (adapted from Marshall et al. 1991). Shaded boxes indicated negative charge layers, white boxes indicate positive charge layers. Boxes contain values for charge density (nC $km^{-3}$), layer thickness (m), and temperature (°C).

# CHAPTER 2

# THE DOWN UNDER DOPPLER AND ELECTRICITY EXPERIMENT (DUNDEE)

In an effort to better understand tropical convection and its effects on the Earth's general circulation and the global electrical circuit, the DUNDEE was conducted during the wet seasons of November 1988-February 1989 and November 1989-February 1990 centered on Darwin, Australia. The DUNDEE was a collaborative effort between Colorado State University, the Massachusetts Institute of Technology, NASA (National Aeronautics and Space Administration), and the Australian BMRC (Bureau of Meteorology Research Centre). As indicated by world mean thunderday maps (e.g., Fig. 2.1 in Uman 1987) and DMSP (Defense Meteorological Satellite Program) observations (Fig. 2.1), convection and lightning occur on a regular basis in the Darwin area (12.4° S, 130.9° E) placing the DUNDEE in an ideal location for meeting its scientific objectives.

## 2.1 Scientific objectives of the DUNDEE

The scientific objectives of the DUNDEE (as listed in Rutledge et al. 1992a) were as follows:

1) to collect information relating the dynamical and electrical characteristics of tropical continental and oceanic convection to previously observed differences between land and ocean lightning frequencies (e.g., Orville and Henderson (1986) reported a mean land/ocean lightning ratio of 3.2 based on DMSP satellite observations and an area normalized ratio of 7.7; Fig. 2.1).

2) to help answer questions regarding the role of tropical lightning and thunderclouds in the global electrical circuit (i.e., the role of thunderstorm induced corona currents and cloud-to-ground lightning in the maintenance of the ionospheric potential difference).

3) to document and explain the high ratios of in-cloud to cloud-to-ground lightning found in the tropics (Prentice and MacKerras 1977; Fig. 2.2) relative to our current understanding of the electrical charge structure of thunderstorms.

4) to relate flash rates to cloud depth in order to test scaling laws (formulated with middle-latitude data) that state total lightning flash rates vary as the fifth power of the cloud-top height (Williams 1985).

5) to document relationships between cloud-to-ground lightning activity and cloud cluster life cycles (e.g., Rutledge et al. (1990) found that spatial patterns in positive and negative CGs evolved with the growth of several middle-latitude MCS stratiform regions).

6) to conduct structural and lifecycle studies of monsoon (i.e., oceanic) and continental cloud clusters.

7) to study the kinematics (e.g., vorticity budgets) of tropical mesoscale convective systems.

## 2.2 Observational network

To accomplish the objectives stated above, a wide array of instruments were deployed.(Figs. 2.3, 2.4). Radar measurements (Fig. 2.3) were made with the MIT (Massachusetts Institute of Technology) and NOAA-TOGA (National Oceanic and Atmospheric Administration-Tropical Ocean and Global Atmosphere) C-band Doppler radars. The radars were situated on a 29 km baseline oriented approximately east-west, which allowed dual-Doppler scanning of storms (Rutledge et al., 1992a). In conjunction with the NOAA and MIT radar measurements, a 50 MHz vertically pointing wind profiler (installed and operated by NOAA and BMRC) was also used for obtaining vertical velocities.

Measurements of temperature, humidity, wind, pressure, and rainfall at the surface (Fig. 2.3) were recorded by a surface mesonet consisting of 10 automated weather stations (AWS) that were developed by the BMRC. The AWSs were complimented with a network of Woefle chart recorders (for additional wind information), and a network of tipping bucket raingauges (Rutledge et al. 1992a). In addition to surface measurements, radiosonde observations (thermodynamic) were taken every 12 hours at the Bureau of Meteorology (BOM) in Darwin with wind soundings at 6 hour intervals. When needed, vertical soundings of the atmosphere were also taken at the MIT radar site using an OMEGAsonde system developed by the National Center for Atmospheric Research (NCAR) and at Noonamah, using the Monash University Digicora Sounding system (Rutledge et al. 1992a).

Electricity measurements were made with several different sensors. During the 1988-89 season, five corona point sensors mounted on 5-meter masts were used to

detect total lightning and electric field changes (Rutledge et al. 1992a). For the 1989-90 season, the corona point network was removed and replaced with a lightning location and detection network consisting of four magnetic direction finding (DF) lightning sensors (Fig. 2.4). The sensors were installed by Lightning Location and Protection Inc. (LLP) of Tucson, AZ. During both seasons of the DUNDEE an electric field mill of the type used at Kennedy Space Center Florida (Jacobson and Krider, 1976) and two flat plate antennas were also used for electricity measurements.

## 2.3. Lightning detection network and flash detection method

A network of four direction-finding (DF) antennas similar to those described by Krider et al. (1976) were deployed at Darwin, Jabiru, Tindal and the Douglas Daly Experimental Station in the Northern Territory to record cloud-to-ground flash data (Fig. 2.4). The average distance between stations in this network was approximately 220 km. The majority of ground flashes used for our analysis occurred within 200 km of the center of the DF network. Information provided by the DUNDEE DF network included the position of each flash (relative to the MIT radar), time of occurrence (to the nearest millisecond), multiplicity (number of return strokes in each flash), polarity and the peak current (in kiloamps, kA) of the first return stroke.

For the DUNDEE lightning data set, the position of a ground flash was calculated using triangulation when at least two stations detected the same flash. If more than two stations detected the same flash (signals received coincident in time at each DF), the position of the flash could be statistically optimized. CG flash detection efficiencies for DF networks are generally $\geq 70\%$ for flashes within a 300 km radius of the center of the network and errors in position have been found to be on the order of 10

km or less (Mach et al., 1986). Detection efficiencies can improve to ≥ 90% for CGs occurring at locations *within* LLP DF networks (personal communication from Mr. Ron Holle and Dr. Raúl López, National Severe Storms Laboratory). Site errors at the antennas for the DUNDEE network were approximately 0.5 degrees in azimuth. Errors in peak currents are ten percent or less (personal communication from Bill Hiscox, LLP Inc.).

## 2.4 Background and selected results from the 1988-89 season

The mesoscale convective systems (MCSs) observed during the DUNDEE can be subdivided into two broad categories; monsoon and break period MCSs. During Southern Hemisphere summers, the position of the intertropical convergence zone (ITCZ) largely dictates the synoptic flow regime over the northern portion of the Australian continent which, in turn, determines the weather regime observed in the Darwin area. In break periods when the ITCZ is north of Darwin, the area experiences low level southeasterly flow off the continent, placing Darwin under the influence of a continental tropical (cT) airmass that has high values of convective available potential energy (CAPE) (sometimes exceeding 2000 J $kg^{-1}$; Rutledge et al., 1992a). During monsoon periods, the ITCZ moves to the south of Darwin and the low level flow changes to a more northwesterly direction off of the ocean placing Darwin in a maritime tropical (mT) airmass of lower CAPE with values of 500-1000 J $kg^{-1}$ (Rutledge et al., 1992a).

From data collected during the 1988-89 DUNDEE season, Rutledge et al. (1992a) showed that the electrification of monsoon and break period MCSs is correlated to the CAPE and hence, from parcel theory, the strength of convective updrafts. The

observations further revealed that monsoon MCSs forming in a lower CAPE environment were only weakly electrified, yielding relatively low lightning flash rates (cloud-to-ground and in-cloud flashes) of 15 $min^{-1}$ or typically, much less (Fig. 2.5; adapted from Rutledge et al. 1992a). Conversely, MCSs forming in a break period regime (higher CAPE) were highly electrified, yielding much higher flash rates of up to 60 $min^{-1}$. Rutledge et al. (1992a) attributed the lower electrical intensity of monsoon MCSs to the absence of deep mixed phase regions, which are required for vigorous non-inductive charging to take place (Takahashi 1978). An example of the weaker mixed phase region of a monsoon MCS is seen in Fig. 2.6a (adapted from Rutledge et al., 1992a). In Fig. 2.6a, reflectivities greater than 40 dBZ below the melting level (5 km) decrease rapidly to 10-20 dBZ just above the melting level, likely indicating glaciated conditions. Break period convection on the other hand, was generally observed to be much deeper with reflectivities in excess of 40 dBZ well above the melting level, likely indicating a deep mixed phase region (Fig. 2.6b).

It should be noted that the explanation offered above by Rutledge et al. (1992a) for the difference in lightning flash rates between monsoon and break period MCSs primarily addressed the lightning associated with the convective portions of tropical MCSs, not the trailing stratiform regions. This provides the opportunity for research of a more specific nature to be conducted on the electrification of stratiform regions associated with the tropical MCSs observed during the DUNDEE. Such research is the focus of this thesis.

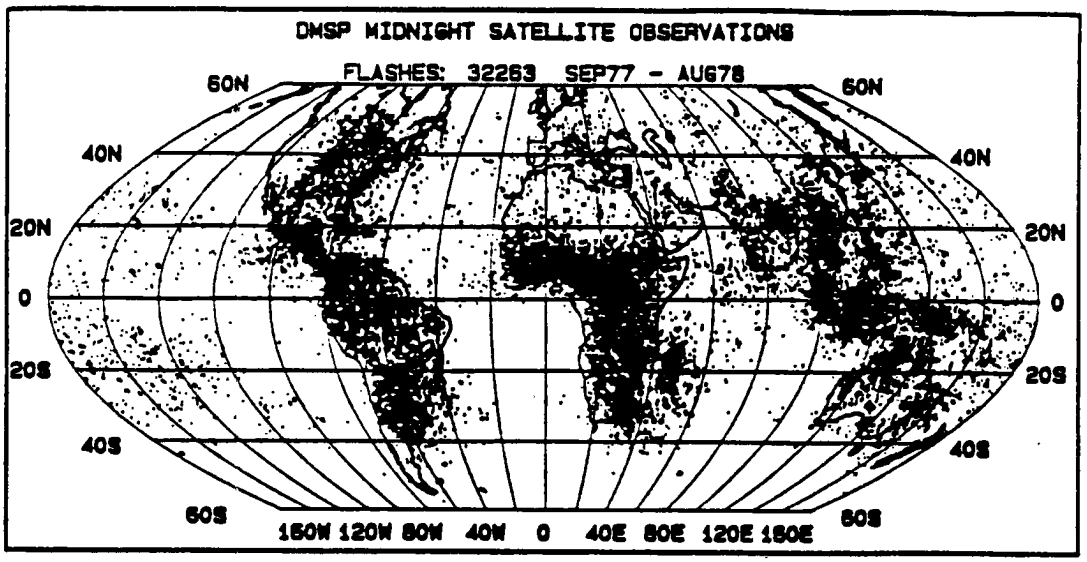


Figure 2.1 September 1977 to August 1978 DMSP midnight satellite observations of total lightning from 60° N-60° S (adapted from Orville and Henderson, 1986).

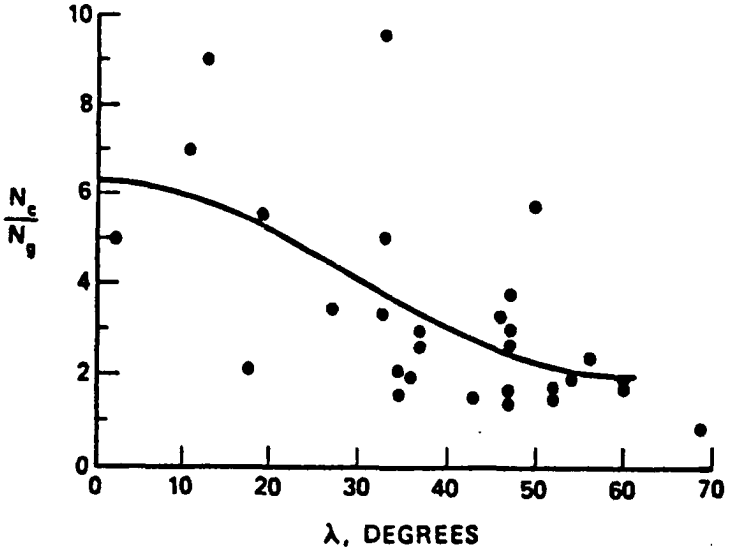


Figure 2.2 Ratio of in-cloud to cloud-to-ground flashes vs. latitude (adapted from Prentice and MacKerras, 1977).

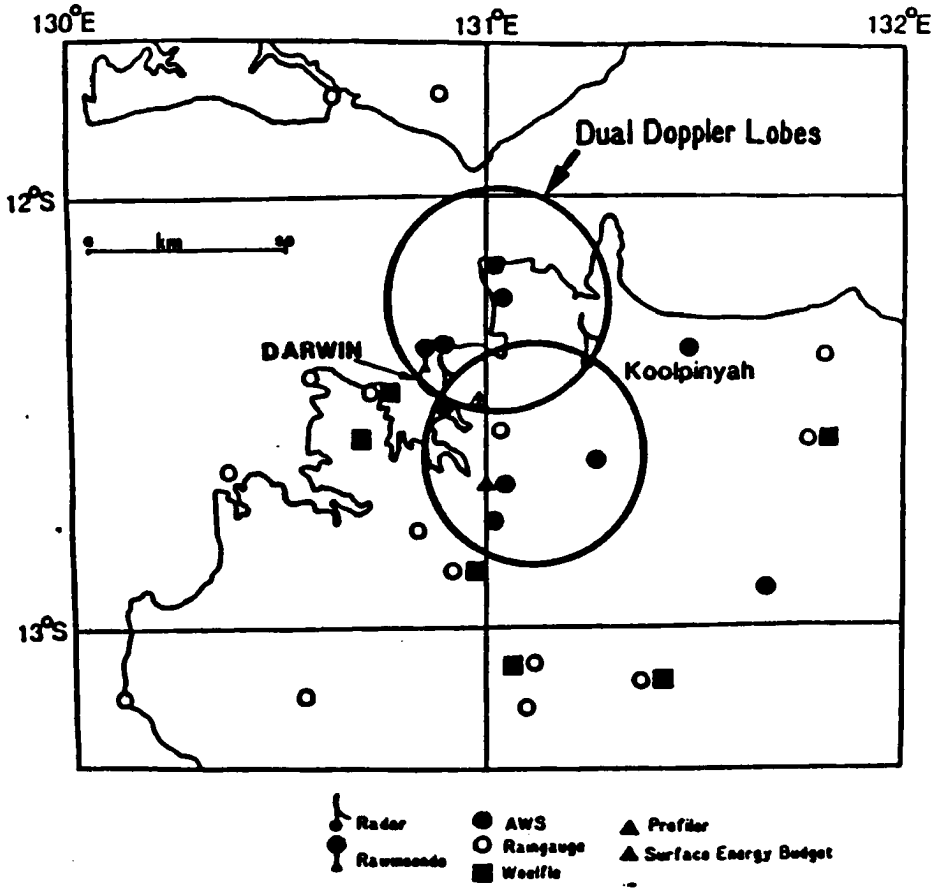


Figure 2.3 Map of the observational network used during the DUNDEE.

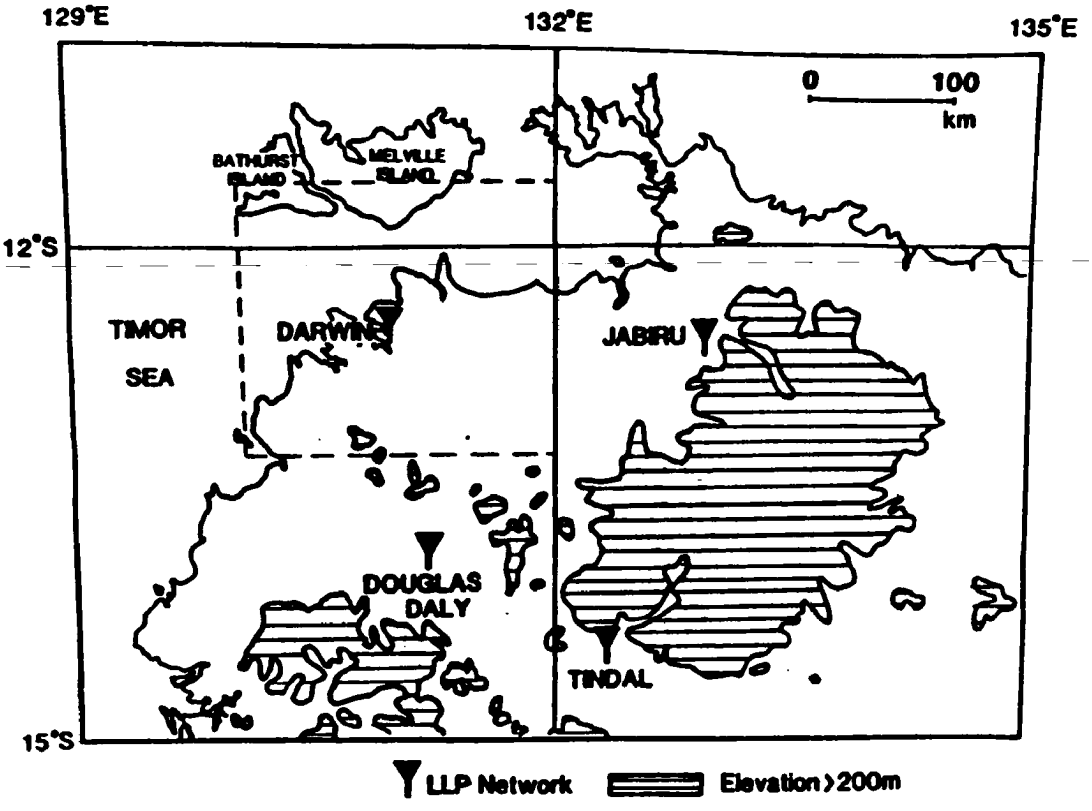


Figure 2.4 Map of the LLP network used during the 1989-1990 observational phase of the DUNDEE. Dashed box represents area shown in Fig. 2.3.

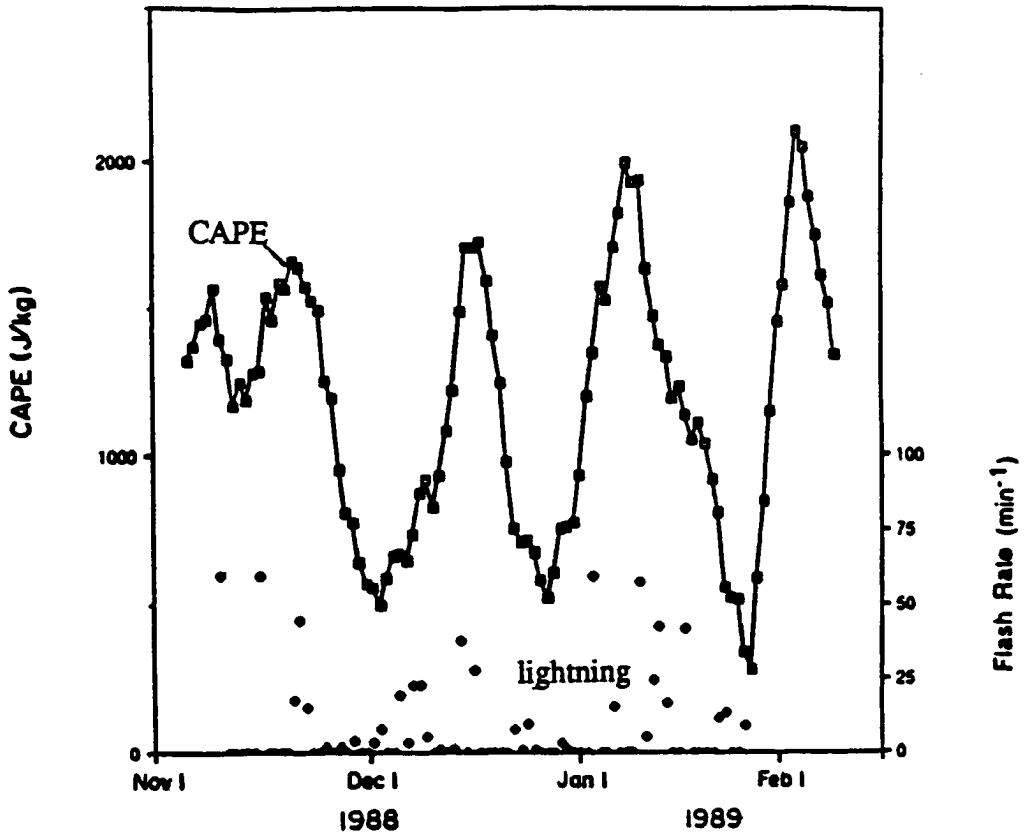


Figure 2.5 DUNDEE 1988-89 season CAPE vs. total lightning flashes (adapted from Rutledge et al. 1992a).

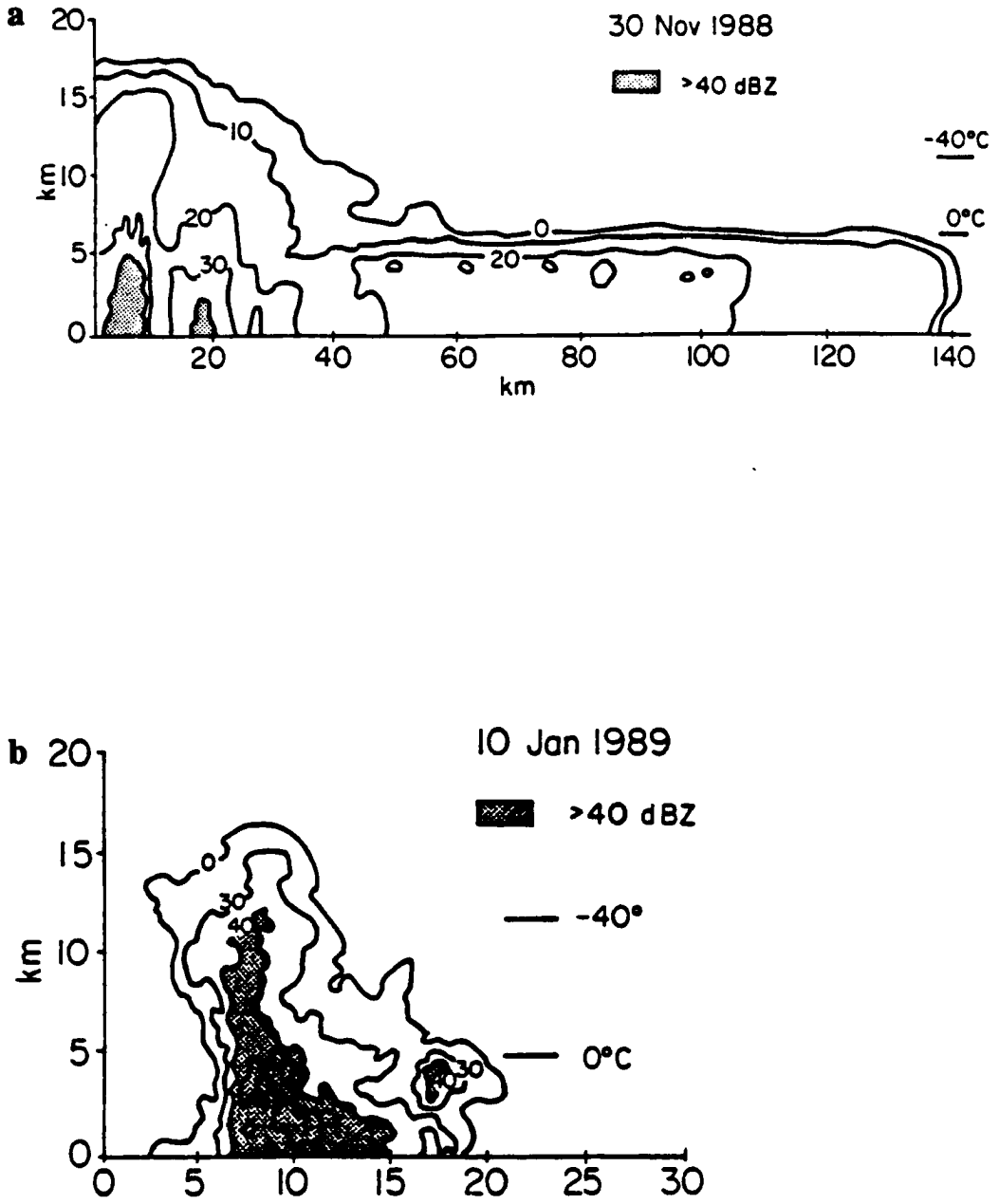


Figure 2.6 Vertical cross-sections of radar reflectivity from the (a) 30 November 1988 monsoon MCS and (b) 10 January 1989 break period MCS; (adapted from Rutledge et al. 1992a).

# CHAPTER 3

## AN OVERVIEW OF MESOSCALE CONVECTIVE SYSTEMS: STRUCTURE, MICROPHYSICS AND ELECTRIFICATION

Mesoscale convective systems are precipitation systems associated with significant convection that occurs during some portion of their lifetime, spatial scales of 10-500 km and lifetimes on the order of 10 hours (Rutledge, 1991). MCSs have been the subject of numerous investigations over the past several decades. They are significant to forecasting since they are often associated with severe weather (e.g., hail, tornadoes, strong winds, frequent cloud-to-ground lightning, and flooding), and they also modify the large-scale synoptic flow of the troposphere through transports of heat and momentum (e.g., Fritsch and Maddox, 1981; Johnson, 1984). Subsets of MCSs include the mesoscale convective complex (as defined by Maddox, 1980), squall lines, tropical cloud clusters and large supercell thunderstorms. Herein we will be primarily concerned with mature tropical squall lines having lifetimes on the order of 5-10 hours. In this chapter we focus on describing the relevant dynamical, microphysical and electrical properties of MCSs as identified in previous studies. This overview will then set the stage for new electrical (lightning and electric field) observations of MCSs to be presented later in Chapter 5.

## 3.1 MCS dynamical structure

Mature MCSs (Fig. 3.1) can be described using a conceptual model similar to that presented by Houze et al. (1989). The model is a composite made from many observations of middle-latitude and tropical squall lines (Houze et al. 1989). Major features of the MCS in Fig. 3.1 include a convective line with associated large radar reflectivities, heavy convective showers and a surface gust front. Trailing the convective line is a stratiform anvil cloud (typically referred to as the trailing stratiform region) characterized by a radar "bright band" (Leary and Houze, 1979; Smull and Houze, 1987; Rutledge and Houze, 1987; Rutledge et al. 1988), and a broad area of stratiform precipitation (Leary and Houze, 1979; Gamache and Houze, 1982; Smull and Houze, 1987; Rutledge et al. 1988).

In Fig. 3.1 two major flow structures are exhibited. General upward motion is indicated at the edge of the gust front with the vertical slope of the motion becoming more pronounced as it enters the convective line, then decreasing as it enters the stratiform region. This storm-relative flow is called the ascending front-to-rear flow (Houze et al., 1989) and is superimposed onto vigorous updrafts and downdrafts in the cells of the convective line (Houze et al., 1989; Rutledge, 1991). The second flow structure (descending rear inflow) slopes gently downward from mid-levels in the stratiform region, through the bright band, and descends sharply at low levels into the back of the convective line where it may merge with convective downdrafts to strengthen the leading gust front (e.g., Smull and Houze, 1987; Rutledge et al. 1988). New cells form at the leading edge of the gust front ahead of mature and decaying cells in the convective line. The older cells and their associated heat, momentum and condensate are advected rearward in the front-to-rear flow, thus developing and

maintaining the trailing stratiform region ( Smull and Houze, 1985, 1987; Rutledge et al. 1988; Biggerstaff and Houze, 1991).

Mean mesoscale vertical motions in the stratiform region (possibly driven by spatially varying convective scale circulations; e.g., Biggerstaff and Houze, 1991; Keenan and Rutledge, 1992) are characterized by mesoscale ascent in the front to rear flow above the bright band and mesoscale descent below the bright band (e.g., Leary and Houze, 1979; Gamache and Houze, 1982; Smull and Houze, 1987; Rutledge and Houze, 1987; Rutledge et al. 1988). The mesoscale updraft and downdraft are typically 20-50 cm $s^{-1}$ in magnitude (e.g., Gamache and Houze, 1982; Rutledge et al. 1988) and are associated with mid-level convergence above the bright band (note the position of the stratiform meso-low at mid-levels in Fig. 3.1) and lower level divergence below the bright band. A narrow region of subsidence and low radar reflectivities called the transition zone often exists between the convective line and trailing stratiform region (Rutledge et al. 1988; Biggerstaff and Houze, 1991).

While the conceptual model (Fig. 3.1) presented by Houze et al. (1989) is generally representative of both tropical and middle-latitude MCSs, some differences do exist. For example, strong reflectivity cores in tropical MCSs of oceanic origin rarely extend much above the 0° C level (e.g., Jorgensen and Lemone, 1989; Rutledge et al. 1992a). Furthermore, peak convective updrafts in middle-latitude MCSs are two to three times stronger than those of tropical MCSs (Jorgensen and Lemone, 1989). For stratiform regions, Smull and Houze (1987) noted that the storm-relative rear inflows of tropical MCS stratiform regions are typically much weaker than those of their middle-latitude counterparts.

## 3.2 Microphysical observations in the stratiform regions of MCSs

The microphysical structures of MCSs are only partially documented owing to limited observational capabilities. In-situ samples of the upper portions of MCSs with aircraft capable of making microphysical observations are basically non-existent. We therefore present microphysical observations made in the lower and middle levels of MCSs. Heymsfield and Hjelmfelt (1984) presented detailed in-situ observations of the hydrometeors present in the middle-levels of convective lines associated with several middle-latitude MCSs. Similar observations were presented by Houze and Churchill (1984) and Gamache (1990) with regard to the microphysical characteristics of tropical MCSs. Herein we will limit our discussion of MCS microphysical observations to those associated with the trailing stratiform region.

Modeling studies and observations point to two primary steps in the growth of the stratiform region. Step 1: Advection of ice particles rearward from the convective line into the stratiform region by the storm-relative front-to-rear flow (e.g., Smull and Houze 1985, 1987; Rutledge and Houze, 1987). Step 2: Further growth of the ice particles and the production of new ice particles in the mesoscale updraft (e.g. Rutledge and Houze, 1987). As the stratiform region grows, a radar bright band (a horizontal band of locally higher reflectivities) develops immediately below the 0°C level as ice falling through the melting level acquires an outer layer of liquid water (Leary and Houze, 1979), producing a sharp increase in reflectivity (Battan, 1973). The rapid decrease in reflectivity below the bright band is due to evaporation of hydrometeors, higher terminal velocities of raindrops and possibly drop break up (Battan, 1973).

The stratiform region is composed almost entirely of ice with average concentrations of 10-70 $L^{-1}$ (e.g., Houze and Churchill, 1984; Gamache, 1990; Willis and Heymsfield, 1989; Yeh et al. 1991). Though the stratiform region is thought to be mainly glaciated, several observational studies have inferred the presence of small amounts of supercooled liquid water (amounts generally $\leq .3$ g $m^{-3}$ ; e.g., Leary and Houze, 1979; Houze and Churchill, 1984; Rutledge et al. 1990; Yeh et al. 1991). In addition to the observations, a modeling study by Rutledge and Houze (1987) also suggested the presence of slight amounts ($\leq 0.1$ g $m^{-3}$) of supercooled liquid water in the stratiform region.

Ice particle observations in the stratiform region have revealed large numbers of aggregates (many of which appear to be aggregates of broken dendrites and ice fragments; e.g., Willis and Heymsfield, 1989) and branched crystals, indicating that in-situ ice particle growth is due primarily to aggregation and deposition (e.g., Leary and Houze, 1979; Houze and Churchill, 1984; Willis and Heymsfield, 1989; Gamache, 1990; Ye et al. 1991). While deposition and aggregation are thought to be the primary growth regimes in the stratiform region (and do not require cloud water), some studies have observed or inferred the presence of rimed aggregates and graupel in the stratiform region (e.g., Leary and Houze, 1979; Yeh et al. 1991) indicating that some riming may be taking place. Kinematic modeling studies by Rutledge (1986) and Rutledge and Houze (1987) also diagnosed the presence of graupel in the stratiform regions of an MCSs.

Leary and Houze (1979) inferred from raindrop size distributions collected during GATE (Global Atmospheric Research Program's Atlantic Experiment) that liquid water above the 0° C level was possibly present in sufficient amounts to cause riming

and the production of graupel. This finding is consistent with Yeh et al. (1991) who observed small concentrations of graupel (.07 $L^{-1}$) and numerous aggregates composed of rimed crystals (believed to be dendrites and fractured dendrites) in the stratiform region of a middle-latitude MCS. These results coupled with the modeling results of Rutledge and Houze (1987), support some limited riming growth of ice and the presence of modest amounts of graupel in the stratiform regions of MCSs.

Houze and Churchill (1984) and Gamache (1990) both conducted studies of ice-particle concentrations and liquid water contents (LWCs) observed in the stratiform regions of tropical MCSs studied during WMONEX and SMONEX (Winter, Summer Monsoon Experiment; 1978 and 1979) respectively. Both studies reported that stratiform regions were dominated by aggregates, vapor grown crystals and a large number of particles whose shapes were indeterminable (though thought to be aggregates and ice fragments by Houze and Churchill). In both studies the concentrations of each type of ice particle were summarized in a tabular format. For example, Houze and Churchill (1984) grouped ice concentrations at the 7-8 km level (-14° C to -19° C) according to size, shape and the strength of the stratiform precipitation reflectivity. Strong stratiform precipitation ($\geq$ 20 dBZ) had concentrations of 20-70 $L^{-1}$ and small amounts of liquid water (always < 0.2 g $m^{-3}$). Weak and very weak stratiform precipitation (1-20 dBZ) had concentrations of ice that were almost always < 10 $L^{-1}$.

In summary, it appears that the stratiform region is seeded by ice particles from the convective line (e.g., Smull and Houze, 1987) and that this condensate grows in the mesoscale updraft by vapor deposition and aggregation (Rutledge and Houze, 1987). Liquid water is sometimes present in the stratiform region, though in small amounts, so some riming of ice particles may take place (Leary and Houze, 1979; Rutledge and

Houze, 1987; Yeh et al. 1991). Particle concentrations vary in the stratiform region with average concentrations on the order of 10-70 $L^{-1}$ (Houze and Churchill, 1984; Willis and Heymsfield, 1989; Gamache, 1990; Yeh et al. 1991). Ice is present in the stratiform regions primarily in the form of aggregates, branched crystals and fragments with slight concentrations of graupel observed (.07 $L^{-1}$; Yeh et al. 1991). In addition, a significant number of ice-ice collisions may take place in the stratiform region based on observations which show aggregates of dendrite branches and fragments (e.g., Yeh et al. 1991), and the presence of numerous individual ice fragments (Houze and Churchill, 1984; Willis and Heymsfield, 1989; Yeh et al. 1991).

## 3.3 A brief review of electrification hypotheses

To better understand hypotheses advanced to explain MCS electrification, a brief review of thunderstorm charging mechanisms is in order. Mechanisms forwarded to explain lightning in thunderstorms can be grouped into two categories: 1) precipitation-based theories (non-inductive and inductive); and 2) a convective theory. Since this thesis concentrates on the mechanisms responsible for producing lightning as observed in the stratiform regions of MCSs, we will concentrate on precipitation-based theories (more specifically the non-inductive charging mechanism) and not the convective theory. The convective theory of charging (reviewed in Williams, 1989) invokes strong vertical air motions inside of developing thunderstorms to transport space charge (created by corona emission and cosmic radiation) against local electric fields. However, the convective theory does not adequately explain the observed charge structures in thunderstorms nor does it produce lightning on time scales relevant to the developing thunderstorm (Williams, 1989).

Precipitation-based theories can be separated into the non-inductive (e.g., Takahashi, 1978: Jayaratne et al. 1983) and inductive charging mechanisms (Elster and Geital, 1913; Illingworth and Latham, 1977). The inductive charging mechanism states that the fair weather electric field polarizes precipitation particles as they are falling (positive charges collect on the bottom of the particle, negative on top in a downward directed electric field). When hydrometeors such as ice or water droplets collide, the smaller particle (being carried upward in an updraft) acquires positive charge, while the larger particle acquires negative charge, thus leaving the cloud with negative charge in lower layers and positive charge aloft (a positive dipole). It has been demonstrated by several researchers that the inductive charging mechanism cannot produce large enough electric fields for breakdown to occur (e.g., Gaskell, 1979; Rawlins, 1982). In comparison to convective and inductive charging mechanisms, the non-inductive mechanism is considered a viable charging mechanism for thunderstorm electrification (Williams, 1989).

The non-inductive charging mechanism is based on the laboratory experiments of Takahashi (1978), Jayaratne et al. (1983), Keith and Saunders (1989), and Saunders et al. (1991). These experiments indicate that significant charge is transferred in collisions between ice crystals and a riming ice surface (e.g., graupel). The amount and sign of charge transferred has been shown to be a strong function of the liquid water content (LWC) and the temperature. Takahashi's (1978) laboratory results are in the best agreement with observations (Williams, 1989).

Fig. 3.2a shows results from Takahashi's (1978) laboratory experiments. The electric charge transferred to the rimer (in electrostatic units) is shown as a function of temperature and liquid water content. The shaded area represents temperatures and

liquid water contents where the rimer charges negatively, the light area represents positive charging of the rimer. The boundary separating the two charge polarities represents the charge reversal temperature (which is a function of the LWC). In addition to the liquid water content and temperature, the sign of charging has also been shown by Takahashi (1978), Baker et al. (1987), Caranti et al. (1991) and Williams et al. (1991) to be a function of the growth state of the ice surface (i.e., when the graupel surface is in a depositional (sublimational) state it acquires positive (negative) charge).

The non-inductive mechanism believed to be responsible for the electrification of clouds works as follows (e.g., Fig. 3.2b): graupel growing by riming are carried by updrafts above the melting level along with liquid water (regions B-C in Fig. 3.2b). Above the charge reversal temperature (typically -10°C to -20°C) graupel colliding with small ice crystals in the mixed phase region are charged negatively. The smaller ice crystals are charged positively and lifted into the upper regions of the storm by updrafts. Thus positive charge is situated in the upper levels in a thunderstorm. The negatively charged graupel meanwhile stay in the mixed phase region at the particle balance level (the level at which the terminal velocity of the graupel equals the updraft velocity) and continue to grow while continually undergoing collisions with smaller ice particles. This concentrates the negative charge residing on the graupel in the mixed phase regions of the cloud (centered generally between -10°C and -20°C). Later, when the graupel grow large enough to fall through the level of the charge reversal temperature (or the suspending updrafts weaken) they undergo collisions in the lower levels of the thundercloud and charge positively (region A in Fig. 3.2b). Hence, a net positive space charge also develops lower in the cloud below the charge reversal temperature. The layers of lower positive charge, middle negative charge and upper positive charge (Fig.

3.2b) thus result in observations of a tripolar charge structure in thunderclouds (Williams, 1989).

The non-inductive charging mechanism in thunderclouds is supported by: 1) in-situ measurements of the vertical charge structure in thunderstorms (e.g., Dye et al. 1988; Breed and Dye, 1989; Williams, 1989; Selvam et al., 1991); 2) observations that clouds dominated by warm rain processes and weak mixed phase regions produce little or no lightning (e.g., Chauzy et al. 1985; Williams, 1989; Selvam et al. 1991; Rutledge et al. 1992a), and by recent in-situ measurements of the charge, size and shape of hydrometeors in cumulonimbus clouds and thunderstorms (e.g., Dye et al. 1988; Selvam et al. 1991; Weinheimer et al. 1991). Dye et al. (1988) and Weinheimer et al. (1991) discovered significant charge residing on graupel particles in New Mexico thunderstorms. Charge measured on the graupel by Weinheimer et al. were on the order of 10-20 pC with peak charges of approximately 200 pC (consistent with the theoretical results of Bourdeau and Chauzy, 1989). Dye et al. measured slightly lower charge of 1-6 pC on a very small number (65) of 1 mm graupel particles. The measurements of Weinheimer et al. also indicated a charge reversal temperature of -17°C to -22° C with liquid water contents of 0 to 2 g $m^{-3}$ which is somewhat consistent with the results of Takahashi, 1978. In the tropics, Selvam et al. (1991) also inferred the presence of a non-inductive charging mechanism in cumulus clouds observed during the Indian summer monsoon. In-situ measurements of the electric potential gradient, temperature, liquid water contents, and the charge residing on raindrops were found by Selvam et al. to be consistent with the results of Takahashi (1978). Thus far we have only considered the non-inductive charging mechanism in thunderclouds however, the non-inductive charging mechanism can also generate electric charge in the trailing stratiform region of an MCS (region D in Fig. 3.2b).

In the stratiform region the mesoscale updraft carries smaller ice crystals upward. It may also carry small amounts of liquid water with the ice in the development of a mixed phase region (recall the observations of small LWCs in stratiform regions presented earlier in this chapter). Therefore, collisions and charge transfer may still take place between ice particles (some of which may be graupel) in the presence of small amounts of liquid water. Gravitational settling would then separate the larger particles from the smaller, promoting charge separation. Indeed, since depositional growth of ice in stratiform regions sometimes takes place in the presence of slight amounts of liquid water, it would be expected that graupel or ice undergoing depositional growth (e.g., Fig. 3.2b) would charge positively in collisions with smaller ice particles (Takahashi, 1978; Baker et al. 1987; Caranti et al. 1991; Williams et al. 1991). The smaller, negatively charged ice particles would then be transported aloft by the mesoscale updraft. Hence, an inverted dipole (negative overlying positive charge) may possibly develop in the stratiform region which would favor positive discharges to ground (e.g., Rutledge et al. 1990). Recent electrical observational studies of MCSs lend support to the existence of an in-situ, non-inductive charging mechanism in the stratiform region.

## 3.4 Summary of MCS electrification studies

Herein we review several recent middle-latitude studies of CG patterns relative to MCS reflectivity structure including Rutledge and MacGorman (1988), Orville et al. (1988), Stolzenburg (1988), Rutledge et al. (1990), and Engholm et al. (1990). Similar radar studies conducted in the tropics and reviewed in this thesis include Chauzy (1985), Rutledge et al. (1991), and Petersen and Rutledge (1992). We also review recent in-situ measurements of the vertical charge structure in middle-latitude and tropical MCS stratiform regions (e.g., Chauzy et al. 1985; Marshall and Rust, 1991; Schuur et al.

1991). We begin the review of MCS electrification by presenting a short summary of the middle-latitude observations of CG lightning relative to observed radar reflectivity structures in MCSs, paying special attention to observations of the positive CGs in the stratiform region.

### 3.4.1 Observations of MCS electrification in the middle-latitudes

Rutledge and MacGorman (1988) (hereafter referred to as RM) presented radar and CG lightning data collected during the 10-11 June 1985 PRE-STORM MCS (e.g., Figs 3.3, 3.4). The lightning data (locations shown as (+) for positive flashes and (-) for negative flashes) were presented at 30 minute time intervals centered spatially and temporally on the National Weather Service (NWS), Wichita, Kansas WSR-57 low level (1.2°) radar scans. The data were analyzed by RM for approximately five hours of the storm's lifetime, from the development of a strong convective line to the development of a mature-dissipating stratiform region.

Fig. 3.3a (0123 UTC) shows a well defined squall line (approximately 2 hours after formation) with contours of reflectivity in the convective line > 40 dBZ (RM classified convective regions as those regions enclosed by 30 dBZ reflectivity contours oriented along a NE-SW line). Weak stratiform precipitation is indicated NE and NW of the convective line. The CG lightning data revealed a bipolar pattern with negative CGs occurring primarily in the convective line and positive CGs in the developing stratiform region. Several hours later at 0423 UTC (Fig. 3.3b), the stratiform region had matured as evidenced by a large area with reflectivities of 20-30 dBZ well behind the leading convective line. As at 0123 UTC (Fig. 3.3a), the CG's were arranged in a bipolar pattern with positive CGs occurring just behind and well to the rear of the convective

line (indeed, a bipolar pattern was evident in each of the 10 time periods studied by RM). An important finding of RM was that the peak positive CG flash rate at 0423 UTC (Fig 3.3b) coincided with the peak in areally integrated rainfall (Fig 3.4). RM also pointed out that peaks in the negative CG flash rate correlated well with the peaks in convective rainfall and that the time lag between the peak flash rates (negative and positive) is similar to the lag between the peaks in convective and stratiform rainfall respectively.

To investigate the correlations between the rainfall (convective and stratiform) and CG flash rates, and the observations of bipolar CG patterns, RM calculated the trajectories ice particles would take from the upper regions of the convective line, into the stratiform region. RM found that large ice crystals in the convective line (above 8.4 km) with fall speeds of 1.5 - 2 m $s^{-1}$, could have been transported 45 km into the stratiform region in 1-3 hours before reaching the melting level. This result led RM to suggest that positive CGs in the stratiform region were associated with the rearward transport of positively charged ice from the upper regions of the convective line into the stratiform region. This conclusion is consistent with the development of stratiform precipitation by the rearward transport of ice from the convective line (Smull and Houze,1985, 1987; Rutledge and Houze, 1987), the existence of positive charge in the upper regions of a thunderstorm (Williams, 1989), and the charge advection mechanism (e.g., Orville et al. 1988).

Orville et al. (1988) and Stolzenburg (1990) documented the occurrence of several bipolar patterns in MCSs occurring in the Eastern United States (e.g., Fig. 1.1) using NWS radar summaries and the SUNYA (State University of New York at Albany) lightning detection network. Bipole lengths (horizontal distance from the center

of negative CGs to the center of positive CGs) were on the order of 100-300 km and were oriented approximately parallel to the geostrophic wind vector. The positive ends of the bipoles were located in downshear anvils while the negative ends of the bipoles were situated in the convective regions. Orville et al. (1988) noted that the bipolar patterns occurred preferentially in fall and winter season mesoscale weather systems, while Stolzenburg inferred a seasonal dependence for the length of the bipoles (summer bipoles being shorter than winter bipoles). Stolzenburg attributed the seasonal dependence on length to seasonal differences in convective intensity (upright convection being stronger in the summer) and to seasonal differences in wind shear (i.e., higher shear in the more baroclinic environment of fall and winter would tend to move the upper positive and lower negative charge regions further apart).

Both Orville et al. (1988) and Stolzenburg (1990) concluded that charge advection by the geostrophic wind led to the observed bipolar patterns. This conclusion was based on several observations. First, the bipoles were always aligned with the geostrophic wind vector. Second, vertical shear of the horizontal wind exceeded 1.5 m $s^{-1}$ $km^{-1}$ (a threshold proposed by Brook et al. (1982) to explain the occurrence of positive CGs 10-20 km away from the convective regions of thunderstorms in Japan (i.e., the tilted dipole mechanism). Third, charge relaxation calculations based on the conductivity of cloudy-air ($2x10^{-15}$ mho $m^{-1}$; Rust and Moore, 1974) revealed a characteristic time for charge relaxation by ion attachment of 4400s (implying a 30 m $s^{-1}$ wind could advect the positive charge approximately 130 km in 60 minutes before the charge was neutralized, which is on the order of observed bipole lengths). It is interesting to note that Orville et al. (1988) also suggested that local charge separation in the stratiform clouds might be partly responsible for the enhanced electric fields needed for positive CGs to occur.

Additional observations of CG patterns with respect to the radar reflectivities associated with MCSs were made by Engholm et al. (1990). More specifically, Engholm et al. (1990) concentrated on the conditions under which positive CGs and bipolar patterns occurred. They found a positive correlation between the vertical wind shear and: 1) relative displacement between positive and negative CGs and 2) percentage of positive CGs (Fig. 3.5). Further, Engholm et al. found that winter bipoles were oriented with the geostrophic wind while summer bipoles tended to align with stronger ageostrophic convective circulations (i.e., storm relative shear vectors).

In studies of the bipolar lightning patterns associated with two winter season and three summer season MCSs, Engholm et al. (1990) pointed out that even though vertical wind shear and the occurrence of bipolar patterns were highly correlated, the bipole length seemed to be equally well correlated to the depth of the surrounding clouds. Indeed, in the winter season MCSs examined, positive CGs (on the positive end of the bipole) tended to be located under an anvil within 10-20 km of upright convection, or within 10-20 km of embedded convection in stratiform cloud (which was also aligned with the geostrophic wind). It was also noted that there seemed to be no correlation between the length of the bipoles and the strength of the geostrophic winds aloft. This lead Engholm et al. to conclude that convective scale tilting of a positive dipole by vertical wind shear (tilted dipole mechanism; Brook et al. 1982) was responsible for the bipolar patterns observed, not charge advection over mesoscale distances. Indeed, Engholm et al. (1990) abandoned the hypothesis of charge advection over mesoscale distances in favor of an in-situ charging mechanism on the convective scale for the production of positive charge in stratiform clouds.

Engholm et al. (1990) supported their position with electric field measurements of several summer season MCSs made with a surface based corona point network. It was argued that if charge advection were the primary mechanism involved in the electrification of the stratiform region and the formation of bipolar patterns, one would expect to measure primarily positive charge overhead in the region just behind the convective line and into the stratiform region. However, MCS stratiform regions passing over the corona point network revealed both positive and negative charge layers overhead, in conflict with charge advection hypothesis (e.g., Orville et al. 1988; Rutledge and MacGorman, 1988; Stolzenburg, 1990).

For example, in one case studied by Enholm et al., (21 June 1987) as the stratiform region (still attached to the convective line and only 20-40 km in width) passed over the network, a global change to positive charge overhead was observed except at one station where negative charge was observed overhead. In another case (12 July 1988), a mature stratiform region, completely detached from the convective line, approached the corona point network from the west. Fig. 3.6 represents the corona point measurements of the electric field (positive values indicate negative charge overhead) recorded with the passage of the stratiform region. Note that the vertical electric field became strongly positive (negative charge overhead) as the stratiform region passed over the radar and then became negative (positive charge overhead) as the trailing edge of the stratiform region left the network. Engholm et al. (1990) attributed this to the local tilting of a positive dipole in the stratiform region. Since this stratiform region was completely independent of the convective line, and the electric field did not change until the stratiform region was over the network, Engholm et al. considered this to be strong evidence of in-situ charge generation in the stratiform region.

Another important finding by Engholm et al. (1990) was that both winter and summer MCS cases which produced lightning, exhibited significant reflectivity in the mixed phase regions of the storms (i.e., 0°C to -40°C). Storms that were not vertically extensive (i.e., no mixed phase region), did not produce lightning. Note that the existence of a mixed phase region is required for charging by the non-inductive mechanism (Takahashi, 1978; Jayaratne et al. 1983). Also, the positive end of the CG bipoles observed by Enholm et al. (1990) contained many negative CGs (as in RM also). This is not explained by the charge advection mechanism.

The last radar study of CG positions in middle-latitude MCSs considered here was conducted by Rutledge et al. (1990). This study concentrated on the positive CGs observed in several MCSs that occurred during PRE-STORM. The CG patterns observed were quite similar to those presented in the studies above. Positive CGs occurred preferentially in the stratiform regions (but not exclusively) while negative CGs tended to occur in closer proximity to convective lines. Rutledge et al. (1990) acknowledged the possible importance of the charge advection mechanism in producing some of the positive CGs in the stratiform region. However, after conducting a modeling study (discussed in more detail later in this section) Rutledge et al. (1990) concluded that considerable charge could be generated in the stratiform region in-situ by ice-ice collisions in the presence of supercooled liquid water (i.e., non-inductive charging mechanism; Takahashi, 1978). Their result offers an explanation for positive CGs in the stratiform region, but more importantly, the mechanism also explains the presence of negative CGs in the stratiform region (which are not adequately explained by the charge advection mechanism). Rutledge et al. (1990) referred to the charging of the stratiform region as an "in-situ" mechanism.

### 3.4.2 Studies of Tropical MCS electrification

Radar studies of MCSs and their associated CGs in tropical northern Australia by Rutledge et al. (1991) and Petersen and Rutledge (1992) indicate CG patterns similar to those observed in the middle-latitudes. Compared to middle-latitude MCSs (e.g., Rutledge and MacGorman, 1988; Rutledge et al. 1990), the tropical MCSs studied by Rutledge et al. (1991) and Petersen and Rutledge (1992) produced a relatively small number of CGs. However, similar to middle-latitude observations the tropical CGs in both studies exhibited bipolar patterns. In addition, Rutledge et al. (1991) inferred the existence of an inverted dipole in the stratiform region of one tropical MCS based on electric field measurements that indicated positive charge overhead in the lowest levels of the stratiform region. Petersen and Rutledge (1992) linked the temporal increase in positive peak current maximums to the growth of the stratiform region, thus demonstrating a dependence of positive peak current magnitudes on the growth stage of the stratiform region. Both Rutledge et al. (1991) and Petersen and Rutledge (1992) presented further evidence for in-situ charging in the stratiform regions of MCSs to explain the occurrence of lightning therein.

Chauzy et al. (1985) examined a tropical MCS that occurred during COPT-81 (Convection Profonde Tropicale) over the northern Ivory Coast region. The MCS consisted of a weakly electrified convective line (reflectivities > 40 dBZ were well below the -10° C level) with an extensive trailing stratiform region (Figs. 3.7a, b). Chauzy (1985) noted that a relatively small number of negative CGs were associated with the rear of the convective line and that no positive CGs were observed in the stratiform region. However, electric field records (Fig. 3.7c) did indicate increases in electrical activity (either in-cloud or CGs) that coincided with the development of an ice phase just

to the rear of the convective line. In the stratiform region, a field change to positive charge overhead occurred approximately 100 km behind the convective line (just below the stratiform bright band in Fig 3.7b) with some excursions to negative charge overhead near 130 km and 160-180 km behind the convective line (consistent with the dominant charge measured on rainfall below each region; Fig. 3.7b). Chauzy et al. (1985) attributed the weak CG activity in the convective line to the lack of a strong mixed phase region. This observation lends support to the importance of an ice-phase in the electrification of clouds (Williams, 1989; Rutledge et al. 1992a).

## 3.5 Studies of the vertical charge structure in stratiform regions

In addition to surface electric field measurements such as those presented by Chauzy et al. (1985), Engholm et al. (1990), and Rutledge et al. (1991), several studies have taken in-situ observations of the vertical component of the electric field in MCSs. These studies infer the vertical distribution of space charge density using Gauss' law (which reduces to evaluating the slope of the vertical component of the electric field as a function of height assuming a horizontally infinite sheet of charge; e.g., Schuur et al. 1991; Marshall and Rust, 1991).

Chauzy et al. (1985) produced two soundings of the vertical electric field from the tropical MCS they examined. One sounding was launched into the rear portion of the convective line, where negative charge was inferred near the 0° C level and positive charge aloft. The other electric field meter was launched into the trailing stratiform region and terminated just above the melting level. The stratiform sounding revealed an area of strong negative charge near the height of the bright band and the beginning of a reversal to positive charge just above the negative charge layer as the sounding

terminated. Based on the collocation of a negative charge layer and the bright band, Chauzy et al. (1985) concluded that a mixed phase region in stratiform clouds may have been important to the generation of charge therein.

Similar vertical electric field soundings were conducted in the trailing stratiform regions of middle-latitude MCSs by Schuur et al. (1991) and Marshall and Rust (1991). All of these soundings revealed a complex charge structure in the stratiform regions examined (e.g., Fig. 1.3). For example, Schuur et al. (1991) presented observations of an electric field meter sounding into the leading edge of a stratiform region (transition zone) associated with a squall line in Oklahoma (these results were also reported in Marshall and Rust, 1991; see Fig. 1.3). The charge structure (as explained by Schuur et al.) consisted of a thick (1.2 km) negative charge layer centered at 4 km with other negative charge layers between 6.5 - 7 km and 10.5 - 11.2 km. Positive charge layers were found between 5 and 6.5 km ($-6°C \leq T \leq -14°C$), 8 - 8.7 km and 8.7 - 8.9 km. Charge densities in the layers were on the order of 0.5 - 4 C $km^{-3}$. Schuur et al. (1991) concluded that the lower and upper negative charge layers located on the cloud boundaries were charge screening layers (formed in response to positive charge in the cloud). The positive charge layers from 5 - 6.5 km and the negative charge layers from 6.5 - 7 km formed an inverted dipole and were attributed by Schuur et al. to the possible existence of an in-situ, non-inductive charging mechanism. Charge advection from the convective line was suggested as a possible mechanism for the generation of the layers of positive charge between 8 and 8.9 km since they existed in a region of strong front to rear flow behind the squall line. It is also worth noting that Schuur et al. observed a higher percentage of positive CGs in the stratiform region than in the convective line.

## 3.6 Model evaluations of the non-inductive and charge advection mechanisms in the trailing stratiform region of an MCS.

Herein we concentrate on the studies of Hill (1988), Rutledge et al. (1990) and Rutledge et al. (1992b). Both Hill (1988) and Rutledge et al. (1992b) addressed the charge advection mechanism. The results of Hill (1988) supported the charge advection mechanism (i.e., positive charge in the upper portions of a convective line is advected by the storm relative flow into the stratiform portions of the cloud thus producing positive CGs and a bipolar lightning pattern). The results of Rutledge et al. (1992b) supported the charge advection mechanism over short distances (i.e., $\leq 30$ km; essentially the tilted dipole mechanism) but concluded that the charge advection mechanism cannot supply the needed charge concentrations ($\geq 1$ C km$^{-3}$) to produce positive CGs at distances $\geq 30$ km from the convective line. The modeling study results of Rutledge et al. (1990) strongly supported an in-situ, non-inductive charging mechanism for the trailing stratiform region of an MCS.

Rutledge et al. (1990) modeled (1-D model) the local charge production in MCS stratiform regions using laboratory charging data from Jayaratne et al. (1983), and Saunders and Jayaratne (1986) coupled with observed and modeled ice concentrations. Charging rates were computed in the model by multiplying the amount of charge transferred in collisions between graupel particles and ice crystals (as determined by Saunders and Jayaratne, 1986) by the mass weighted velocity of the graupel particles, the number concentrations of ice and graupel, and the charge separation efficiency. The model produced charge densities of 2-4 C km$^{-3}$ ( values typically observed in lightning producing clouds; Uman, 1987) and volume charging rates on the order of $2 \times 10^4$ C hr$^{-1}$. The significance of the non-inductive charging mechanism (as demonstrated by

Rutledge et al.) can be realized as follows: if we assume that each positive CG transfers roughly 100 C of charge to ground (Brook et al. 1982), then based on the volume charging rate above the non-inductive mechanism could support a flash rate of 200 flashes $hr^{-1}$ in the stratiform region. It is also important to note that the modeling study of Rutledge et al. (1990) produced an inverted dipole with positive charge situated below negative charge. Thus negative CGs might also be possible in a highly sheared flow that tilted the dipole.

The viability of the charge advection mechanism was explored in a study by Hill (1988). He considered the radial expansion of a spherical volume of cloudy air (initial radius 1 km) containing 41 C of positive charge situated on ice particles. The expansion was due only to the repulsive Coulombic force which acted outward on the positive charge volume. Hill did not consider turbulent diffusion of the charge and also neglected ion attachment since the volume was assumed to be in cloudy air where conductivities are low ($2 \times 10^{-15}$ mho $m^{-1}$; Rust and Moore, 1974). With these assumptions Hill calculated the time required for the radius of the charge sphere to double. Hill calculated this time to be 62,750 seconds, which is an order of magnitude greater than the 4400 second time interval calculated by Orville et al. (1988) for neutralization of a positive charge volume advected some 130 km at a speed of 30 m $s^{-1}$. This lead Hill (1988) to conclude that charge advection might be a reasonable explanation for lightning bipoles. As Rutledge et al. (1992b) note, in a time period of 60,000 seconds and an advection speed of 15 m $s^{-1}$ the charge volume would travel 950 km before the volume radius doubled placing the charge volume well outside the cloudy domain of an MCS.

Rutledge et al. (1992b) also addressed the charge advection mechanism (and the results of Hill, 1988) with a modeling study. Rutledge et al. (1992b) first proceeded to verify the results of Hill (1988) using an alternative expression for the coulombic radial expansion of a 1 km radius, spherical charge volume. The calculation yielded results similar to Hill (1988) with 38,000 seconds being the time required for the charge volume to expand to twice its initial radius.

The analyses of Hill (1988) and Rutledge et al. (1992b) indicated rather long dissipation times for a charge volume when only Coulombic expansion of the charge volume was considered. Hence long advection distances of the charge volume were indicated within a cloudy environment, suggesting the possible relevance of the charge advection mechanism. However, charge volumes expand not only by a Coulombic force but are also subject to turbulent diffusion (Rutledge et al. 1992b). To examine the effects of turbulent diffusion, an analogy to the dispersion of a point source (say a smoke plume) from a continuous source (say a smoke stack) at some effective emission height can be made. The source also supplies the effluent at some constant rate (in our case we will use a charging rate in Coulombs per second for one cubic kilometer). The aim here will be to estimate some type of "upper bound" for the space charge densities that can be maintained in the area behind the convective region (e.g., the trailing stratiform region in a squall-type MCS) due soley to charge advection, considering turbulent diffusion of the charge volume.

The turbulent diffusion of a charge volume for two cases will be calculated. For the first case a rather vigorous charging rate of $4 \times 10^{-2}$ C $s^{-1}$ is used, which will produce 41 coulombs of charge in a sphere of 1 km radius (space charge density 10 C $km^{-3}$) in 4 minutes (equivalent to the values used by Hill, 1988). For the second

case the charging rate is reduced to $2 \times 10^{-2}$ C $s^{-1}$, yielding a space charge density of 2-5 C $km^{-3}$ (a value that is on the order typically found in lightning producing clouds; Uman, 1987). The particular charging rates are assumed to be independent of time. Additionally, the following assumptions are required:

1. The sphere will represent a point source of continuous, uniform emission of charged particles once the respective initial charge densities are reached (10 C $km^{-3}$ and 3 C $km^{-3}$).
2. The charged particles consist of ice particles with negligible fall speeds so that the ice particles remain suspended in the horizontal flow.
3. Following Panofsky and Dutton (1984) and also Taylor's (1921) theorem for point source dispersion, the turbulence is assumed to be homogeneous and stationary.
4. The wind velocity will be horizontal and uniform along the major axis of the charge plume with a speed of 15 m $s^{-1}$. (Calculated charge concentrations will be along the major axis of the plume parallel to the wind).
5. The charge plume will have a Gaussian distribution in both the horizontal and vertical directions with the standard deviation interpreted as the width of the plume in the respective plane. The initial plume radius is set at 1000 m.
6. Standard deviations of the plume width in the lateral ($s_y$) and vertical dimension ($s_z$) can be derived from a power law relationship using neutral stability as in Seinfeld (1986).
7. Ground height will correspond to the center of the plume as will the effective emission height.

A solution to the atmospheric diffusion equation was used with the above assumptions to perform the necessary calculations. The form of the equation used, following Turner (1969) is

$$\langle c \rangle = \frac{Q}{\pi \sigma_y \sigma_z \bar{u}} \exp\left(-\frac{1}{2} \frac{H^2}{\sigma_z z}\right) \tag{3.1}$$

where Q is the source rate (charging rate), $s_y$ and $s_z$ are dispersion parameters, and H is the distance above or below the horizontal centerline of the plume. If we choose to examine the concentration $\langle c \rangle$downwind a distance x from the source, (6) reduces to,

$$\langle c \rangle = \frac{Q}{\pi \sigma_y \sigma_z \bar{u}} \tag{3.2}$$

For $\bar{u} = 15 ms^{-1}$, $\sigma_y = R_y x^{r_y}$ and $\sigma_z = R_z x^{r_z}$, ($R_y$=.32, $R_z$=.22, $r_y$=.78, $r_z$=.78; Seinfeld, 1986) dispersion calculations were performed for both $Q = 4 \times 10^{-2}$ C $s^{-1}$ and $Q = 2 \times 10^{-2}$ C $s^{-1}$. It is further assumed that H = 0 and $\langle c \rangle$represents the concentration at the center of the dispersing plume.

The results of these calculations are shown in Fig. 3.8. Notice that the charge density of 10 C $km^{-3}$ (corresponding to the extreme charging rate of $4 \times 10^{-2}$ C $s^{-1}$) decreases by 2 orders of magnitude to 0.1 C $km^{-3}$ just 60 km downwind of the convective core. This value is an order of magnitude smaller than charge densities typically found in lightning-producing clouds (Uman, 1987). The second case corresponding to a charge density of 3-5 C $km^{-3}$ shows the charge density decreasing at an even faster rate. In this case the charge density has decreased by an order of magnitude in 30 km and more than an order of magnitude by 50-70 km.

The case can certainly be made from the calculations that turbulent diffusion plays a much greater role in the process of charge advection than the Coulombic force. It should be noted again that these results are only intended to show the existence of an "upper bound" on the charge densities available due to the effect of turbulent diffusion in the charge advection process. In the real atmosphere we might expect the charge densities to be smaller since turbulent processes are not generally uniform and homogeneous in all three dimensions. Furthermore the stability might not be neutral, and the wind is not horizontal or uniform in magnitude.

It would appear from the analyses presented above that positive CGs occurring at large distances from the convective line are not supported by simple charge advection. However, the analyses do support the charge advection mechanism (in the form of a tilted dipole) for positive CGs occurring at distances $\leq 30$ km from the convective line. We note however, that the charge advection mechanism does appear to supply *some* charge (0.1 - 0.5 C $km^{-3}$) to the stratiform region and it is entirely possible that this charge is a significant contribution to that produced by in-situ charging processes such as the non-inductive mechanism.

The non-inductive mechanism operating in MCS stratiform regions (and the importance of mixed phase microphysics) as modeled by Rutledge et al. (1990) is supported by the following: 1) in-situ and surface-based measurements of the vertical electric field in the trailing stratiform regions of MCSs reveal varied, complex structures (e.g., Marshall and Rust, 1991) and in some cases, inverted dipoles (e.g., Schuur et al. 1991) or normal positive dipoles (Chauzy et al. 1985, Engholm et al. 1990; Rutledge et al. 1990; Rutledge et al. 1991); 2) similar measurements taken in ordinary winter stratiform clouds over Florida indicate that stratiform clouds with stronger mixed phase

regions are more electrified (e.g., Mach et al. 1991); 3) occurrence of both positive and negative CGs in MCS stratiform regions point to some independent charging mechanism in the stratiform regions (e.g., Rutledge and MacGorman, 1988; Orville et al. 1988; Engholm et al. 1990, Rutledge et al. 1990); 4) modeling results testing the validity of a non-inductive charging mechanism in stratiform regions by Rutledge et al. (1990) produced large amounts of charge; 5) when turbulent diffusion of charge is considered in charge advection calculations, positive charge densities decrease rapidly with distance away from the convective line (i.e., the charge advection mechanism alone does not appear to be effective beyond 30 km from the convective line). In the following chapters we present evidence that offers further support for the presence of an in-situ, non-inductive charging mechanism in the trailing stratiform regions of MCSs.

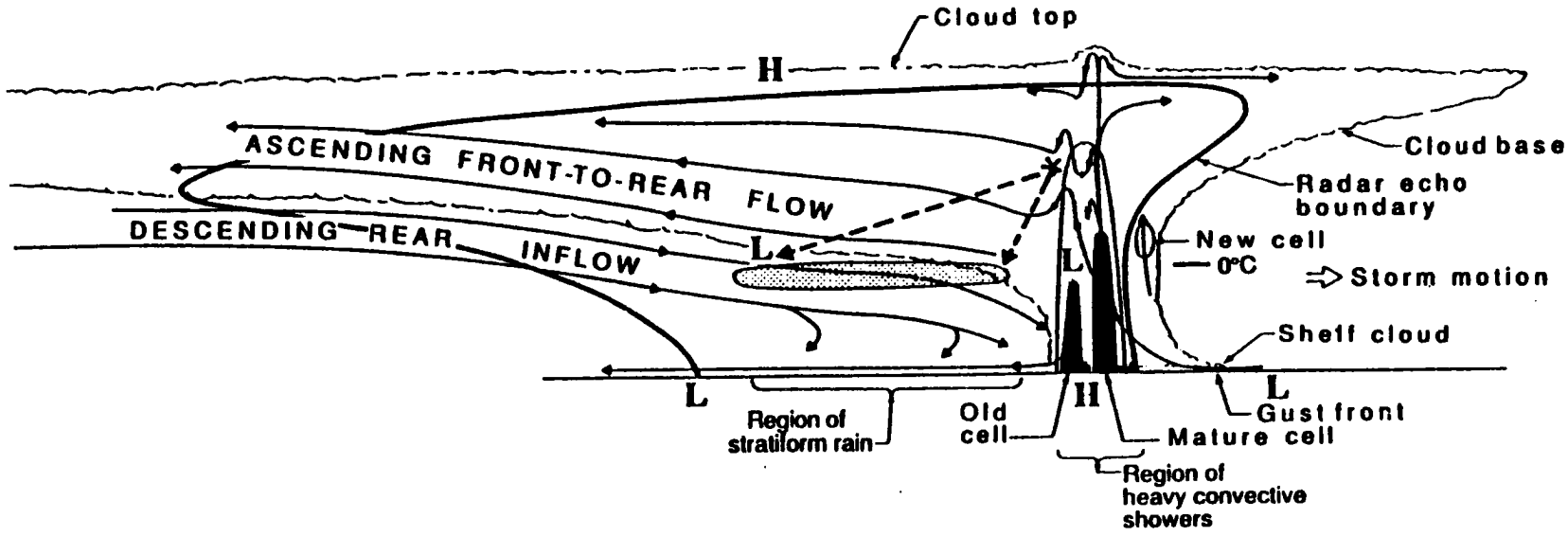


Figure 3.1 Conceptual model of an MCS (adapted from Houze et al. 1989).

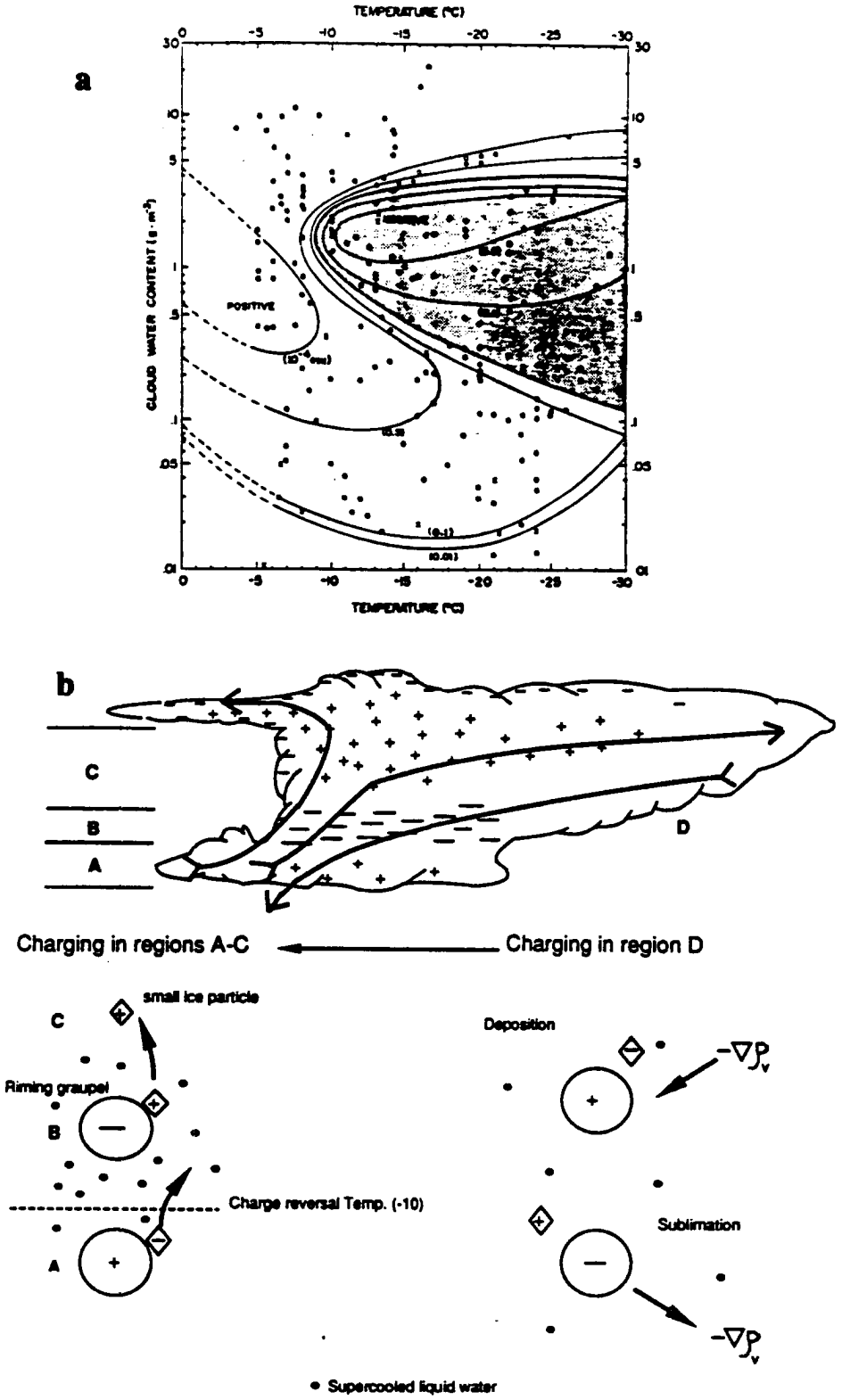


Figure 3.2. Non-inductive charging of ice in the presence of supercooled liquid water (a) laboratory results of Takahashi (1978), shaded (white) area represents negative (positive) charge transfer to the rimer and (b) illustration of charging process for ice (explanation in text).

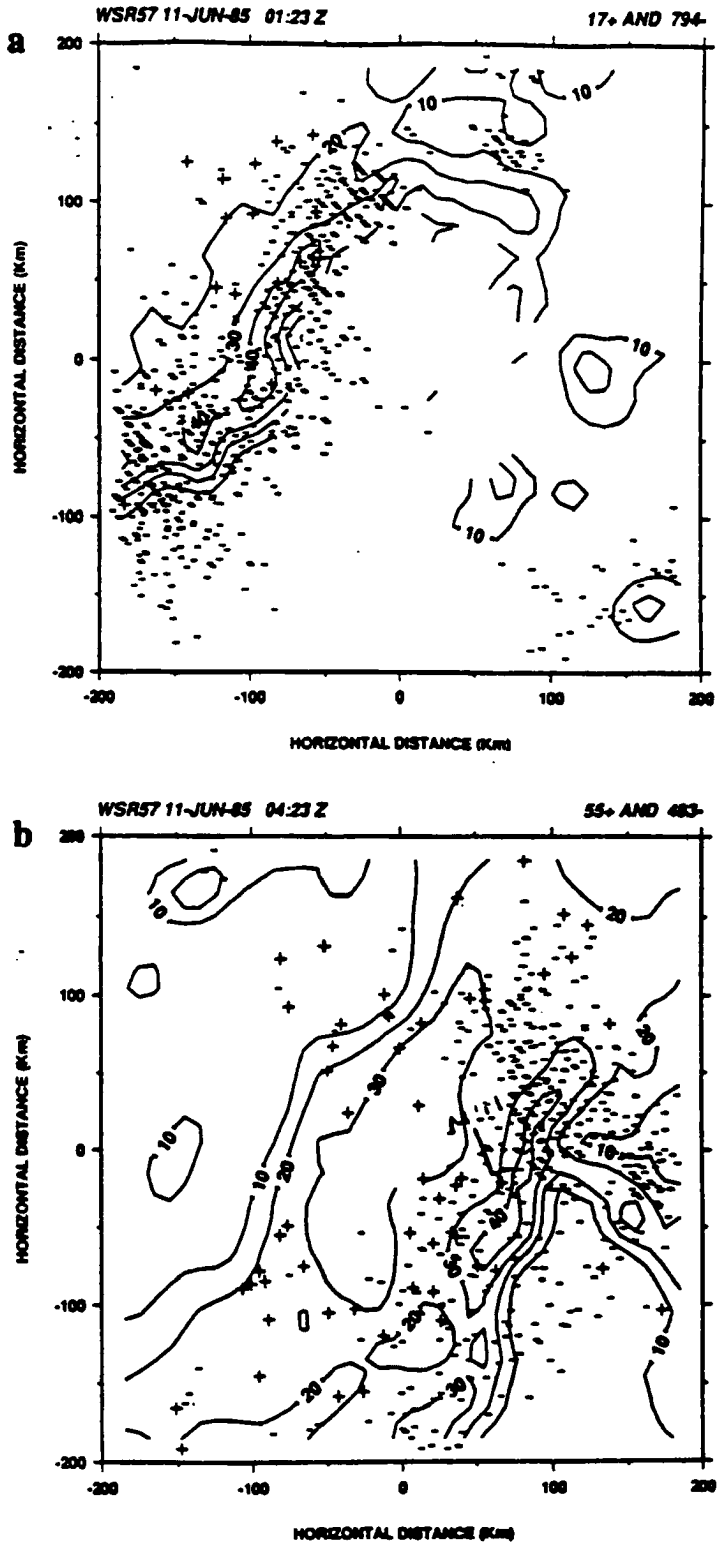


Figure 3.3 WSR-57 low level PPIs of radar reflectivity and cloud-to-ground lightning for the 10-11 June 1985 MCS at (a) 0123 UTC and (b) 0423 UTC; (adapted from Rutledge and MacGorman, 1988). The location and polarity of cloud-to-ground flashes which occurred during a 30 minute time interval centered on the time of the radar are indicated by a (+) for positive flashes and a (-) for negative flashes.

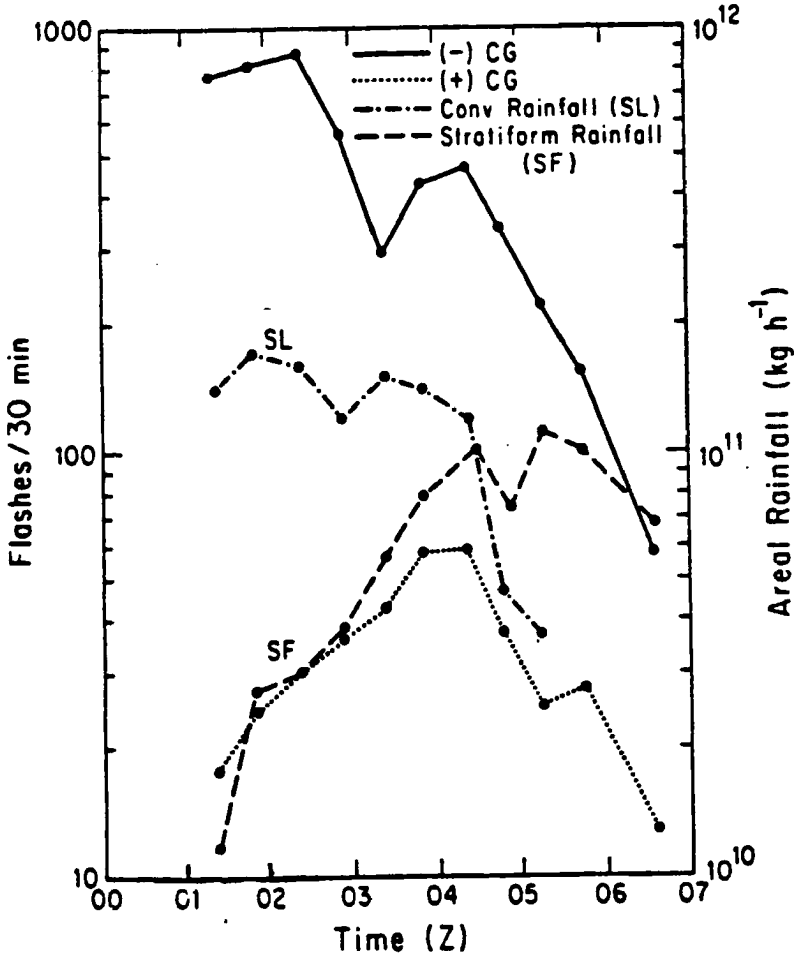


Figure 3.4 Cloud-to-ground lightning flash rates and areally integrated rainfall rates from the 10-11 June 1985 MCS from 0123-0656 UTC (adapted from Rutledge and MacGorman, 1988). Rainfall rates were computed for convective precipitation (—•—•—) and stratiform precipitation (——). Negative flashes/ 30 minutes area indicated by a solid line (—), positive flashes/30 minutes by the dotted line (• • •).

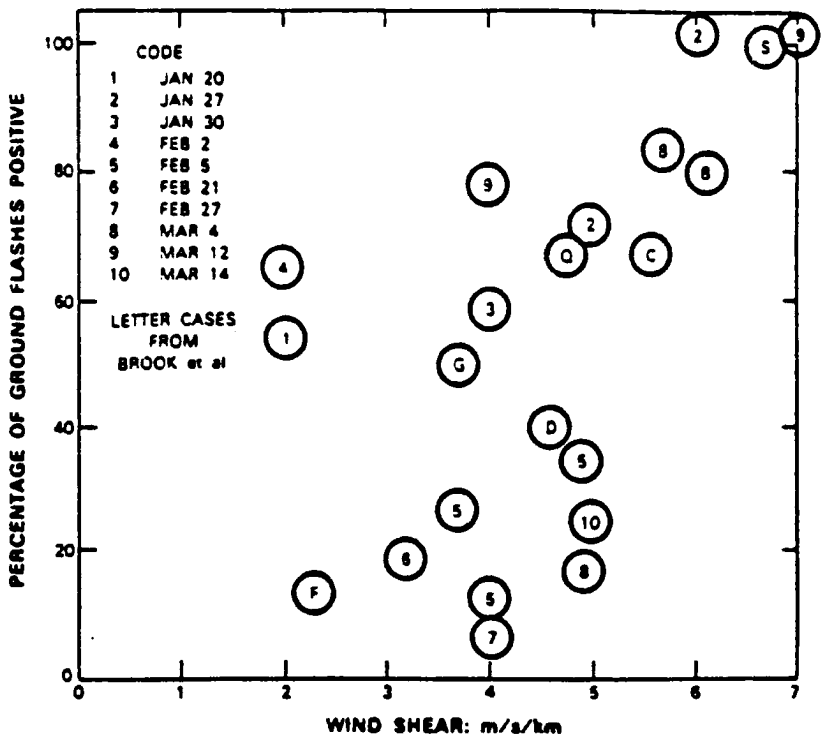


Figure 3.5 Vertical wind shear vs. the percentage of positive CGs that occurred in 10 winter season MCSs (numbered) [adapted from Engholm et al. 1990]. Lettered cases from Brook et al. (1982).

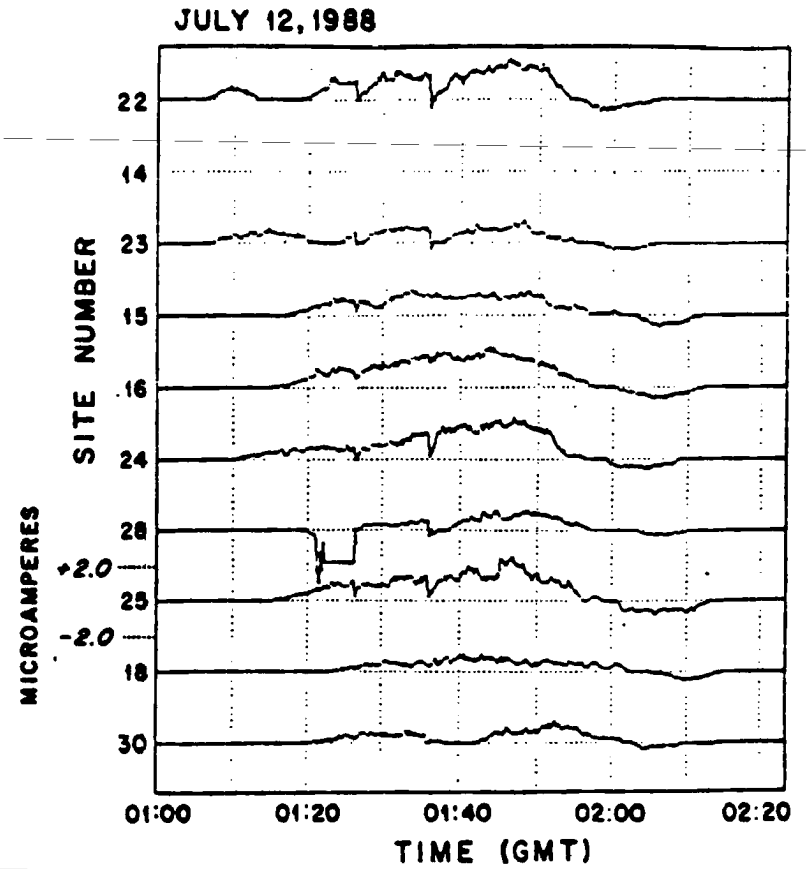


Figure 3.6 Surface based corona point measurements from the 12 July 1988 MCS stratiform region (adapted from Engholm et al. 1990). Positive values of current (μA) indicate negative charge overhead, negative values indicate positive charge overhead.

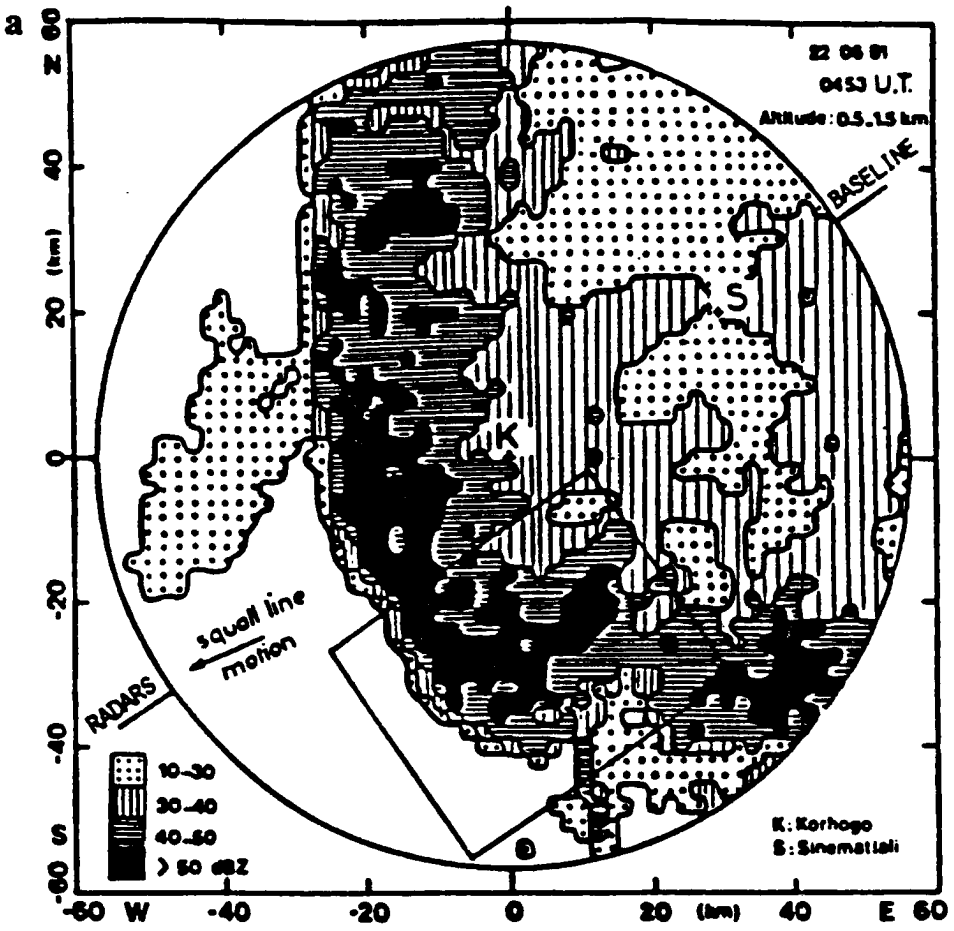


Figure 3.7 (a). Horizontal radar reflectivity contours at the 0.5-1.5 km levels from the Korhogo radar (COPT-81), 22 June 1981 (adapted from Chauzy et al. 1985). The rectangle represents an area of dual Doppler coverage.

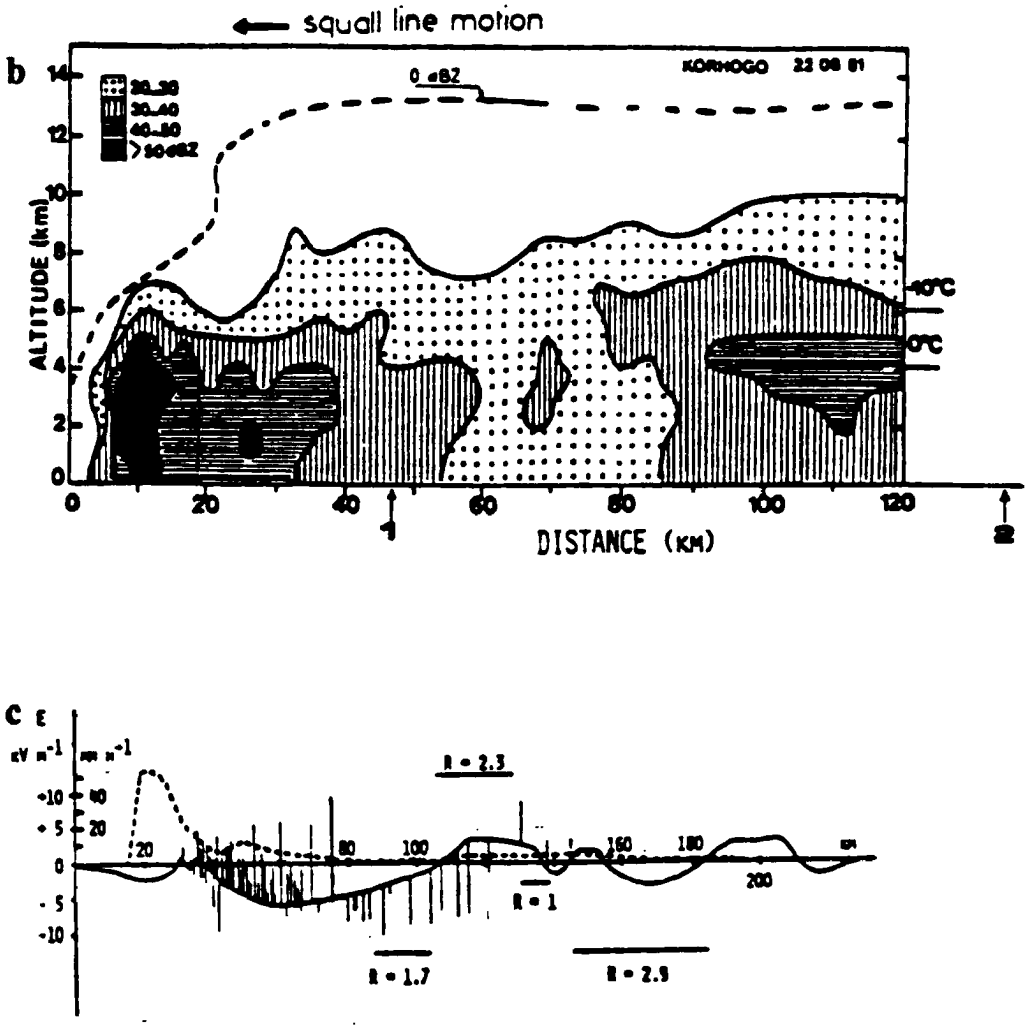


Figure 3.7. (b) Vertical cross-section of radar reflectivity normal to the direction of propagation for the 22 June 1981 MCS; (c) corresponding average vertical electric field including field steps due to lightning, rainfall rates, and ratio of raindrop polarity [above (below) horizontal axis indicates positive (negative) charged drops most frequent].

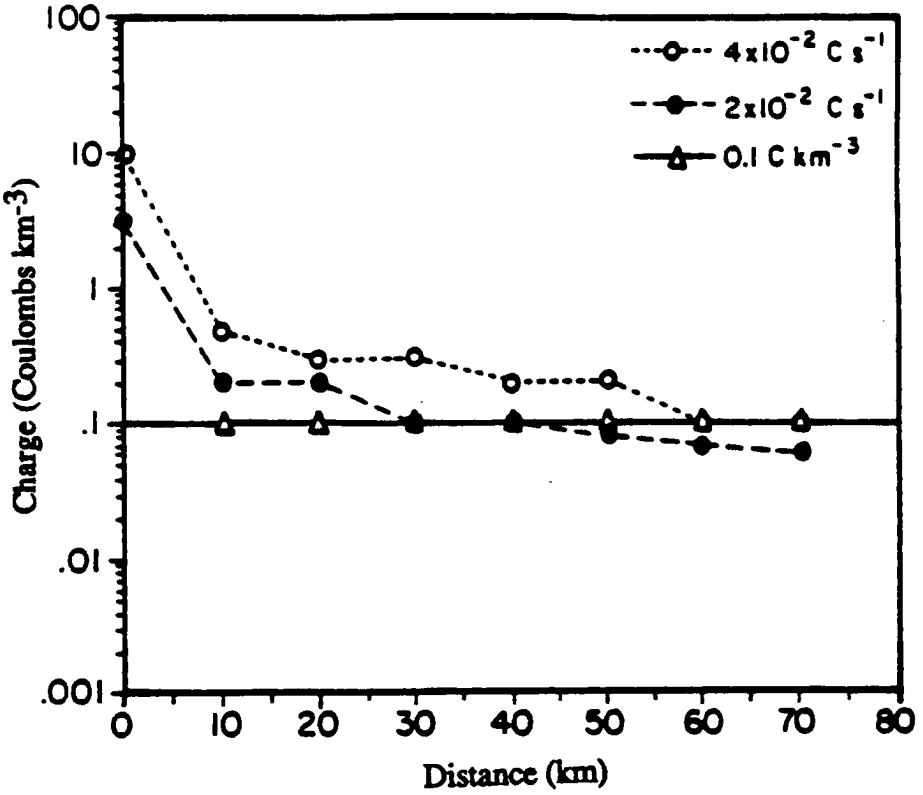


Figure 3.8 Space charge density (C $km^{-3}$) vs. advection distance behind the convective line (see text for explanations; adapted from Rutledge et al. 1992b).

# CHAPTER 4

## AN OVERVIEW OF THE MCSs STUDIED AND ANALYSIS METHOD

In this chapter we review the specific MCS cases examined in this thesis and the method of analysis. First, we present a short description of each MCS chosen for study. Next, we describe the Doppler radar data, wind profiler data, upper-air soundings, lightning data, and electric field data used for analyzing each case along with the method of analysis. We also discuss the development of a simple one-dimensional model used to assess the probability of supercooled liquid water in several of the stratiform regions studied herein.

### 4.1 The MCSs selected for study

Seven MCSs and associated cloud-to-ground lightning are studied in detail in this thesis. Of the seven MCSs examined, six are continental break period storms and one is a monsoon period storm. All of the MCSs studied were characterized by a well defined leading convective line with radar reflectivities of 30-55 dBZ, and a trailing stratiform region with reflectivities of $\leq$ 30 dBZ. To a good approximation, the majority of the MCSs studied herein were linear and quasi two-dimensional (ref. Fig 3.1; Houze et al. 1989). As in Rutledge et al. (1992a), the break period MCSs exhibited a higher degree of electrification (in terms of lightning flash rates) than the monsoon case. The

following is a short description of each case examined (values reported for the CAPE are from the pre-storm environment):

1) 5 December 1989; break period squall line (CAPE of 650 J $kg^{-1}$), examined for 5 hours of the lifecycle. The squall line formed approximately 60 km south of the MIT and TOGA radars and moved north at approximately 8-10 m $s^{-1}$. Peak cloud top heights of 16-17 km were observed in the convective line. As the squall line moved north over the MIT radar, it developed a broad, long-lived trailing stratiform region with cloud tops of 11-13 km. At its peak electrical intensity the squall line produced 111 CGs in a 30 minute period, 15 of which were positive.
2) 12 January 1990; monsoon squall line (CAPE 300 J $kg^{-1}$), examined for the last 2.5 hours of the lifecycle. The squall line was oriented west-southwest to east-north east and formed over the ocean approximately 50 km northwest of Darwin. The convective line had maximum cloud top heights of 11-12 km and moved toward the south-southeast at 7-9 m $s^{-1}$, leaving a large area of trailing stratiform precipitation over Darwin. Stratiform cloud tops were approximately 10 km in height. No CGs were recorded by the LLP network during the observation period.
3) 22 January 1990; break period squall line (CAPE 1100 J $kg^{-1}$), examined for 3 hours of the lifecycle. This squall line formed 50 km southeast of the MIT radar and was oriented northeast to southwest. Maximum cloud top heights were 15 km in the convective line and 12 km in the stratiform region. The squall line moved rapidly to the northeast at 12-14 m $s^{-1}$ leaving a very large region of stratiform precipitation behind. Initially, the squall line was moderately electrified producing 159 CGs in the first 30 minute period studied. However, the number of CGs rapidly decreased to just 37 in the next 30 minutes and continued to decrease for

the remainder of the storm lifecycle. Very few CGs were associated with the stratiform precipitation region.

4) 24 January 1990; break period squall line (CAPE 800 J $kg^{-1}$), examined for 3.5 hours of the lifecycle. The squall line approached the MIT radar from the east moving at approximately 13 m $s^{-1}$. Maximum cloud tops in the convective line approached 14-15 km in height and cloud tops in the stratiform were 8-10 km in height. A long, relatively narrow stratiform region, trailed the convective line and dissipated as it moved over the MIT radar. This MCS was weakly electrified, producing only 27 CGs (within the range of the MIT radar) at its peak in one 30 minute time interval. In the stratiform region four to five CGs occurred 10 km behind the convective line; three of these flashes were positive.

5) 28 January 1990; break period squall line (CAPE 2000 J $kg^{-1}$), examined for 7 hours of the lifecycle. A 270 km long squall line formed approximately 130-150 km east of the TOGA radar. The main portion of the line moved west at approximately 13 m $s^{-1}$ while the southeastern portion of the line broke off and moved west-northwest at approximately the same speed. A deep, horizontally extensive stratiform region developed behind the convective line as the MCS passed over the TOGA radar. The central and northern portions of the convective line dissipated 2-3 hours after passing over the radar, however the southeastern portion of the MCS accelerated to the west-northwest moving over the TOGA radar and then out to sea. The stratiform region persisted for at least four hours after the convective line passed over the radar. This particular MCS was highly electrified producing 300 CGs in the first 30 minute time period studied. Approximately 40 positive CGs occurred in the trailing stratiform region, particularly as the stratiform region was developing. Unfortunately the MIT radar

site had a power outage this day and no electric field or MIT radar data could be collected (Table 4.1)

6) 14 February 1990; break period squall line (CAPE 1500 J $kg^{-1}$), examined for 4 hours of the lifecycle. The squall line developed 90 km east-southeast of the MIT radar and moved west at an average speed of 14 m $s^{-1}$. Stratiform regions developed in the northeast and southeast sections of the MCS as the convective line began to split. A small portion of the convective line and northeastern stratiform region then passed over the MIT radar. However, the largest area of stratiform precipitation remained stationary at a position well south and east of the MIT and TOGA radars, dissipating approximately two hours after forming. CGs were quite numerous in the convective line during the first two hours of the storm with a peak of 206 flashes recorded in 30 minutes. As the convective line split the flash rate decreased markedly to only 45 flashes in 30 minutes. A total of seven positive CGs were observed in the broad stratiform region southeast of the MIT and TOGA radars.

7) 15 February 1990; break period squall line (CAPE 300 J $kg^{-1}$) examined for 3 hours of the lifecycle. This particular squall line was quite vigorous for approximately one hour. It developed southeast of the MIT radar and moved toward the west at approximately 12 m $s^{-1}$. A very weak, disorganized stratiform region began to develop behind the convective line but dissipated within approximately two hours of genesis. The line produced a peak of 123 CGs in 30 minutes but just one hour later the rate had dropped to only 29 flashes in 30 minutes. Only one positive CG occurred in weak stratiform precipitation, approximately 20 km behind the convective line.

In this thesis emphasis is placed on squall line numbers 1, 2, 3 and 5 since these MCSs exhibited broad, long-lived stratiform regions that moved over the MIT radar site and the electric field mill (except for 28 January 1990; see Table 4.1), which allowed in-depth study of their electrical characteristics. Squall lines 4, 6, and 7 were used primarily to supplement cloud-to-ground lightning observations, though some limited field mill data was available for cases 4 and 6 (see Table 4.1).

## 4.2 Methodology used for radar analysis

Single-Doppler radar analysis was performed on the seven case studies mentioned above. The MIT 5 cm radar (Table 4.2) provided the primary reflectivity and velocity data used in analyzing all but one of the case studies, 28 January 1990. On this date the MIT radar site experienced a power outage, hence the TOGA radar (also described in Table 4.2) was utilized. MIT radar data were used preferentially in this study since 1) the data were more readily accessible; 2) it had a smaller gate spacing (500 m) than the TOGA data (1000 m); 3) it contained volume scans spaced at regular time intervals; and 3) the majority of data volumes contained scans up to 45° elevation angles (many of the TOGA scans ended at elevation angles of 25°). In addition, CG lightning positions were centered on the position of the MIT radar and the electric field mill was located at the MIT radar site.

The radar data were viewed and edited using the Research Data Support System (RDSS) software (Mohr et al., 1986) developed by the National Center for Atmospheric Research (NCAR). RDSS was used primarily to dealias velocity data and to remove unwanted noise and ground clutter. After editing the data with RDSS, several different products were constructed from the volume scans including low level PPI's (Plan

Position Indicator), vertical slab averages (cross-sections) of reflectivity and horizontal velocity, and EVADs (Extended Velocity Azimuthal Display; Srivastava et al.1986; Matejka and Srivastava, 1991).

Low level PPIs of reflectivity data from the MIT (1.2° elevation) and TOGA radars (0.8° elevation) were interpolated to horizontal grids with resolutions of 1 and 2 km respectively. The reflectivity value plotted at each grid point represented a smoothed average of the reflectivity values at surrounding gates in the elevation cone. The low-level PPIs were centered on the respective radars with horizontal ranges of 113 km for the MIT radar (range limited by signal processing constraints) and approximately 160 km for the TOGA radar. Vertical cross-sections of reflectivity and horizontal velocity were constructed using software described in Rasmussen and Rutledge (1992). The vertical cross-sections are very similar to RHI's and were constructed along a line perpendicular to each squall line. Cross-sections were specified to be 10 km in width. The vertical reflectivity and velocity profiles were both corrected for storm advection that took place during the volume scan. The vertical slab average technique (Rasmussen and Rutledge, 1992) is very versatile since it allows for slicing through a storm at different azimuths to view the vertical reflectivity structure. For horizontal velocities, the slab average technique was used only to make line-normal slices through the storm assuming a quazi two-dimensional structure to the MCS (Rasmussen and Rutledge, 1992). For this study, the vertical slab averaging technique worked well since the majority of the cases examined were approximately 2-D in structure.

As in previous studies (e.g., Rutledge and MacGorman, 1988; Rutledge et al. 1990), PPI's of reflectivity were used to identify the stratiform (reflectivity $\leq$ 30 dBZ and wide-spread echoes) and convective (reflectivity > 30 dBZ) components of each

MCS. Vertical cross-sections of reflectivity were used to identify the depth of each MCS and to identify the height of the 15 - 25 dBZ reflectivity region in the stratiform regions relative to the height of the 0°C and -10°C isotherms. The height of the 15-25 dBZ reflectivity region is used to evaluate the presence and depth of a mixed phase region, using the microphysical observations of Houze and Churchill (1984). In addition, reflectivity values supplied by the vertical cross-sections were used as input to a one-dimensional model of water vapor flux in which ice particle concentrations were a function of stratiform reflectivity (Houze and Churchill, 1984). Line-normal vertical cross-sections of horizontal velocity were used to calculate the vertical shear of the horizontal wind from 700-400 mb and 450-280 mb (7-10 km) in four of the break period stratiform regions studied herein. The vertical shear was then correlated to the number of positive CGs and the total number of CGs (positives and negatives) observed in each respective stratiform region.

When possible (Table 4.1), radar volume scans were used to generate EVADs (see Matejka and Srivastava, 1991) in order to gain estimates of the mean vertical velocity profile in the stratiform regions studied. EVADs yield estimates of the mean vertical velocity in layers of stratiform clouds at specified levels of a cylinder centered on the radar. The vertical velocities are generated by invoking mass continuity after divergence of the horizontal wind is calculated at each level in the cylinder. Cylinder radii in the EVADs were set at 20-40 km and layers were 0.5 - 1 km thick (depending on the particular gate spacing of the radar data). The top of the EVAD cylinder was located at the radar echo top as indicated by the VAD (Velocity Azimuth Display) "Cone Profiles" software which is used prior to applying the EVAD technique. As in Matejka and Srivastava (1991), the vertical velocities at the top and bottom of the EVAD cylinders were assumed to be zero. Virtual temperature profiles and densities were input

from the 0000 UTC radiosonde observations taken at Darwin. EVADs were only attempted when assumptions of continuous reflectivity and smooth variation of the radial velocity over the radar were valid (i.e., when only stratiform cloud completely covered the radar; Matejka and Srivastava, 1991). Unfortunately the assumptions made in generating vertical velocities from the EVAD technique were not always met in the cases studied herein. Therefore, the primary method used to determine vertical velocities in the stratiform regions was analysis of vertically pointing wind profiler data.

## 4.3 Profiler data analysis

The primary source of vertical velocity data for the MCS stratiform regions examined herein was the NOAA 50 MHz vertically pointing wind profiler located approximately 5 km east of the TOGA radar (Fig. 2.3). The profiler recorded samples of vertical velocity every 100 s, at 500 m height intervals from 1.5 km to approximately 20 km in the vertical (e.g., Fig. 4.1). To obtain estimates of the vertical velocity, raw spectral data were plotted by a computer. Vertical velocities were then estimated to the nearest 0.1 - 0.2 m $s^{-1}$ by subjectively identifying the peak in the clear-air turbulence power spectra and the corresponding vertical velocity. This subjective method for determining vertical velocity is presently considered to be as accurate as any computer algorithm developed for determining the vertical velocity of the *air* when there are *multiple, coincident* peaks (i.e., from air, rain and snow) in the Doppler spectra present (personal communication, Dr. Tony Riddle, NOAA Aeronomy Research Laboratory).

## 4.4 Use of sounding data

As mentioned in Chapter 2, upper-air soundings were taken at several different locations in the Darwin area. Unfortunately, many of the soundings taken at the Koolpinyah site (where the MIT radar was located) terminated shortly after entering cloud in the stratiform regions. Therefore, sounding data collected by the BMRC in Darwin was used for this study. The sounding data was used primarily to determine the CAPE, the height of the 0°C and -10°C isotherms, and to provide temperature and specific humidity input for a simple one-dimensional model of water vapor flux.

## 4.5 Use of radar, profiler and sounding data in a simple one-dimensional model

In lieu of in-situ microphysical measurements, a simple one-dimensional model was developed to assess the possible existence of small amounts of supercooled cloud liquid water (and hence a mixed phase region) between the 0°C and -20°C levels in the stratiform regions. The model essentially represents continuity of water vapor as measured by the saturated specific humidity ($q_S$) in a water saturated environment. The model is based on the following equations:

$$\partial q_s / \partial t + U \cdot \nabla q_s = S \tag{4.1}$$

$$\frac{dM}{dt} = \sum n \frac{dm}{dt} \tag{4.2}$$

$$\frac{dm}{dt} = \frac{4\pi C (S_{ice} - 1)}{[R_V T_\infty / e_{si} D_V] + (L_S / kT_\infty)[L_S / R_V T_\infty - 1]} \tag{4.3}$$

The variables and constants used in equation (4.3) are the following:

C = ice crystal capacitance, (formulae in Rogers, 1979)

$e_{si}$ = ambient equilibrium vapor pressure over ice (Pa)

$e_{sw}$ = ambient equilibrium vapor pressure over water (Pa)

$D_V$= diffusivity of water vapor: ($m^2\ s^{-1}$):

$$D_V = 2.11 \times 10^{-4} [T_\infty/273.15]^{1.94}[1013.25/P]$$

P= pressure (mb)

k= thermal conductivity of air (0.023 J $s^{-1}$ $K^{-1}$)

$L_S$= latent heat of sublimation ($2.84 \times 10^6$ J $kg^{-1}$)

$R_V$= ideal gas constant for moist air (461 J $kg^{-1}K^{-1}$)

$SS_{ice} = e_{sw}/e_{si}$

$T_\infty$= temperature of the environment (K)

Equation (4.1) represents the continuity of saturated specific humidity (units of kg $m^{-3}$) with a source-sink term (S). Equation (4.2) is the *total* deposition rate (units of kg $m^{-3}$ $s^{-1}$) for all strengths of stratiform precipitation (strong, weak and very weak; Houze and Churchill, 1984), particle types, and number concentrations in the vertical column. The right side of (4.2) is a summation over the product of the number concentrations (n) in units of $m^{-3}$, and individual depositional growth rates (dm/dt) in units of kg $s^{-1}$ for ice crystals of a particular size and shape found in each type of stratiform precipitation. Equation (4.3) is the depositional growth equation for a single ice crystal.

The following assumptions were made for the modelling study:

1) Horizontal homogeneity;

2) Steady-state saturated specific humidity;

3) Water saturated environment (no evaporation);

4) Water vapor was either deposited on ice surfaces (depositional growth) or condensed into liquid water (i.e., S= condensation + deposition).

With these assumptions, equation (4.1) reduces to:

$$w\partial q_s / \partial z = C + D \qquad (4.4)$$

Where C= condensation rate in g $m^{-3}$ $s^{-1}$, and D= total deposition rate (dM/dt) in g $m^{-3}$ $s^{-1}$. Thus the condensation rate can be estimated by subtracting the total deposition rate (calculated in eq. 4.2) from the vertical flux of water vapor in (4.4).

Data for variables used in the equations were taken from the vertical cross-sections of reflectivity, profiler data and upper-air sounding data. Stratiform region ice concentrations (for the tropics) were parameterized using the results of Houze and Churchill (1984). Total ice particle number concentrations were set at 30 $L^{-1}$, 10 $L^{-1}$, and 2 $L^{-1}$ for strong (≥ 20 dBZ), weak (5 - 20 dBZ) and very weak (0 - 5 dBZ) stratiform precipitation respectively. The vertical velocity at each level (w) was estimated from profiler data. Temperature was taken from upper-air soundings in the vicinity of the stratiform regions being examined. Saturation vapor pressures over ice and water were calculated from temperatures using a form of the Magnus equation (Murray, 1967; Elliot and Gaffen, 1991). The variable $q_S$ was then calculated from the equilibrium vapor pressure over water and converted to units of g $m^{-3}$ using a standard tropical density profile. Outputs at 500 m intervals between the 4.5 - 9 km height levels consisted of the steady state vertical vapor flux (g $m^{-3}$ $s^{-1}$), the total deposition rate (g $m^{-3}$ $s^{-1}$), and the condensation rate (g $m^{-3}$ $s^{-1}$). To test the sensitivity of the model,

updraft speeds and particle concentrations were adjusted and the subsequent effect on the condensation rate was noted.

## 4.6 Analysis of atmospheric electricity observations

Cloud-to-ground lightning associated with the DUNDEE MCSs were detected by a four station, high gain DF network (described in Chapter 2). By using radar data concomitantly with lightning location network data, CG flash positions, polarities, and peak currents could be correlated with the various stages of evolution of tropical MCSs. The electric field mill located at the MIT radar site was used to detect total lightning and to identify the sign (positive or negative) of charge in clouds overhead. Used exclusively, the LLP sensors provided raw data for the computation of basic statistics such as the mean peak current (independent of polarity) in the first return stroke, the median positive and negative peak currents, maximum and minimum peak currents, flash rates and polarity percentages.

### 4.6.1 Statistical analysis of CG flash data

Statistics describing the peak current means, medians, maxima, and minima were calculated for each MCS. In addition to the peak current statistics, polarity percentages (percentage of positive and negative CGs) and CG flash rates were also computed. To enable comparisons to be made with other studies (e.g., Orville et al. 1987; Orville, 1990), the above calculations were performed on a total of 5000 CGs associated with MCSs examined in the process of completing this thesis.

4.6.2 CG polarity and peak current analysis

Several tropical MCSs and their associated ground flash patterns were examined for relationships between peak current magnitude and position of occurrence relative to MCS radar reflectivity patterns. The radar reflectivity data in turn allowed identification of convective and stratiform precipitation regions within the MCS. The position, polarity and numbers of ground flashes were overlaid on PPI's of reflectivity for each time period examined. The CGs thus plotted represent flashes occurring over a 30 minute time interval centered on the time of the radar data.

The magnetic field strength associated with the first return stroke of each flash observed during the DUNDEE was converted to peak current in kiloamps (kA) by using an appropriate range normalization factor (supplied by LLP software). This thesis also revisits LLP data from a seven station network of DFs as used in the central United States during PRE-STORM. In PRE-STORM the magnitude of the ground flash current was also recorded as a dimensionless measure of the magnetic field strength associated with the first return stroke of the flash, but was range normalized to a 100 km distance from each DF. This dimensionless unit is commonly called an "LLP" unit and can be converted to peak current (in kiloamps, kA) by using the conversion formula from Orville, (1991):

$$I(kA) = 0.19(LLP) + 2.3 \qquad (4.5)$$

where $I(kA)$ is the peak current in kiloamps, and $LLP$ is the range normalized signal strength in LLP units. Eq. (4.5) is strictly valid for peak currents less than 60 kA; however, by assuming a linear dependence of peak current on signal strength (e.g.,

Brook et al. 1989; Orville, 1991), Eq. (1) can be used to arrive at *estimates* for peak currents greater than 60 kA. This type of conversion will be used for our analysis of ground flash peak currents associated with the 3-4 June and 10-11 June 1985 PRE-STORM cases. The relationship between ground flash locations and radar reflectivity patterns in the 3-4 June case and the 10-11 June case have been previously studied by Rutledge et al. (1990) and Rutledge and MacGorman (1988) respectively.

To classify CG peak current extrema relative to position within the DUNDEE and PRE-STORM MCSs (specifically to the position of convective and stratiform components of the MCS), the peak current maximums and minimums were placed into one of two categories: flash position within 10 km of the convective line, or flash position >10 km from the convective line and within stratiform precipitation. In addition to classifying the positive peak current extrema relative to position, when possible the positive peak current maxima were also classified relative to the growth stage of the stratiform regions associated with several of the MCSs examined. The positive maximum peak current-stratiform growth stage classification was attempted primarily for linear MCSs characterized as having large, long-lived stratiform regions and relatively large numbers of positive CGs (10-11 June 1985, 5 December 1989, 28 January 1990, 14 February 1990 cases).

### 4.6.3 Electric field mill data

The electric field mill was located at the MIT radar site. When available (Table 4.1), the electric field mill data were used to infer the sign of charge in clouds overhead, to detect the onset of electrification in nearby clouds, and to detect the presence of both in-cloud and cloud-to-ground lighting. Electric field data were routed to a strip chart

recorder and indicated fair or foul weather electric fields and lightning (Fig. 4.2). Two outputs were recorded by the field mill strip charts (e.g., Fig. 4.2). In Fig. 4.2 the trace characterized by large deviations across the center-line represents the most sensitive measure of the ambient electric field. If moderate electric fields were present nearby or directly overhead, the trace would go off scale. Short, amplified deviations in the sensitive trace indicate rapid changes in the electric field due to lightning. The other trace, located approximately in the center of the chart, is a low gain (less sensitive) output from the field mill that only deviated appreciably from the center of the chart when moderate electric fields were overhead. The field mill data from the strip charts were digitized to yield output in units of kV $m^{-1}$ with a positive value indicating negative charge overhead and a negative value indicating positive charge overhead.

The above analysis methods and their application to several MCSs observed during the DUNDEE will be presented in the following chapter. Radar, profiler, upper-air soundings, electric field data, and a simple 1-D model will be combined to provide an in-depth study of the cloud-to-ground lightning associated with the trailing stratiform regions of tropical MCSs.

**Table 4.1: MCS case studies and data analysis type.**

| Date | Radar | Profiler | Evad | LLP | E-Field | Raob. | Model |
|---|---|---|---|---|---|---|---|
| 12/5/89 | X | X | X | X | X | X | X |
| 1/12/90 | X | X | X | X | X | X | X |
| 1/22/90 | X | X | X | X | X | X | X |
| 1/24/90 | X | X | | X | * | X | |
| 1/28/90 | X | X | X | X | | X | X |
| 2/14/90 | X | | | X | * | X | |
| 2/15/90 | X | | | X | | X | |

* Limited data

**Table 4.2:** Characteristics of the MIT and TOGA radars used in the DUNDEE (adapted from Rutledge et al. 1992a).

| Characteristic | MIT | TOGA |
|---|---|---|
| Wavelength (cm) | 5.4 | 5.3 |
| Peak power (kW) | 250 | 250 |
| Pulse length (μs) | 1.0 | 0.5, 1.9 |
| Beamwidth (°) | 1.4 | 1.65 |
| Minimum detectable signal (dBm) | -106 | -113 |
| Pulse repetition frequency ($s^{-1}$) | 921 | 921 |
| Number of gates | 226 | 224 |
| Polarization | Horizontal | Horizontal |

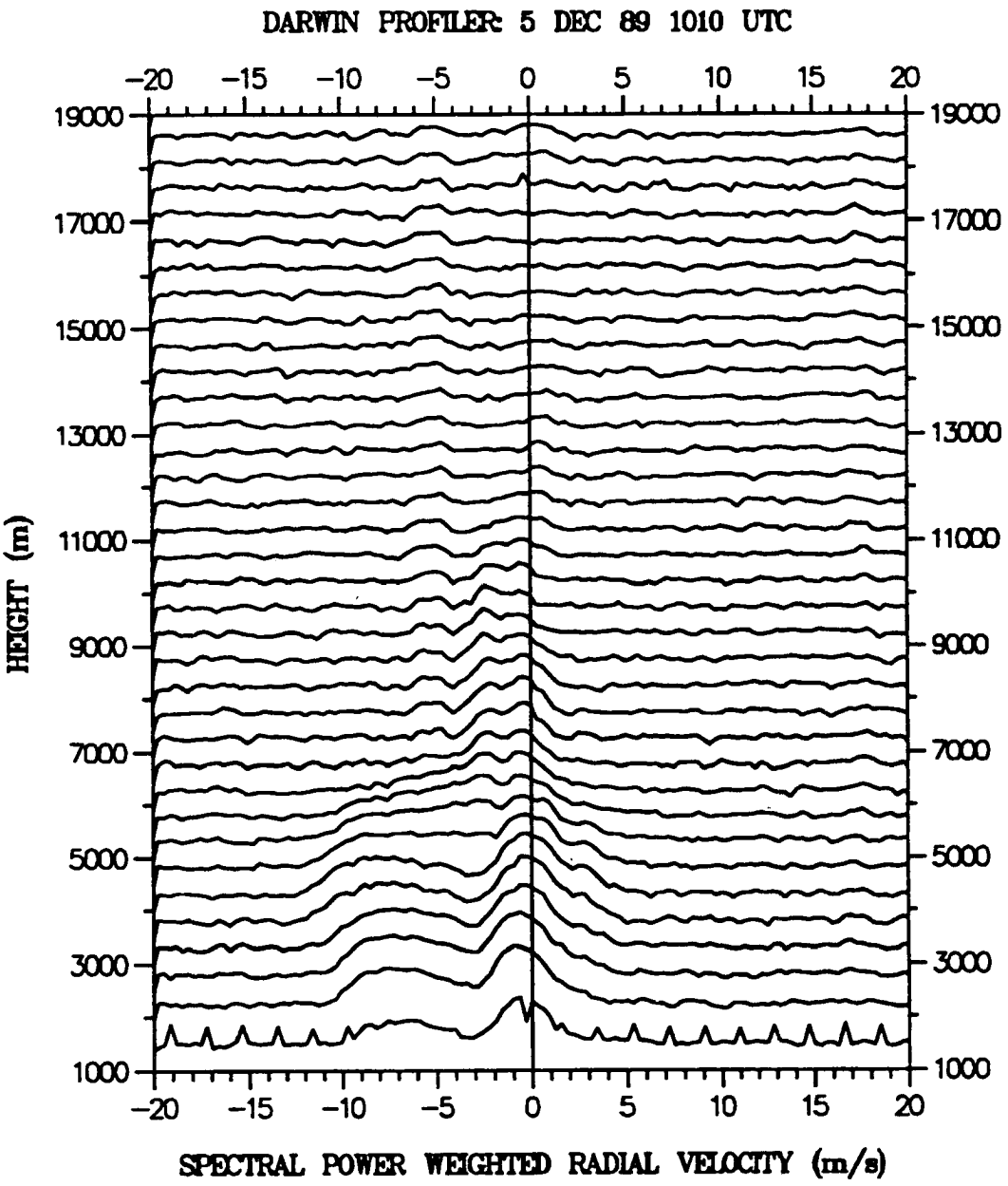


Figure 4.1 Example of vertical velocity spectra as measured by the Darwin wind profiler at 1010 UTC, 5 December 1989. Note that precipitation peaks in the spectra are located between -6 to -9 m s $^{-1}$ and -1 to -2 m s $^{-1}$. Clear-air (turbulent) spectra are located between -1 and +1 m s $^{-1}$.

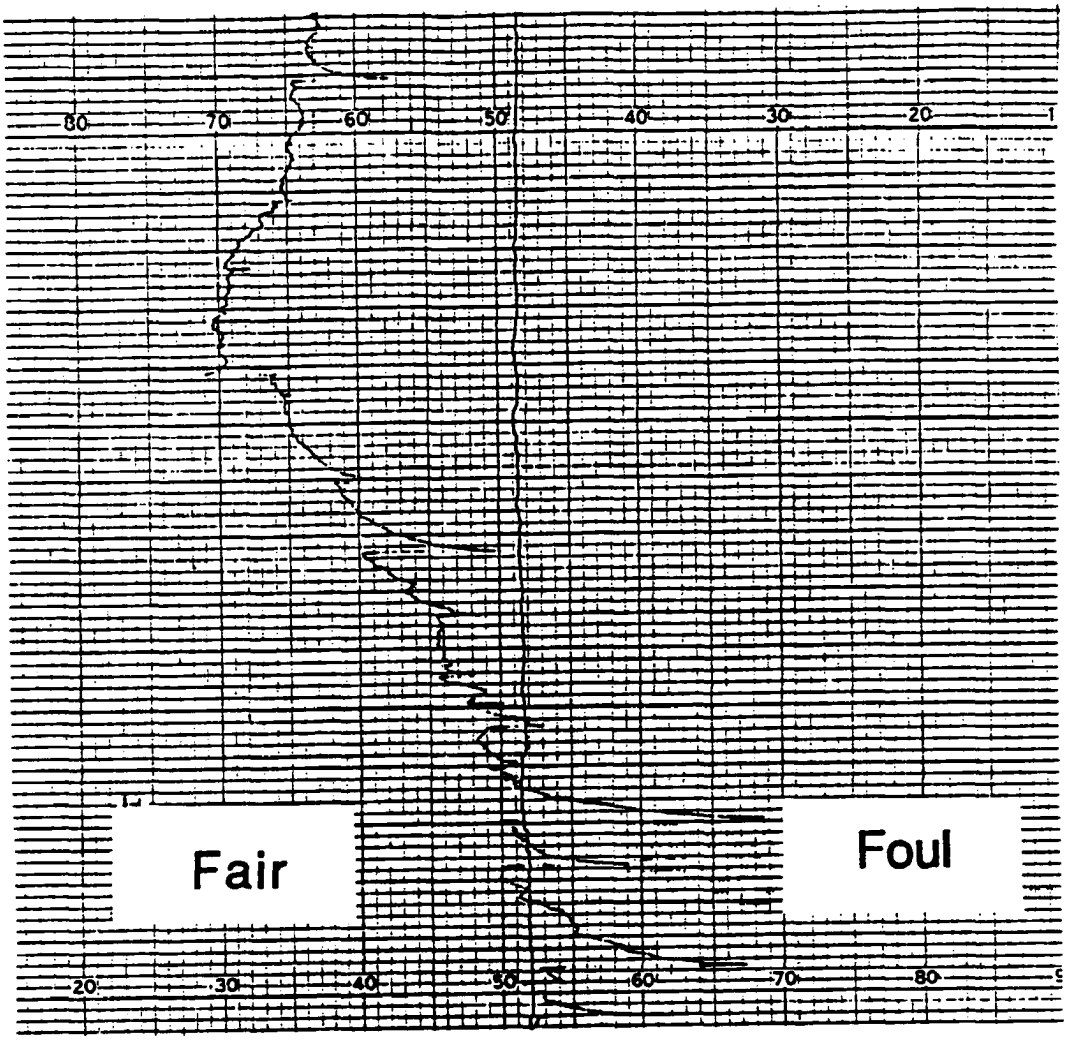


Figure 4.2 Example of electric field data recorded from 1230-1245 UTC on 14 February 1990 at the MIT radar site. "Fair" values indicated positive charge overhead, "Foul" values indicate negative charge overhead.

# CHAPTER 5

## CASE STUDY ANALYSIS

Herein, the analysis of seven DUNDEE MCSs (see Chapter 4) is presented. The first section of the chapter is comprised of radar and electrical analyses of the seven MCSs. We then present vertical velocity data for four of the MCS stratiform regions. Following the vertical motion section, we present the results of a simple one-dimensional modelling study to test for the presence of supercooled water in the stratiform regions. Modelling and vertical motion results are then discussed relative to the electrification of break and monsoon period stratiform regions. Next, in order to evaluate the potential for a charge advection mechanism in four of the break period stratiform regions studied, the number of positive cloud-to-ground flashes observed in each respective stratiform region is correlated to the 700-400 mb and 450-280mb (approximately 7-10 km) vertical shear of the horizontal wind (storm-relative). We then examine the peak currents associated with positive cloud-to-ground lightning relative to their location and time of occurrence in several stratiform regions observed during the DUNDEE and in two middle-latitude MCSs observed during PRE-STORM. The results of the above analyses are offered in support of an in-situ, non-inductive charging mechanism in the trailing stratiform regions of tropical MCSs.

## 5.1. Radar and electrical analysis of seven DUNDEE MCSs

In this section the horizontal and vertical structure of seven MCSs together with LLP cloud-to-ground lightning data and electric field mill data when available (see Table 4.1) are analyzed. Recall from Chapter 4 that all figures showing vertical cross-sections of radar reflectivity and horizontal velocity (storm relative), were constructed along a line-normal radial 10 km in width that contained the radar (unless otherwise noted). The horizontal coordinate system in the vertical cross sections is oriented such that positive distances coincide with the direction of squall line movement. Thus squall lines will always appear to move left to right in the vertical sections. Several vertical cross-sections of reflectivity contain arrows (x's) along the horizontal axis to indicate the approximate surface position of a positive (negative) cloud-to-ground lightning flash as determined by the LLP network.

Radar reflectivity PPI's (lowest elevation scans) are centered on the MIT radar (with the exception of the 28 January 1990 case which is centered on the TOGA radar) located at (0,0). The plots also denote the position of the wind profiler (designated by an open circle) located to the west (east) of the MIT (TOGA) radar (also see Fig. 2.3). The locations of cloud-to-ground flashes that occurred in a 30 minute time interval centered on the time of the radar scan are overlaid on the radar reflectivity plots. Positive CGs are indicated by a (+), negative CGs with a (-). In several of the PPI figures the positive peak current extrema (kA) are identified. We will conduct the analysis for each MCS separately beginning with those that occurred during the break period.

5.1.1.a 5 December 1989

On 5 December 1989, a vigorous squall line developed south of the MIT radar at 0740 UTC (Fig. 5.1). The convective line had cloud tops of 16 km and peak reflectivities within the convective line of 45-60 dBZ that extended nearly 7 km in the vertical. One hour later at 0840 UTC (Figs 5.2a, 5.3a, 5.4a) the squall line (Fig. 5.3a) had broadened considerably (Fig. 5.2a) and was located over the MIT radar site. The convective line remained intense with cloud tops near 16-17 km and reflectivities of 25-35 dBZ extending above the 7 km level (Fig. 5.3a). The LLP network detected a total of 111 CGs during this time period. Almost all of the 96 negative CGs and 11 of the 15 positive CGs were associated with convective line. However, four of the positive CGs (including the positive peak current maxima of 108 kA) were located near what appeared to be only patchy stratiform precipitation, 60 - 80 km southwest of the radar. However, a low level surveillance scan taken by the TOGA radar indicated that stratiform precipitation was more widespread 60-80 km southwest of the MIT radar. Apparently the low-level scan taken at the MIT radar was attenuated by heavier precipitation located at the radar (Fig. 5.2a). The stratiform precipitation that developed southwest of the MIT radar at 0840 UTC is more readily observed in the PPI made from the time period at 0910 (Fig. 5.2b).

At 0910 UTC (Figs. 5.2b, 5.3b, 5.4b) the convective line was located just north of the MIT radar and seemed less organized. A broad stratiform region had developed south through west of the radar. Ninety CGs were detected during this 30 minute time period with a total of 9 positive flashes recorded. The majority of the negative CGs appear to have been associated with the convective line. Positions calculated by the LLP network for the cluster of negative CGs (and some of the postive CGs) located just

behind the convective line (Fig. 5.2b) may be subject to error since those CGs occurred near the baseline of the two DFs that were operational on this date (position errors are greatest along the baseline since triangulation is not possible). Six positive flashes occurred near the convective line and only two to three positives occurred in stratiform precipitation. Note that the maximum positive peak current (123 kA) was associated with a positive CG that occurred approximately 80 km southwest of the radar in stratiform precipitation, while the minimum positive peak current (10 kA) occurred near the convective line (Fig. 5.2b).

Vertical cross-sections of horizontal velocity and reflectivity at 0910 UTC (Figs. 5.3b and 5.4b) indicate that the leading convective line was still quite erect, however peak reflectivities in the line decreased to only 25-35 dBZ. As indicated by cross sections of the horizontal velocity (Fig. 5.4b), a very weak rear-inflow existed below the 0°C level. A moderate front-to-rear flow existed (9-12 m $s^{-1}$) and the 700-400 mb shear had was approximately 2.0 x $10^{-3}$ $s^{-1}$.

At 0940 UTC (Figs. 5.2c, 5.3c, 5.4c), the convective line continued to weaken as it moved north. Conversely, the stratiform region continued to broaden and began to develop in the southeastern section of the MCS. Only 37 CGs were detected by the LLP network during this time period. The CG lightning pattern at 0940 UTC was bipolar since the majority of the positive CGs were located to the rear of the convective line or in stratiform precipitation away from the negative CGs. Both the maximum (72 kA) and minimum (16 kA) positive peak currents were located near the convective line.

The vertical reflectivity structure normal to the convective line at 0940 (Fig. 5.3c) was characterized by a decrease in low level reflectivity in the convective line with

peak reflectivities of 25-35 dBZ confined to elevations well below the 0°C level. This may have been related to a decrease in mixed phase processes in the convective line associated with a general weakening of the convection (and hence electrical charging; e.g., Takahashi, 1978; Jayaratne et al. 1983), thus explaining the substantial decrease in cloud-to-ground lightning observed during this time period. A very weak low level rear-inflow still existed in the MCS (Fig. 5.4c) and the front-to-rear flow strengthened slightly to peak values of 12 m $s^{-1}$. The 700-400 mb shear increased to a value of 2.7 x $10^{-3}$ $s^{-1}$.

By 1010 UTC (Figs. 5.2d, 5.3d, 5.4d) the convective line resembled a disorganized line of discrete convective cells, but the stratiform region still continued to grow and intensify south and southeast of the radar. Forty two CGs were detected by the LLP network during this time period (40 negatives, 2 positives). The CG pattern during this time period was bipolar, however only two positive CGs (peak currents of 54 kA and 40 kA) were detected in stratiform precipitation. Therefore, the term "bipolar" can only be loosely applied at this time.

The vertical cross-section of reflectivity for 1010 UTC (Fig 5.3d) showed that a deep region of 15-25 dBZ reflectivity values existed above the -10°C level approximately 30 km south of the radar where the stratiform region was still developing. Also shown in Fig. 5.3d is an arrow indicating the position of the positive CG (54 kA) that occurred 25-30 km south of the MIT radar and in the domain of the vertical slab. This particular positive CG was located under the area of 15-25 dBZ reflectivity that extended above -10°C level. Fig. 5.4d indicates that this location may have been associated with speed convergence in the mid-levels (Fig. 5.4d). Thus a local enhancement in the vertical motion field may have been responsible for this positive CG

if non-inductive charging were taking place (assuming the CGs originated in the stratiform cloud). The magnitude of the shear remained constant at a value of approximately 2.7 x $10^{-3}$ $s^{-1}$.

The final time period examined for the 5 December 1989 MCS was at 1110 UTC (Figs. 5.2e, 5.3e, 5.4e). The convective line now consisted of just two cells located approximately 60 km north of the radar. All of the 45 negative CGs and 1 positive CG recorded during this time period were associated with these two cells. The areal coverage and intensity of the trailing stratiform precipitation had decreased slightly during this time period but remained over the radar for another one to two hours prior to dissipating completely. The LLP network recorded no additional CGs in the stratiform precipitation for the remainder of the stratiform region's lifetime.

It is important to note that the positive CGs detected by the LLP network in the stratiform region of the 5 December 1989 MCS seemed to occur in areas where reflectivities of 15-25 dBZ extended well above the elevation of the 0°C level (4.7 km). For example, at 0910 UTC (Fig. 5.5a; radial azimuth 210°) the single positive CG that occurred some 80 km southwest of the radar was located in a region of stratiform precipitation where 15-25 dBZ reflectivities extended well above the 0°C level. The current associated with this flash was 123 kA. Note that a negative CG also occurred near the same area at 0910 UTC (designated by the "x" in Fig. 5.5a). Positive CGs in the stratiform regions at 0940 UTC (Fig. 5.5b; radial azimuth 140°) and at 1010 UTC (Figs 5.3d and 5.5c; radial azimuth 205°) also occurred in regions where the area of 15-25 dBZ reflectivities extended well above the 0 °C level.

5.1.1.b Electric field observations for 5 December 1989

Fig. 5.6 shows the vertical electric field measured by the electric field mill (kV $m^{-1}$) as a function of time. Lightning flashes are indicated by rapid fluctuations in the trace. Positive values of the electric field indicate negative charge overhead (foul weather field), negative values indicate positive charge overhead (fair weather field). The field mill registered no significant deviation in the vertical electric field until approximately 0810 UTC when the squall line approached the radar. As the convective line moved over the radar near 0830 UTC, the field mill detected a strong foul weather field (negative charge overhead) with peak values of the electric field at the surface approaching 6-8 kV $m^{-1}$. The field remained foul until approximately 0950 UTC when it abruptly reversed indicating positive charge overhead. Note that the reversal to positive charge overhead occurred nearly coincident with the time that stratiform precipitation moved over the radar (see Fig. 5.2c). Positive charge remained over the radar until approximately 1110 UTC when the field again reversed to positive values (negative charge overhead). By 1140 UTC the magnitude of the electric field returned to a value near the zero (actually the fair weather value of approximately 100 V $m^{-1}$).

The negative charge overhead detected by the field mill in the convective line is most likely related to the strong lower negative charge region often observed in thunderstorm electrical dipoles (e.g., Krehbiel, 1986; Williams, 1989). The strong negative electric field (8-10 kV $m^{-1}$) located at the leading edge of the stratiform region (indicating positive charge overhead) may indicate the presence of an inverted dipole (Rutledge et al. 1990, 1991). The field reversal to positive values (negative charge overhead) from 1110 - 1140 UTC may have been an end of storm oscillation (EOSO) (Krehbiel, 1986). An alternative explanation for the positive field reversal at 1110 UTC

might be the local tilting of an inverted dipole by the storm relative winds, with positive charge underlying negative charge (e.g., Engholm et al. 1990).

In summary, the 5 December 1989 MCS was characterized as having a vigorous convective line that was trailed by a broad area of stratiform precipitation. A moderate number of negative CGs were associated primarily with the convective line, while positive CGs were associated with both the convective line and the stratiform region. There was an apparent preference for CGs that occurred in the stratiform region to be positive, though a few negative CGs also occurred in stratiform precipitation. Bipolar lightning patterns were discernable at 0940 and 1010 UTC (Figs. 5.2c, d). The electric field record (Fig. 5.6) indicated negative charge overhead as the convective line passed over the field mill which is consistent with previous observations of lower negative charge regions in thunderstorms (e.g., Krehbiel, 1986; Williams, 1989). As the stratiform region moved overhead, the electric field reversed to indicate positive charge overhead, indicating the possible presence of an inverted dipole (e.g., Rutledge et al. 1990, 1991).

5.1.2.a 22 January 1990

On 22 January 1990, a squall line developed 30 km southeast of the MIT radar and moved toward the northwest at a speed of approximately 12 m $s^{-1}$. At 1023 UTC (Figs. 5.7a, 5.8a, 5.9a) the convective line exhibited cloud tops of 14 km with reflectivities of 25-35 dBZ extending well above the 0°C level (Fig. 5.8a). To the rear of the convective line, finger like regions of stratiform precipitation were developing coincidentally with a rear-inflow jet of 6 m $s^{-1}$ at low levels (< 4 km) and a strong front to rear flow of 15 m $s^{-1}$ aloft (Fig. 5.9a). A total of 159 CGs were recorded in the 30

minute period centered on 1023 UTC (Fig. 5.9a). Three of the CGs were positive and were associated with the northeastern portion of the convective line over the Van Diemen Gulf. All of the negative CGs were associated with the convective line.

By 1100 UTC the convective line had moved over the radar and was beginning to dissipate (Figs. 5.7b, 5.8b, 5.9b). The stratiform region continued to broaden and intensify behind the convective line (Fig. 5.7b). A broadening of the storm relative flow structure with the development of the stratiform region is indicated by Fig. 5.9b. It should be noted that the shear in the 700-400 mb layer stayed virtually constant throughout the time periods studied at a relatively high value of $4.1 \times 10^{-3}$ $s^{-1}$.

Cloud-to-ground lightning activity decreased significantly during the time period centered on 1100 UTC, with the LLP network detecting only 37 CGs. This may have been due to the rapid decrease in the area of strong reflectivities (i.e., > 25 dBZ) observed above the 0°C isotherm indicating a weakening in the mixed phase region (Fig. 5.8b). One positive and one negative CG appear to have been associated with the developing stratiform region in the southern portion of the MCS. However, it is also possible that the these CGs were a result of the decaying convection on the southern end of the convective line. It is interesting to note the cluster of positive CGs which were located in isolated convection on the far northeastern edge of the convective line. It is not clear why the CGs associated with this isolated convection would be *only* positive in polarity.

At 1140 UTC (Figs. 5.7c, 5.8c, 5.9c) the stratiform region had broadened considerably and was approaching its mature state (Fig. 5.7c). A bright band began to develop near the 4 km level (Fig. 5.8c) and the 15-25 dBZ reflectivity region was

situated just above the 0°C level in a region of strong vertical shear of the horizontal wind (Figs. 5.8c, 5.9c). During this time period cloud-to-ground lightning activity was virtually non-existent in the convective line (2 positives, 1 negative). Two of the six positive CGs located northeast of the radar appeared to be associated with the stratiform region (Fig. 5.7c). The positive peak current extrema (i.e., associated only with the MCS being studied) both occurred in the stratiform region and were 45 and 114 kA respectively (Fig. 5.7c).

Near 1200 UTC (Figs. 5.7d, 5.8d, 5.9d) the convective line began to separate from the stratiform region (Fig. 5.7d) as it moved northwest and out over the ocean (see Fig. 2.3). Almost no lightning was associated with the convective line and reflectivities > 25 dBZ were confined to elevations with temperatures ≥ 0°C (Fig. 5.8d). Only one negative CG and one positive CG (the positive peak current maximum of 82 kA) were associated with the convective line while several positive CGs appeared to be associated with stratiform precipitation over the ocean. However, only one positive CG (the peak current minimum, 40 kA) appears to have been associated with the stratiform region of the MCS being examined here. The stratiform region at 1200 UTC increased in areal extent (Fig. 5.7d) as the front-to-rear flow became more uniform at 15-18 m $s^{-1}$ (Fig. 5.9d). In addition to expanding in the horizontal, the stratiform region also intensified vertically as indicated by the height of the 15-25 dBZ reflectivity contour in Fig. 5.8d.

In the last time period examined (1300 UTC; Figs. 5.7e, 5.8e, 5.9e) the convective line had moved out of range of the radar and all of the CGs detected by the LLP network (10 negatives) were associated with discrete cells in the convective line (Fig. 5.7e). No CGs were detected by the LLP network in stratiform precipitation during this or any later time periods. For future discussion note in Fig. 5.8e that the 15-

25 dBZ reflectivity region was still located above the 0°C level over the radar, but that an area of heavier precipitation (and increased elevation of the 15-25 dBZ region) that formed over the radar between 1200 and 1300 UTC had moved just to the right (northwest) of the radar.

5.1.2.b Electric field observations for 22 January 1990

The electric field data for the 22 January 1990 case is shown in Fig. 5.10. Similar to the 5 December 1989 case (and consistent with observations made in other studies; e.g., Krehbiel, 1986), the electric field showed a departure to positive values (indicating negative charge overhead) as the convective line moved over the radar at 1120 UTC (PPI not shown). The electric field remained positive (500-700 V $m^{-1}$) until approximately 1200 UTC at which time it reversed to indicate weak positive charge overhead. Recall that a region of stronger stratiform precipitation developed over the radar between 1200 UTC and 1300 UTC (Figs. 5.8d-e) as indicated by the height of the 15-25 dBZ reflectivity region. Therefore, the transition to weak positive charge overhead near 1200 UTC may have been related to slightly enhanced vertical development of the stratiform region over the radar (Figs. 5.8d-e). Consequently, the reversal to negative charge overhead at 1235 UTC may have been associated with the local tilting of an inverted dipole (as opposed to an end of storm oscillation).

The change to positive charge overhead at 1200 UTC may also have been due to the local tilting of an upper positive charge region in the dissipating convective line (i.e., tilted rearward by the storm relative shear). Tilting of a dipole seems plausible since the convective line was only 25-30 km to the northwest of the radar and the value of the storm relative 700-400 mb shear was relatively high at 4.1 x $10^{-3}$ $s^{-1}$ (Brook et al.

1982). The change back to negative charge overhead at 1235 UTC would then be presumably due to an EOSO (end of storm oscillation).

It is possible that the electric field mill was not located in the most vertically extensive portion of the stratiform region. Figs. 5.11a-b show vertical cross-sections of reflectivity made along an azimuth of 250° at 1200 and 1230 UTC (positive distances in the direction of 250°). The cross-sections show vertical reflectivities that existed along a line containing the positive CG which occurred at 1207 UTC approximately 60 km to the east-northeast of the radar (Fig. 5.7d). Note in Figs. 5.11a-b the vertical extent of the 15-25 dBZ contour to the right (northeast) of the radar and the position of the CG (as indicated by the arrow in Fig. 5.11a).

Reflectivities of 15-25 dBZ at 1200 UTC (Fig 5.11a) were located at approximately the level of the 0°C isotherm, but by 1230 UTC (Fig. 5.11b) there was some vertical development in the stratiform region in the area where the positive CG occurred at 1200 UTC. Given that the positive flash was located under this region, it is possible that a greater degree of charging occurred near this section of the stratiform region after 1200 UTC and that the field mill detected only the weaker trailing edge of the charge. Recall that the peak magnitudes of the electric field on 22 January 1990 were generally weak (i.e., $< 1$ kV $m^{-1}$) at the MIT radar site. When compared to the 5 December 1989 case, (which produced approximately 7 positive CGs in the stratiform region), these values are smaller by a factor of eight. Note also that the 5 December 1989 stratiform region exhibited a deeper region of 15-25 dBZ reflectivities above the 0°C level.

In summary, the 22 January 1990 MCS began its lifecycle as an intense squall. Frequent cloud-to-ground lightning accompanied this intense stage as 159 CGs were recorded in one 30 minute period. However, the number of CGs decreased rapidly as the line propagated over the radar, dissipated, and developed a large region of stratiform precipitation with a relatively high 700-400 mb shear ($4.1 \times 10^{-3}$ $s^{-1}$; Figs. 5.9 a-e). Approximately three positive CGs were associated with the stratiform region. At least one of these positive CGs occurred near an area where 15-25 dBZ reflectivities extended above the 0 °C level (Figs. 5.11a-b). With the exception of the northeastern portion of the stratiform region, 15-25 dBZ reflectivities remained at or below the 0 °C level, indicating a rather weak stratiform cloud. This may be the reason so few positive CGs occurred in the stratiform region of 22 January 1990.

The electric field data (Fig. 5.10) exhibited weak negative charge overhead as the convective line passed over the radar, and then a switch to weak positive charge overhead as stratiform precipitation moved over the radar. There is some indication that larger amounts of charge may have been located in stratiform precipitation to the northeast of the radar where the stratiform region appeared to be more vigorous (as indicated by the height of 15-25 dBZ reflectivity region in Figs. 5.11a-b) and positive CGs occurred.

5.1.3.a 24 January 1990

On 24 January 1990 a weakly electrified squall line formed approximately 80-100 km east of the MIT radar. The squall line moved westward at a speed of 13 m $s^{-1}$. By 0800 UTC (Fig. 5.12a, 5.13a, 5.14a) the MCS was located approximately 60 km east of the radar with radar echo tops in the convective line of 12 km (Fig. 5.13a). The

LLP network detected 21 CGs during this time period, but only eight of the flashes were associated with the squall line. Of the eight flashes associated with the squall line at 0800 UTC, three were positive and located approximately 10 km to the rear of the convective line. At 0830 UTC (not shown), two negative CGs were detected by the LLP network approximately 20 km behind the convective line.

By 0900 UTC (Figs. 5.12b, 5.13b, 5.14b) the shallow convective line (followed by a relatively narrow stratiform region) was located just 5 km east of the radar (Fig. 5.12b). An area of rear-inflow began to form at low levels behind the convective line (Fig. 5.14b) producing a 700-400 mb shear of $2.7 \times 10^{-3}$ $s^{-1}$. Only 28 negative CGs were recorded by the LLP network with approximately 10 of them being associated with the southeastern portion of the convective line. The other flashes were associated with isolated convection to the southeast of the radar. No CGs occurred in the shallow stratiform precipitation (Fig. 5.13b).

At 1000 UTC the squall line was 30 km to the west of the radar (Fig. 5.12c). The convective line seemed to intensify somewhat as the leading edge became more vertical (Fig. 5.13c). The squall line exhibited a weak rear-inflow ($\leq 3$ m $s^{-1}$) and the 700-400 mb shear increased from $2.7 \times 10^{-3}$ $s^{-1}$ (0900 UTC) to $3.4 \times 10^{-3}$ $s^{-1}$ (Fig. 5.14c). The LLP network registered a total of 18 CGs in this time period, eleven of which appeared to be associated with the convective line. No CGs were associated with the stratiform region.

At 1035 UTC the squall line moved out over the ocean and accelerated away from the patchy, dissipating stratiform region (Fig. 5.12d). Interestingly, the small patch of stratiform precipitation left over the radar at 1035 UTC had a small region of

15-25 dBZ reflectivities located well above the 0°C level (Fig. 5.13d). However, as in the previous time period no CGs were detected in the stratiform region.

The low number of CGs associated with this squall line may have been a consequence of the relatively weak intensity of the MCS. Note in Figs. 5.13 a-d that 25-35 dBZ reflectivities in the convective line did not extend substantially above the 0°C level until 1035 UTC (Fig.5.13d), which was just prior to when the convective line dissipated. A similar situation existed in the stratiform region. At 1035 UTC the 15-25 dBZ reflectivity region finally extended well above the 0°C level over a horizontal distance of approximately 30 km, but this area rapidly dissipated as did the remainder of the stratiform precipitation and no cloud-to-ground lightning was detected.

5.1.3.b Electric Field observations for 24 January 1990

Prior to 1000 UTC the electric field data (non-digitized, 1020-1100 UTC; Fig. 5.15) were somewhat limited for this case due to chart recorder problems. From 1000-1030 UTC the field mill indicated negative charge overhead at the MIT radar site. Interestingly, a swing to dominant positive charge overhead took place for 15 minutes at 1030 UTC. Recall that it was near 1035 UTC (Fig. 5.13d) when the 15-25 dBZ reflectivity region extended above the 0°C isotherm in the stratiform region over the radar. Later, at 1045 UTC, the field again reversed indicating negative charge overhead for approximately 15 minutes. Since the convective line was located nearly 60 km west of the detached stratiform region, it seems possible that some in-situ charging briefly occurred in the small patch of stratiform precipitation that was located over the radar.

To summarize, the 24 January 1990 squall line was a shallow, weakly electrified MCS. The convective line never produced more than 11 CGs in any one 30 minute period. This is attributed to the lack of a deep mixed phase region as indicated by weak reflectivities above the 0°C isotherm (e.g., Williams, 1989; Engholm et al. 1990; Rutledge et al. 1992a). Three positive CGs occurred in stratiform precipitation but were located only 10 km behind the convective line. For the remainder of the time periods examined, no CGs were detected in the stratiform region and with the exception of 1035 UTC, the region of 15-25 dBZ reflectivities did not extend above the 0°C level. The electric field data indicated that some weak charging may have taken place in the stratiform region. Positive charge was located over the radar in stratiform precipitation at 1030 UTC, near the time that 15-25 dBZ reflectivity region extended into the 0°C to -10°C temperature regions. The electric field then reversed to indicate negative charge overhead at 1045 UTC.

### 5.1.4 28 January 1990

The 28 January 1990 MCS was perhaps the most intense squall line observed during the 1989-1990 DUNDEE observational phase. It was characterized by a very deep convective line (radar echo tops near 20 km), a very broad long-lived stratiform region, and large numbers of cloud-to-ground flashes. As mentioned in Chapter 4, the MIT radar unfortunaly experienced a power outage (and generator failure) on this date, so no radar or electric field data were available from the MIT site. Therefore, the analysis of the 28 January 1990 MCS is restricted to the examination of TOGA radar data and the LLP network data.

The 28 January 1990 MCS began as an intense 240-300 km line of convection situated to the east of the TOGA radar. At 1132 UTC (Fig. 5.16) the line was located approximately 50-70 km east of the TOGA radar. Cloud tops in the line were 18-20 km in height, and a region of 35-45 dBZ reflectivities extended to nearly 10 km (near the -35°C level). The LLP network recorded 300 CGs during the 30 minute period centered on 1132 UTC. Of these CGs, 291 were negative and located at scattered locations around the convective line (Fig. 5.16). There were a total of nine positive CGs with the majority located to the rear of the most intense convection (Fig. 5.16). Some negative CGs associated with a distant portion of the MCS were located to the southeast, beyond the effective range of radar coverage.

By 1306 UTC (Figs. 5.17a, 5.18a, 5.19a) the central and northern portion of the convective line had weakened considerably (Fig. 5.17a). Convection in the southeastern portion of the MCS continued to intensify at 1306 UTC and produced a large number of CGs (Fig. 5.17a). A total of 60 positive flashes were detected by the LLP network, approximately 12 of which were located along developing fingers of stratiform precipitation behind the convective line (note the position of the positive peak current maxima in Fig. 5.17a). Several negative CGs were also located along the same projections, though in much smaller numbers. The projections of weaker precipitation behind the convective line contained small regions of enhanced reflectivity (Fig. 5.18a; azimuth 078°) located 60-120 km behind the convective line. The enhanced reflectivities in turn were located in close proximity to the positions of several positive and negative CGs (positive CGs shown by arrows, negative CGs by "x" in Fig. 5.18a). These enhancements in weaker reflectivity may have been associated convective scale circulations embedded in the developing stratiform precipitation.

After 1306 UTC there was an 80 minute gap in the TOGA radar volume scans. However two surveillance scans taken at 1331 UTC and 1358 UTC (not shown) indicated the development of a broad region of stratiform precipitation by 1426 UTC. The growth of this stratiform region appeared to take place along the finger-like projections of weaker reflectivity observed at 1306 UTC (Fig. 5.17a).

The TOGA radar volume scan taken at 1426 UTC (Figs. 5.17b, 5.18b, 5.19b) showed that a very large stratiform region had developed behind the original convective line, which dissipated between 1306 and 1426 UTC (Fig. 5.17b). In addition to the large stratiform region, an area of intense convection located in the southeastern portion of the MCS moved northeast to a location 60-80 km south of the radar. This area of convection is believed to be associated with patchy convection that developed earlier in the extreme southeastern portion of the convective line. Heavier precipitation associated with dissipating convection was located over and northwest of the radar. The heavier precipitation approximately 80 km northeast of the radar appeared to be stratiform in nature (from inspection of radar data), though it may have ultimately resulted from weak dissipating convection that was present in the 1331 UTC surveillance scan.

A total of 271 CGs were recorded during the 1426 UTC time period, 30 of which were positive. The majority of the 241 negative CGs detected by the LLP network were associated with strong convection south of the radar, though 5 negative CGs were also located near what appeared to be heavy stratiform precipitation situated approximately 80 km northeast of the radar. As in the 5 December 1989 case, only two DFs were operational on 28 January 1990. Many of the negative flashes located 80-100 km southeast of the TOGA radar (associated with strong convection in that area) occurred very close to the DF baseline. Therefore, it is assumed that the majority of the

negative flashes that extended in a linear fashion behind the convection in the southeast, were actually associated with the convective line located 60-70 km south-southeast of the radar. Note that a bipolar pattern in the cloud-to-ground flashes is evident to the south of the radar, and to a lesser extent, east of the radar. Approximately 15 of the 30 positive CGs that occurred during this time period were associated with stratiform precipitation. The positive peak current maxima (84 kA) was associated with stratiform precipitation and the positive peak current minima (15 kA) was located near convective precipitation (Fig. 5.17b).

Vertical cross sections of the reflectivity (Fig. 5.18b) and horizontal velocity (5.19b) indicate that a very deep stratiform region existed at 1426 UTC. In the vertical cross section of velocity (Fig. 5.19b) there did not appear to be a well organized velocity structure in the stratiform region (e.g., Fig. 3.1) and the 700-400 mb shear was relatively low ($1.4 \times 10^{-3}$ $s^{-1}$). There were however areas of convergence between 30-60 km and at 90 km, which may have provided enhanced upward motion in those areas of the stratiform region. Note that the 15-25 dBZ reflectivity region was elevated to the -10°C contour over relatively large distance. Also, the positive CGs which occurred approximately 80 km due east of the radar were located under an area associated with 1) elevated 15-25 dBZ reflectivities (Fig. 5.18b), and 2) enhanced convergence in the mid-levels (Fig. 5.19b).

At 1445 UTC (Figs. 5.17c, 5.18c, 5.19c) there was virtually no change in the horizontal or vertical structure of the MCS. However, the number of CG's detected decreased substantially to only 107 flashes (12 positive CGs). As in the time periond centered on 1426 UTC, negative CGs were located near the DF baseline southeast of the radar and are assumed to be associated with the convective line 40-60 km south of the

radar. Two of the 12 positive flashes indicated in Fig. 5.17c (one in heavier precipitation just northwest of the radar and another in stratiform precipitation 80 km southeast of the radar) were also plotted in Fig. 5.17b due to overlapping 30 minute time intervals. The overall decrease in the total number of CGs recorded during this time period was most likely due to a decrease in the cloud-to-ground lightning associated with the convective line south of the radar. However a bipolar CG pattern still existed, with approximately 6 of the 12 positive CGs detected being located in stratiform precipitation. During this time period, the positive peak current maximum (64 kA) was located in a region of heavier precipitation which may have been associated with dissipating convection, though cross-sections of reflectivity through this region (not shown) indicated a stratified structure. The peak current minimum (20 kA) was located on the edge of stratiform precipitation.

By 1545 UTC (Figs. 5.17d, 5.18d, 5.19d) the stratiform region had weakened slightly as it moved west of the radar. Active convection southwest of the radar and dissipating convection (part of the convective line located south of the radar at 1445 UTC) west of the radar, produced the majority of the 157 CGs detected by the LLP network (Fig. 5.17d). Seven positive CGs were located well south of the radar. Four of the seven positive CGs were located in stratiform precipitation thus producing an approximate bipolar CG pattern. The positive peak current maxima (103 kA) was located in stratiform precipitation, and the minima (27 kA) was located in convective precipitation (Fig. 5.17d).

The vertical cross sections from 1545 UTC (Figs. 5.18d, 5.19d) identify the convection that existed west of the radar and the dissipating stratiform region located east of the radar. The region containing 15-25 dBZ reflectivities in Fig. 5.18d was still

located above the -10°C contour over the radar, but descended rapidly to the 0°C level in the eastern portion of the stratiform region. In the horizontal velocity cross-section, a weak rear-inflow jet developed near the 0°C isotherm and the shear in the 700-400 mb layer was approximately 1.4 x $10^{-3}$ $s^{-1}$. Note that rear-inflow developed well after the stratiform region had reached its peak intensity near 1426-1445 UTC, and that its position coincided with an area of eroded radar echo (Fig. 5.18d). Therefore, the developing rear-inflow may have ultimately been associated with the dissipation of the stratiform region.

At 1645 UTC, the last time period examined (Figs. 5.17e, 5.18e, 5.19e), a disorganized convective line and associated cloud-to-ground lightning were oriented northwest to southeast at a distance of 100-140 km from the radar (Fig. 5.17e). All of the 83 CGs that occurred during this time period were associated with the convective line. The stratiform region continued to dissipate (Figs. 5.17e) and moved to the west. A small portion of the 15-25 dBZ reflectivity region (a remnant of earlier convection at 1545) still existed above the 0°C level to the west of the radar (Fig. 5.18e). Reflectivities ≥ 30 dBZ that existed over the radar at 1645 UTC in Fig. 5.17e were actually due to ground clutter and heavier stratiform precipitation.

The 28 January 1990 MCS was the most electrified squall line of the 7 MCSs examined in this thesis. The initial convective line produced 300 CG flashes in just 30 minutes. The convective line became disorganized by 1306 UTC (Fig. 5.17a) with stronger convection located to the southeast of the radar. This convection produced numerous CGs and moved rapidly east-northeast with the rest of the decaying convective line. A very broad stratiform region developed behind the convective line and produced approximately 40-50 positive CGs during the storm lifecycle.

It was noted that stratiform precipitation appeared to develop at 1306 UTC behind the convective line from finger-like projections of weaker precipitation that contained embedded convective circulations at (Figs. 5.17a, 5.18a). Many positive CGs associated with this time period (and a few negative CGs) were located along these projections in close proximity to areas of enhanced elevation of the 15-25 dBZ reflectivity region (Fig. 5.18a). During the time periods from 1426-1445 UTC (Figs. 5.17b-c) the stratiform region was horizontally extensive and deep with reflectivities of 15-25 dBZ located near the -10°C isotherm over its entire width (Figs. 5.18b-c). Approximately 25 positive CGs were associated with stratiform precipitation during the 1426-1445 UTC time period and were arranged in somewhat of a bipolar pattern with respect to the negative CGs located in the convective line. Several of the 26 positive CGs were located in a region of enhanced precipitation and mid-level convergence (e.g., Figs. 5.18b, 5.18c) in the stratiform region.

Positive CGs located in stratiform precipitation decreased in number at 1545 UTC (Fig. 5.17d) to a total of four, all of which were located approximately 40 km behind convection southwest of the radar. Vertical cross-sections of reflectivity at 1545 UTC (Fig. 5.18d) indicated that the stratiform region east of the radar had decreased in intensity and depth (note the decreased region of 15-25 dBZ reflectivities above the 0°C level). A relatively weak rear-inflow jet was also observed to form near this time (Fig. 5.19d). One hour later at 1645 UTC (Fig. 5.17e), the stratiform region was dissipating and moved west of the radar. The only cloud-to-ground lightning detected during the 30 minute time period centered on 1645 UTC was associated with disorganized convection along the leading edge of the MCS.

The large number of positive CGs (relative to MCS cases previously examined in this Chapter) and the elevated height of the 15-25 dBZ reflectivity region observed in this particular stratiform region, may indicate the presence of a stronger mixed phase region. Based on the locations of positive CGs relative to precipitation enhancements and local middle-level convergence (as shown in several of the vertical cross sections), it is possible that non-inductive charging in the stratiform region may have taken place on the convective scale, or that the stratiform region consisted of isolated, enhanced pockets of charge associated with variations in microphysics or dynamics.

### 5.1.5 14 February 1990

The 14 February 1990 MCS provides a good example of the bipolar cloud-to-ground lightning pattern that is often associated with MCSs (e.g., Orville et al. 1987, Rutledge and MacGorman 1988). The MCS formed south of the MIT radar and only a small decaying portion of the convective line moved over the radar. Hence we present only reflectivity and lightning data for several of the time periods studied (no electric field data are presented). Bipolar patterns were prevalent in the cloud-to-ground lightning detected by the LLP network.

An example of the bipolar lightning patterns observed on 14 February 1990 is shown in a low-level sector scan taken by the MIT radar at 1110 UTC (Fig. 5.20a). A total of 87 CGs (6 positives) were detected during this time period. Four of the six positive flashes detected by the LLP network, appeared to be associated with stratiform precipitation located to the southeast of the radar, including the maximum positive peak current (66 kA). The minimum positive peak current (22 kA) was located in the convective line. Note that several negative CGs also appeared to be located in the

stratiform precipitation at 1110 UTC. Similarly, at 1140 UTC (Fig. 5.20b) the flashes were arranged in a bipolar pattern with four of the six positives detected (including the maximum positive peak current of 113 kA) being associated with stratiform precipitation southeast of the radar. The minimum positive peak current (10 kA) was associated with the northern end of the convective line. Two negative CGs were located approximately 60 km east of the radar in stratiform precipitation, however they occured coincidentaly with a dissipating convective cell which was located in the same area approximately 10 minutes earlier.

By 1210 UTC (Fig. 5.20c), the convective line in the northern portion of the MCS became a disorganized group of cells trailed by a small, dissipating region of stratiform precipitation. The convective line in the southern portion of the MCS was reduced to just one active cell and a large region of stratiform precipitation. Only 14 CGs were detected during this time period, three of which were positive. The positive peak current maxima (minima) of 68 (23) kA was located in the southern stratiform (convective) region (Fig. 5.20c). The region of reflectivities $\geq$ 30 dBZ located in the stratiform region is associated with heavier stratiform rain and persisted for approximately 30-60 minutes prior to dissipating with the rest of the stratiform region.

### 5.1.6 15 February 1990

On 15 February 1990 a short-lived squall line developed south of the MIT radar that also exhibited a bipolar CG pattern in one of seven time periods examined. The line remained south of the radar for the entire time of study, hence only reflectivity and LLP network data will be presented herein (electric field data not available). The squall line

was characterized by a strong leading convective line and a weak trailing stratiform region, which persisted for approximately one hour before dissipating.

Fig. 5.21 shows the developing MCS at 1135 UTC. The leading convective line was well organized and it appeared that small finger-like projections of stratiform precipitation were developing to the rear of the line, similar to the 22 January 1990 and 28 January 1990 cases discussed earlier. A total of 98 CGs (5 positives) were associated with the squall line during this time period and were arranged approximately in a bipolar pattern. All five of the positive flashes were located to the rear of the convective line and at least one of the five positive CGs (the positive peak current maximum; 31 kA) appeared to be associated with developing stratiform precipitation 25 km behind the convective line (though the flash was located in close proximity to the baseline of the two DFs that were operational during this time period). The squall line dissipated approximately 45 minutes later without developing a large area of stratiform precipitation, and did not produce any more positive CGs.

5.1.7.a The 12 January 1990 Monsoon MCS

Up to this point we have examined six break period MCSs. The majority of these systems (with the exception of 24 January 1990) produced relatively large numbers of CGs during some point of their lifecycle. In addition, the break period stratiform regions produced limited numbers of positive CGs. Now we examine the radar reflectivity and velocity structure of a monsoon MCS for which no cloud-to-ground lightning was detected. Electric field data is also examined in an effort to determine if any charging took place within the stratiform region of the monsoon MCS.

The 12 January 1990 MCS was one in a series of monsoonal MCSs that formed over the ocean and moved onshore over Darwin on 12 January 1990. Earlier time periods (i.e., beginning at 0730 UTC) were previously studied by Keenan and Rutledge (1992). We begin our study of the MCS at 1010 UTC (Figs. 5.22a, 5.23a, 5.24a) after the convective line and trailing stratiform region moved onshore. During this time period a bow-shaped convective line was located over and just to the east of the MIT radar. Peak reflectivities in the line, 25-35 dBZ, were confined to below the 0°C level. Trailing the convective line was a broad area of patchy stratiform precipitation that was approximately 8-10 km deep. As shown in the vertical cross section of reflectivity (Fig. 5.23a), 15-25 dBZ reflectivities covered a relatively small area and were generally located below the 0°C isotherm in the stratiform region. Vertical cross sections of the storm relative velocities indicated general mid-level flow into the back side of the system with front-to-rear flow at lower and middle levels (Fig. 5.24a).

At 1100 UTC (Figs. 5.22b, 5.23b, 5.24b) the convective line was located southeast of the radar and was trailed by an area of heavier stratiform precipitation that was located over the radar (Fig. 5.22b). Reflectivities of 15-25 dBZ extended above the height of the 0°C isotherm in heavier precipitation over the radar (Fig. 5.23b). As in the previous time period (1010 UTC; Fig. 5.24a) a deep region of rear-inflow existed at mid-levels in the stratiform region but did not appear to descend into the rear of convective line (Fig. 5.24b).

By 1200 UTC (Figs. 5.22c, 5.23c, 5.24c) the MCS was only weakly organized and beginning to dissipate. The stratiform region to the southeast of the MIT radar still contained an area of heavier precipitation that was approximately 30 km wide (Fig. 5.23c). Again, the 15-25 dBZ reflectivity region was primarily confined to levels below

the 0°C isotherm. Storm-relative rear inflow still existed at mid-levels (Fig. 5.24c) but the front-to-rear flow had decreased in intensity aloft. By 1230 UTC (not shown) the MCS had nearly dissipated entirely.

5.1.7.b Electric field observations for 12 January 1990

As noted in the discussion at the beginning of section 5.1.7.a, no cloud-to-ground lightning was observed with the 12 January 1990 MCS. However, this does not imply that the clouds were not electrified. Indeed, when high gain (sensitive) output from the electric field data was reviewed it was found that some weak charging had obviously taken place in both the convective line and the stratiform region (Fig. 5.25).

Fig. 5.25 shows the electric field record from 1000 to 1139 UTC. Note that the chart speed was 1 cm $hr^{-1}$ between the times of 1000 UTC and 1116 UTC (Fig. 5.25) and was then changed to 1 cm $min^{-1}$ at 1116 UTC. In Fig. 25 between 1000 and 1139 UTC, two distinct reversals are indicated in the electric field data. At 1000 UTC a foul weather field existed, indicating negative charge overhead. This coincides with the time that the convective line was over the radar (Fig. 5.22a). Between 1010 and 1020 UTC, the electric field reversed to indicate positive charge overhead for approximately 30 minutes. The reversal to positive charge overhead immediately behind the convective line may be due to a layer of positive charge located in the trailing anvil (i.e., a tilted dipole). Between 1050 and 1100 UTC, the electric field became foul again, indicating negative charge overhead. Recall from Fig. 5.22b that stratiform precipitation was over the MIT site at 1100 UTC. The field mill indicated that negative charge remained over the MIT site until 1200 UTC (not shown) at which time the electric field reversed to indicate very weak positive charge overhead.

It is interesting to note that the electric field over the radar indicated weak *negative charge* overhead in the stratiform region from 1100 to 1200 UTC (Fig. 5.25). This is opposite to what occurred in the 5 December 1989 and 22 January 1990 cases (Figs. 5.6 and 5.10 respectively). In the 5 December 1989 (22 January 1990) case *positive charge* was located over the radar for approximately 80 (30) minutes, coincident with stratiform cloud overhead. Also, positive CGs were observed to occur in the stratiform regions of 5 December 1989 and 22 January 1990, while no CGs were detected in the 12 January 90 stratiform region. The primary difference between the stratiform regions of 5 December 1989, 22 January 1990, and 12 January 1990, was the area of strong reflectivity observed between the 0°C and -10°C isotherm (i.e., the height of the 15-25 dBZ reflectivity region). It is therefore possible that mixed ph- microphysics (or the lack thereof) played an important role in the electrification of these stratiform regions.

## 5.2 Vertical velocities observed in four DUNDEE MCSs

In order for the non-inductive charging process to produce charge in a cloud, a mixed phase region and some process for separating regions of differing charge polarity must exist. In the stratiform region it has been hypothesized that the mesoscale updraft supplies water vapor that is condensed to produce small amounts of supercooled liquid water (e.g., Rutledge et al. 1990). Separation of the charge regions is conjectured to occur through gravitational settling of larger ice particles and the lifting of smaller ice particles in the weak mesoscale updraft (e.g., Rutledge et al. 1990). To this end, we present a short summary of observations made of the vertical velocities (as determined from the NOAA wind profiler and EVAD technique) in four of the DUNDEE MCS stratiform regions examined above.

5.2.1 Vertical velocity observations in the 5 December 1989 stratiform region

Two observations that were characteristic of the vertical velocities observed in the 5 December 1989 stratiform region are shown in Figs. 5.26a-b and 5.27a-b. Figs. 5.26a-b present wind profiler observations made at 1040 and 1111 UTC respectively and Figs. 5.27a-b are vertical velocities (determined from EVADs) for the same time periods made from MIT radar data. In Figs. 5.26a-b the peaks observed in the power spectra were due to rain (downward velocities between -6 and -9 m $s^{-1}$), snow (downward velocities of 0 to -2 m $s^{-1}$), and clear air (upward or downward velocities with magnitudes generally $\leq$ 1m $s^{-1}$). Note in Figs. 5.26a-b that all three peaks are discernable near the melting level between 4.5 km and 5 km. The EVADs in Figs. 5.27a-b represent average vertical velocities (m $s^{-1}$) at each height level for a circle (30 km in radius) centered on the MIT radar. Recall from Chapter 4 that the vertical velocities are calculated using an average divergence profile and the mass continuity equation (Matejka and Srivastava, 1991).

At 1040 UTC (Fig. 5.26a) the wind profiler detected relatively strong upward vertical velocities (unless otherwise stated the term vertical velocities will imply vertical velocity in the clear-air return) above the melting level between the elevations of 5.5 km and 8.5 km. Vertical velocities became zero to slightly negative near the 8.5-9.5 km levels and reversed to upward vertical velocities (0.2-0.3 m $s^{-1}$) between the 10-12 km levels. Upward vertical velocities were approximately 0.4-0.6 m $s^{-1}$ between the 6 km and 8 km levels, and the total updraft depth in middle-levels was approximately 3-4 km. Conversely, the EVAD vertical velocity profile for 1040 (Fig. 5.27a) does not show upward motion at any point above the melting level. Indeed the EVAD analysis shows subsidence (peak of -0.3 m $s^{-1}$) from the 10 km level to well below the melting level. It

is possible that the EVAD vertical velocity profile was affected by subsidence found in a weak transition zone behind the convective line which covered a large area of the 30 km radius EVAD cylinder. It is also possible that the upper boundary condition of w=0 at the radar echo top used in the integration of the continuity equation was improperly placed in the vertical due to the inability of the DUNDEE radars to observed the small ice crystals near cloud top.

At 1111 UTC both the profiler (Fig. 5.26b) and the EVAD technique (Fig. 5.27b) showed upward vertical velocities in the stratiform region. The profiler showed upward motions of 0.1 - 0.3 m $s^{-1}$ at levels above 7 km, while the EVAD indicated peak vertical velocities centered in a layer from 5 to 6 km. It is important to note here that the EVAD represents an average vertical velocity over a 2800 $km^2$ *area* , where as the profiler vertical velocities are a *temporal* average over approximately two minutes. Thus it would seem likely that the two measurements of vertical velocity would differ in certain circumstances. For example, at 1110 UTC the wind profiler was located further into the stratiform region than the MIT radar (see Fig. 5.2e) and hence may have been sampling a region with a deeper updraft. It is also likely that the "mesoscale" updraft in stratiform regions is far from being spatially or temporally uniform (e.g., Biggerstaff and Houze, 1991; Keenan and Rutledge, 1992). Indeed, temporal variations in the depth, location and magnitude of updraft were observed between 1040 (Fig. 5.26a) and 1111 UTC (Fig. 5.26b) in the profiler data.

The items worth noting in the vertical velocity observations for 5 December 1989 (Figs. 5.26a-b and 5.27a-b) are 1) upward motion (3-4 km in depth) was detected by the profiler in the stratiform region; 2) the vertical motion was relatively strong with peak vertical velocities of approximately 0.5-0.6 m $s^{-1}$; 3) temporal and spatial

variations existed in the depth, location and magnitude of the mesoscale updraft in the stratiform region lending further support to the suggestion that the mesoscale updraft is simply an average of convective scale circulations (e.g., Keenan and Rutledge, 1992).

5.2.2 Vertical velocity observations in the 22 January 1990 stratiform region

Figs. 5.28 and 5.29 show vertical velocity profiles somewhat characteristic of the 22 January 1990 stratiform region (observation at 1230 UTC). Note that the wind profiler data (Fig. 5.28) and the EVAD data (Fig. 5.29) approximately agree on the location and depth of the updraft in this portion of the stratiform region. At 1230 UTC the profiler indicated a deep updraft between 4.5 km and 11.5 km with peak velocities on the order of 0.4 m $s^{-1}$ (Fig. 5.28). Similarly, the EVAD analysis at 1230 UTC (Fig. 5.29) also shows that a deep updraft (4.5-11 km) existed in the area over the radar. Peak vertical velocities computed for the area covered by the EVAD analysis were approximately 0.25 m $s^{-1}$. It should be noted that the base of the updraft detected by the profiler varied with time and was located from 4.5 to 5.5 km within 10 minutes either side of 1230 UTC.

Between 1200 and 1300 UTC (when the stratiform region was over the profiler) the profiler did indicate some change in the depth and magnitude of the upward motion (i.e., pulsing) between 4.5 km and 11 km. On average, the updraft persisted until approximately 1310 UTC at which point it decreased in depth and magnitude. The EVAD analysis done at 1300 UTC (not shown) changed very little from that of 1230 UTC (Fig. 5.29). Thus it appears that a deep updraft with a peak vertical velocity of 0.4 m $s^{-1}$ was present in the stratiform region of 22 January 1990.

### 5.2.3 Vertical velocity observations in the 28 January 1990 stratiform region

Wind profiler data from 1449 UTC is shown in Fig. 5.30a. An updraft existed between the 4 and 8 km levels with peak vertical velocities of approximately 0.4-0.5 m $s^{-1}$. In fact, it appears that a layer containing vertical motions of 0.4 m $s^{-1}$ extended from 6-7.5 km. Downward motion was detected by the profiler above 8.5 km. The EVAD analysis at 1445 UTC (Fig.5.31a) verified the strength of the updraft (average velocities of 0.4 m $s^{-1}$) observed by the profiler above 4 km, but extended the depth of the updraft to nearly 12.5 km. Consistent with the extended depth of the updraft shown by the EVAD, the profiler data showed updrafts at elevations up to 11 km at 1430 and 1440 UTC. This illustrates to some extent the non-uniformity of the updraft strength, depth and location on smaller spatial and time scales. By 1509 UTC the updraft diminished as the profiler and radar appeared to come under the influence of subsidence on the eastern edge of convection which had approached from the south moving northeast (see Fig. 5.17c).

At 1620 UTC (Fig. 5.30b) the wind profiler indicated upward velocities in the lower 4.5 km of the troposphere and either zero or very weak negative velocities above 4.5 km. This is consistent with the observed dissipation around this time (see Figs. 5.17d-e). The EVAD results at 1615 UTC (Fig. 5.31b) closely resembled the profiler data except for a region of very weak upward motion (0.05 m $s^{-1}$) that existed at 6 km. By 1645 UTC (see Fig. 5.17e), the EVAD results (not shown) indicated subsidence at all levels and the profiler (not shown) indicated weak subsidence or zero velocities at all levels.

In summary, the profiler indicated upward motion (velocities of 0.4-0.5 m $s^{-1}$) in the stratiform region between the 4.5-8.5 km levels (for the 1449 UTC analysis time; Fig. 5.30a). The EVAD at 1445 UTC (Fig. 5.31a) indicated upward motion of similar magnitudes but over a greater depth. At 1620 UTC both the profiler (Fig. 5.30b) and the EVAD analysis (Fig. 5.31b) indicated subsidence or zero vertical velocity in the dissipating stratiform region.

### 5.2.4 Vertical velocity observations in the 12 January 1990 stratiform region

The vertical velocities in the stratiform region of 12 January 1990 were characterized by relatively weak upward motion situated above the 4.5 km level that varied in magnitude, depth and location. Stronger updrafts (i.e., 30 cm $s^{-1}$) generally occurred at or above the 7.5 km level. The updrafts were neither temporally nor spatially uniform between 1100 and 1230 UTC (when only stratiform precipitation was located over the MIT radar and the profiler). To illustrate this variation, we present the vertical velocities diagnosed at 1059 and at 1200 UTC.

At 1059 UTC (Fig. 5.32a; note that velocities are plotted from -6 to +6 m $s^{-1}$) the profiler indicated that only weak upward motion of 0.1-0.3 m $s^{-1}$ existed in the 6-8 km layer and in the 9-11 km layer Weak subsidence was detected just above and below the 6-8 km layer by the profiler. The EVAD analysis from 1100 UTC (Fig. 5.33a) indicated that upward vertical motion of 0.1-0.15 m $s^{-1}$ existed in the 8-10 km layer. This is quite different from the profiler results at 1059 UTC. However, at 1050 and 1110 UTC (not shown) the profiler did indicate upward motion (0.2-0.3 m $s^{-1}$) in the 8-10 km layer. Indeed, at 1110 UTC the profiler indicated a peak upward velocity of approximately 0.3-0.4 m $s^{-1}$ near the 8 km level. However, the peak vertical velocity of

0.4 m $s^{-1}$ was only measured at one level in stratiform precipitation and only during the 1110 UTC time period.

At 1200 UTC, the profiler (Fig. 5.32b) indicated upward vertical velocities of 0.1-0.2 m $s^{-1}$ from 4-6.5 km and either zero or slightly downward motion above 6.5 km. Weak upward vertical motion between the 4-6.5 km levels (i.e., 10 cm $s^{-1}$) was observed in several time periods between 1100 and 1230 UTC. The EVAD at 1200 UTC (Fig. 5.33b) found that weak upward motion of 0-0.1 m $s^{-1}$ was located from 6.5-11 km and that subsidence was located below 6.5 km. The profiler also indicated some slight upward motion between 8-10 km at 1150 UTC (not shown). These observations make it apparent that some upward motion was present in the stratiform region of the 12 January 1990 monsoon MCS, but that it was generally weaker than the break period cases (with the exception of the 1110 UTC time period), varied in depth and location, and was often observed well above the bright band (i.e., between 8 km and 11 km).

## 5.3. Model results

In this section we present the results of a simple one-dimensional model (described in Chapter 4) that uses observed vertical velocities to evaluate the probability of a mixed phase region existing in two of the stratiform regions examined in section 5.1. After running the model with observed vertical velocities, sensitivity tests were conducted to investigate the effect of a varying mesoscale updraft (as observed in the four cases in section 5.2) on the amount of supercooled water produced. Cases for which the model analysis is made include the break period MCS of 5 December 1989, and the monsoon MCS of 12 January 1990.

5.3.1 Model results for the break period stratiform region of 5 December 1989

Table 5.1 contains output generated by the one-dimensional model for the time period (10-20 minutes) surrounding 1040 UTC. Positive values in the "Water" column indicate water vapor available for condensation. Negative values for "Water" were caused by either movement of water vapor out of the column in downdrafts (e.g., the 4750 m and 5250 m layers in Table 5.1), or by a total deposition rate that exceeded the vertical flux of water vapor in a layer (e.g., the 7750 m and 8250 m levels in Table 5.1).

**Table 5.1:** 5 December 1989 (1040 UTC) water vapor flux model results

| Height (m) | Temperature (C°) | $W_{avg}$ (m $s^{-1}$) | Water (g $m^{-3}$ $s^{-1}$) |
|---|---|---|---|
| 4750 | 0.6 | -0.25 | -0.000440 |
| 5250 | -2.3 | -0.05 | -0.000137 |
| 5750 | -4.9 | 0.25 | 0.000163 |
| 6250 | -6.7 | 0.50 | 0.000224 |
| 6750 | -8.5 | 0.50 | 0.000236 |
| 7250 | -11.8 | 0.30 | 0.000235 |
| 7750 | -15.6 | 0.10 | -0.000141 |
| 8250 | -18.7 | 0.00 | -0.000225 |

In Table 5.1, positive values of water vapor flux occurred between the -5 °C to -12 °C temperature ranges (5750-7250 m). When the excess water in the layers between -5 °C and -12 °C was integrated over a time period of $10^3$ s (on the order of 10-20

minutes), approximately 0.2 g $m^{-3}$ of supercooled liquid water could be realized in each layer through condensation. A value of 0.2 g $m^{-3}$ is consistent with previous observations of supercooled liquid water in the stratiform regions of MCSs (e.g., Rutledge et al. 1990; Yeh et al. 1991). When the observed vertical velocities at 1111 UTC (see Fig. 27b) were used (generally lower than the vertical velocities at 1040 UTC), the layers between 5750-7250 m exhibited less excess water vapor (time integrated values < 0.2 g $m^{-3}$). If slightly higher vertical velocities were used in the middle and upper layers, values of the condensed water increased to 0.3 g $m^{-3}$. Thus it appears that limited amounts of supercooled water may have existed in the lower to middle-levels (-5 °C to -12 °C) of the 5 December 1989 stratiform region. This is consistent with the observations (section 5.1.1) of moderate (15-25 dBZ) reflectivities existing above the 0 °C level in this particular stratiform region. It should also be noted that the 5 December 1989 stratiform region was actually water saturated(or close to water saturation) over much of the model domain (as indicated by a sounding taken at the Darwin Aerodrome by the Bureau of Meteorology).

The excess water vapor flux was also sensitive to the ice particle number concentrations used in each layer. If concentrations were increased (decreased), the total deposition rate increased (decreased) and the "Water" value decreased (increased). Varying the ice particle number concentration from the average used in weak stratiform precipitation (10 $L^{-1}$) affected the model output the most since the majority of the stratiform region between 4.5 and 8.5 km was classified as weak (reflectivities ≤ 20 dBZ). For example, if ice particle concentrations were increased from 10 $L^{-1}$ to 15 $L^{-1}$ in weak stratiform precipitation at 1040 UTC (Table 5.1), the excess water vapor available for condensation decreased to 0.1 g $m^{-3}$. Thus the amount of liquid water that

can be realized in the stratiform region (as indicated by this simple model) is dependent on the strength and location of the updraft, and the ice particle number concentrations.

### 5.3.2 Model results for the monsoon period stratiform region of 12 January 1990

The probability of supercooled liquid water in the stratiform region of the 12 January 1990 monsoon case was assesed using the wind profiler vertical velocity observations between 1050 and 1100 UTC (Table 5.2). Recall from section 5.2.4 that the vertical velocities in the stratiform region of this particular monsoon MCS were somewhat less than what was typically observed in the break period stratiform regions. The weaker updrafts (and their elevated location; i.e., typically above 7 km) had a marked effect on the amounts and locations of excess water yielded by the model.

**Table 5.2:** 12 January 1990 (1100 UTC) water vapor flux model results

| Height (m) | Temperature (C°) | $W_{avg}$ (m $s^{-1}$) | Water (g $m^{-3}$ $s^{-1}$) |
|---|---|---|---|
| 5250 | -0.5 | -0.10 | -0.000141 |
| 5750 | -2.7 | 0.00 | -0.000058 |
| 6250 | -5.1 | 0.10 | 0.000018 |
| 6750 | -7.7 | 0.20 | 0.000022 |
| 7250 | -10.5 | 0.20 | 0.000024 |
| 7750 | -13.6 | 0.25 | 0.000006 |
| 8250 | -17.0 | 0.20 | -0.000060 |
| 8750 | -20.6 | 0.10 | -0.000173 |

In Table 5.2 values in the "Water" column are approximately one to two orders of magnitude lower than what was found in the break period case (Table 5.1). The excess water occurred between the temperatures of -5 °C and -13 °C. Indeed, if the values are integrated over a time of $10^3$ seconds, the only substantial liquid water contents possible would be .02 g $m^{-3}$ between the -5 °C and -11 °C levels. When the updraft was changed to reflect stronger vertical velocities between 7 and 9 km, the only significant water produced was 0.1 g $m^{-3}$ at the 7250 m level. If a weak updraft was introduced in the 5-6 km layer, 0.1 g $m^{-3}$ of liquid water was produced at the 0 °C and -2.7 °C levels. If the particle concentrations were increased from 10 $L^{-1}$ to 15 $L^{-1}$ in the weak stratiform precipitation, no excess water was produced. From these results we conclude that very little liquid water (i.e., of substantial quantity) existed above the 0 °C level in the 12 January 1990 monsoon stratiform region. This is consistent with the observations (section 5.1.7) of weak reflectivity values (as indicated by the height of the 15-25 dBZ reflectivity contour in the vertical cross-sections) in the stratiform region above the 0 °C isotherm. It is also important to note that the sounding taken on 12 January 1990 did not indicate water saturation at many of the levels in the model domain. Therefore, the amount of supercooled liquid water actually present in the 12 January 1990 stratiform region was probably *less* than what the model predicted.

### 5.3.3 Liquid water contents and electrification in the stratiform regions

The break period stratiform region (5 December 1989) and the monsoon stratiform region (12 January 1990) exhibited different reflectivity structures, vertical velocities and modeled liquid water contents. The modeling results suggest that lower vertical velocities and the position of the updraft in the monsoon case may have impeded the formation of substantial liquid water contents above the 0 °C temperature level.

Conversely, the break period stratiform region was associated with relatively strong updrafts and significant amounts of model-predicted supercooled liquid water in the -5 °C to -12 °C region. It seems reasonable to assume that these differences should have some effect on the electrification of the stratiform region.

Now let us consider the modeled liquid water contents in a layer of some specified temperature with respect to a non-inductive charging theory that includes the surface state of the ice particles in the layer (e.g., Fig. 5.34; adapted from Williams et al. 1991). Fig. 5.34 is a graphic illustration of the combined non-inductive charging results of Williams et al. (1991) (theoretical) and Takahashi (1978) (laboratory). Given Fig. 5.34 we can determine the dominant polarity of charge created in layers with a specific liquid water content and temperature. In Fig. 5.34, the sloping dashed and solid lines represent boundaries for different surface states of the ice (Williams et al. 1991) as a function of liquid water and temperature. The lower region (bounded by the dashed line) represents depositional growth of an ice surface and is associated with primarily positive charging of that surface. The middle region represents acretional growth of an ice surface in a sublimational state and primarily negative charging of the ice surface (e.g., Baker et al. 1987; Caranti et al. 1991). The upper region represents an ice surface in a wet growth state and is associated with positive charging. The black and white dots are experimental charging results from Takahashi (1978). Black (white) dots represent negative (positive) charge transfer to a riming ice particle in a collisions with another ice particles.

If we compare our modeling results in Table 5.2 to Fig. 5.34 for the 12 January 1990 monsoon stratiform region, we find that the charging of the ice should be weakly positive. Note that a reversal to weak positive charge overhead was noted in the electric

field record (Fig. 5.25) near 1200 UTC on 12 January 1990. Of course, this does not explain the negative charge that existed over the field mill in the stratiform region until 1200 UTC. Recall however, that the vertical velocities in the stratiform region of 12 January 1990 varied in the lower levels from weak upward to weak downward motion. When weak upward motion was present in the lowest layers, 0.1 g $m^{-3}$ of water was generated by the model between -0.5 °C and -2.7 °C. Fig. 5.34 indicates that ice particles at this temperature and liquid water content would be in a sublimating environment, and therefore should charge negatively. Thus both polarities of charging were likely possible in the 12 January 1990 case (though the values of charge transfer are small; see Fig. 3.2). It is possible that fluctuations in the updraft coupled with low liquid water contents prevented the cloud from becoming strongly electrified with one dominant polarity of charge in the stratiform region.

With regard to Fig. 5.34, the break period case of 5 December 1989 is somewhat complicated. In all of the modeling experiments, liquid water contents of 0.1-0.2 g $m^{-3}$ were created between -5 °C and -12 °C. This places the ice in a depositional environment for temperatures > -7 °C, and hence positive charging would take place (Williams et al. 1991). However, at temperatures of -5 °C and liquid water contents greater than 0.1 g $m^{-3}$, the results of Williams et al. (1991) (Fig. 5.34) indicate that an ice surface could be in either a sublimational (negative charging) or a depositional state (positive charging). The results of Takahashi indicate only positive charging of the ice (Fig. 5.34). Note in Table 5.1 that larger quantities of liquid water (0.2 g $m^{-3}$) were located between -7 °C and -12 °C levels, placing the ice surfaces in a region of depositional growth (positive charging) in Fig. 5.34. Thus it is likely that positive charging of the ice took place between the -5 °C and -12 °C levels in the 5 December 1989 stratiform region. This is consistent with the observed occurrence of positive CGs

in the stratiform region on December 5, and also the field mill observations (Fig. 5.6) which indicated dominant positive charge overhead in the stratiform clouds between 0940 and 1110 UTC.

It appears that the modeling and vertical motion observations support a non-inductive charging mechanism for the stratiform regions. However, this suggestion is made with a note of caution since 1) the assumptions made in the model (i.e., horizontal homogeneity, water saturation, and ice particle parameterizations) may not be representative of the actual conditions; 2) the subjective determination of vertical velocity from profiler data is a possible source of error; and 3) the sensitivity of the model to updraft strengths and particle densities presents questions regarding the accuracy and applicability of the model. Also recall that the sounding of 12 January 1990 at 1200 UTC did not indicate water saturation at all levels. Thus other evidence will be needed to infer the presence of a non-inductive charging mechanism in the stratiform regions examined herein.

## 5.4 Updrafts correlated to positive CG flash rates

An interesting correlation arises when the updraft strengths and the number of positive CGs observed in each stratiform region are compared. Fig. 5.35 is a plot of the total number of positive CGs that occurred in each stratiform region vs. the frequency of 10 minute time periods that contained updrafts > 0.3 m $s^{-1}$ (as indicated by the profiler) for each of the four stratiform regions examined in section 5.2 (each stratiform region examined for approximately the same length of time). Fig. 5.35 indicates that there is a positive correlation between the strength and longevity of the updrafts, and the number of positive CGs observed. This would be expected if the updraft strength is related to

the formation of a strong mixed phase region and the development of in-situ, non-inductive charging. Caution should be exercised in interpreting these results however, since vertical velocities were subjectively determined and only four cases could be compared.

## 5.5 Correlation between the height of the 15-25 dBZ reflectivity contour and the number of CGs observed in the stratiform regions.

In section 5.1 it was observed that the height of the 15-25 dBZ reflectivity region above the 0 °C isotherm in the stratiform region seemed to be related to the number of CGs observed therein. To test this relationship, two plots were created (Figs. 5.36a-b) to compare the normalized number of CGs (positive CGs, Fig. 5.36a; total CGs, Fig. 5.36b) observed in each stratiform region to the relative intensity (as indicated by the area of 15-25 dBZ reflectivities located above the 0 °C isotherm) of each respective stratiform region. The number of positive CGs and the total number of CGs observed in each stratiform region were normalized by factors representing the approximate number of positive CGs (Fig. 5.36a), and the total number of CGs (positive *and* negative CGs; Fig. 5.36b) observed in the trailing stratiform region of the 28 January 1990 MCS respectively. In addition, the region of 15-25 dBZ reflectivities that existed above the 0 °C level in each stratiform region were subjectively normalized relative to that of the 28 January 1990 stratiform region. Thus the 28 January stratiform region was assigned a value of 1 for positive CGs observed, total CGs observed (i.e., positive and negative CGs), and for the area of 15-25 dBZ reflectivity located above the 0 °C level.

It is apparent in Figs. 5.36a-b that the number of CGs observed in a particular stratiform region is related to the elevation of the 15-25 dBZ reflectivity region. Notice that the curve in Fig 5.36a (positive CGs only) is very similar to that of Fig. 5.36b (positive and negative CGs). This similarity occurred for two reasons 1) the number of positive CGs generally outnumbered the negative CGs observed in the stratiform regions examined, and therefore dominated the relationship shown in Fig. 5.36b; and 2) the number of negative CGs observed in each stratiform region (included in the total number of CGs) may also have been related to the height of the 15-25 dBZ reflectivity region (e.g., Figs. 5.3b, 5.17b, 5.18a). If we assume that the height of the 15-25 dBZ reflectivity region is somehow related to the strength of the mixed phase region, then the number of CGs observed in the stratiform region (especially positives since they are the most numerous) should be positively correlated to the strength of the mixed phase region. This is consistent with the existence of an in-situ, non-inductive charging mechanism in the stratiform regions. Thus a strong mixed phase region in stratiform clouds should be linked to more charging in the stratiform clouds and more frequent cloud-to-ground lightning (e.g., 5 December 1989, 28 January 1990). The reverse would be true for a weaker mixed phase region (e.g., 12 January 1990, 24 January 1990). A similar positive correlation between the strength of mixed phase regions in winter stratiform clouds and the degree to which the stratiform clouds were electrified was reported by Mach et al. (1991).

## 5.6 Break period positive CGs vs. the average 700-400 mb and 450-280 mb shear

It was stated in section 5.4 that further evidence would be required to infer the presence of a non-inductive mechanism in stratiform regions. We can indirectly approach this goal by showing that other charging mechanisms cannot explain the

observed lighting in the stratiform regions. For example we can test the validity of the charge advection mechanism by examining the average 700-400 mb shear and the average 450-280 mb (7-10 km) shear in each of the break period storms that produced positive CGs behind the convective line. Since Chauzy (1985) identified a positive charge region at approximately 7.5-8 km (400-350mb) in a tropical convective line, and Krehbiel (1986) identified a main positive charge center near the 10 km (250-300 mb) level in Florida thunderstorms, if the shear is strong in either the 700-400 mb or 450-280 mb layers it seems likely that positive charge would be more efficiently advected to the rear of the convective line, thus producing the likelihood of positive CGs. This assumes that only positive charge is advected rearward in the vicinity of 400 mb (7.5 km) or 280 mb (10 km). If negative charge were advected rearward we would expect to see more negative flashes than positive flashes in the stratiform region, however we have observed that this was not the case in the MCSs examined herein. If no charge is advected rearward then there should be no correlation between the numbers of positive CGs and the shear; of course this implies no charge advection.

Fig. 5.37a is a plot of the average 700-400 mb shear vs total number of positive CGs observed in the stratiform regions of four of the six MCSs examined herein. The average shear in each MCS was calculated using the maximum value of the 700-400 mb shear that occurred during each time period studied for a particular case. In Fig. 5.37a there is a very weak *negative* correlation between the 700-400 mb shear and the total number of positive CGs observed in the stratiform regions. Fig. 5.37b is a plot of the average 450-280 mb (-10 °C to -30 °C) shear vs. the total number of positive CGs observed in the stratiform regions of the same four MCSs. The correlation between the number of positive CGs and the shear in Fig. 5.37b is also weakly negative. Hence, charge advection would not appear to be a major contributor to the occurrence of

positive CGs in these particular break period stratiform regions. Unfortunately this result applies to only four MCSs and therefore may not be representative of squall-line type MCSs in general.

## 5.7 The location of CG peak current extrema relative to MCS structure

The break period MCSs and their associated ground flash patterns were examined to investigate the relationship between peak current magnitude and the position of occurrence relative to MCS radar reflectivity patterns. The same examination was also performed on two middle-latitude MCSs (examples shown in Figs. 5.38, 5.39; adapted from Rutledge and MacGorman, 1988 and Rutledge et al. 1990) which occurred on 3-4 June 1985, and 10-11 June 1985 during PRE-STORM. Peak current magnitudes in the PRE-STORM cases were computed using Eq. (4.5) from Orville (1991) to convert LLP units to kA.

Recall from Chapter 4 that peak current maximums and minimums were placed into one of two categories: flash position within 10 km of the convective line, or flash position >10 km from the convective line, and within stratiform precipitation. When categorized in this fashion, both the minimum and maximum negative peak currents always occurred in the convective line of the 8 (6 tropical, 2 middle-latitude) MCSs studied. Indeed, this should be expected since the negative flashes in all of the MCSs examined were associated primarily with the convective line. However, the positive peak current extrema exhibited a distinctly different behavior.

When the positive peak current extrema in each thirty minute time interval were examined, an interesting pattern was revealed (e.g., see Figs. 5.2a-d, 5.7c-d, 5.12a,

5.17a-d, 5.20a-c, and 5.21a). For the tropical MCSs, 70 percent of the time intervals studied found the maximum positive peak currents situated in stratiform precipitation while the minimum positive peak currents were associated with convective precipitation in approximately 89 percent of the time intervals. For the 3-4 June 1985 PRE-STORM MCS (Fig. 5.38), positive peak current maximums (minimums) were associated with stratiform (convective) precipitation in 75 (75) of the time intervals studied. Similarly, for the 10-11 June 1985 PRE-STORM MCS (Fig. 5.39), positive peak current maximums (minimums) were associated with stratiform (convective) precipitation in 90 (80) percent of the time intervals examined.

Figs. 5.38 (0105 UTC, 4 June 1985) and 5.39 (0256 UTC, 11 June 1985) each represent one of several 30 minute time periods (as shown in Rutledge and MacGorman, 1988 and Rutledge et al. 1990) studied from the 3-4 June 1985 and 10-11 June 1985 PRE-STORM MCSs. Like the tropical MCSs examined in this thesis, these particular middle-latitude MCSs also had the maximum positive peak currents (147 kA for 3-4 June, Fig. 5.38; 202 kA for 10-11 June, Fig. 5.39) in stratiform precipitation (approximately 70-100 km from the convective lines) and the minimum positive peak current s ( 11 kA and 19 kA respectively) in convective precipitation. The maximum positive peak currents in the 3-4 June MCS were located in stratiform precipitation in three out of four time periods (spanning a total time of 4 hours) studied by Rutledge et al. 1990. In the 10-11 June case, positive peak current maxima were located in stratiform precipitation in nine out of the ten time periods (spanning a total time of 5 hours) examined by Rutledge and MacGorman (1988). Likewise, the minimum positive peak currents in the 3-4 June (10-11 June) case were located in convective precipitation in three out of four (eight out of ten) time periods. Note also that the maximum positive peak currents in the stratiform regions of Figs 5.38 and 5.39 are approximately one

order of magnitude larger than their minimum counterparts in the convective precipitation. The large difference in current magnitude between the stratiform and convective region positive peak current extrema was observed in virtually all of the time periods examined in the 3-4 June and 10-11 June 1985 MCSs.

In nearly all of the tropical examples presented herein, the peak current extrema differ by at least a factor of two. In the two middle-latitude MCSs the maximum and minimum positive peak currents differ by at least an order of magnitude. This might lead one to suspect that all of the positive peak currents (not just the extrema) associated with the stratiform region are, on average, greater than those occurring in the convective line. This tendency was not conclusively demonstrated in the majority of the DUNDEE cases presented herein but did exist in both of the middle-latitude PRE-STORM cases. Only one of the DUNDEE cases (14 February 1990, Figs. 5.20a-c) showed a pronounced difference in the average positive peak currents, (stratiform average 55 kA, convective 37 kA), but the averages should be taken with a note of caution as the total number of positive flashes associated with stratiform precipitation was relatively small. The 3-4 June and 10-11 June 1985 PRE-STORM cases showed a marked difference (approximately 37 kA and 27 kA respectively) between the average positive peak currents occurring in the stratiform region (75 kA, 3-4 June; 81 kA, 10-11 June) and those in the convective region (37 kA, 3-4 June; 54 kA, 10-11 June). However, no general conclusions with regard to the difference in average positive peak currents between stratiform and convective regions can be drawn for the middle latitude PRE-STORM MCSs since only two cases were examined.

A possible explanation of the tendency for the positive peak current maximum (minimum) to occur in the stratiform (convective) region of an MCS might be related to

the relative size of the charge volume contributing to the ground flash. Rutledge et al. (1990) suggested that in-situ charging (charge generation through stratiform microphysical processes) coupled with the large areal extent of the stratiform region, could provide a large charge volume and hence ample charge for the flashes observed beneath the stratiform region of an MCS. In the convective region, flashes would presumably draw upon a smaller charge volume (relative to the stratiform region) and might therefore be expected to have smaller associated peak currents. Rutledge et al. (1990) developed a one-dimensional model to examine the rate of charge generation by non-inductive charging associated with microphysical conditions in the stratiform clouds of MCSs. The model indicated that sufficient charge was generated within the stratiform region to account for a flash rate of 200 flashes $hr^{-1}$. Now, if the same modest charging rate as found by Rutledge et al. (1990) is assumed (4 C $km^{-2}$ $hr^{-1}$), over the same large area (typically 100 x 50 $km^2$), and <100 positive flashes occur in a one hour time period (which was the case for all of the MCSs examined herein), there could be more charge available per flash and perhaps a higher probability for a large peak current. However, this hypothesis is presented with a note of caution since other processes such as continuing currents (currents which follow the majority of positive first return strokes) and in-cloud lightning can transport significant amounts of charge out of the cloud volume (Uman, 1987). These two processes would therefore reduce, to some extent, the higher probability of a cloud-to-ground flash occurring with a large peak current by removing any excess charge. It should also be noted that the hypothesized in-situ charging is assumed to be uniformly distributed over a large area of the stratiform region.

To further support the possibility of in-situ charging in the stratiform region, plots of maximum positive peak current magnitude over storm lifetime (Fig. 5.40) are

presented for four of the MCSs (the 10-11 June 1985 middle latitude MCS and three tropical cases) examined herein. The value plotted on the abscissa (from left to right) represents a time spectrum in terms of 30 minute increments for each storm with a value of 1 representing the initiation of an intense convective line to a value of 12 representing dissipation of the MCS. Times 4-7 represent the part of each MCS lifecycle for which the stratiform region was intensifying and developing to peak intensity (as subjectively determined from plots of radar reflectivity). The ordinate represents the maximum positive peak current magnitude recorded in any part of each MCS over a 30 minute period. In order to make a comparison between storms, 30 minute periods for each linear MCS (note that 3-4 June 1985 was not linear and was not studied for its entire lifecycle) were subjectively classified according to the growth stage (i.e., early or late in the storm lifecycle).

For each MCS examined in this manner, the maximum positive peak current occurs during the time of stratiform region growth and intensification (periods 4-7). Also, *each peak in Fig. 5.40 is associated with a positive CG that occurred in a stratiform region.* [A double peak was observed for the 14 February 1990 tropical MCS, corresponding to the growth of a second stratiform region on the southeastern side of the MCS (Fig. 5.20a-c)]. The data presented in Fig. 5.40 suggest that the maximum positive peak current is a function of storm lifecycle, in particular, the lifecycle of the stratiform region. Indeed, the maximum positive peak current associated with the 10-11 June 1985 MCS also corresponded to the maximum rate of increase in areally integrated rainfall in the stratiform region (see Fig. 3.4). The dependence of maximum positive peak current on the growth stage of the stratiform region strongly suggests the presence of an in-situ charging process operating within the stratiform region (as discussed by Rutledge et al., 1990). The stratiform precipitation is linked to

the development of a broad mesoscale updraft (found to exist in several of the MCSs examined in section 5.3), which as Rutledge et al. (1990) suggest, produces a mixed phase environment within which a non-inductive charging process operates (Takahashi, 1978). Recall from the analyses in sections 5.1 that the height of the 15-25 dBZ reflectivity region (from which we infer the strength of the mixed phase region) appeared to be correlated to the cloud-to-ground lightning activity (section 5.2, Fig. 5.26) and electric field magnitudes associated with the stratiform clouds.

Now, if a non-inductive charging mechanism is responsible for the charging and subsequent lightning that takes place in the stratiform region of an MCS, we would intuitively expect the production of charge to be at a maximum during time periods 4-7 (Fig. 5.40) just prior to the onset of the heaviest stratiform rainfall, or as in the 10-11 June 1985 MCS, during the maximum rate of increase in stratiform rainfall. Further, as in Rutledge et al. (1990), we might also expect the charge distribution to be that of an inverted dipole (negative overlying positive charge). This distribution of charge might then manifest itself in the form of an in-cloud or positive cloud-to-ground lightning flash assuming the electric field in the cloud approached break down values ($10^5$-$10^6$ V $m^{-1}$).

Recall that large negative electric fields of 8-10 kV $m^{-1}$ existed at the ground (indicating a large region of positive charge in the cloud overhead) while the stratiform region of the 5 December 1989 DUNDEE MCS (Fig. 5.2c-e) was over the field mill located at the MIT radar site. Also, the model results presented in section 5.5 indicated that supercooled liquid water and positive charge would be located between the -5 and -12 °C levels. It is also likely that during this time of maximum positive charging in the lower stratiform region, the probability of a positive ground flash occurring with a large

peak current would be higher. Note that this argument assumes the presence of an efficient non-inductive charging process in the trailing stratiform regions of an MCS.

## 5.8 Support for a non-inductive charging mechanism in the stratiform regions of tropical MCSs

The analyses in sections 5.1-5.7 appear to support the presence of an in-situ, non-inductive charging mechanism in the the tropical stratiform regions examined herein. The support is summarized as follows:

1) Similar to previous observations of the cloud-to-ground lightning in middle-latitude MCSs (e.g., Orville et al. 1987; Rutledge and MacGorman, 1988; Rutledge et al. 1990), primarily positive CGs were observed to occur in the stratiform regions examined herein (those that produced CGs). However, a few negative CGs were also observed coincidentally with positive CGs in the stratiform regions (e.g., 5 December 1989, 28 January 1990, and 14 February 1990; Figs. 5.2b, 5.17a-b, 5.20a-b ); this is not explained by the charge advection mechanism (unless negative charge is also transported into the stratiform region).
2) The 700-400 mb and 450-280 mb (7-10 km) shears were negatively correlated (weakly) to the number of positive CGs observed in each stratiform region (Fig. 5.37). This is also inconsistent with the charge advection mechanism.
3) Stratiform regions that produced relatively large numbers of CGs (observed to be primarily postive) were associated with stronger mixed phase regions (as indicated by the elevation of the 15-25 dBZ reflectivity region above the melting level; Figs. 5.36a-b). Conversely, stratiform regions with weaker

mixed phase regions (15-25 dBZ reflectivities confined to below the melting level) did not produce large numbers of CGs (e.g., contrast 28 January 1990 [Fig. 5.17b] with 12 January 1990 [Fig. 5.22b]). This result is consistent with the observations of Mach et al. (1991) who found a positive correlation between the electrification of winter stratiform clouds and the strengths of their respective mixed phase regions.

4) Upward vertical motion in the stratiform regions was positively correlated with the production of positive CGs (Fig. 5.35).

5) In a simple one-dimensional model of the vertical water vapor flux in one break period stratiform region (5 December 1989), significant amounts of liquid water (0.2 g $m^{-3}$) were produced between the -5 °C and -12 °C temperature levels (see Table 5.1). These amounts of liquid water are consistent with previous in-situ measurements made in stratiform regions (e.g., Yeh et al. 1991).

6) When model derived liquid water contents and corresponding temperatures from the break period case were mapped to a non-inductive charging diagram from Williams et al. (1991), it was found that positive charging would occur in the -5 °C to -12 °C layers. This is consistent with previous observations of a main positive charge layer existing just below the -12 °C level (e.g., Schuur et al. 1991; Marshall and Rust 1991; see Fig. 1.3), and is also consistent with the surface based electric field measurements for this case (Fig. 5.6) which indicated that positive charge was situated overhead when stratiform clouds were situated over the field mill.

7) As a consequence of the elevated location and smaller magnitude of the mesoscale updraft in the monsoon case of 12 January 1990, the supercooled liquid water contents produced by the model were an order of magnitude

smaller than those produced for the break period case. When the liquid water contents and the respective layer temperatures were mapped to the Williams et al. (1991) diagram, it was found that weak positive charge could have been created in the monsoon stratiform region. However, when updrafts were present near the 0 °C level (i.e., at 1200 UTC), model predicted liquid water contents and the results of Williams et al. (1991) indicated that weak negative charging may have taken place near the 0 °C level. Note that very weak charging of both polarities was observed in the 12 January 1990 case (as indicated by electric field measurements; see Fig. 5.25).

8) The model indicated differences between the amounts of water produced above the 0 °C isotherm in the break period and monsoon cases. The model-predicted differences in the supercooled liquid water contents are consistent with the observed strengths of the mixed phase regions (inferred from the amount of 15-25 dBZ reflectivities located above the 0 °C levels) and the numbers of CGs produced in each type (break or monsoon) of stratiform region. This would strongly suggest that non-inductive charging is the primary mechanism for producing electrified stratiform clouds.

9) Positive peak current maxima (minima) were found to occur in stratiform (convective) precipitation in six DUNDEE MCSs in 70 (89) percent of the time intervals studied. This trend was also observed in two middle-latitude MCSs observed during PRE-STORM. Note that the large distances (typically > 30 km) between the location of the peak current maximums in the stratiform region and the convective line also suggest that an in-situ charging process is responsible for electrifying the stratiform region.

10) The positive peak current maxima that occurred in the stratiform regions were at least twice as large as the positive peak current minima in the convective

line. In fact, in several of the DUNDEE MCSs (and both middle-latitude MCSs) the positive peak current maxima were at least an order of magnitude larger than minima.

11) Maximum positive peak currents were found during the time of maximum growth and intensification of the stratiform region, suggesting that microphysical processes (associated with the generation of a mesoscale updraft) were responsible for electrifying the stratiform region.

It is of course difficult to rule out significant additions of charge to the stratiform region by other mechanisms such as charge advection (see section 3.6), though analysis indicates that charge advection may not be the primary charging mechanism in the stratiform regions. Other possibilities that cannot be ruled out entirely are 1) transfer of charge to the stratiform region via in-cloud flashes and 2) positive CGs located in the stratiform regions due to flashes which emanate from convective lines with horizontal channels of 50-100 km before going to ground (Rust, 1986). Since no data exists to confirm or refute points 1 and 2, we do not address them here. We believe however, that the evidence presented herein strongly supports a non-inductive charging mechanism in the trailing stratiform regions of tropical MCSs.

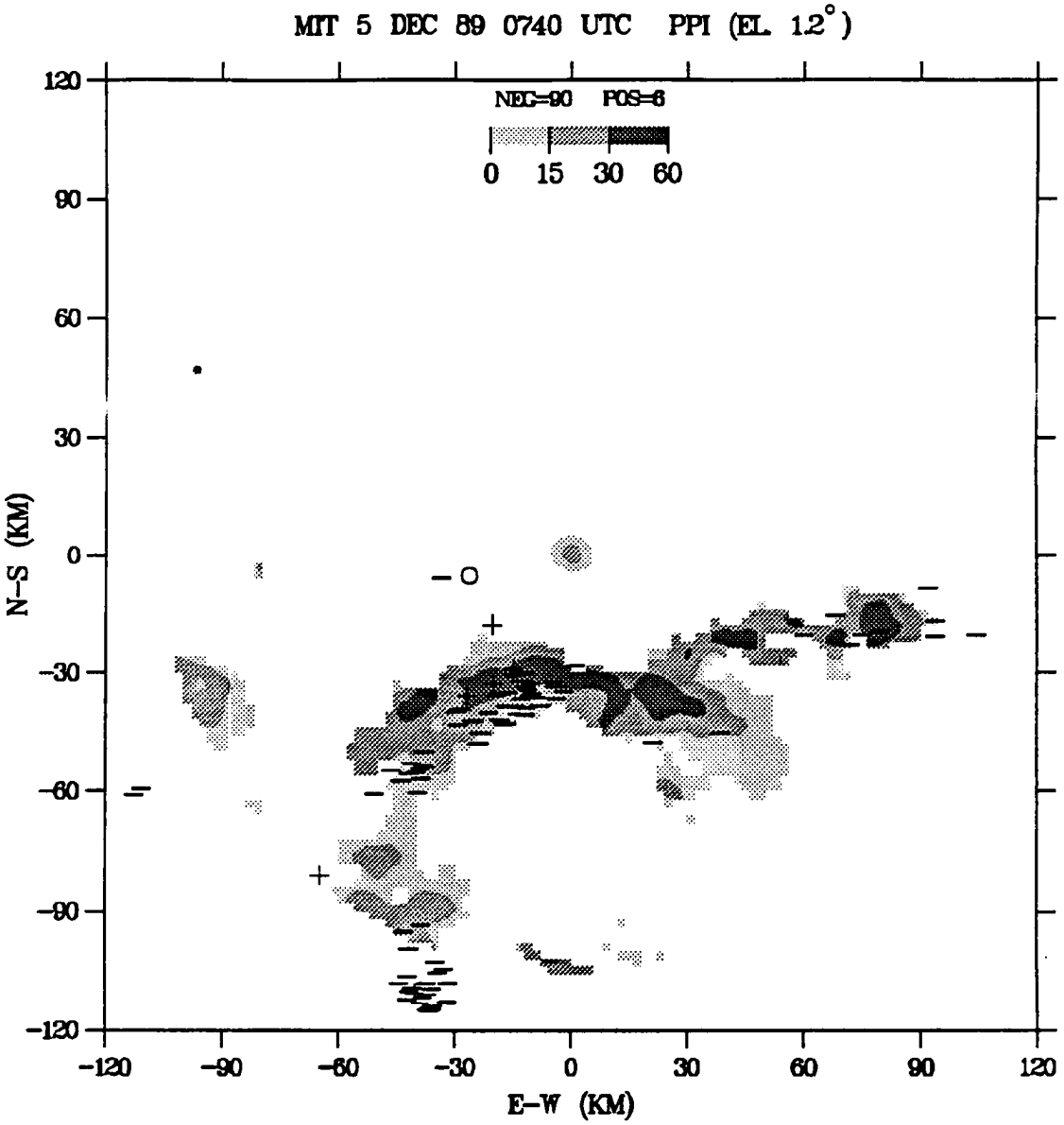


Figure 5.1 MIT radar low level PPI (1.2° elevation) of reflectivity (dBZ) and cloud-to-ground lightning (30 minute interval centered on the time of the radar scan), for 5 December 1989 at 0740 UTC. The MIT radar is centered at (0,0). A (+) indicates a positive flash, (-) indicates a negative flash.

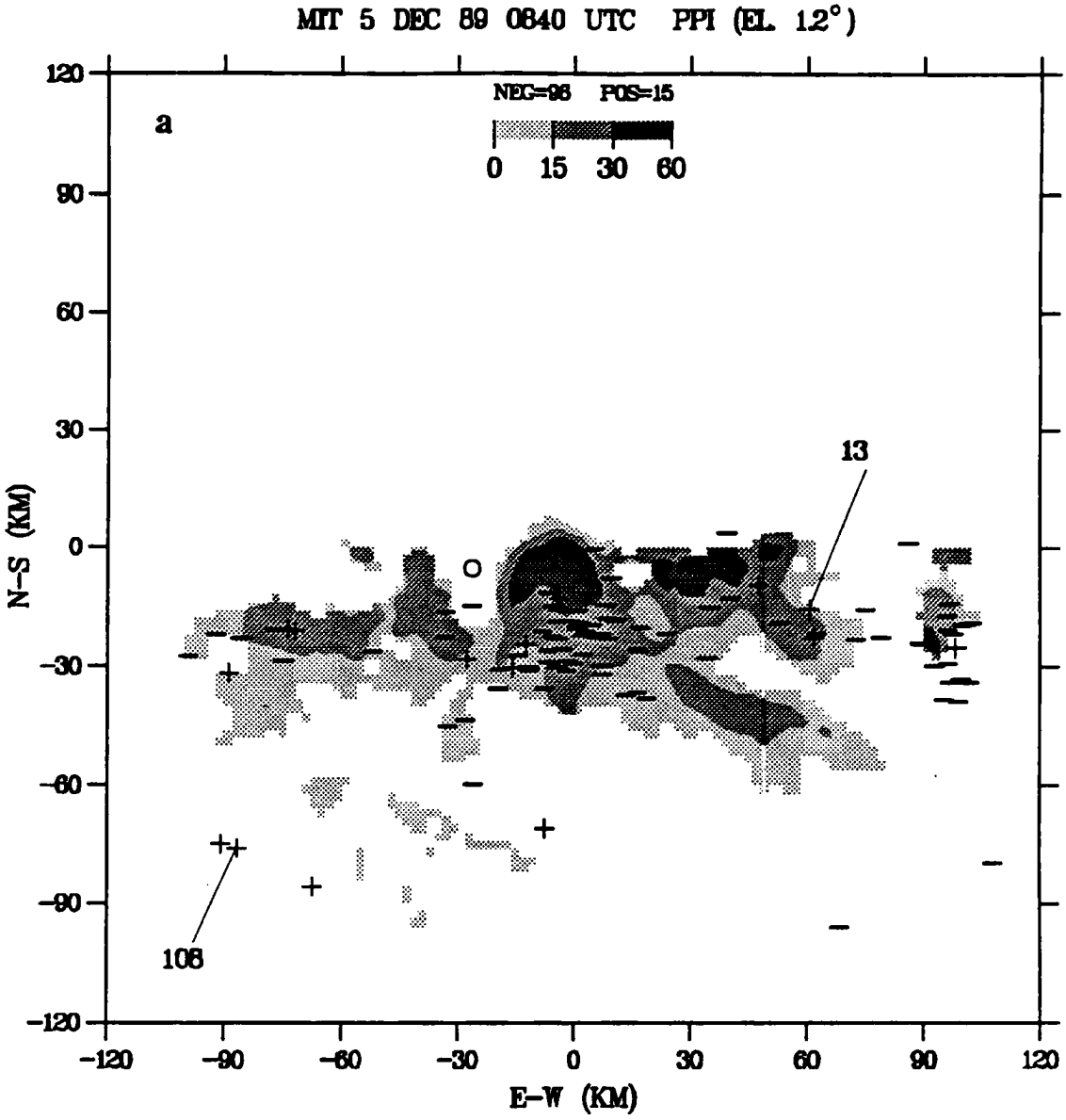


Figure 5.2 Same as (5.1) except (a) 0840 UTC. Positive peak current extrema identified as 13 and 108 kA.

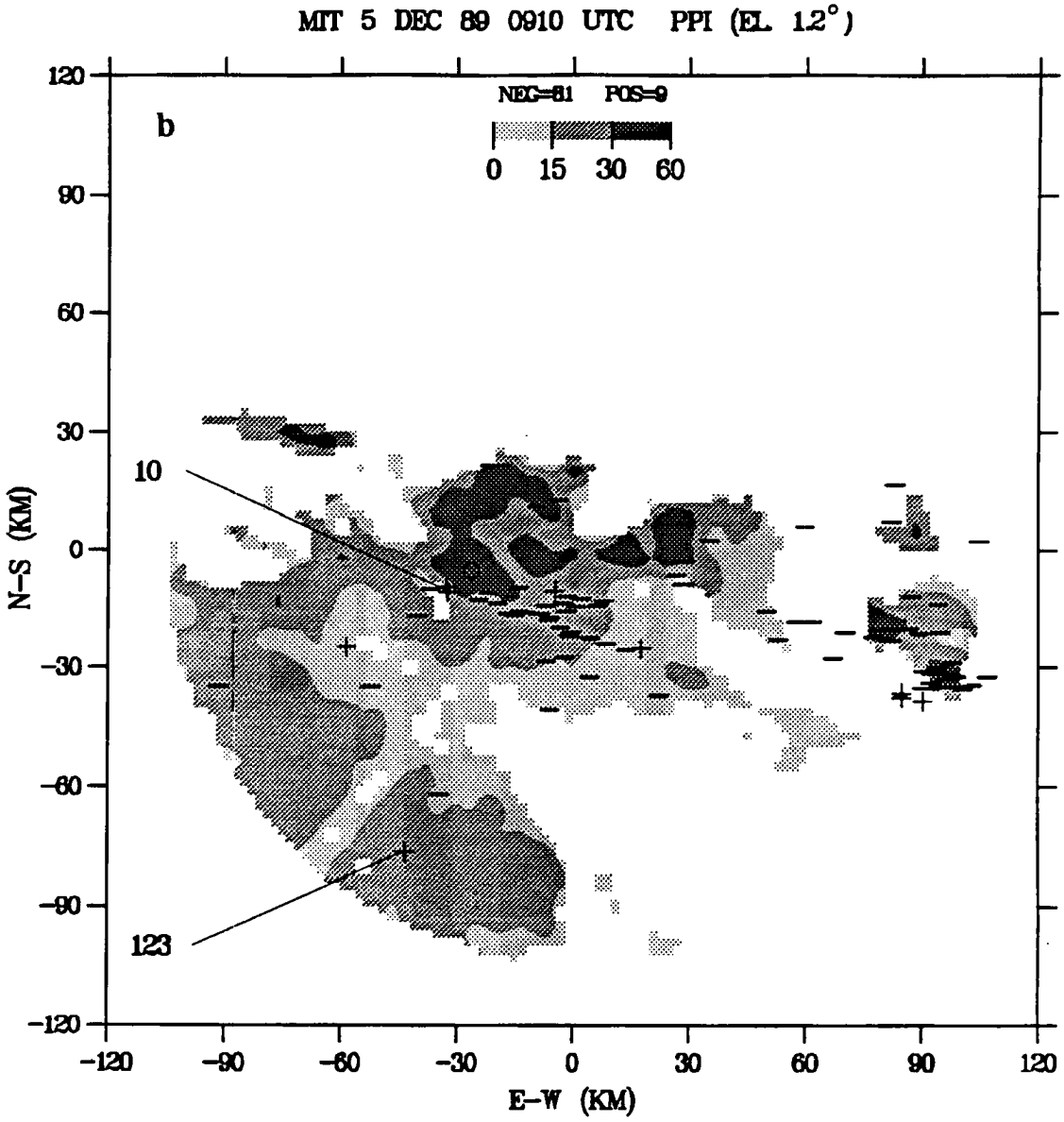


Figure 5.2 (b) 0910 UTC. Positive peak current extrema identified as 10 and 123 kA.

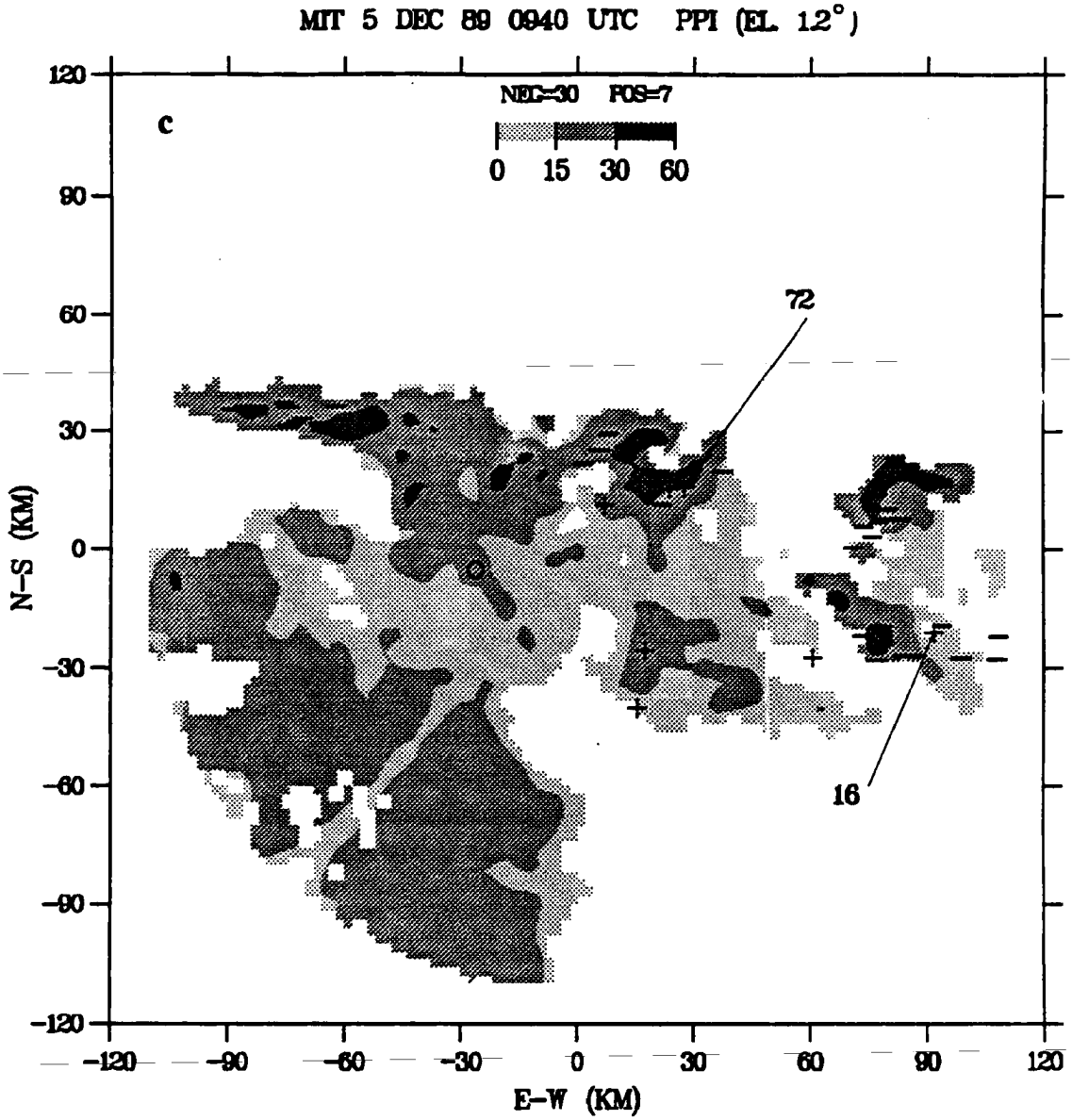


Figure 5.2 (c) 0940 UTC Positive peak current extrema identified as 16 and 72 kA.

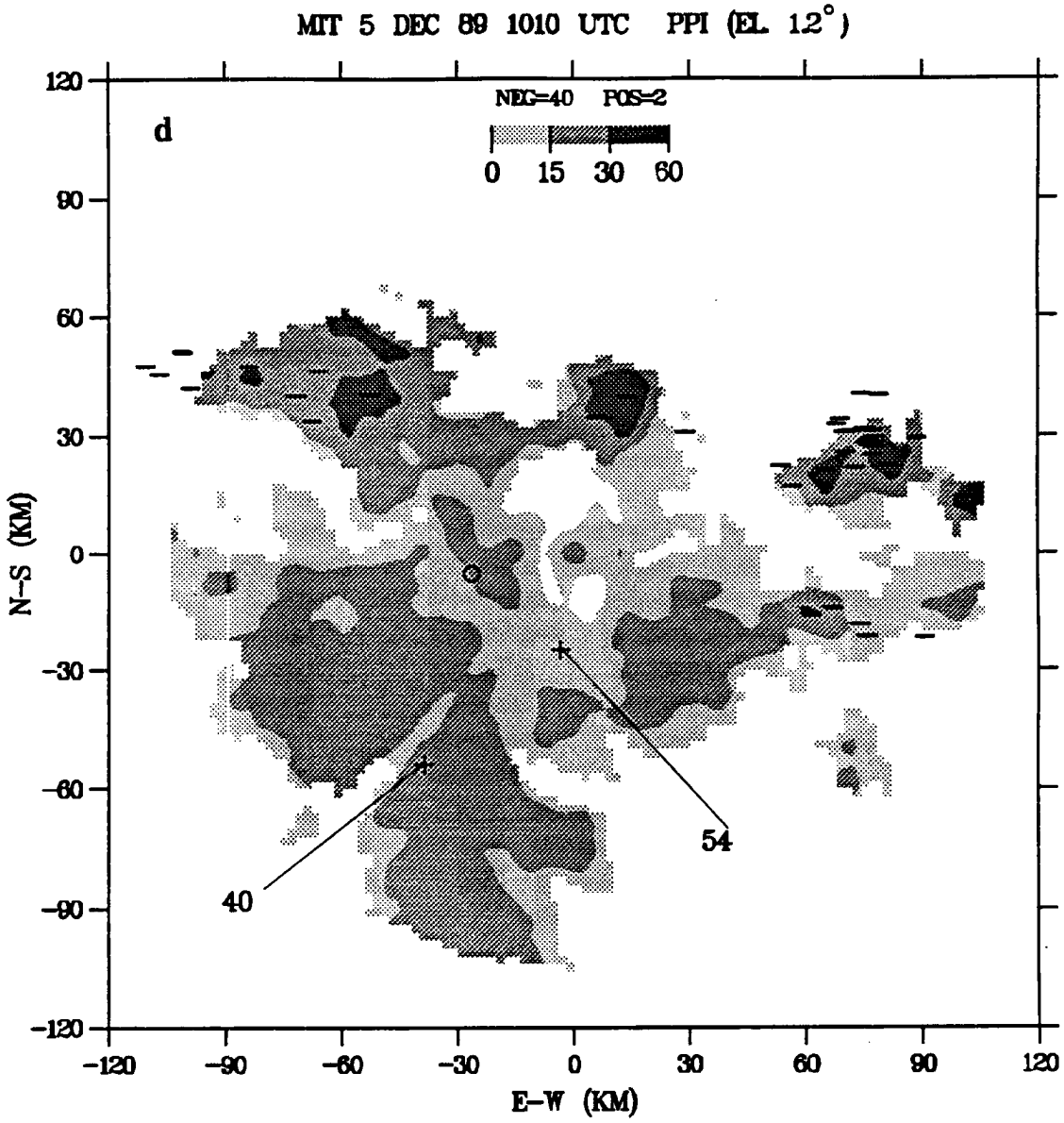


Figure 5.2 (d) 1010 UTC. Positive peak current extrema identified as 40 and 54 kA.

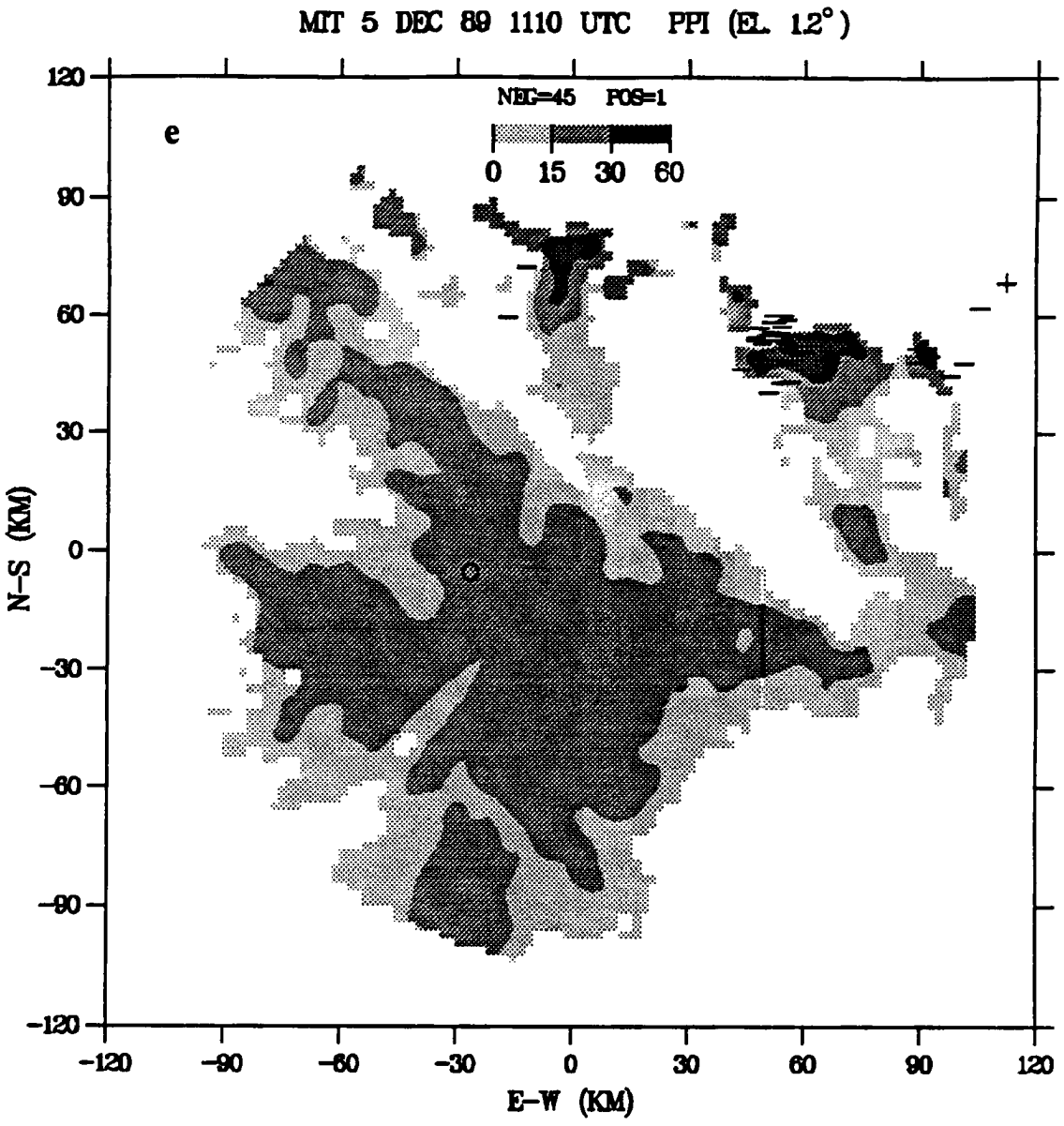


Figure 5.2 (e) 1110 UTC.

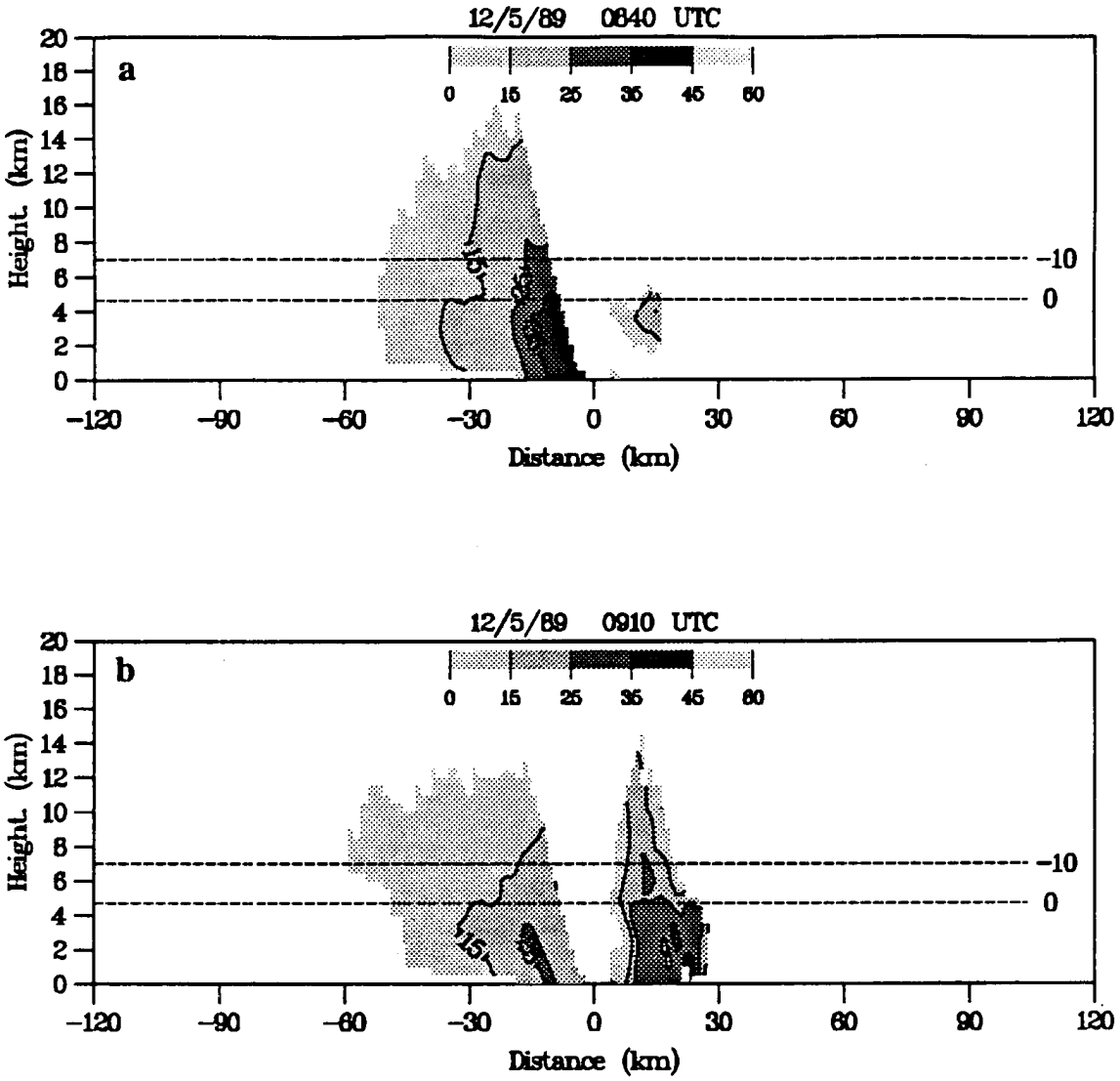


Figure 5.3 MIT radar line-normal (180° azimuth) vertical cross-sections of reflectivity for 5 December 1989 at (a) 0840 UTC and (b) 0910 UTC. Positive values of distance are oriented in the direction of squall line movement, negative values of distance are oriented opposite to the direction of squall line movement. Reflectivities ≥ 15 dBZ are contoured in 10 dBZ increments. Heights of the clear-air 0 °C and -10 °C levels are indicated by a dashed line (------).

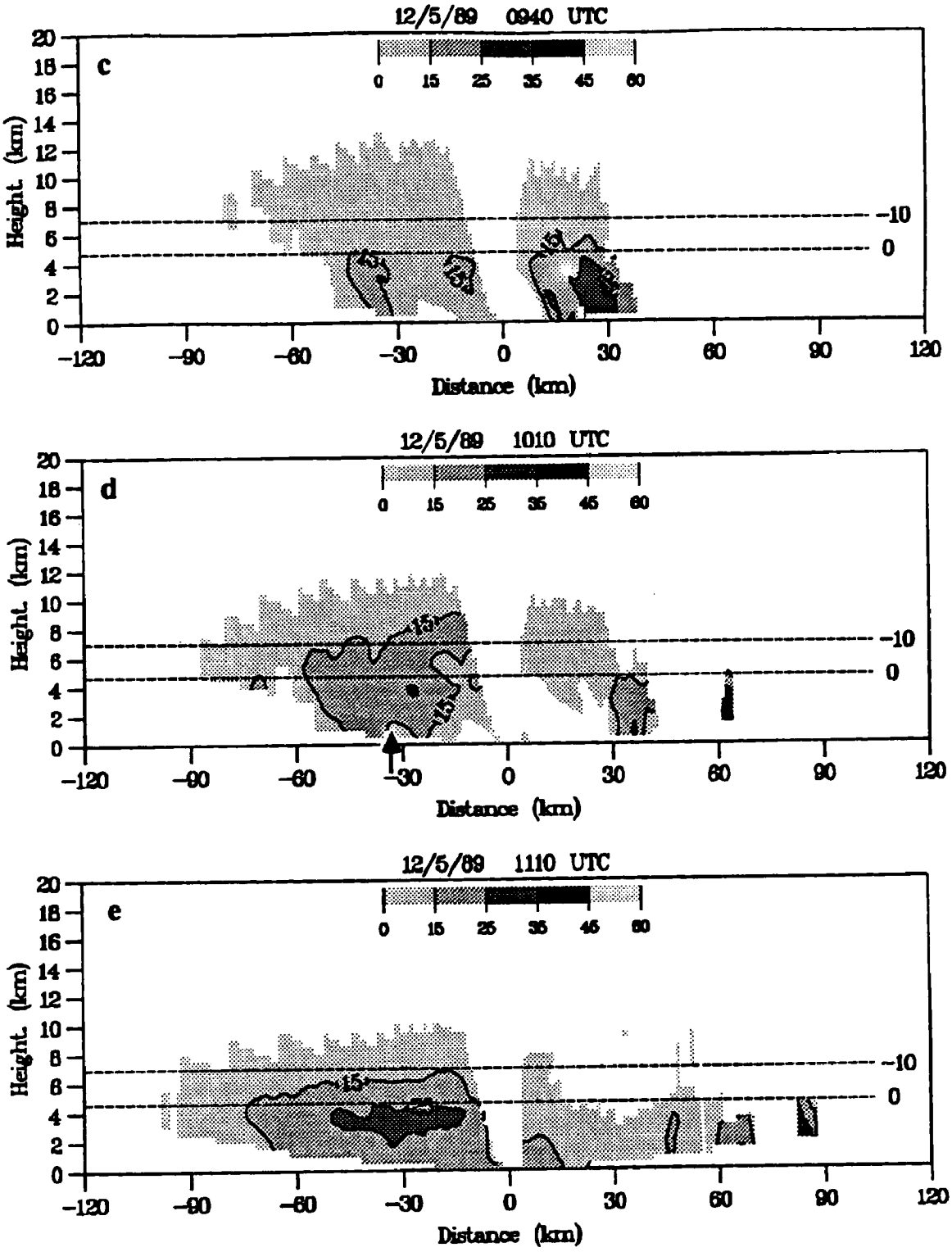


Figure 5.3 (c) 0940 UTC; (d) 1010 UTC (location of positive CG indicated by arrow at -35 km); (e) 1110 UTC.

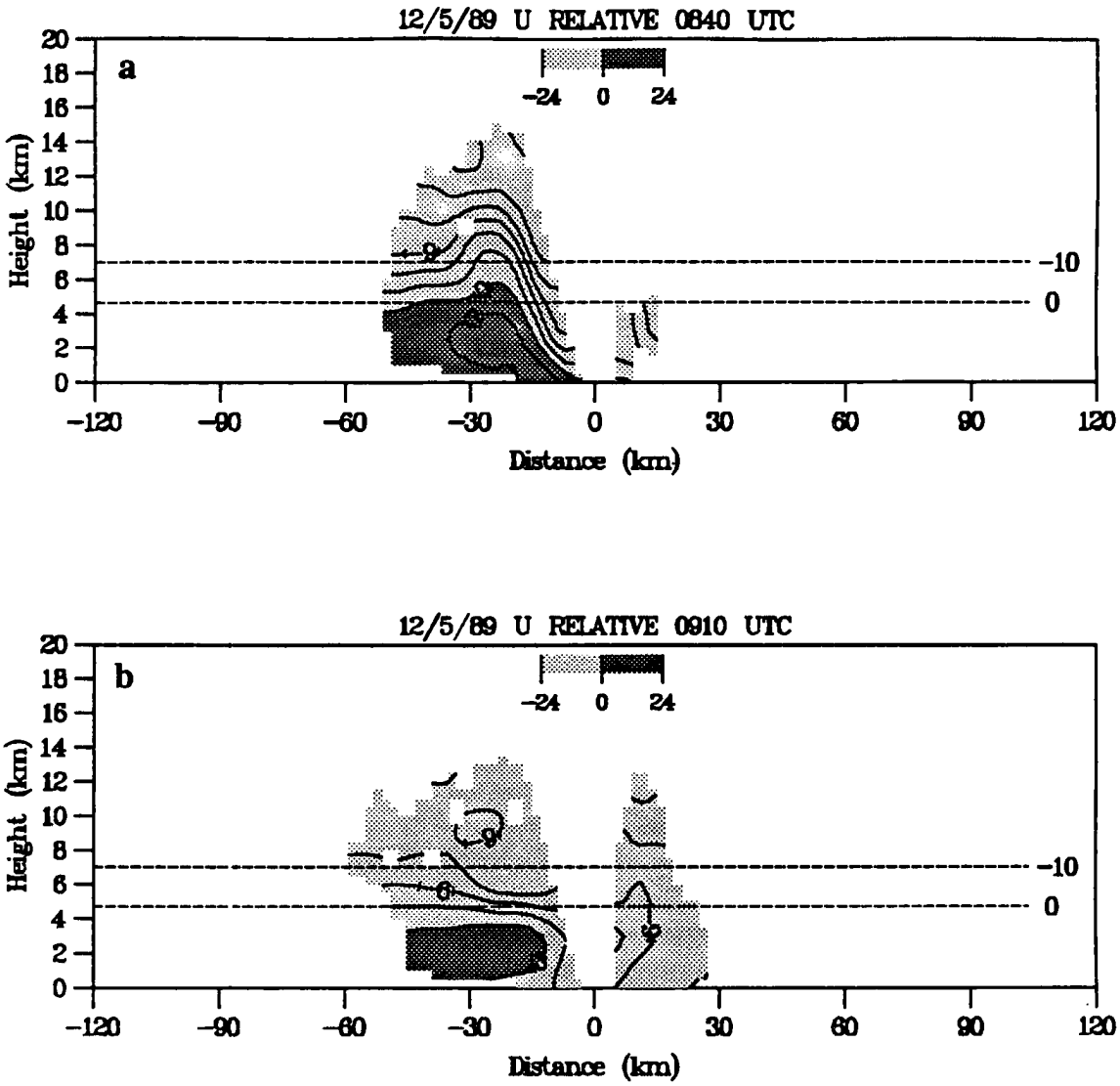


Figure 5.4 MIT radar line-normal (180° azimuth) cross-sections of storm relative horizontal velocities for 5 December 1989 at (a) 0840 UTC and (b) 0910 UTC. Velocities are contoured every 3 m s-1. Dark shaded areas represent velocities < 0 (i.e., storm relative velocity toward the left, oriented opposite to the propagation direction of the squall line), light shaded areas represent velocities > 0 m s-1 oriented parallel to the direction of squall line propagation (i.e., movement toward the right).

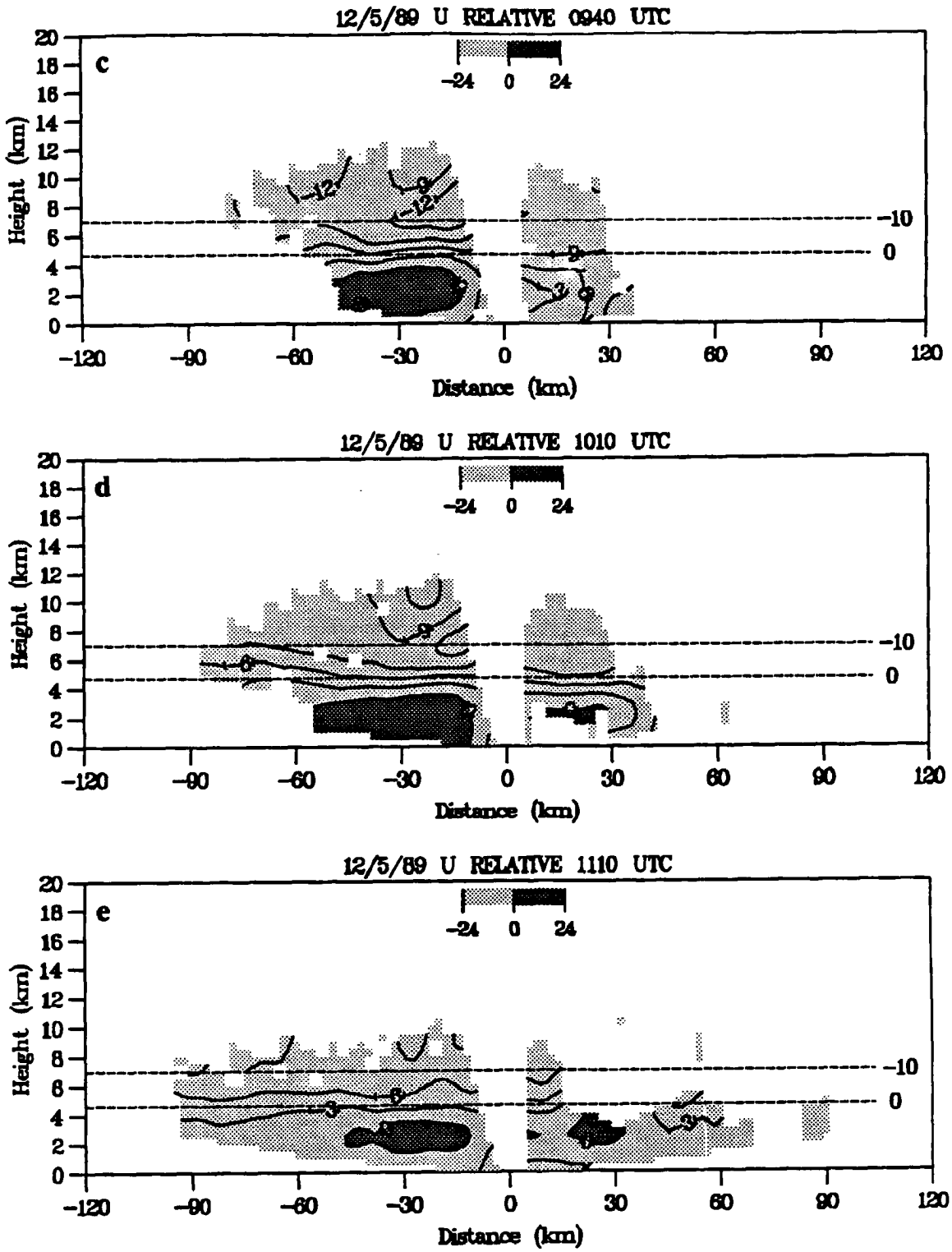


Figure 5.4 (c) 0940 UTC; (d) 1010 UTC; (e) 1110 UTC.

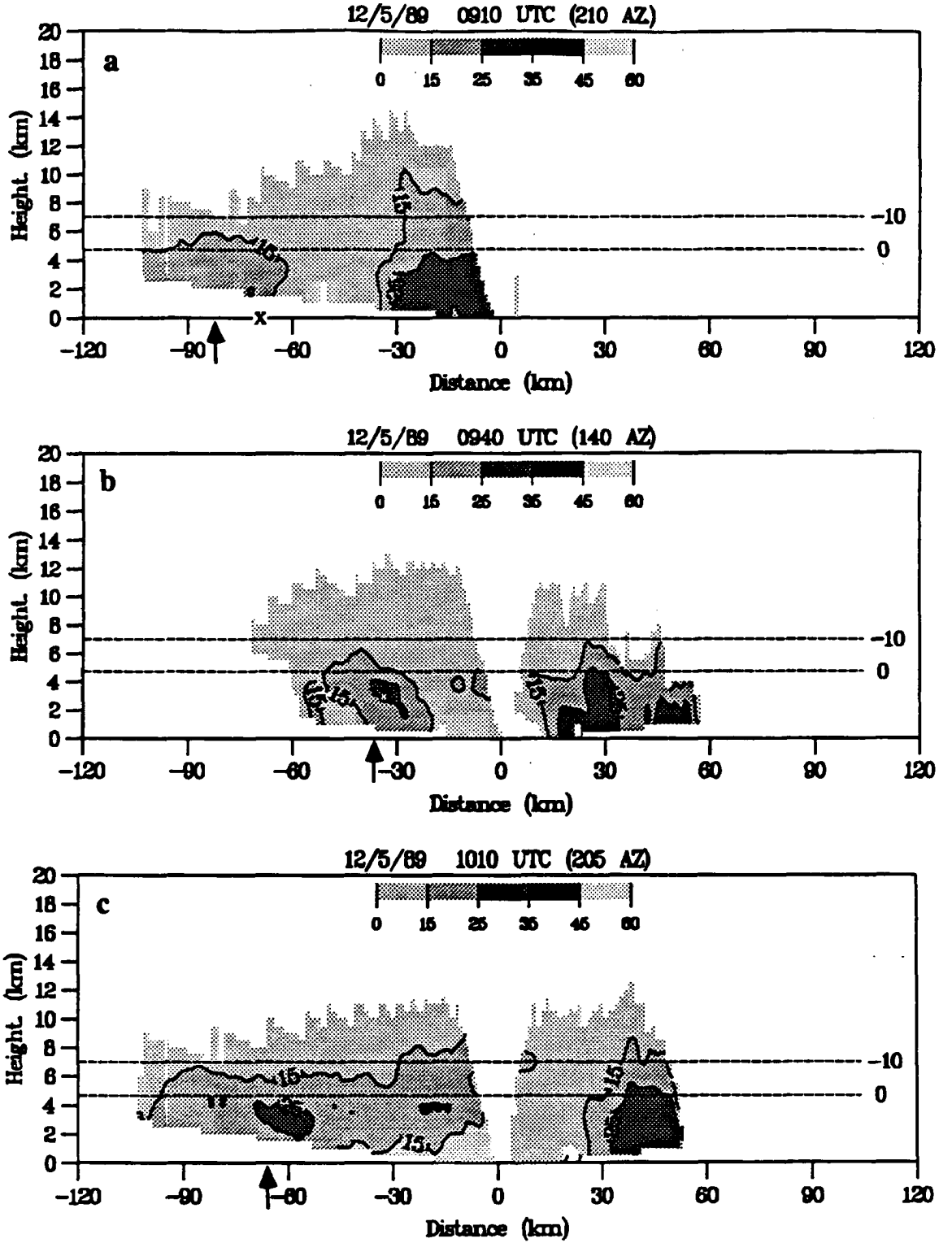


Figure 5.5 Same as Figure 5.3 except for (a) 0910 UTC 210° azimuth; (b) 0940 UTC 140° azimuth; and (c) 1010 UTC 205° azimuth. Arrows indicate positions of positive CGs, an "x" indicates the position of a negative CG.

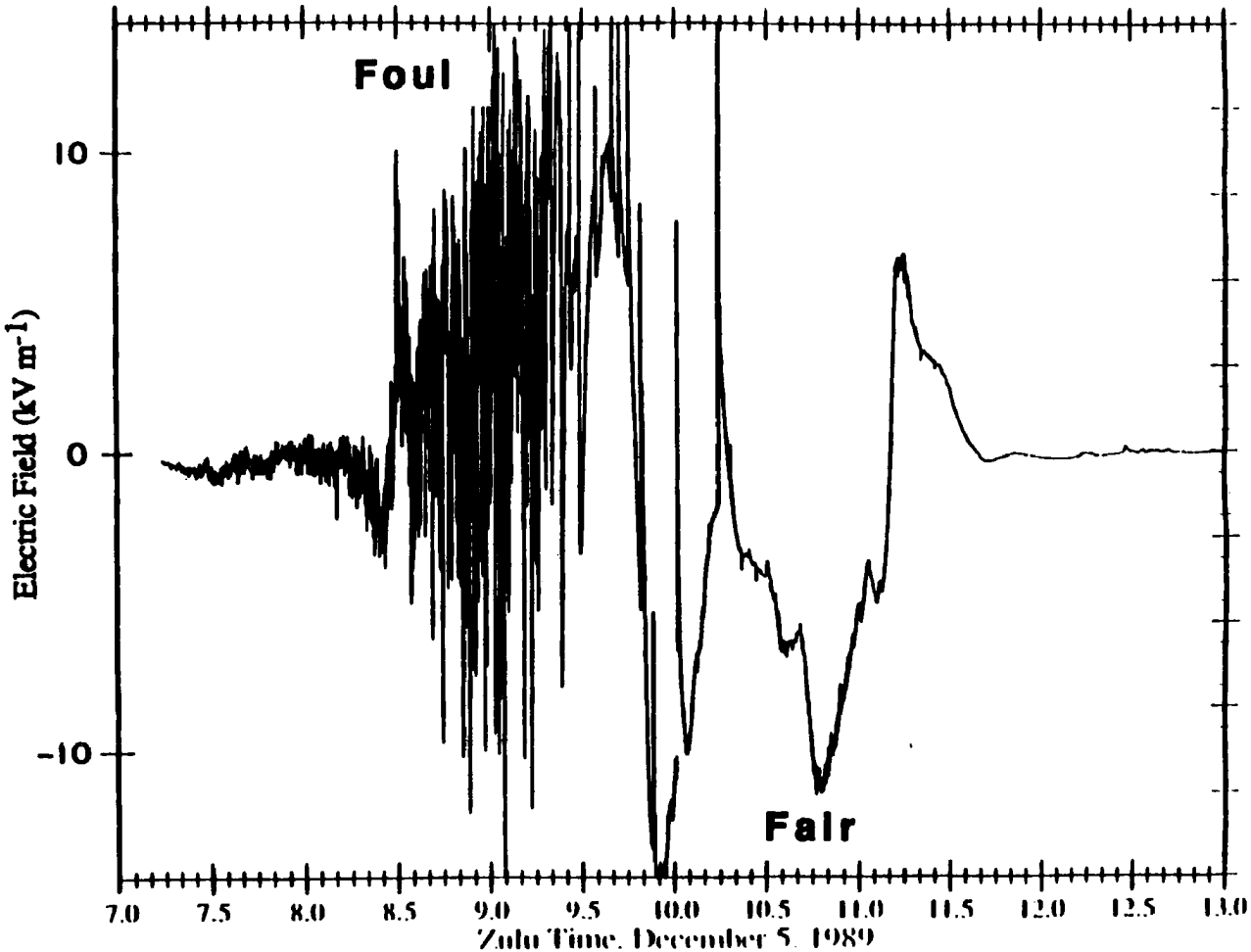


Figure 5.6 Surface electric field record for 5 December 1989 (0700-1300 UTC) measured at the MIT radar site. Positive values of the electric field (kV $m^{-1}$) indicate negative charge overhead, negative values indicate positive charge overhead. Large, rapid deviations in the trace indicate lightning flashes.

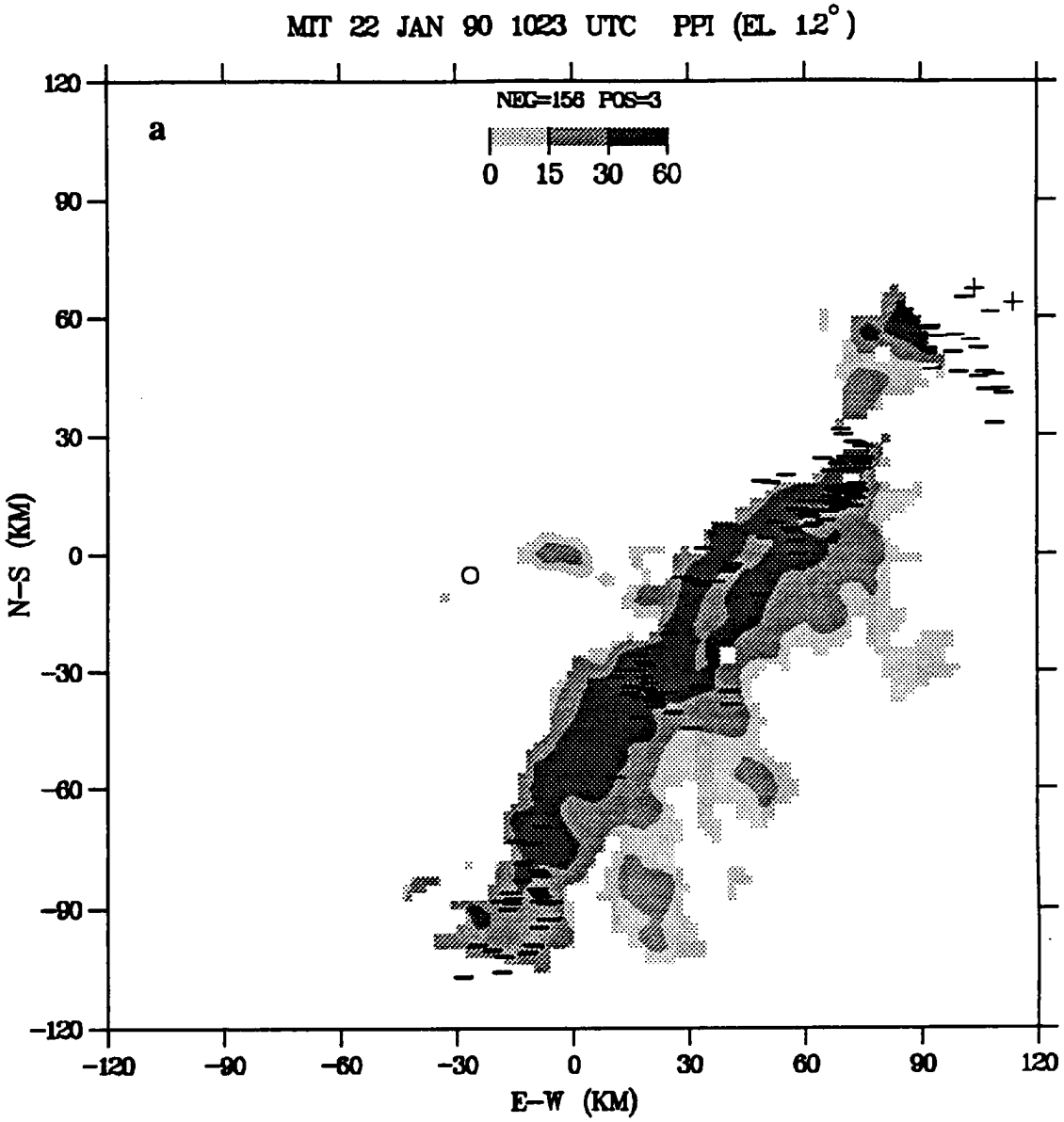


Figure 5.7 Same as Figure 5.1 except for 22 January 1990 at (a) 1023 UTC.

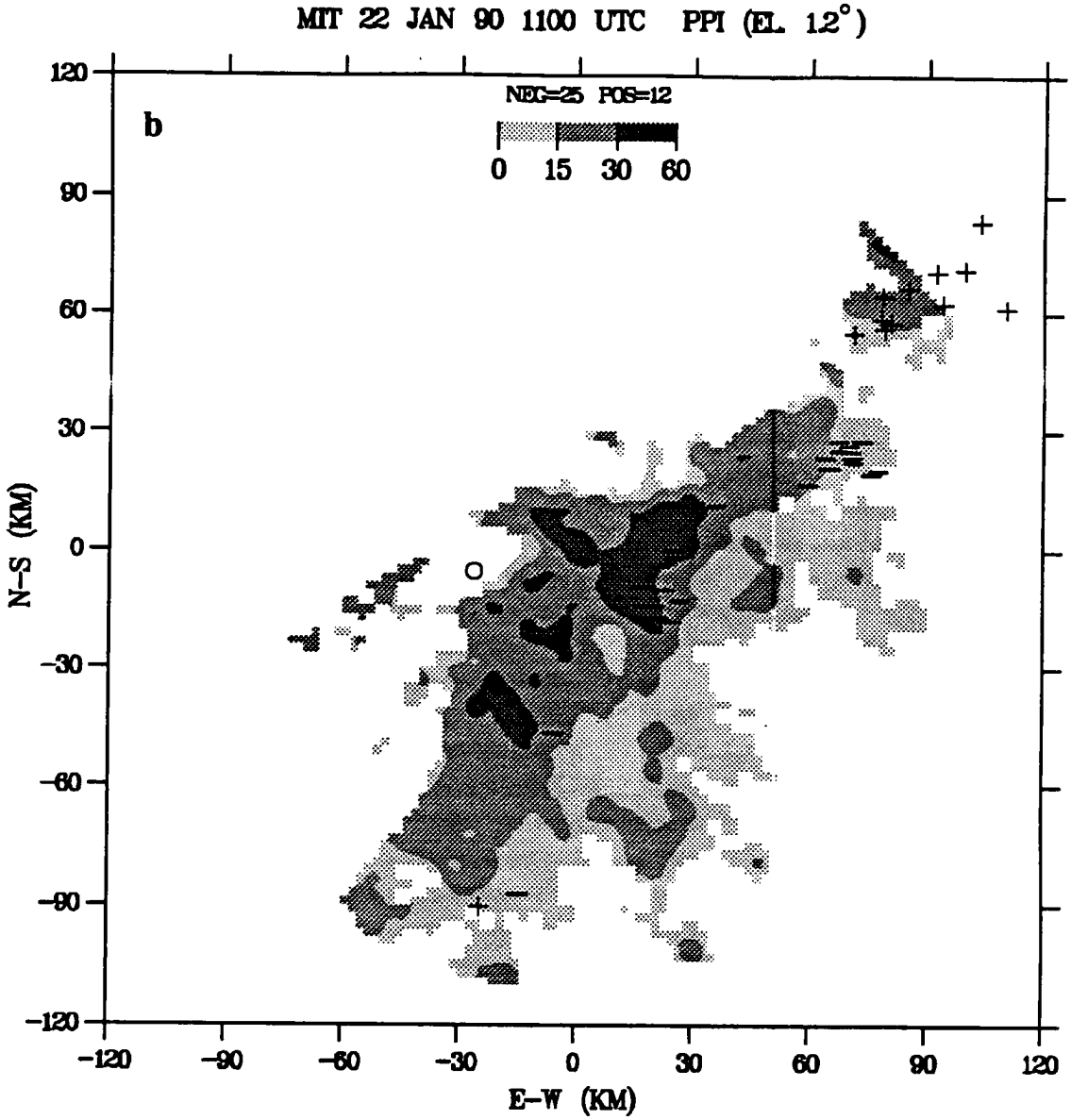


Figure 5.7 (b) 1100 UTC.

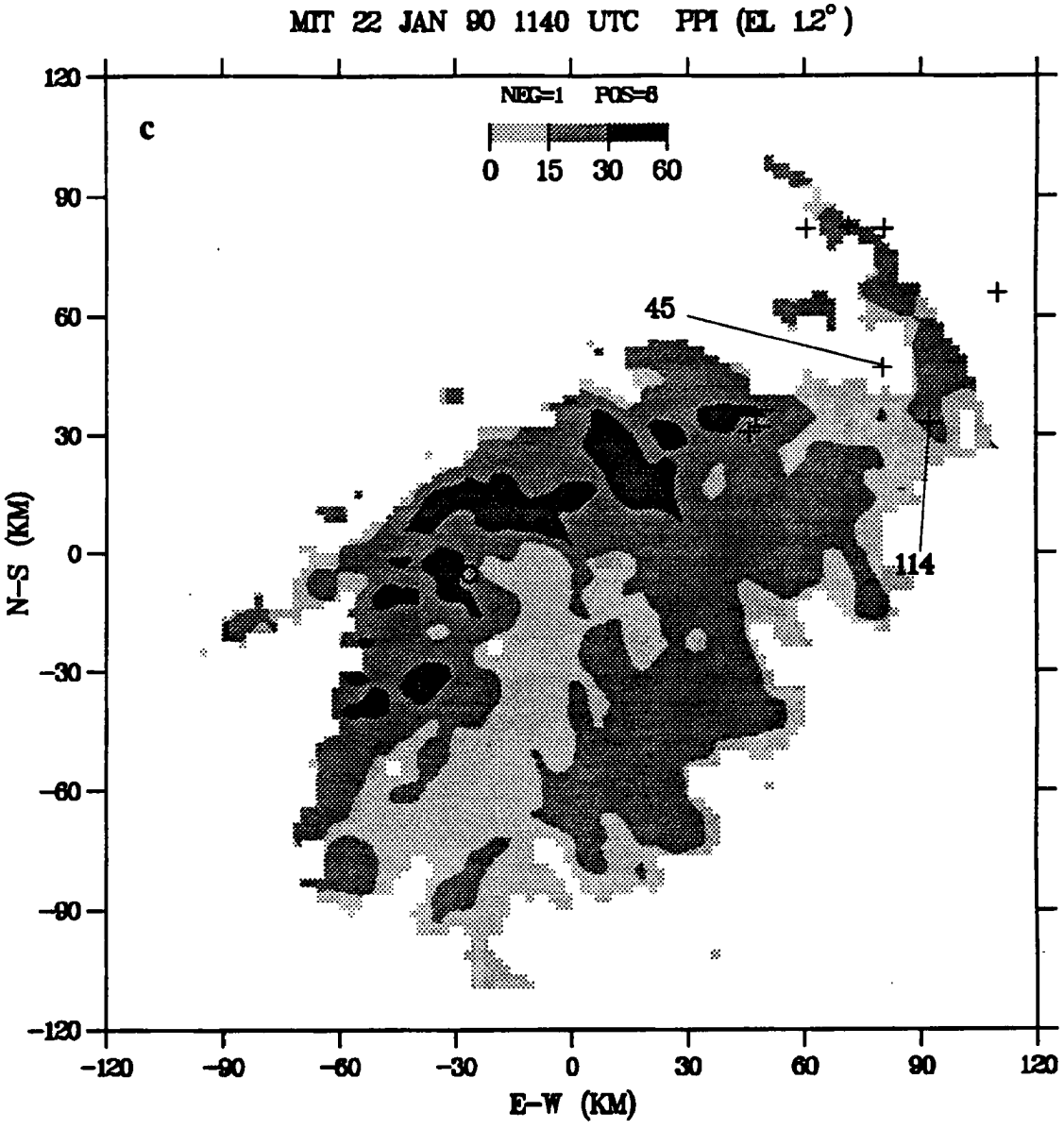


Figure 5.7 (c) 1140 UTC. Positive peak current extrema identified as 45 and 114 kA.

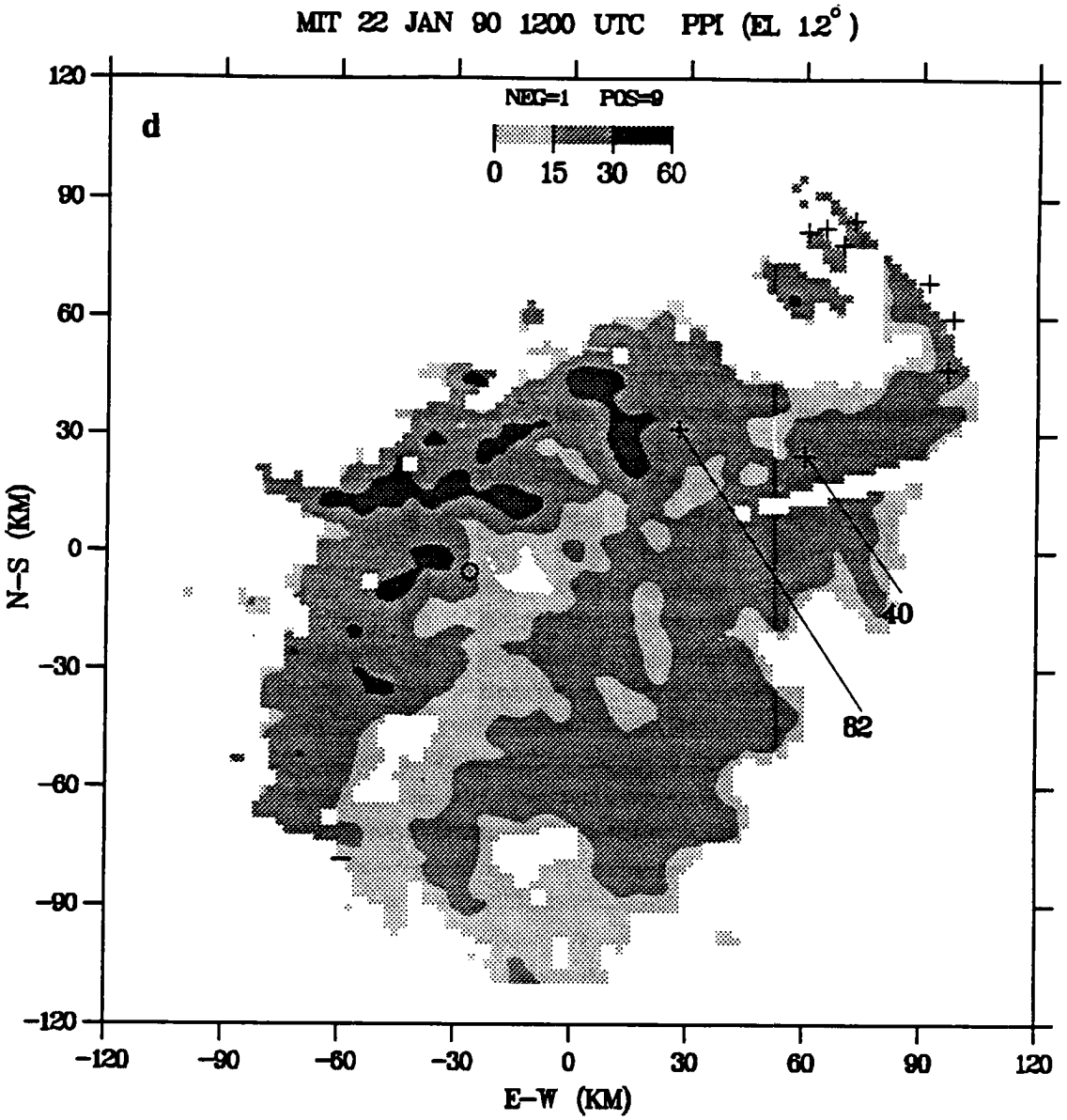


Figure 5.7 (d) 1200 UTC. Positive peak current extrema identified as 40 and 82 kA.

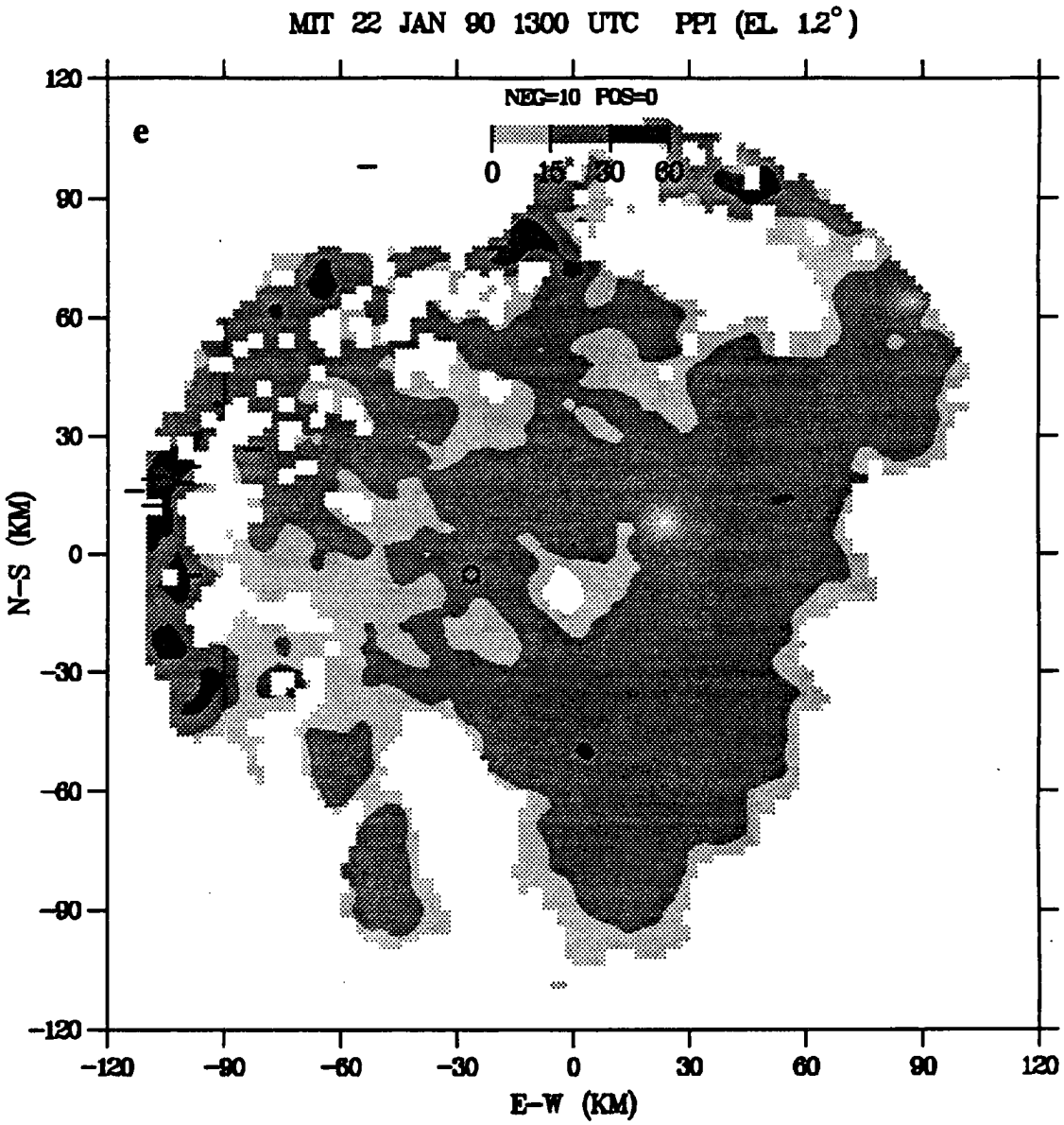


Figure 5.7 (e) 1300 UTC.

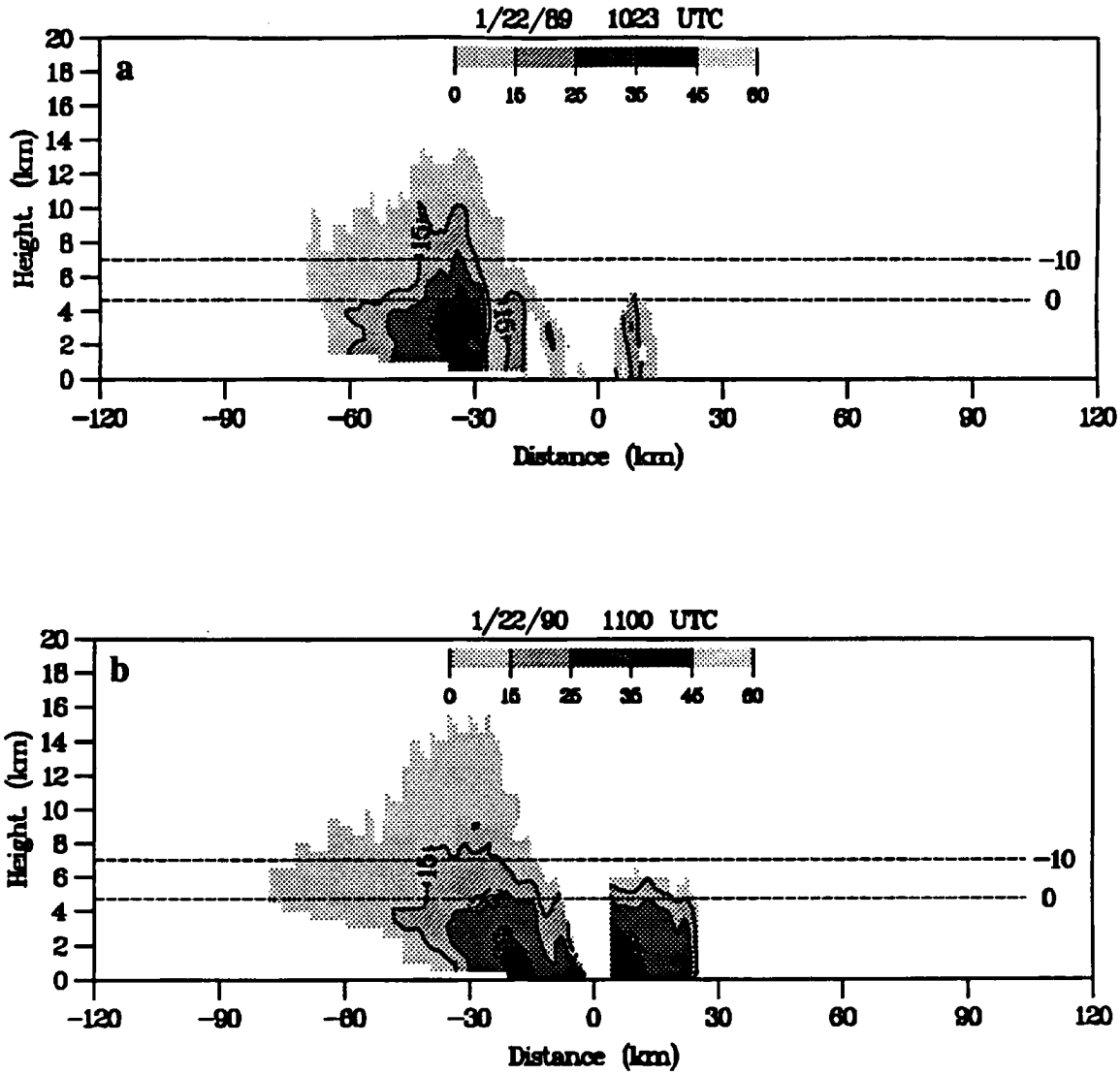


Figure 5.8 Same as Figure 5.3 except for 22 January 1990 (130° azimuth) at (a) 1023 UTC and (b) 1100 UTC.

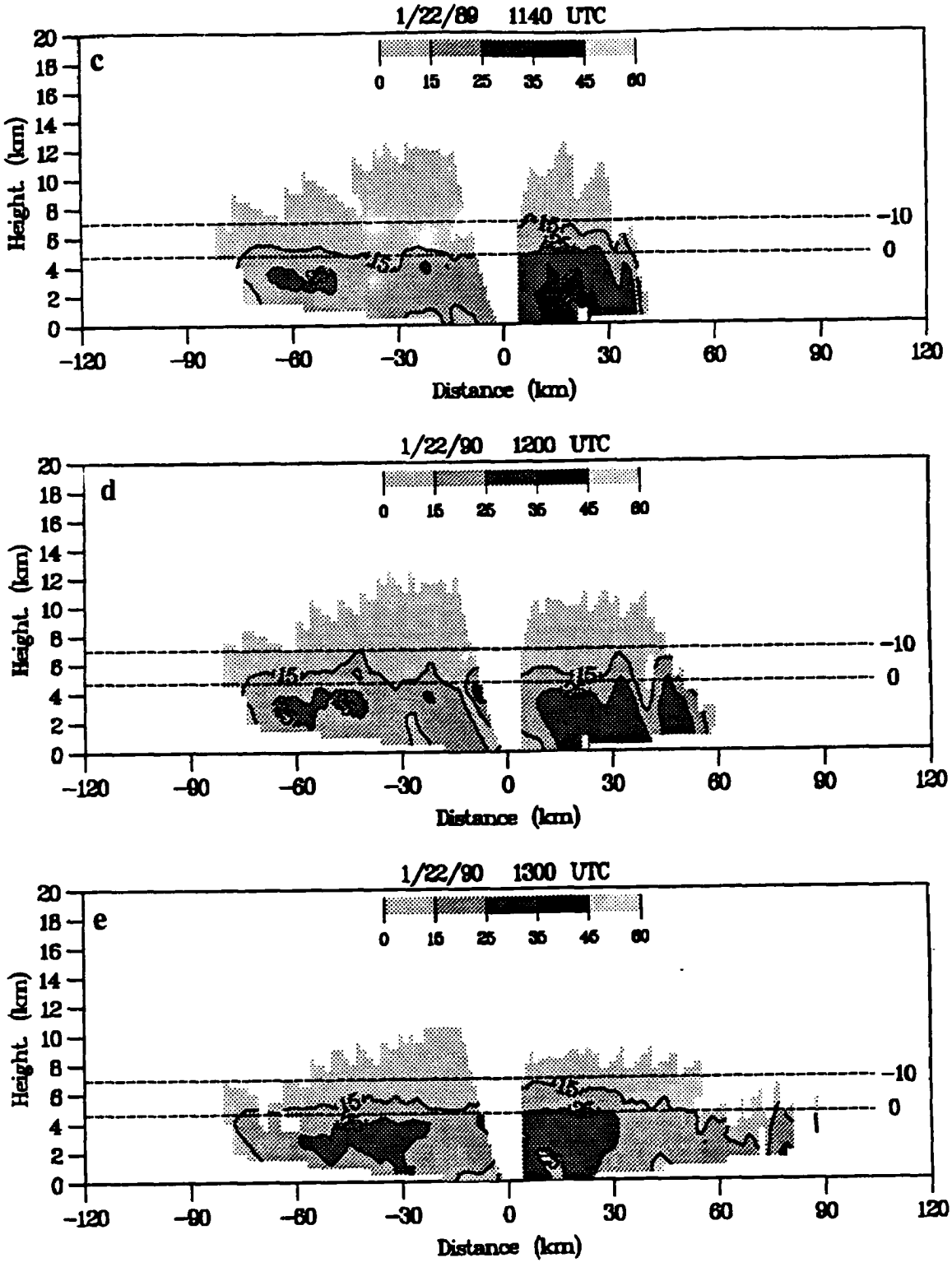


Figure 5.8 (c) 1140 UTC; (d) 1200 UTC; (e) 1300 UTC.

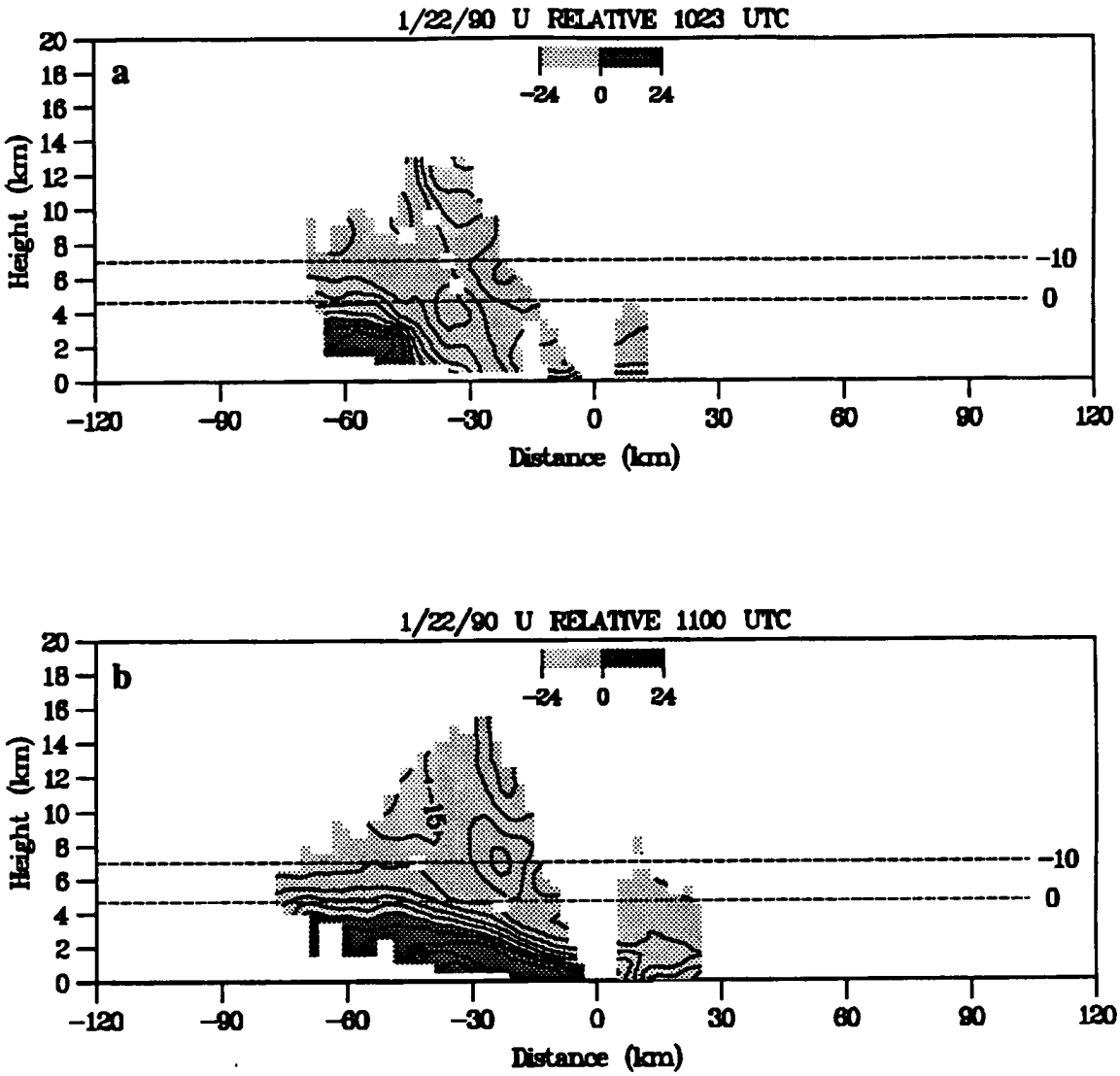


Figure 5.9 Same as Figure 5.4 except for 22 January 1990 (130° azimuth) at (a) 1023 UTC and (b) 1100 UTC.

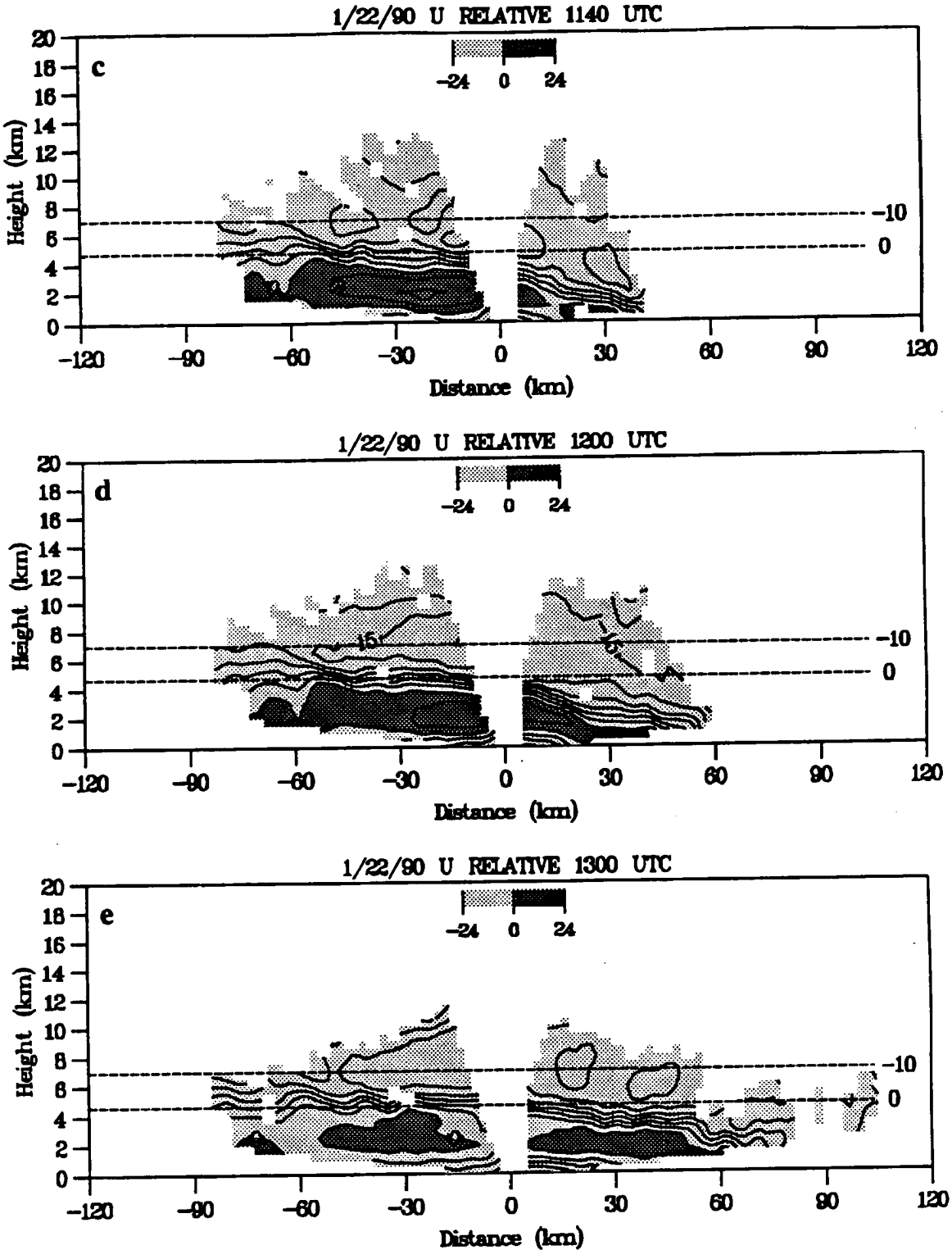


Figure 5.9 (c) 1140 UTC; (d) 1200 UTC; (e) 1300 UTC.

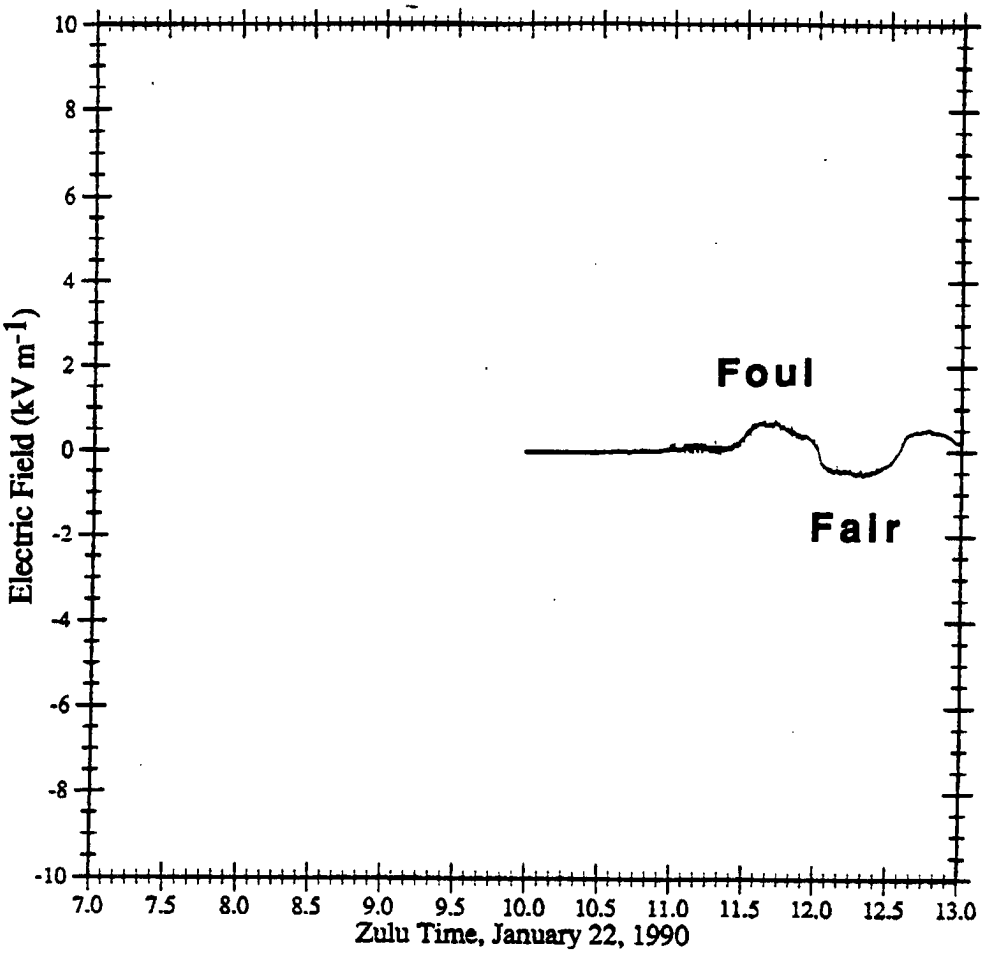


Figure 5.10 Surface electric field record for 22 January 1990 (1000-1300 UTC) measured at the MIT radar site (same sign convention as Figure 5.6).

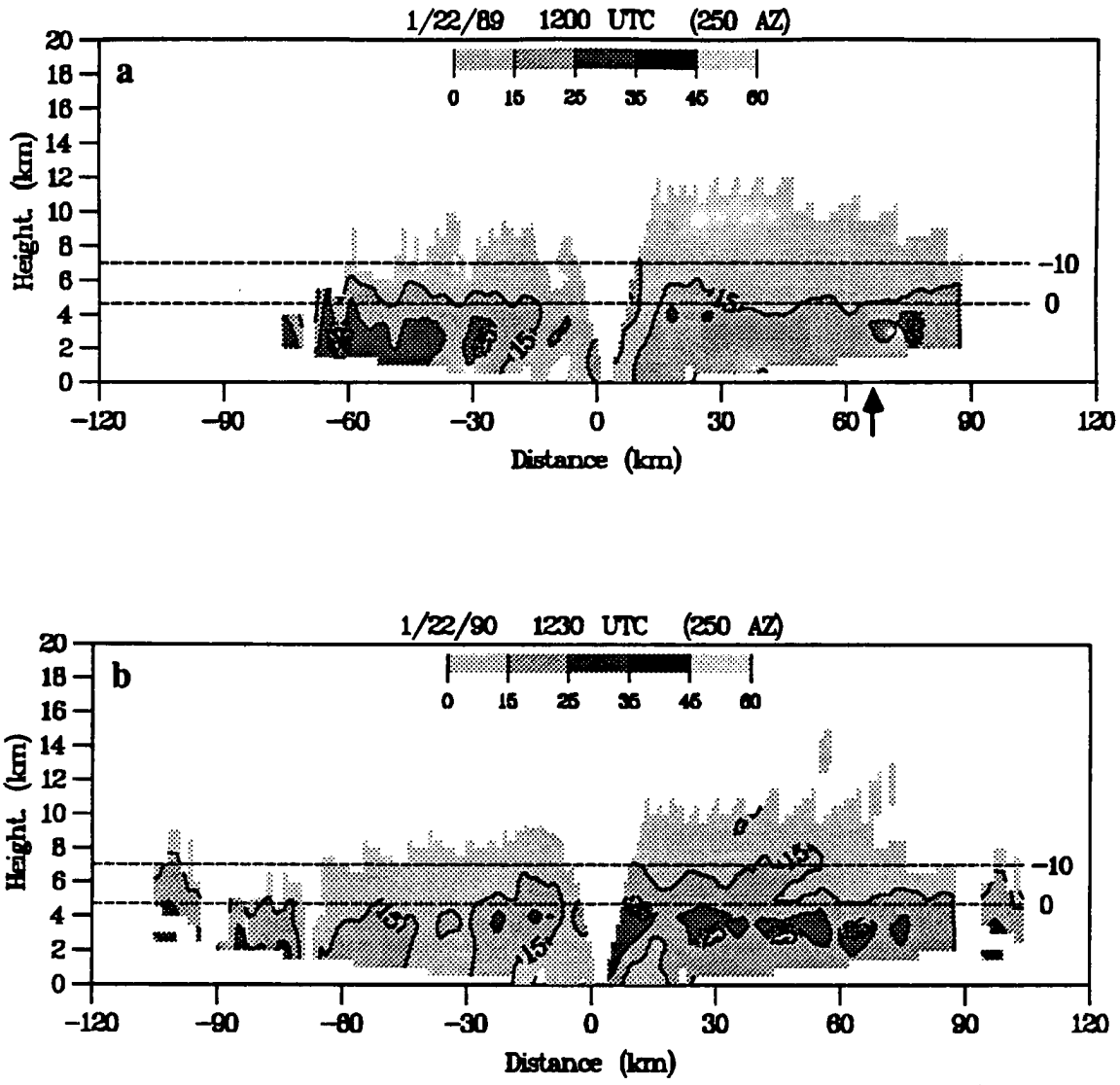


Figure 5.11 Same as Figure 5.3 except for 22 January 1990 at (a) 1200 UTC 250° azimuth (arrow indicates position of positive CG); and (b) 1230 UTC 250° azimuth.

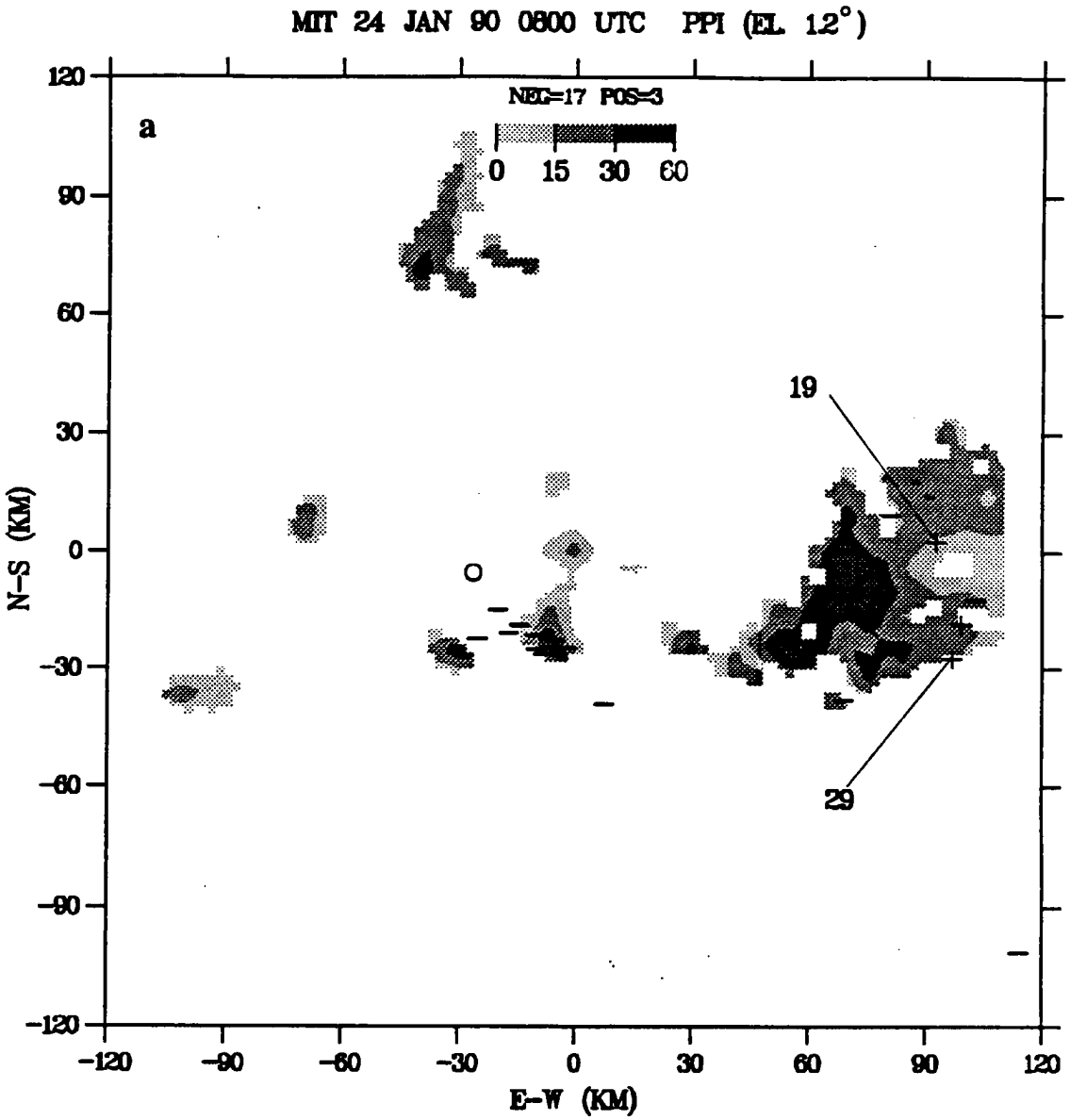


Figure 5.12 Same as Figure 5.1 except for 24 January 1990 at (a) 0800 UTC (positive peak current extrema identified as 19 and 29 kA).

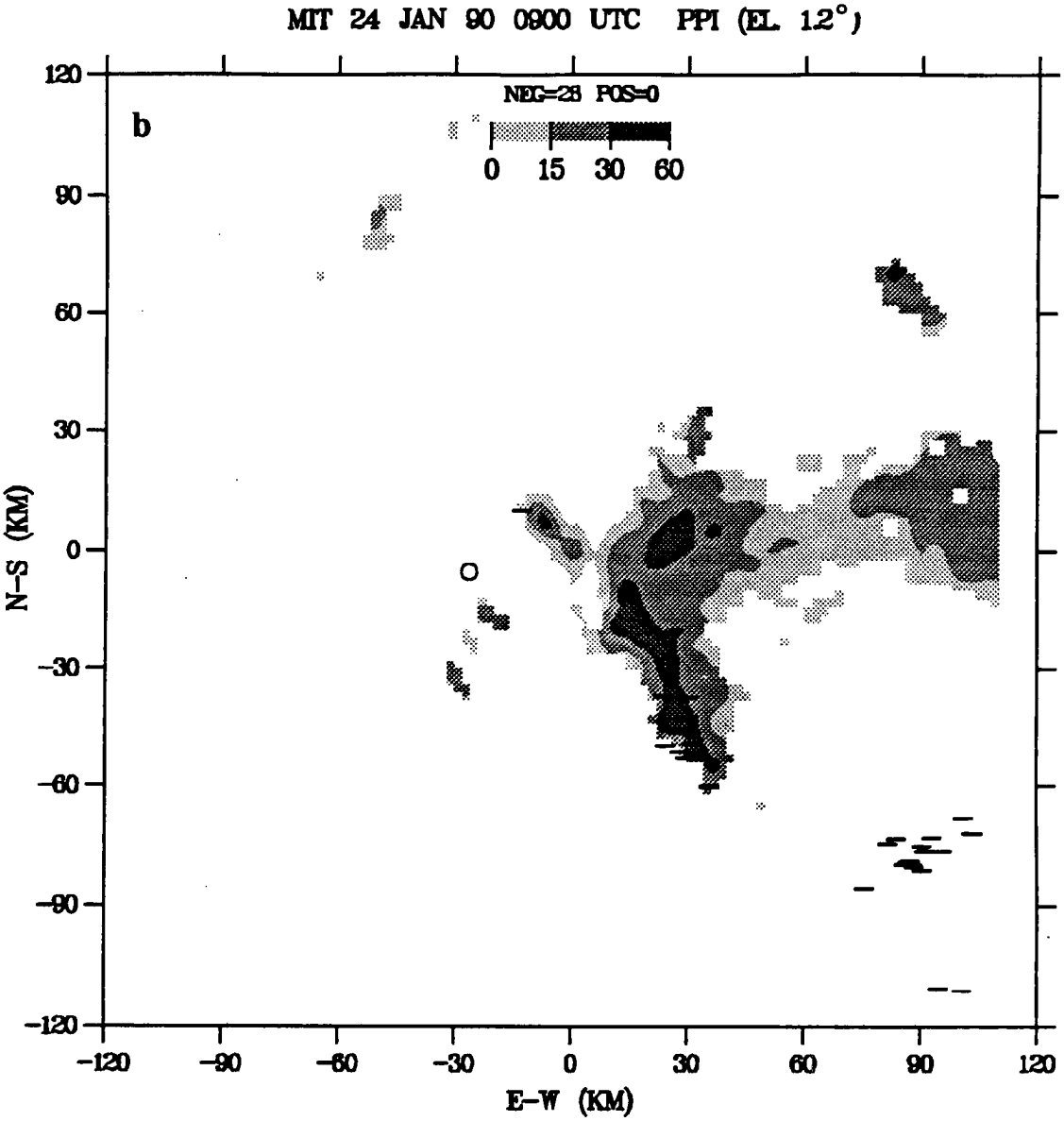


Figure 5.12 (b) 0900 UTC.

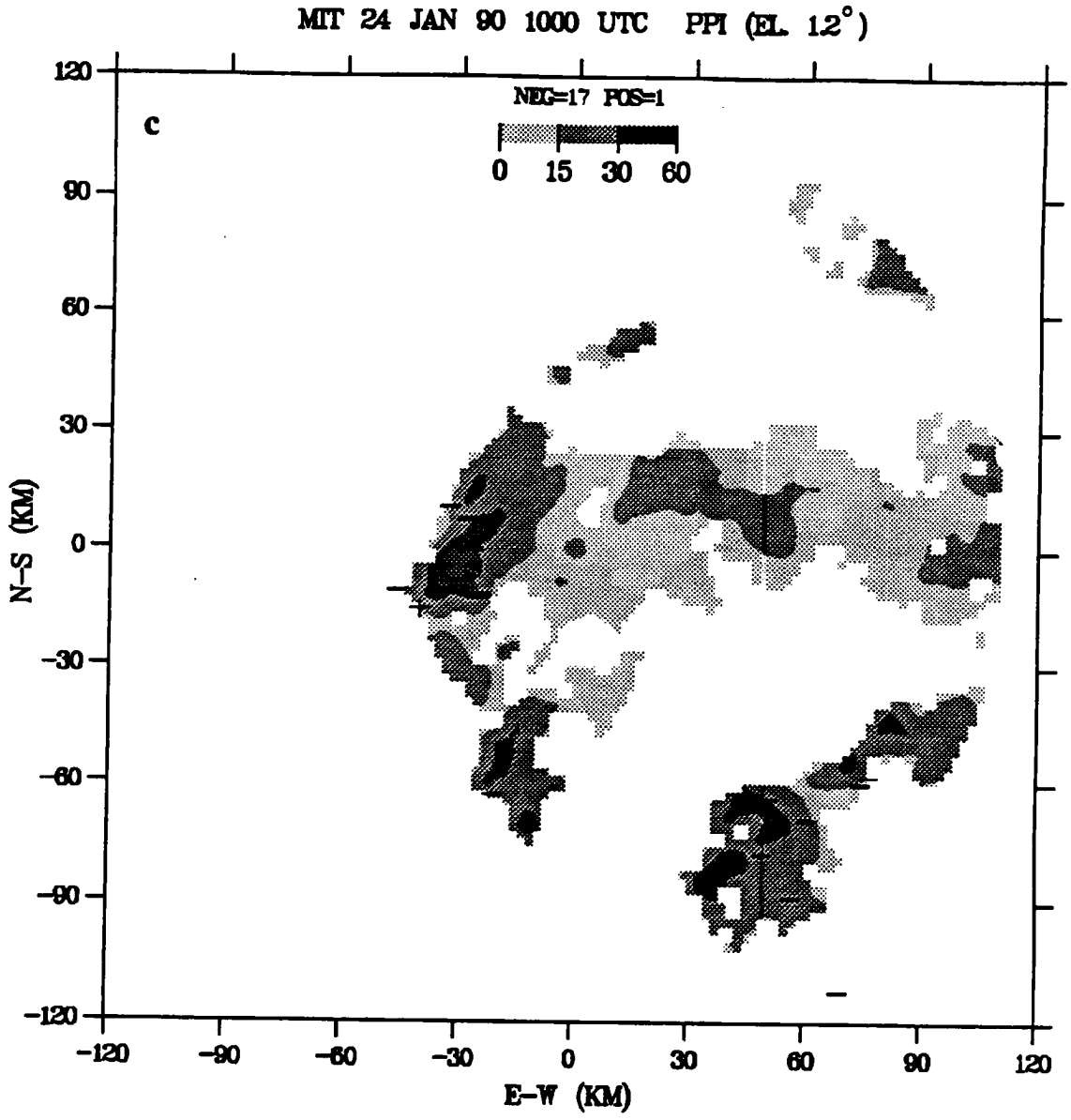


Figure 5.12 (c) 1000 UTC.

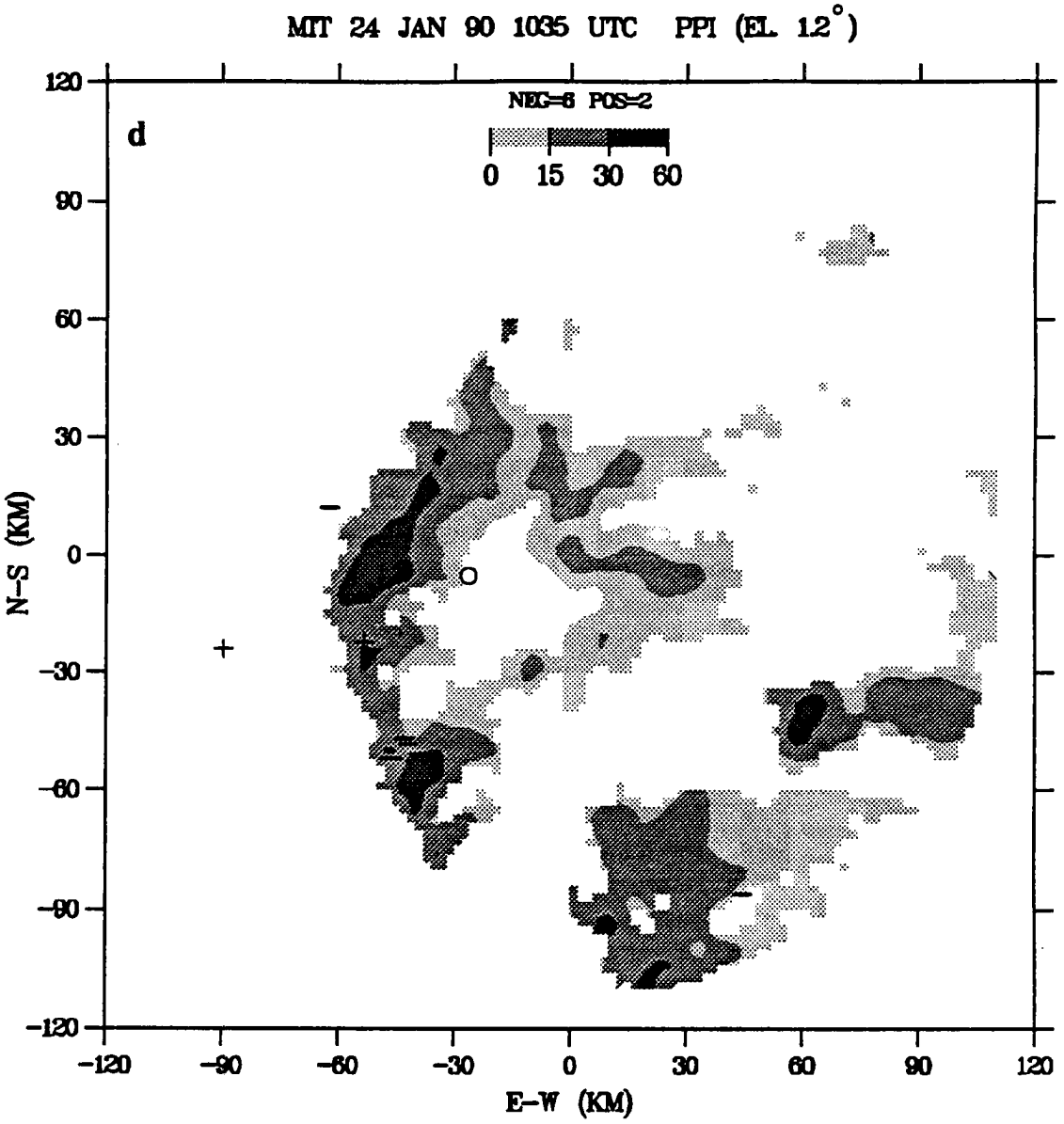


Figure 5.12 (d) 1035 UTC.

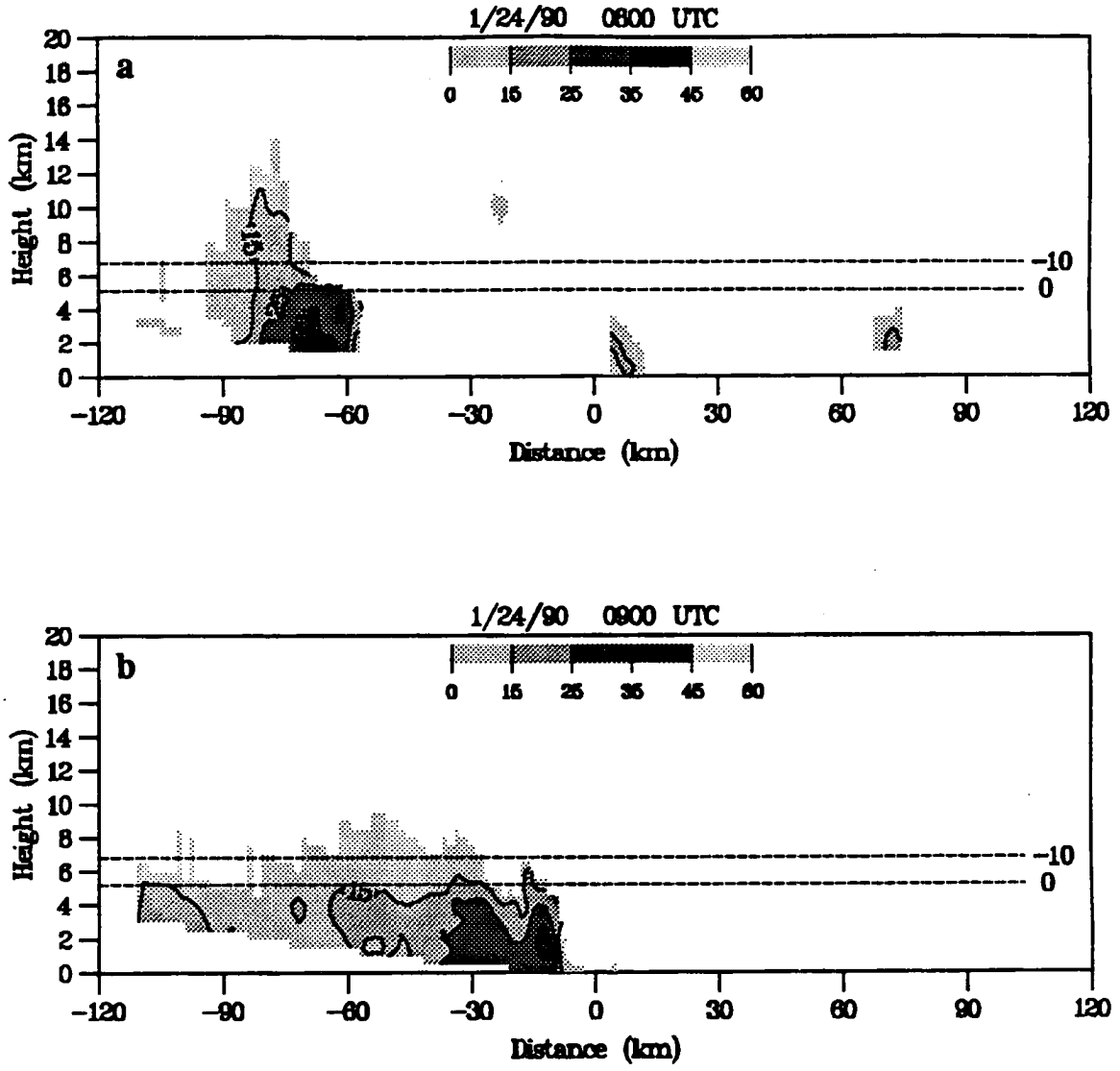


Figure 5.13 Same as Figure 5.3 except for 24 January 1990 (090° azimuth) at (a) 0800 UTC and (b) 0900 UTC.

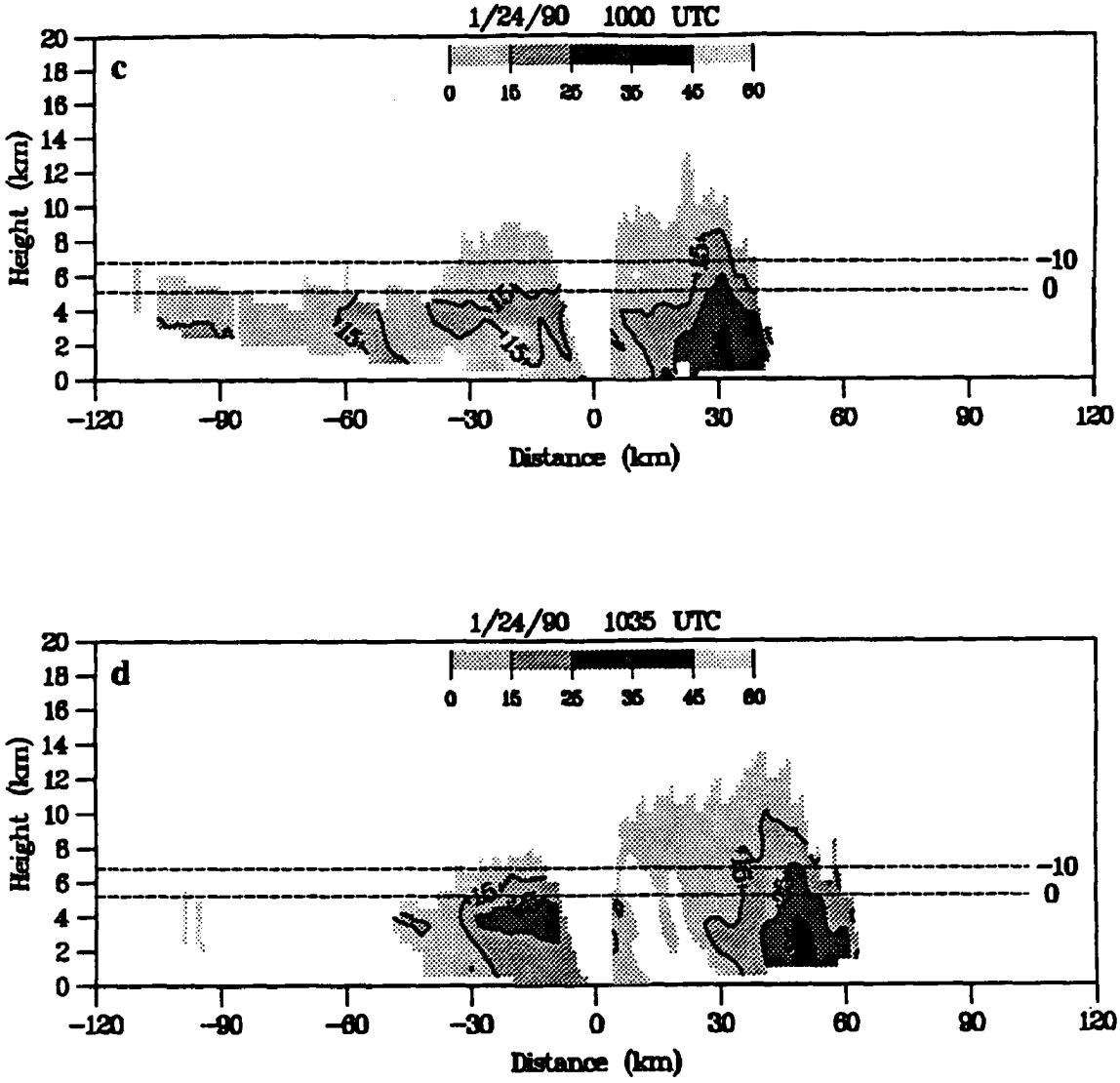


Figure 5.13 (c) 1000 UTC; (d) 1035 UTC.

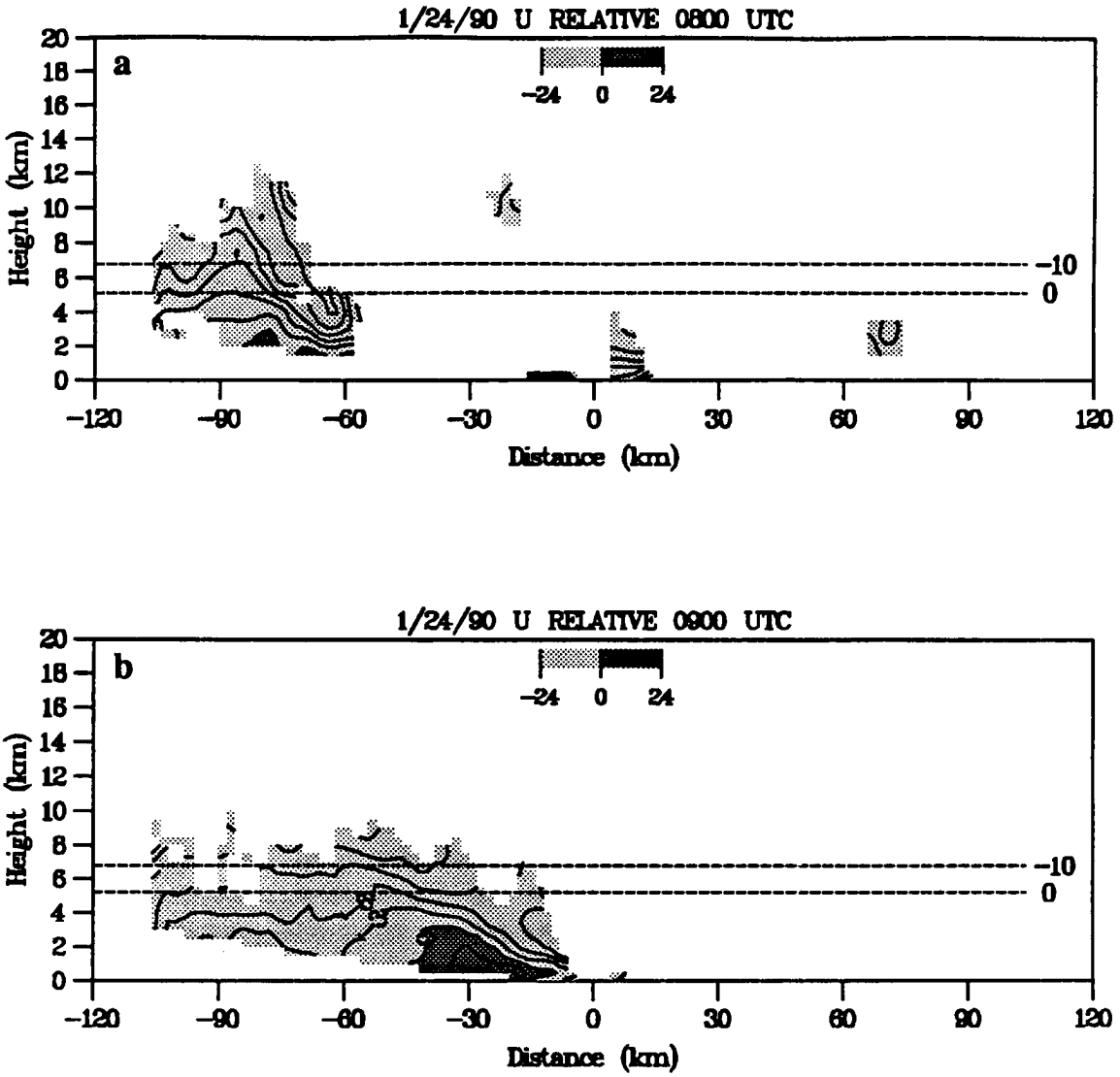


Figure 5.14 Same as Figure 5.4 except for 24 January 1990 (090° azimuth) at (a) 0800 UTC and (b) 0900 UTC.

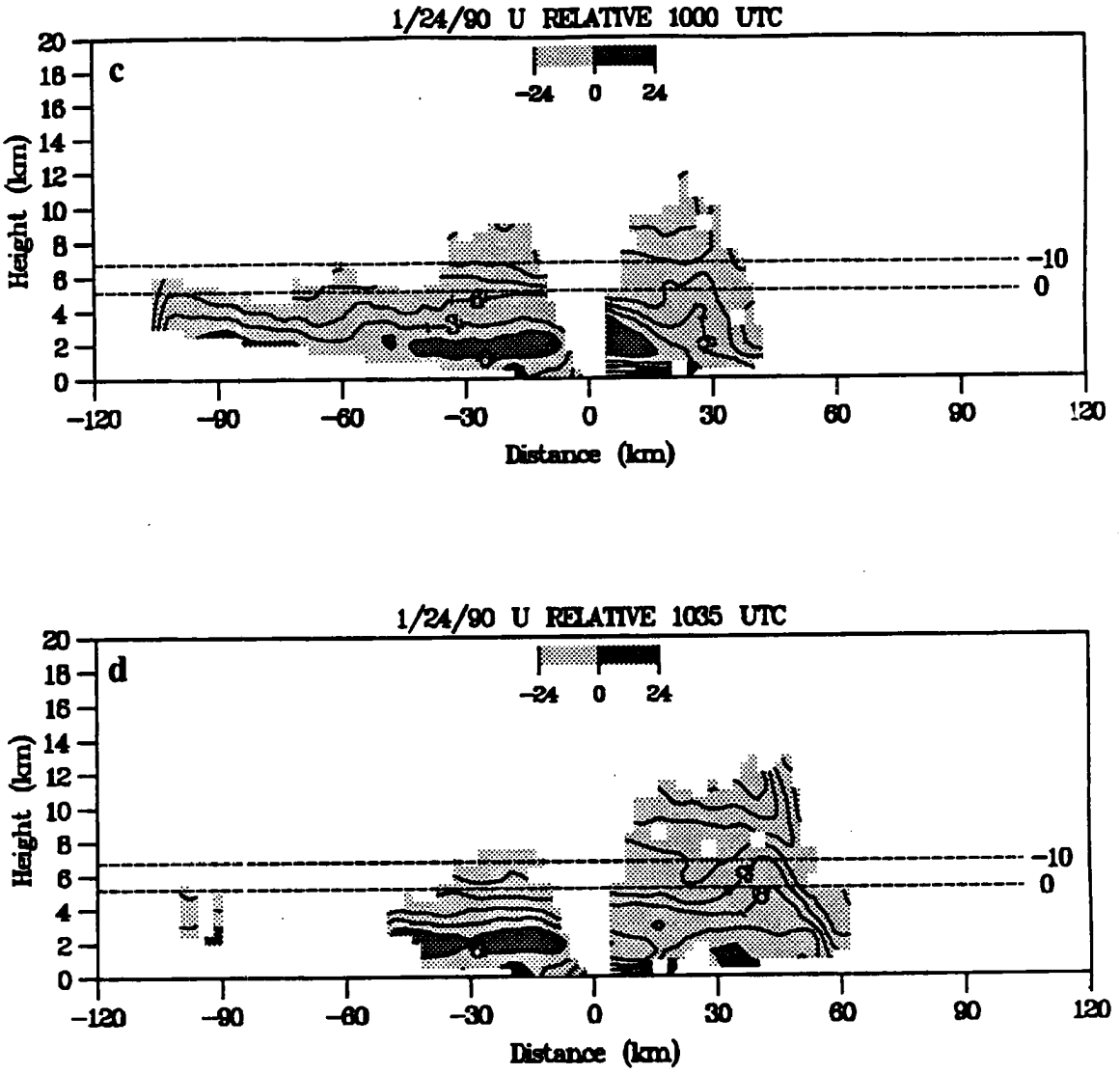


Figure 5.14 (c) 1000 UTC; (d) 1035 UTC.

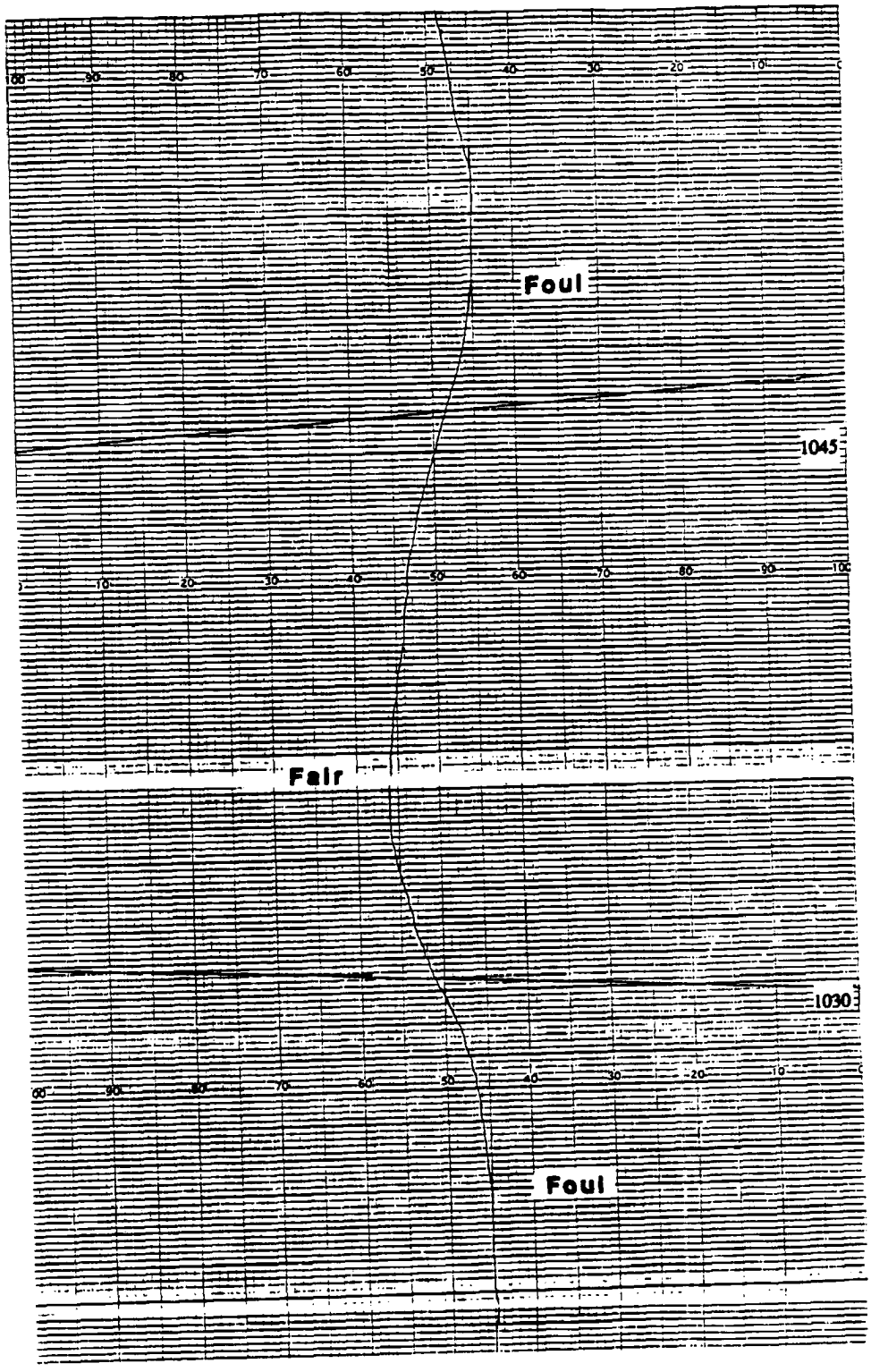


Figure 5.15 Surface electric field record for 24 January 1990 (1020-1100 UTC) measured at the MIT radar site (non-digitized). "Fair" indicates positive charge overhead, "Foul" indicates negative charge overhead.

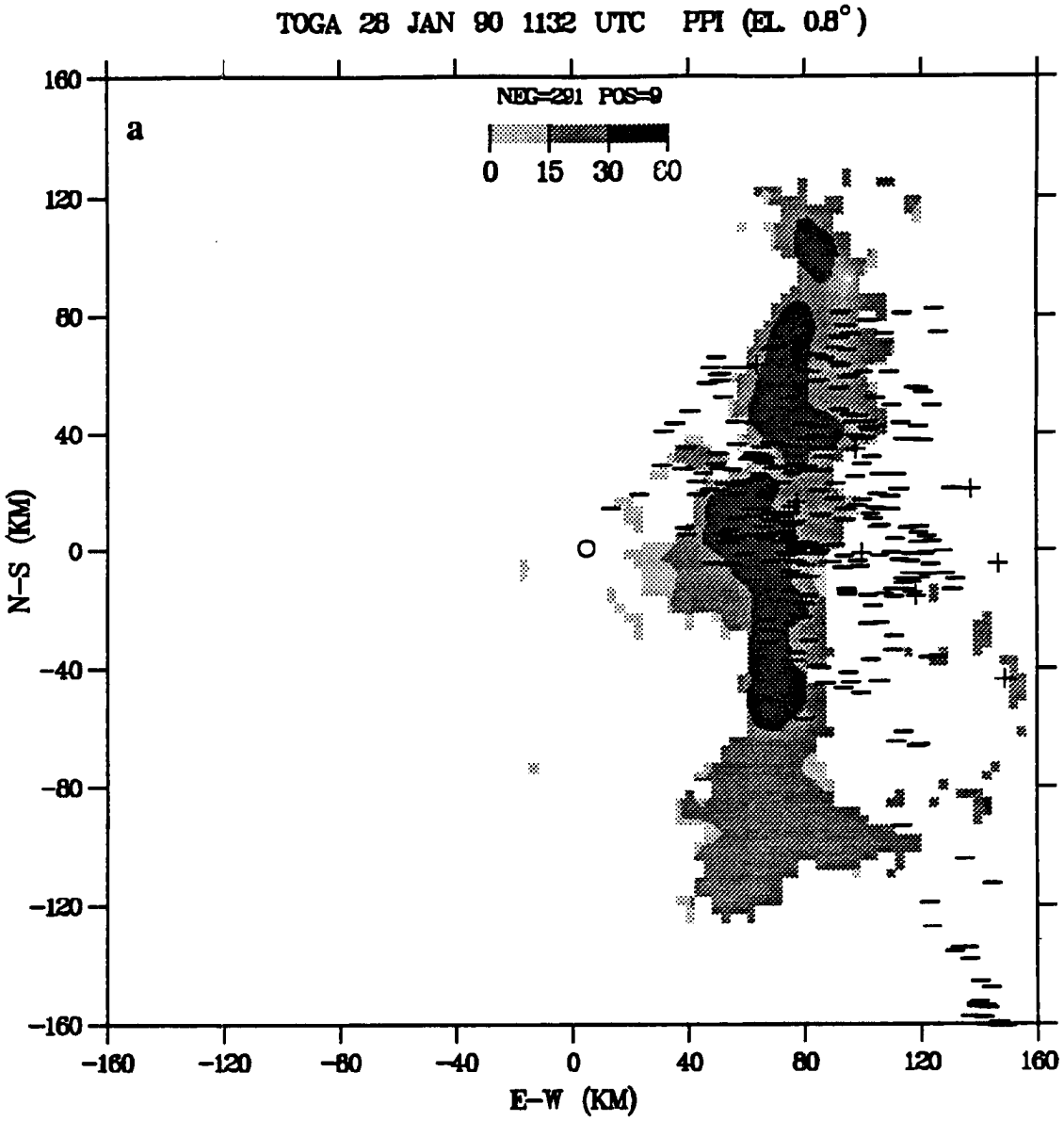


Figure 5.16 TOGA radar low level (0.8° elevation) PPI of reflectivity and cloud-to-ground lightning (30 minute interval centered on the time of the radar scan), for 28 January 1990 at 1132 UTC. The TOGA radar is centered at (0,0) and the labeling convention for lightning is the same as Figure 5.1. The wind profiler (denoted by an open circle) is located 5 km east of the radar.

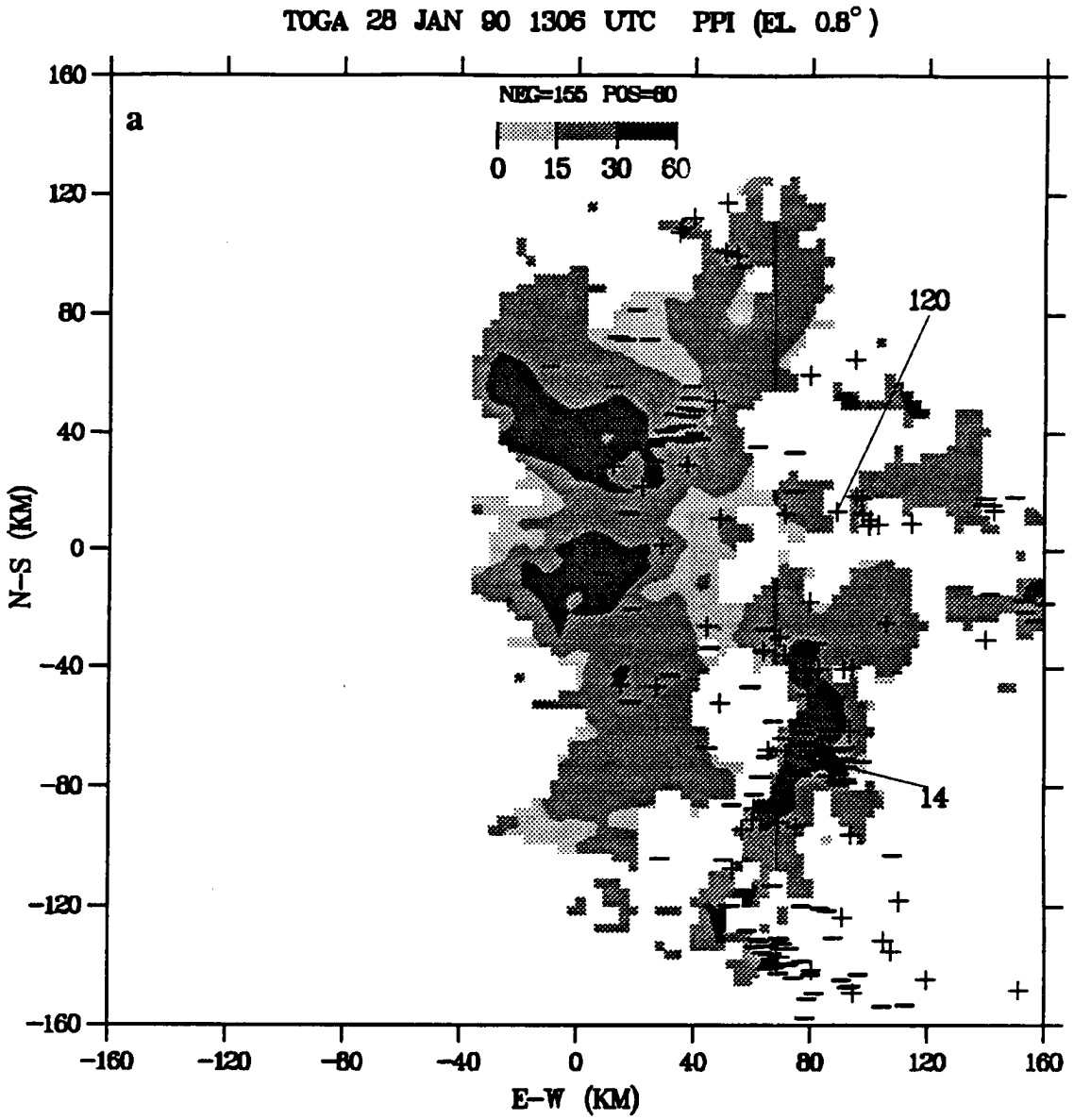


Figure 5.17. Same as Figure 5.16 except for (a) 1306 UTC (peak current extrema identified as 14 and 120 kA).

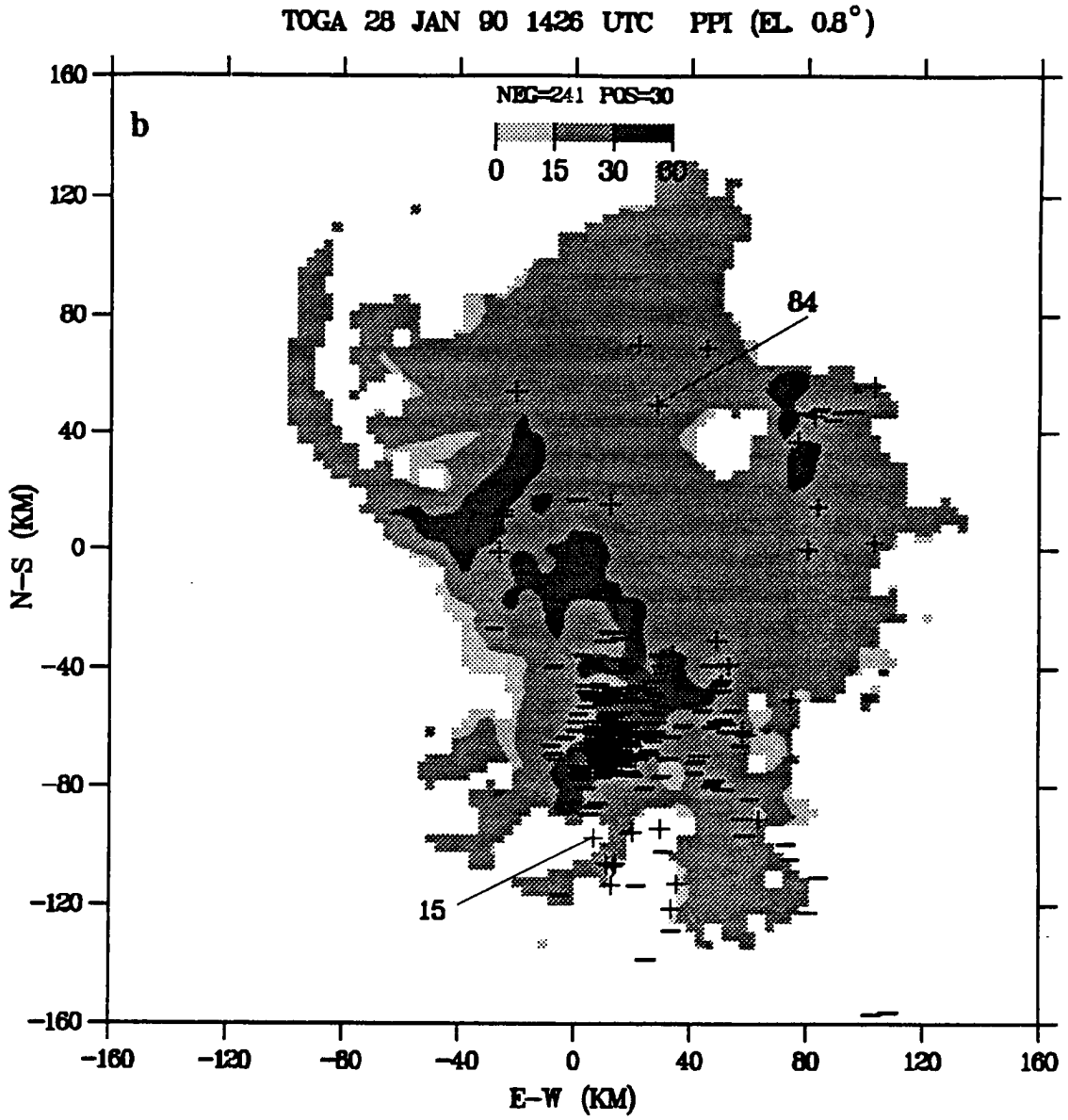


Figure 5.17 (b) 1426 UTC. Peak current extrema identified as 15 and 84 kA.

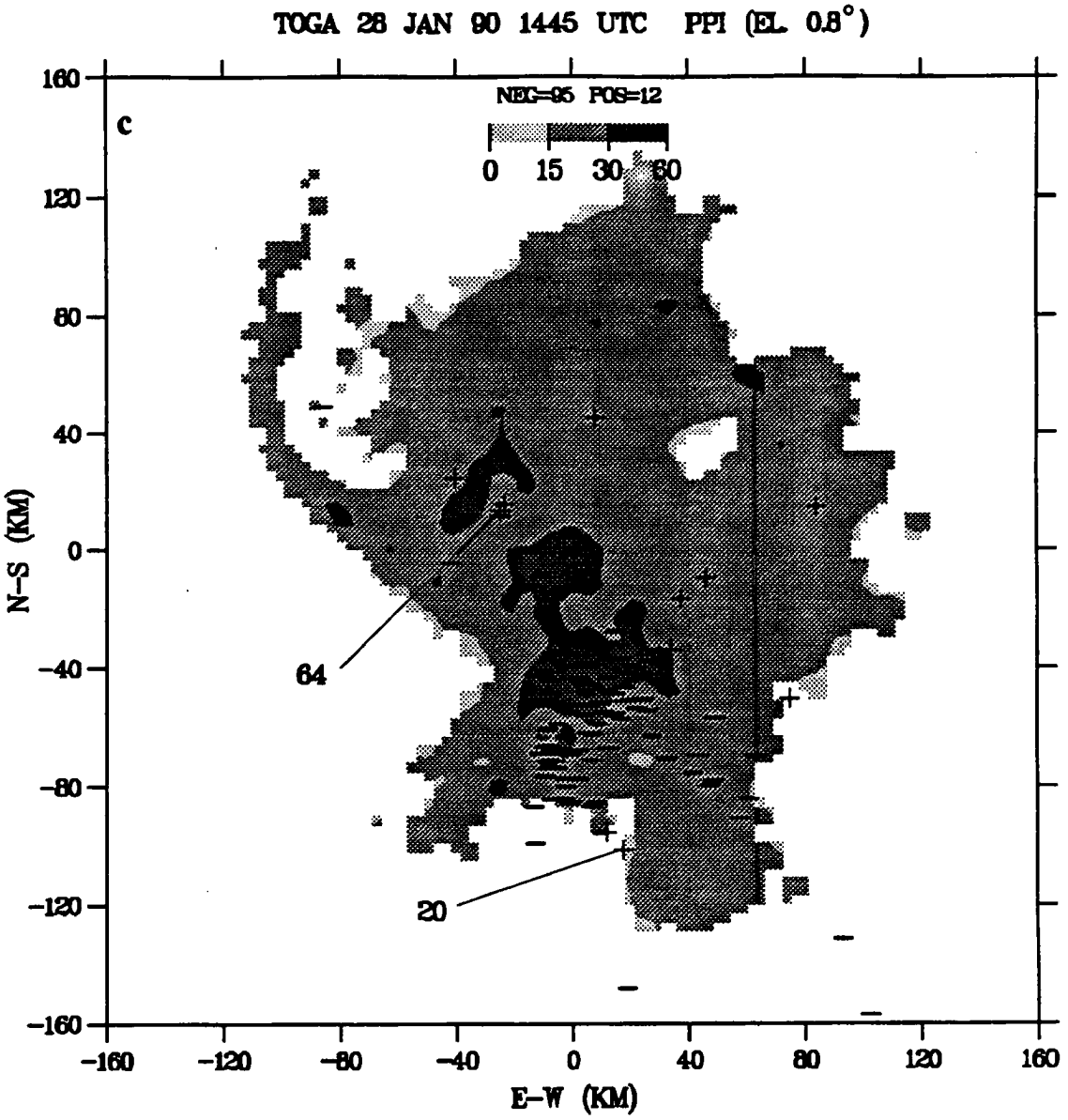


Figure 5.17 (c) 1445 UTC. Peak current extrema identified as 20 and 64 kA.

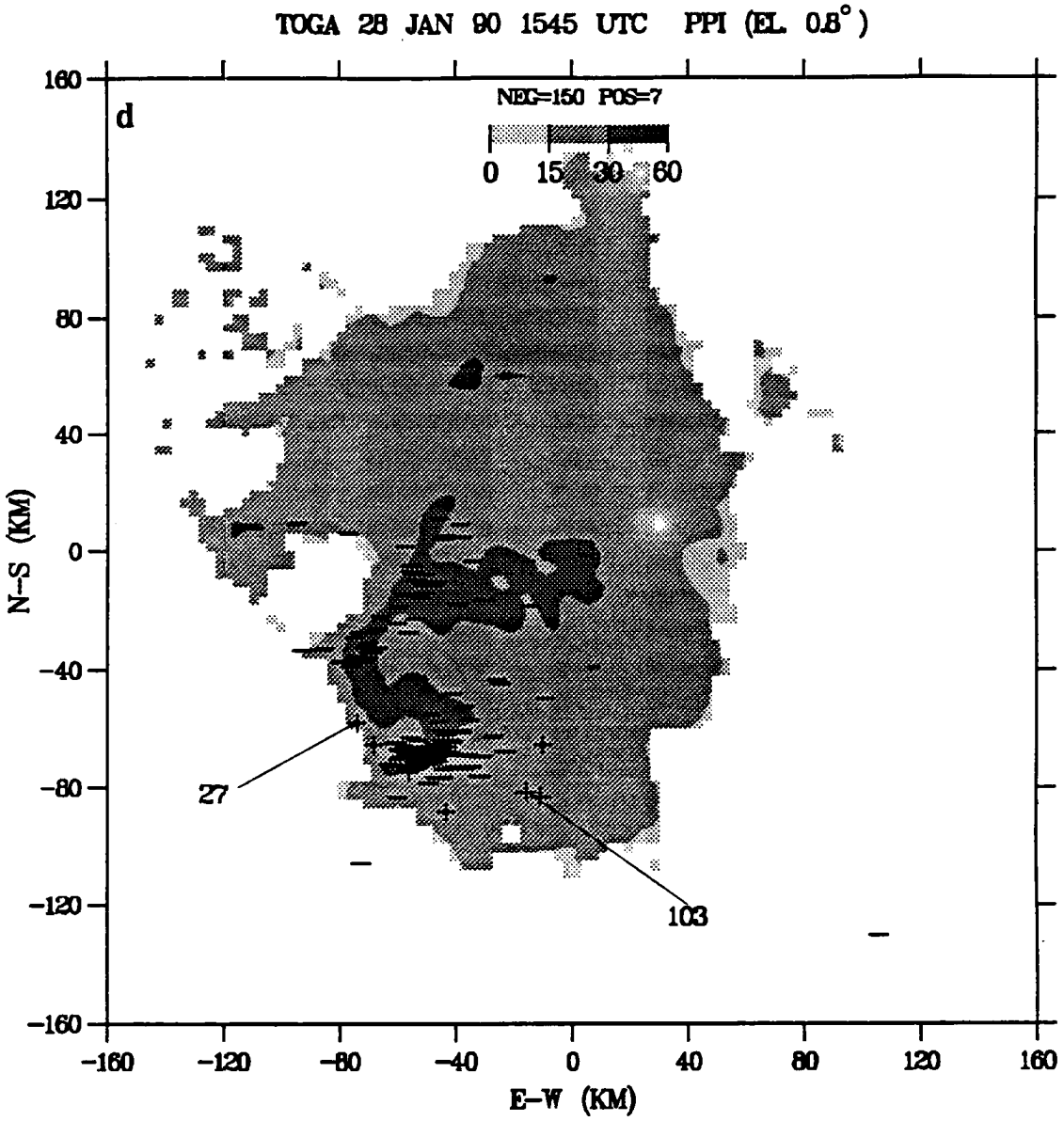


Figure 5.17 (d) 1545 UTC. Peak current extrema identified as 27 and 103 kA.

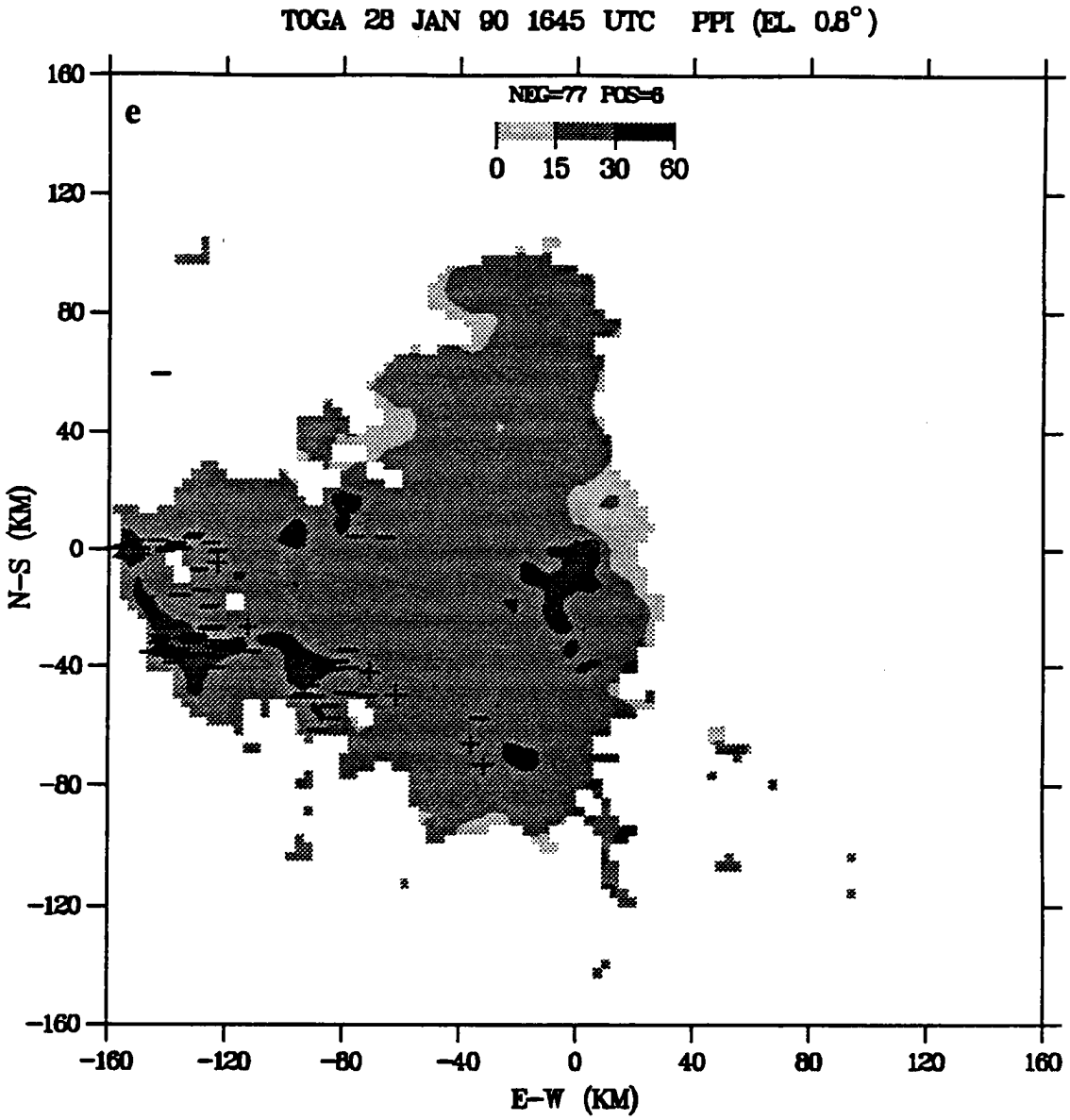


Figure 5.17 (e) 1645 UTC.

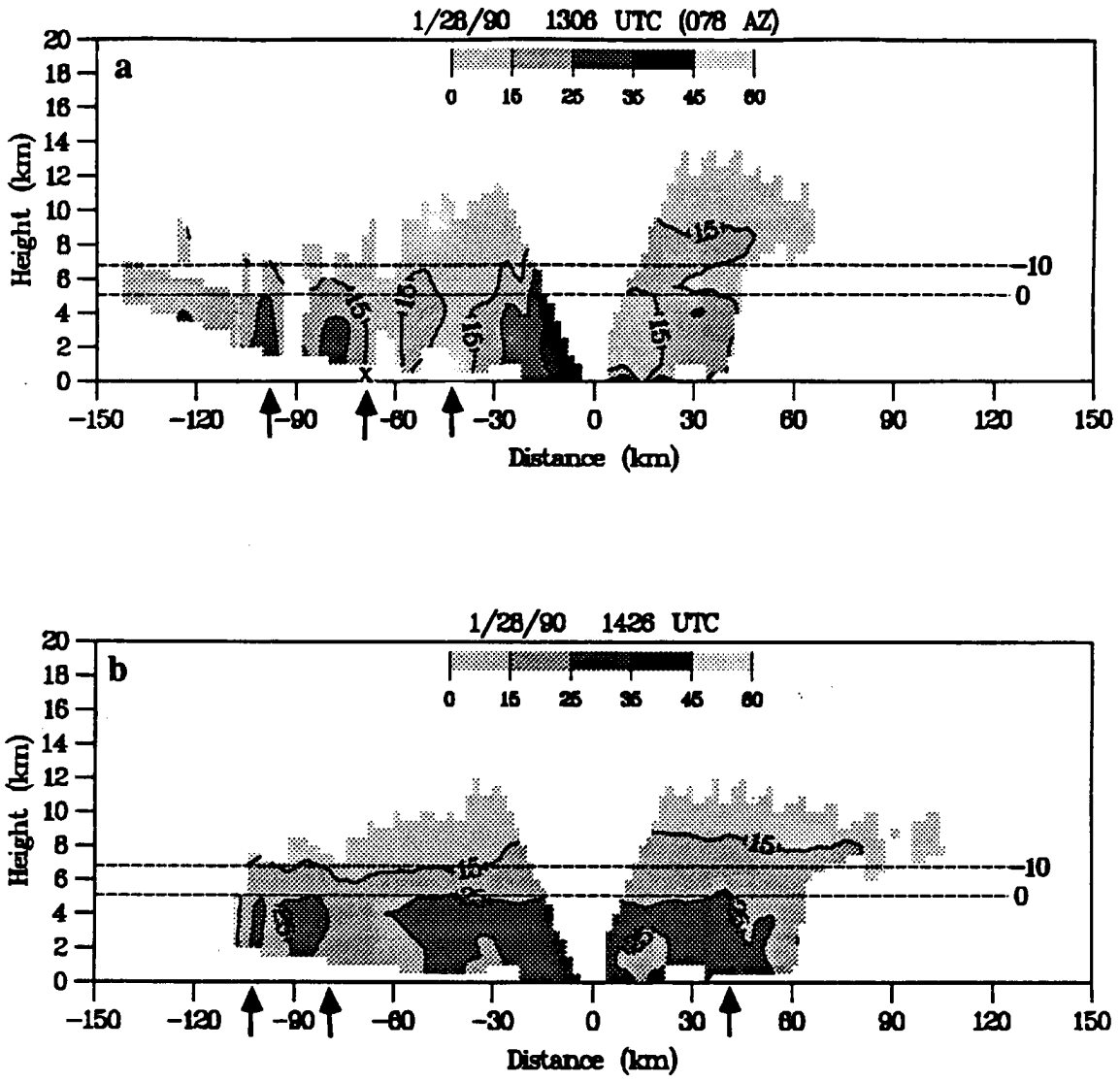


Figure 5.18 Same as Figure 5.3 except TOGA radar (090° azimuth), 28 January 1990 at (a) 1306 UTC (078° azimuth) and (b) 1426 UTC. An arrow indicates the position of a positive flash, "x" indicates the position of a negative flash.

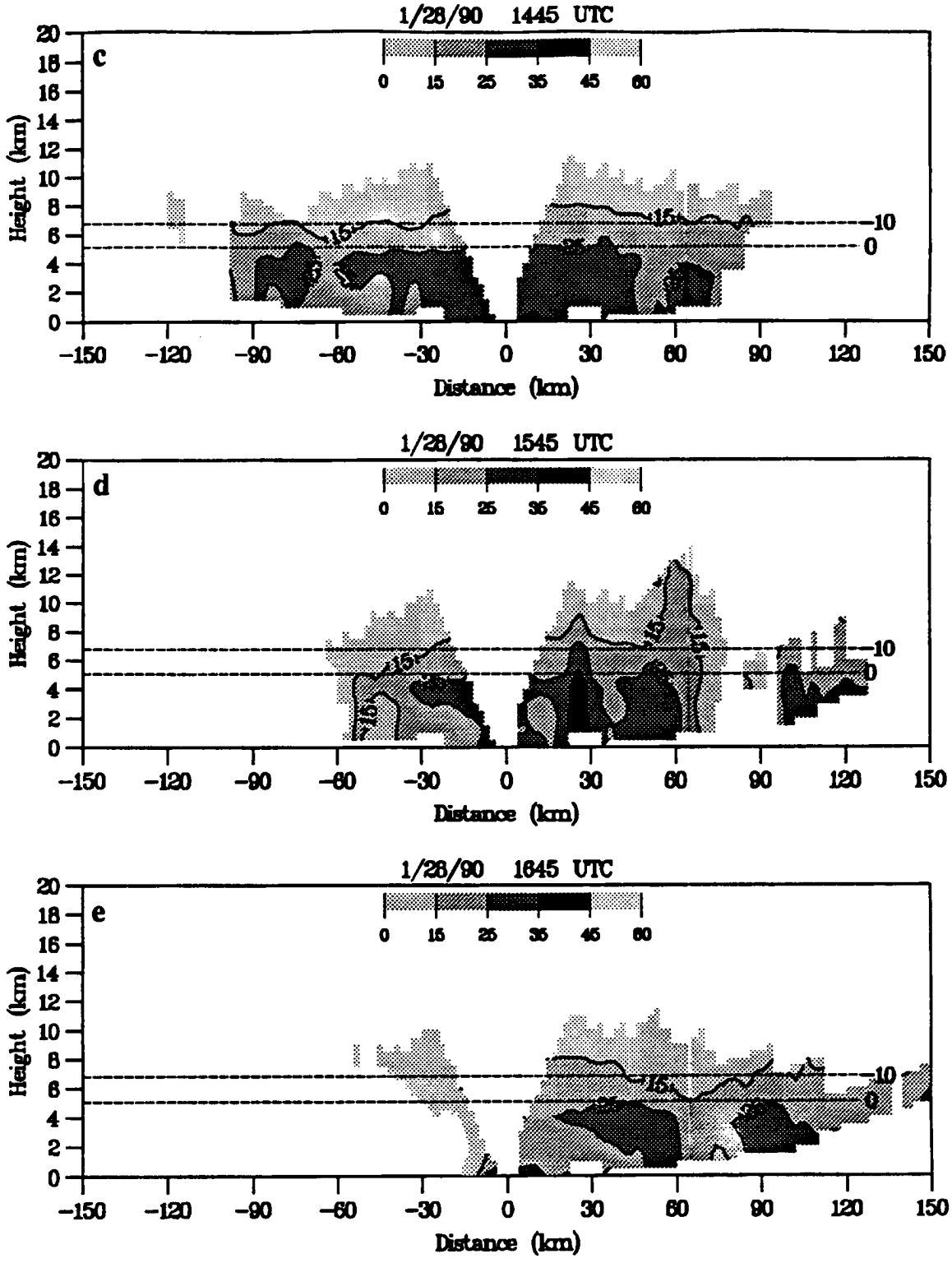


Figure 5.18 (c) 1445 UTC; (d) 1545 UTC; (e) 1645 UTC.

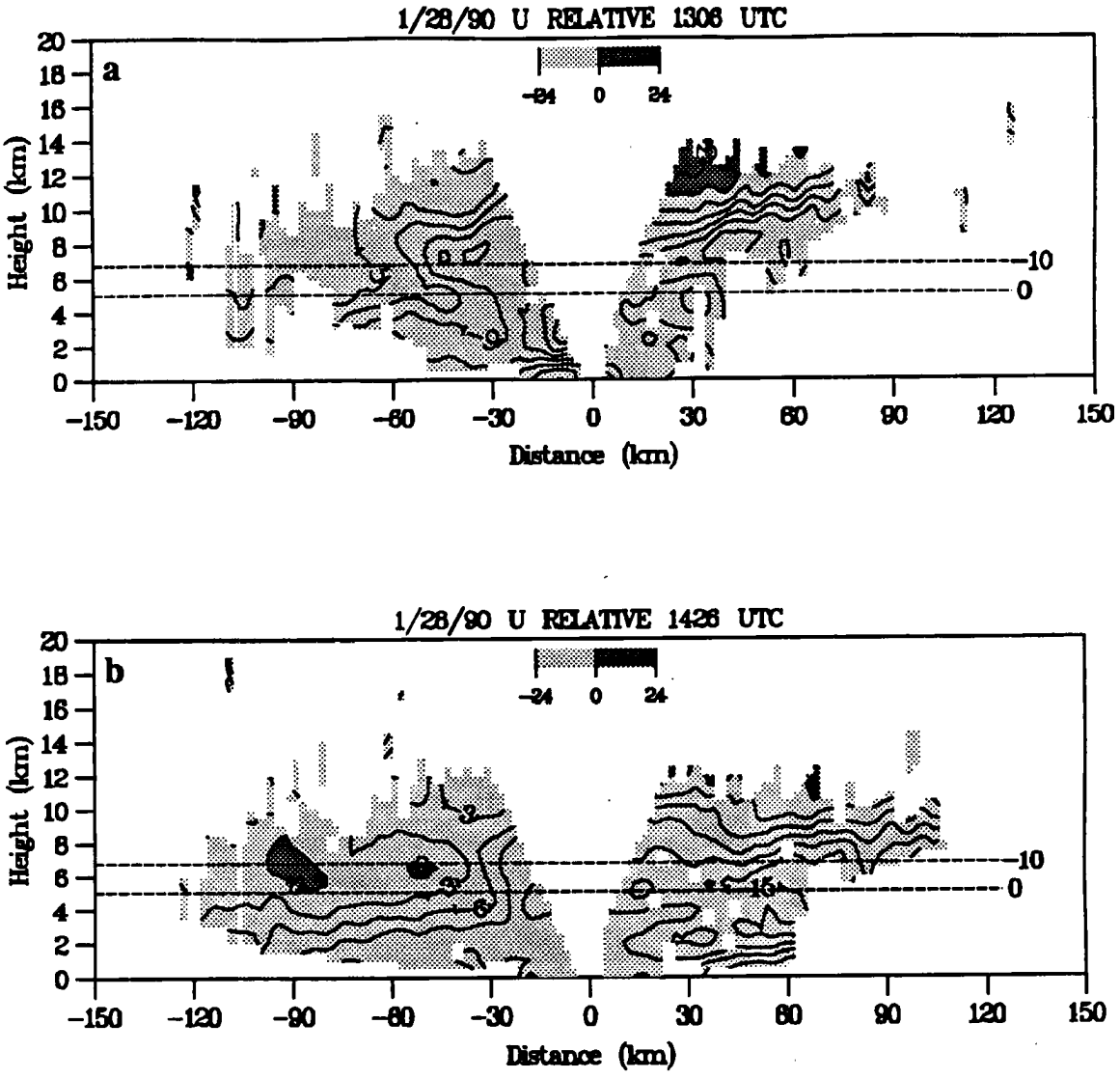


Figure 5.19 Same as Figure 5.4 except TOGA radar (090° azimuth), 28 January 1990 at (a) 1306 UTC and (b) 1426 UTC.

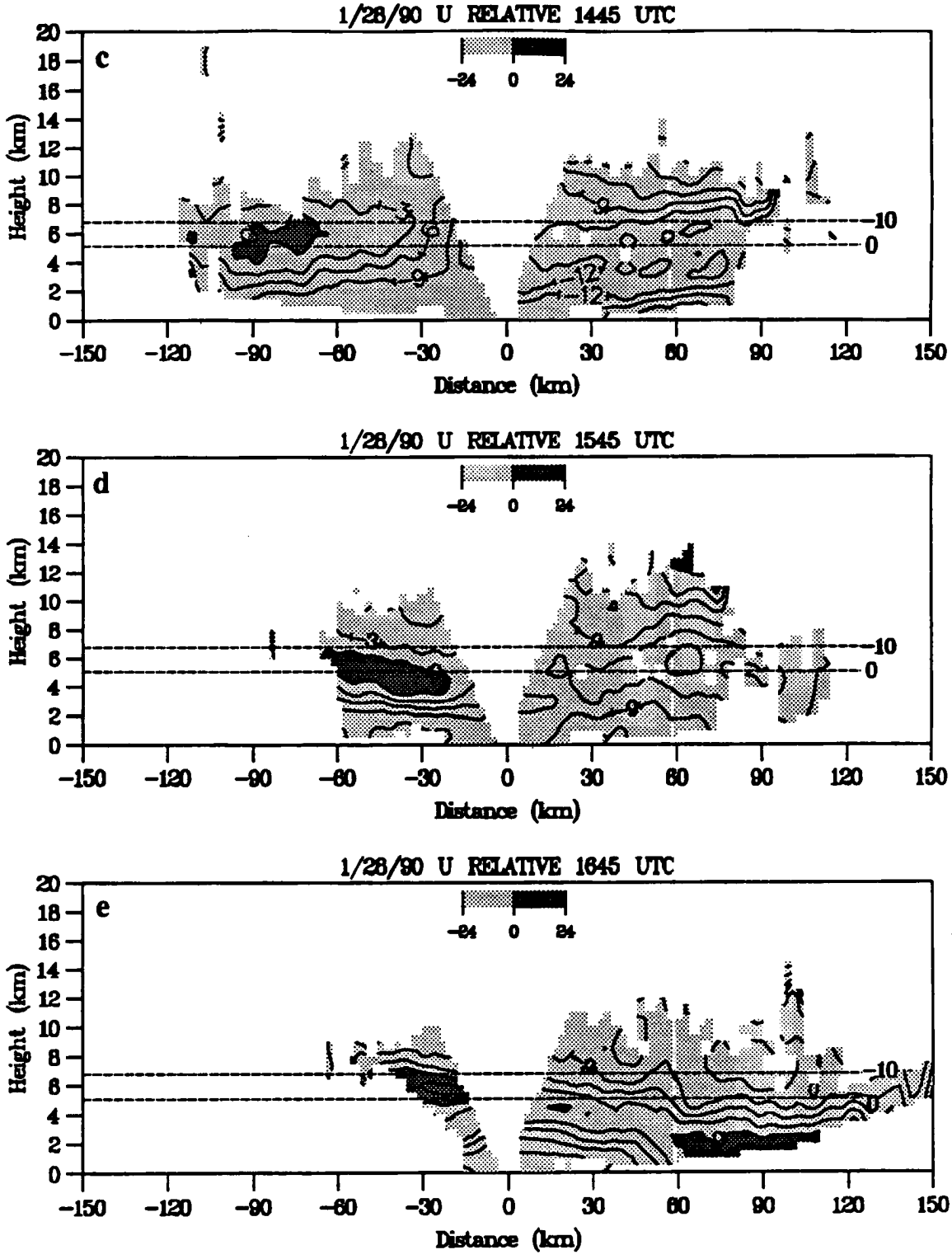


Figure 5.19 (c) 1445 UTC; (d) 1545 UTC; 1645 UTC.

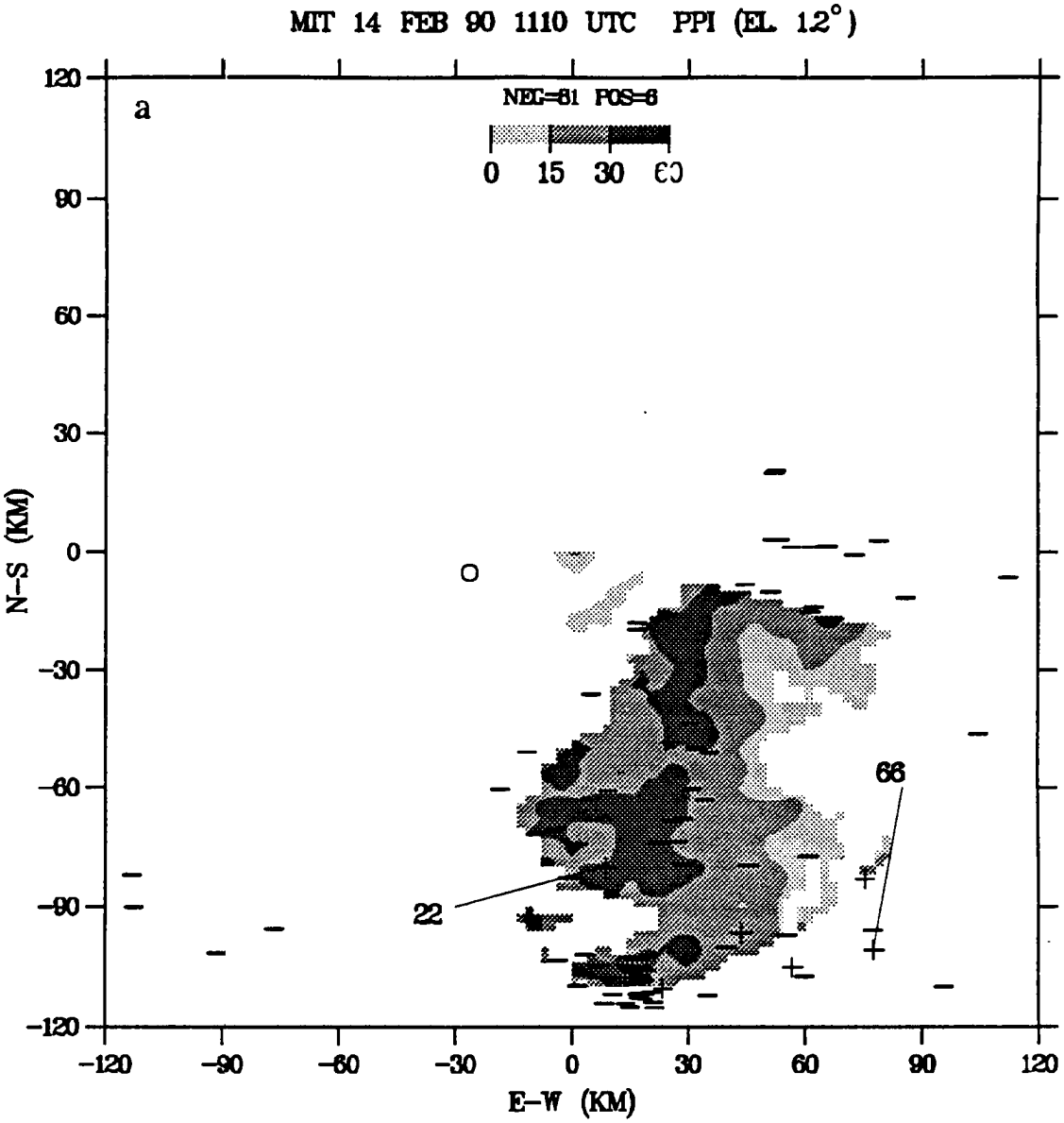


Figure 5.20 Same as Figure 5.1 except for 14 February 1990 at (a) 1110 UTC (peak current extrema identified as 22 and 66 kA).

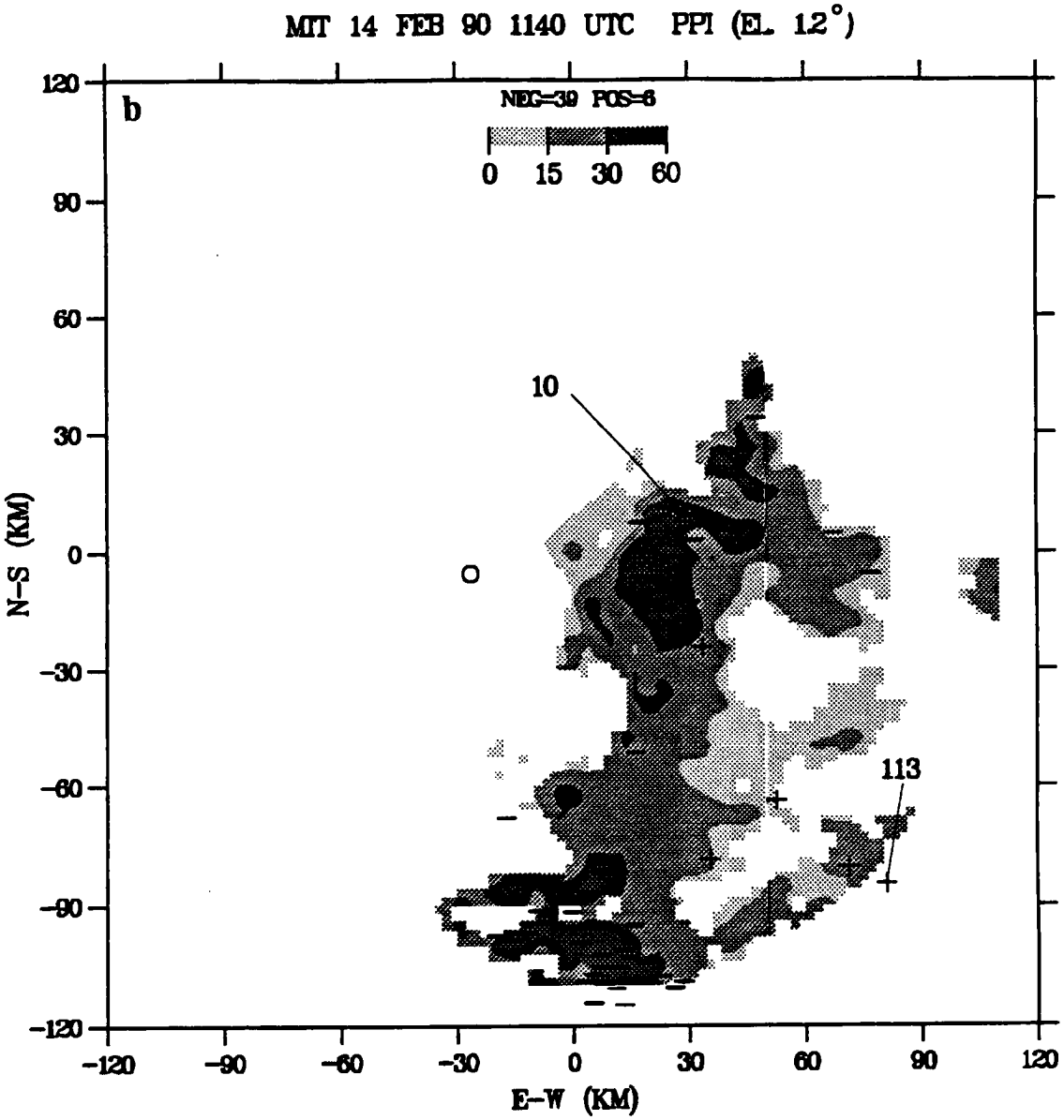


Figure 5.20 (b) 1140 UTC. Peak current extrema identified as 10 and 113 kA.

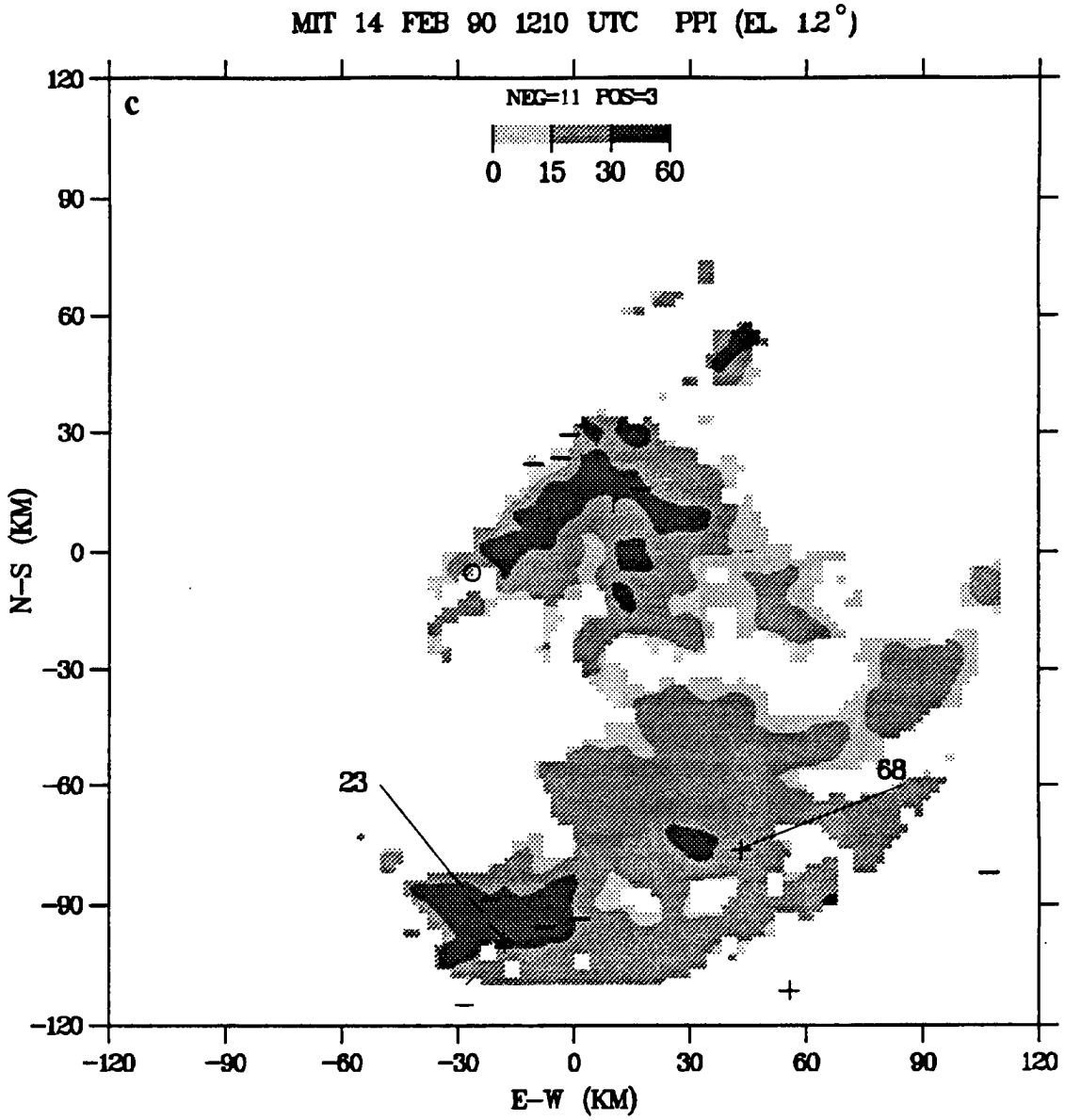


Figure 5.20 (c) 1210 UTC. Peak current extrema identified as 23 and 68 kA.

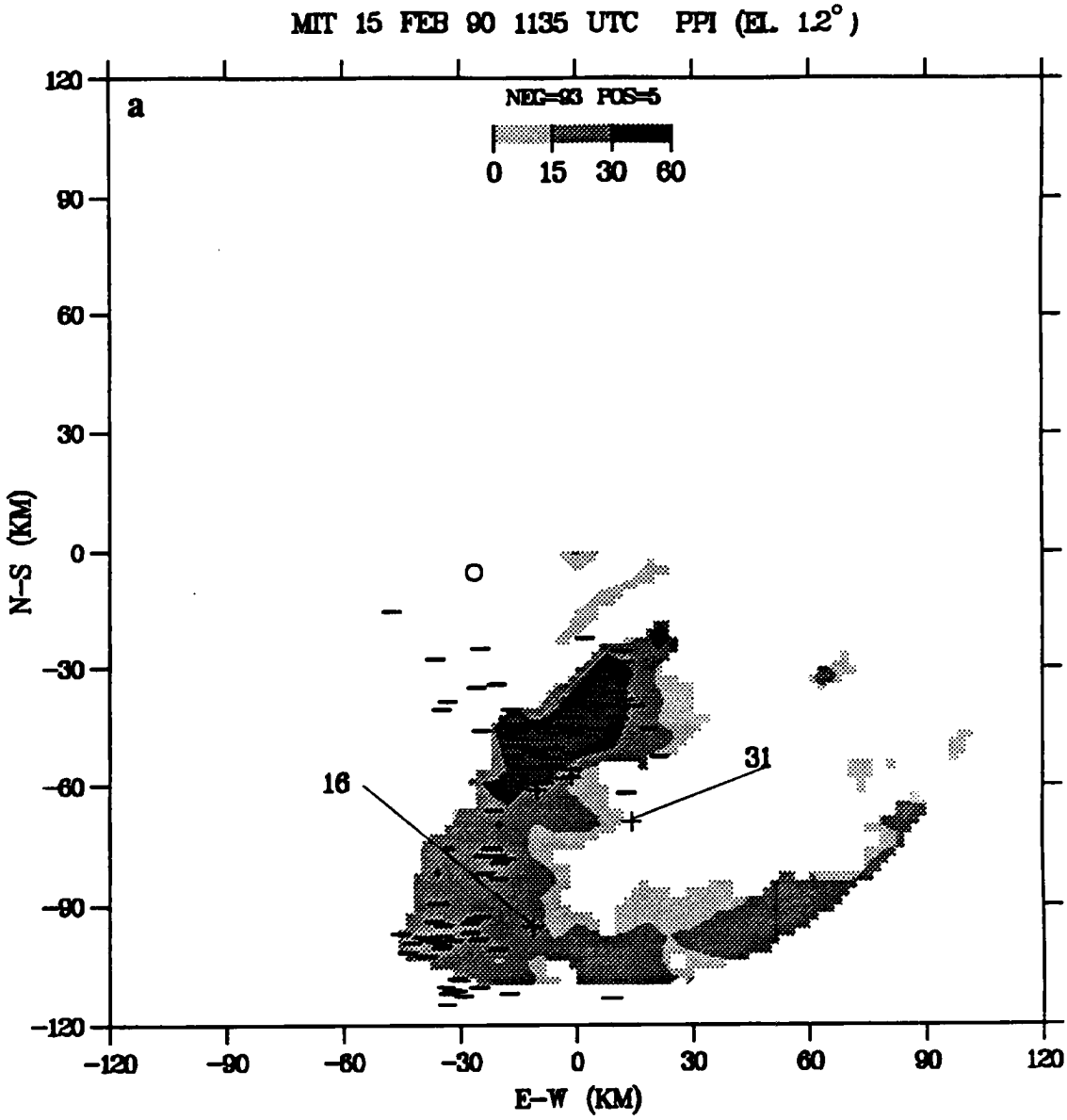


Figure 5.21 Same as Figure 5.1 except for 15 February 1990 at (a) 1135 UTC (peak current extrema identified as 16 and 31 kA).

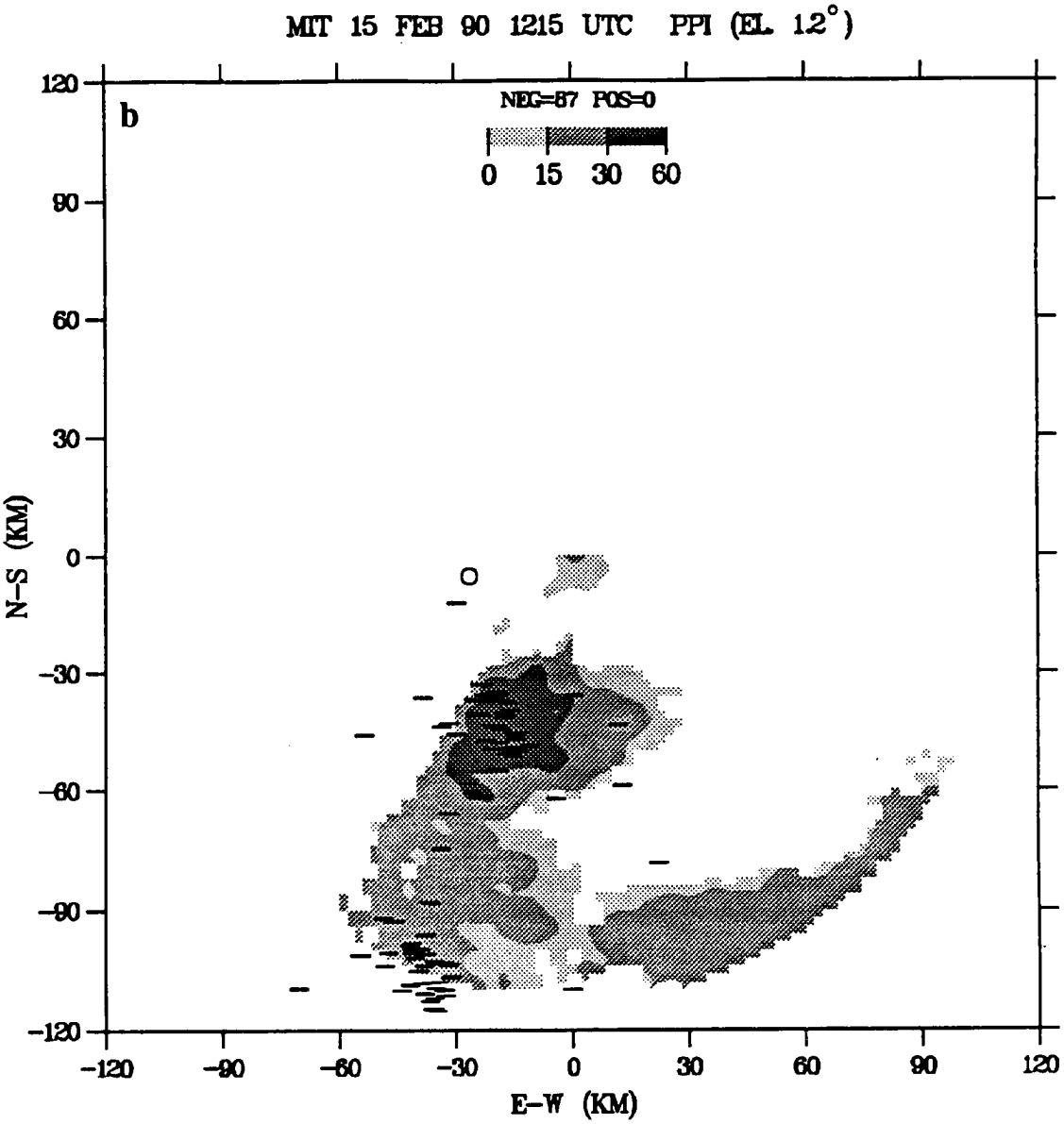


Figure 5.21 (b) 1215 UTC.

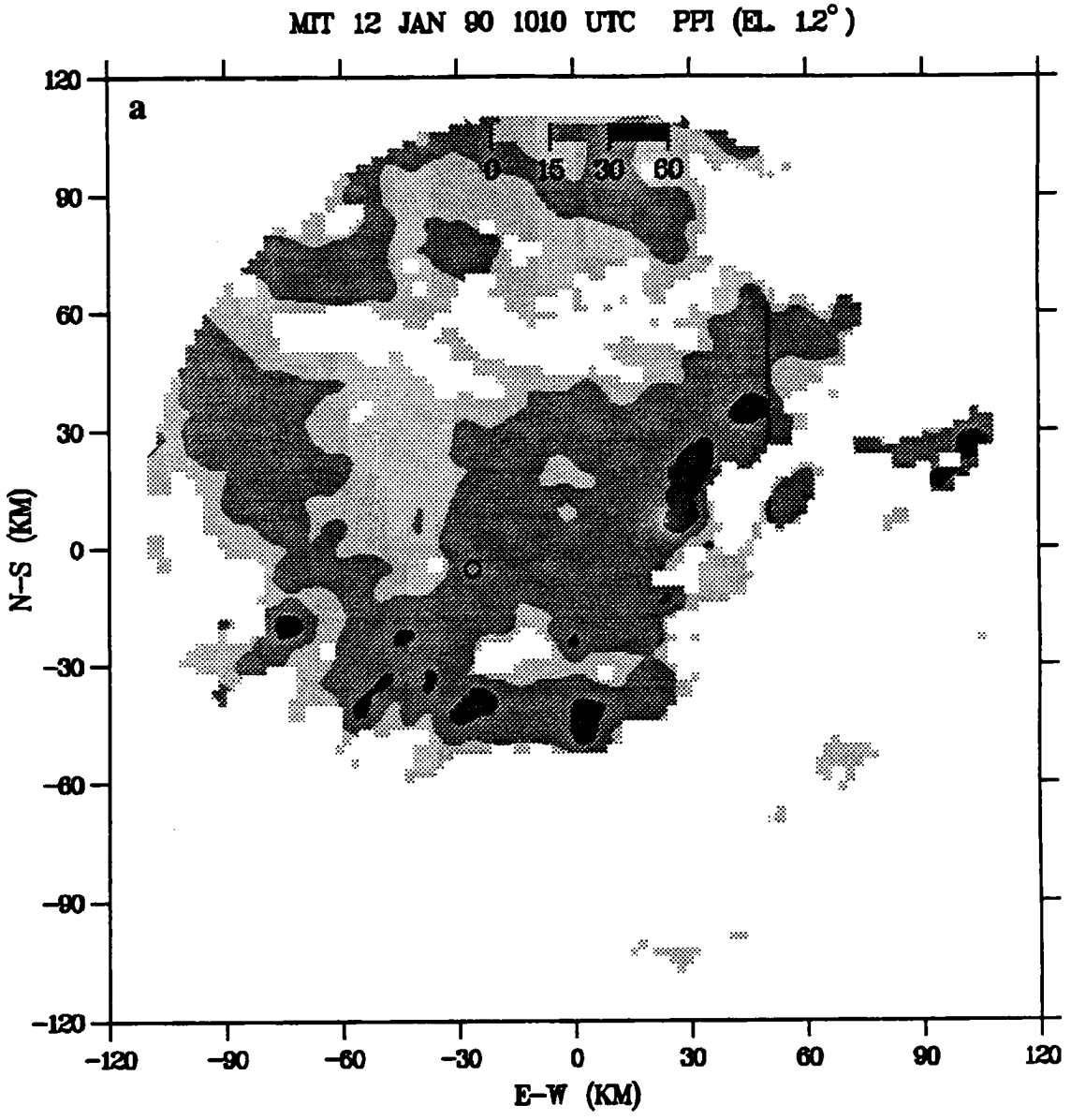


Figure 5.22 Same as Figure 5.1 except for 12 January 1990 at (a) 1010 UTC.

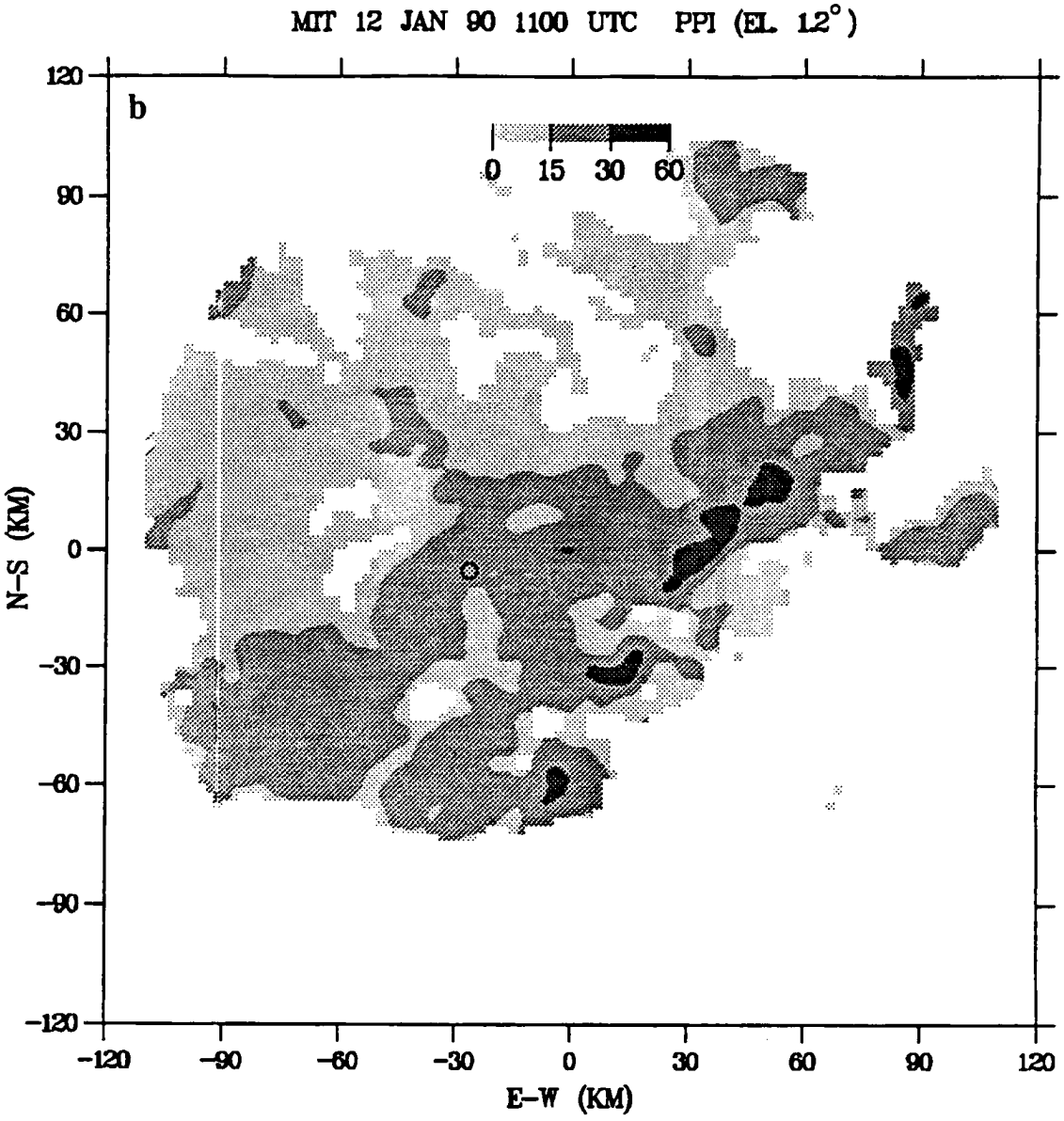


Figure 5.22 (b) 1100 UTC.

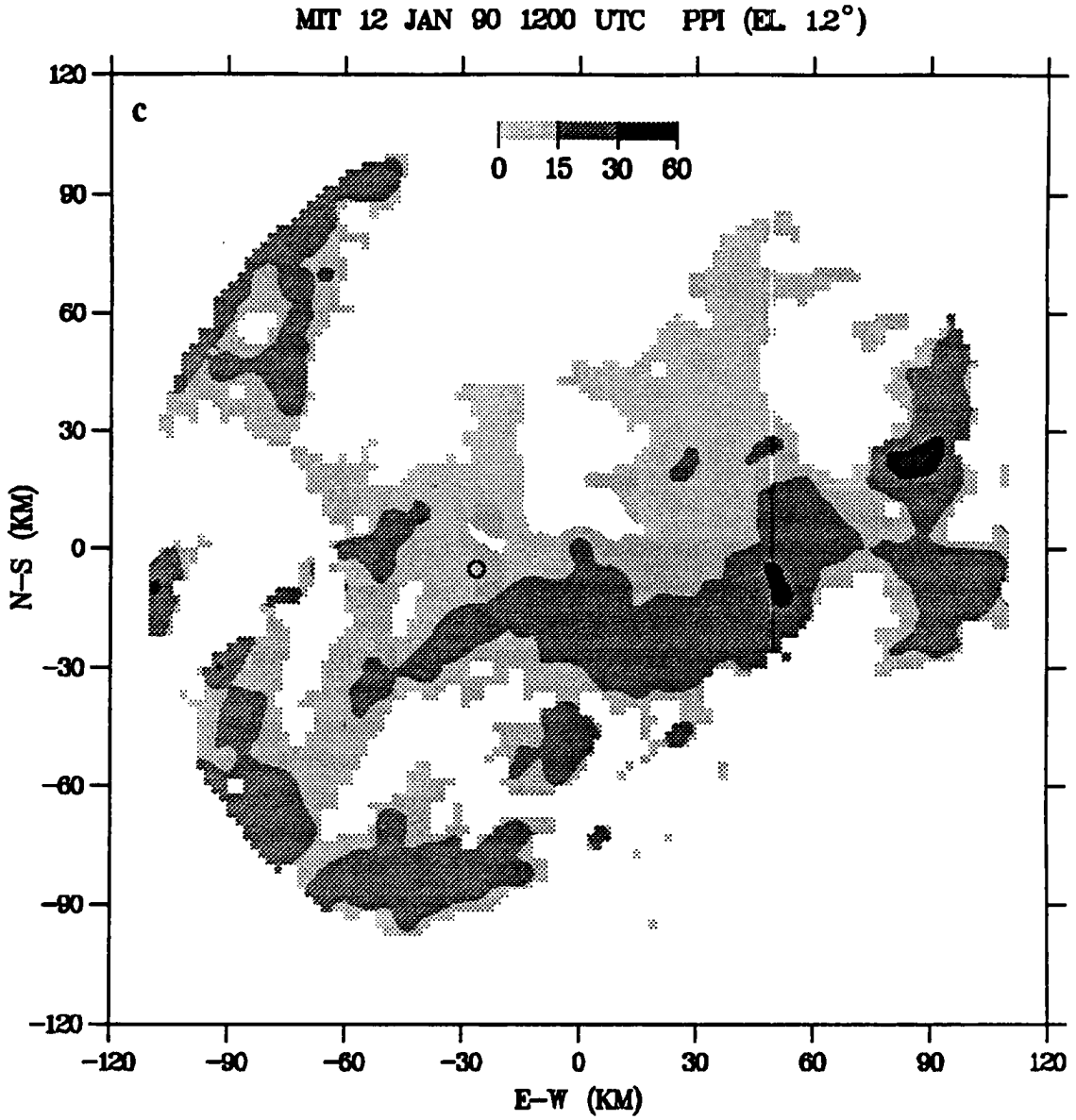


Figure 5.22 (c) 1200 UTC.

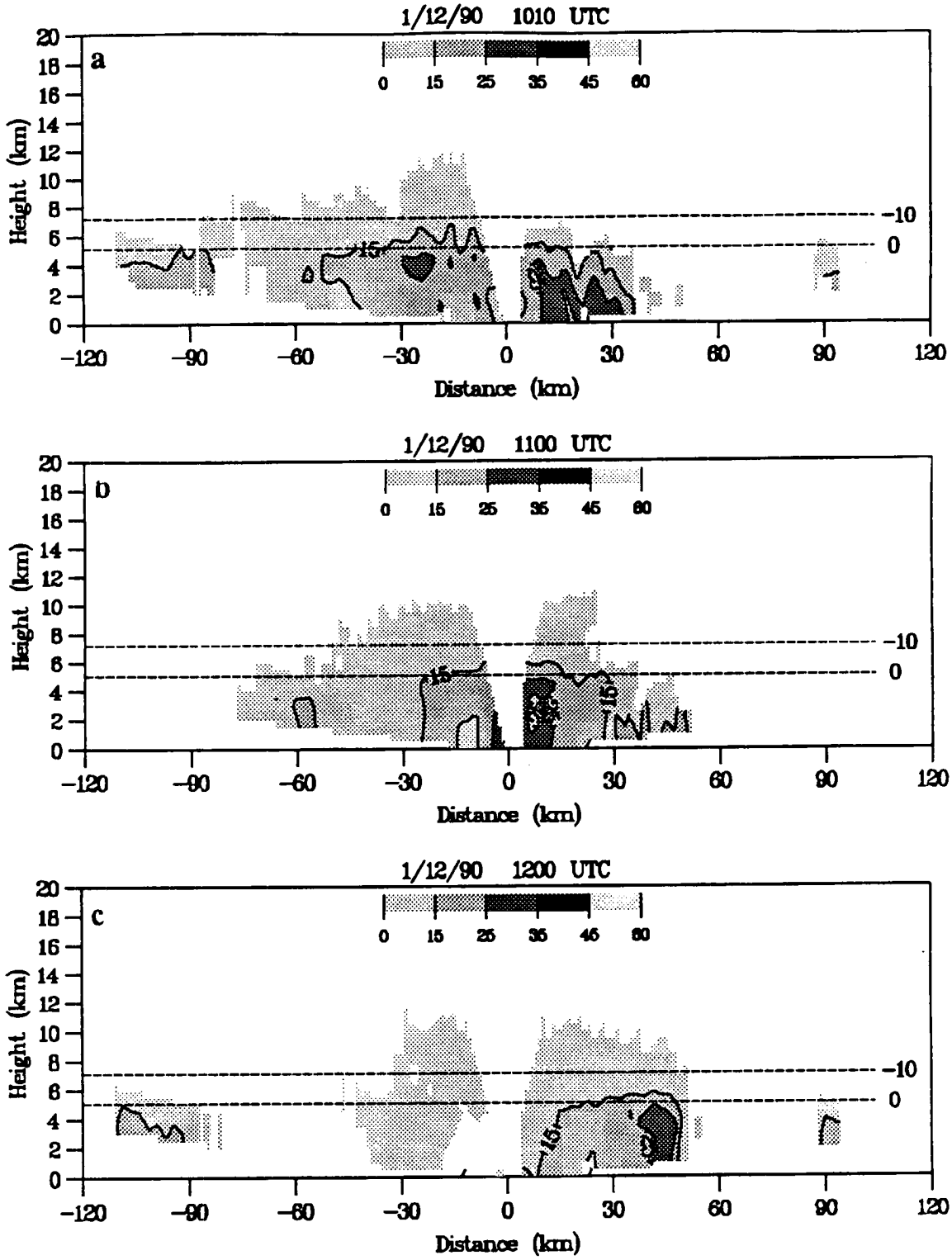


Figure 5.23 Same as Figure 5.3 except for 12 January 1990 (315° azimuth) at (a) 1010 UTC; (b) 1100 UTC; and (c) 1200 UTC.

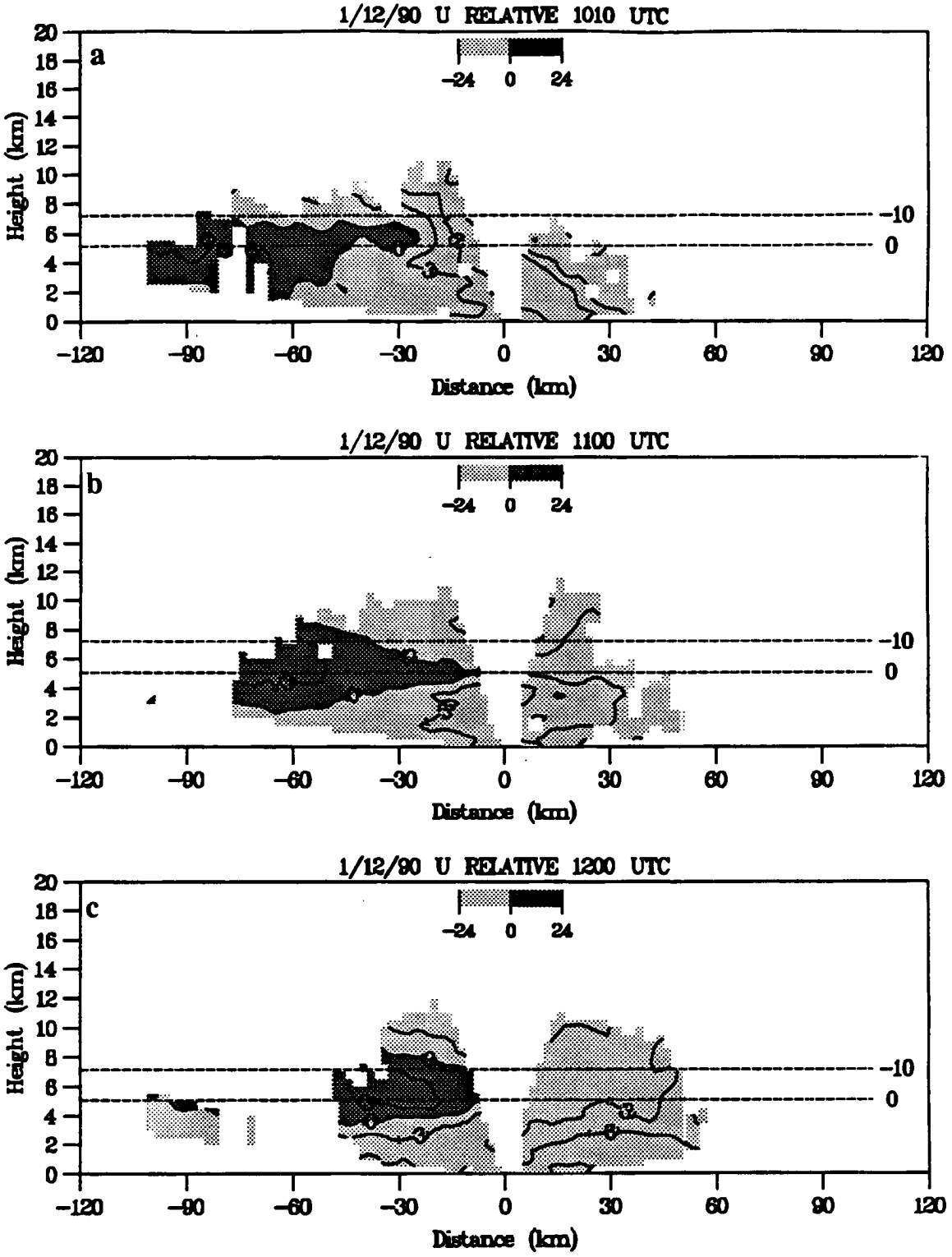


Figure 5.24 Same as Figure 5.4 except for 12 January 1990 (315° azimuth) at (a) 1010 UTC; (b) 1100 UTC; and (c) 1200 UTC.

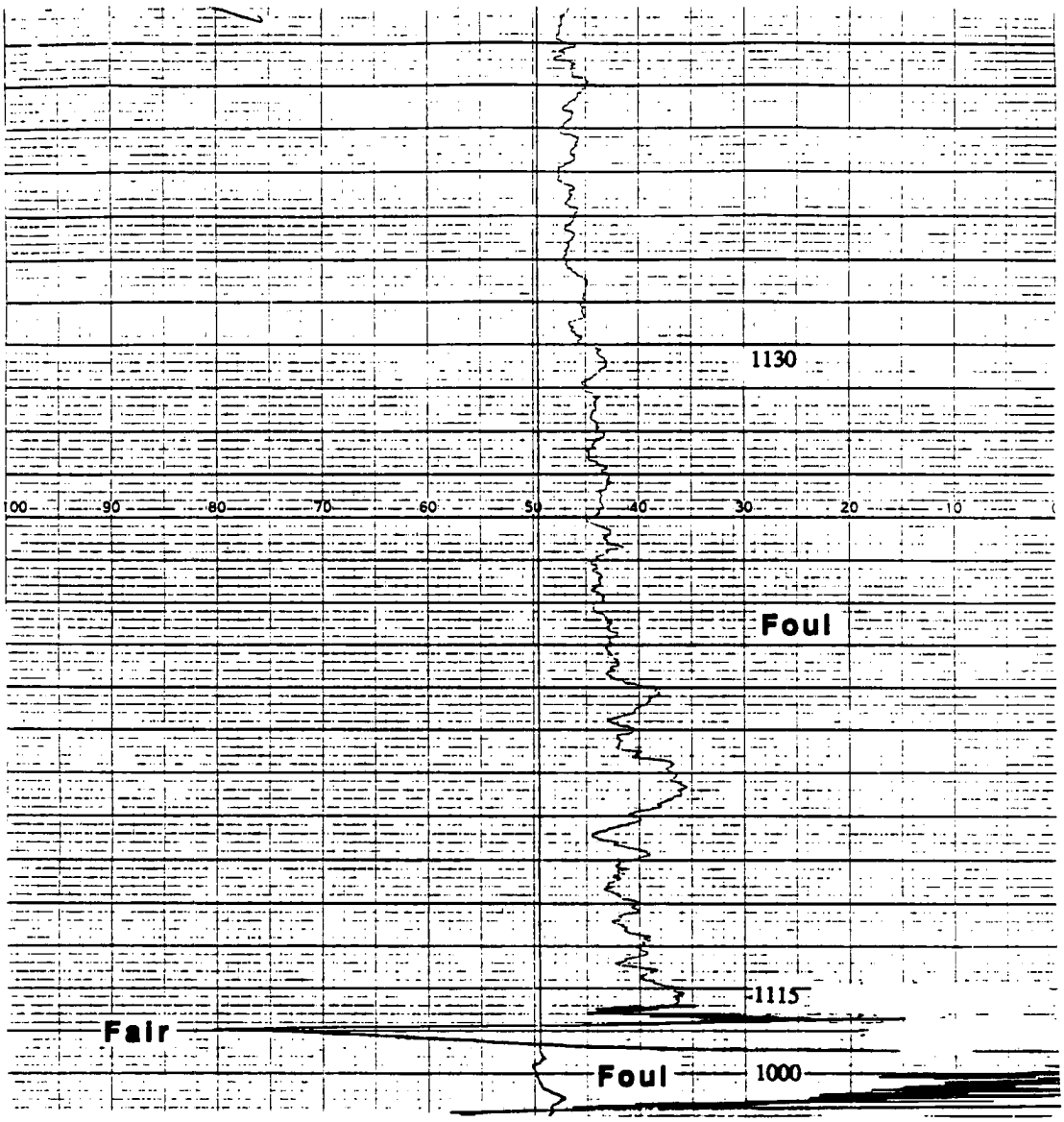


Figure 5.25 Surface electric field record for the MIT radar site, 12 January 1990 (1000-1139 UTC). Chart speed 1 cm $hr^{-1}$ from 1000-1115, 1 cm $min^{-1}$ thereafter. "Fair" indicates positive charge overhead, "Foul" indicates negative charge overhead.

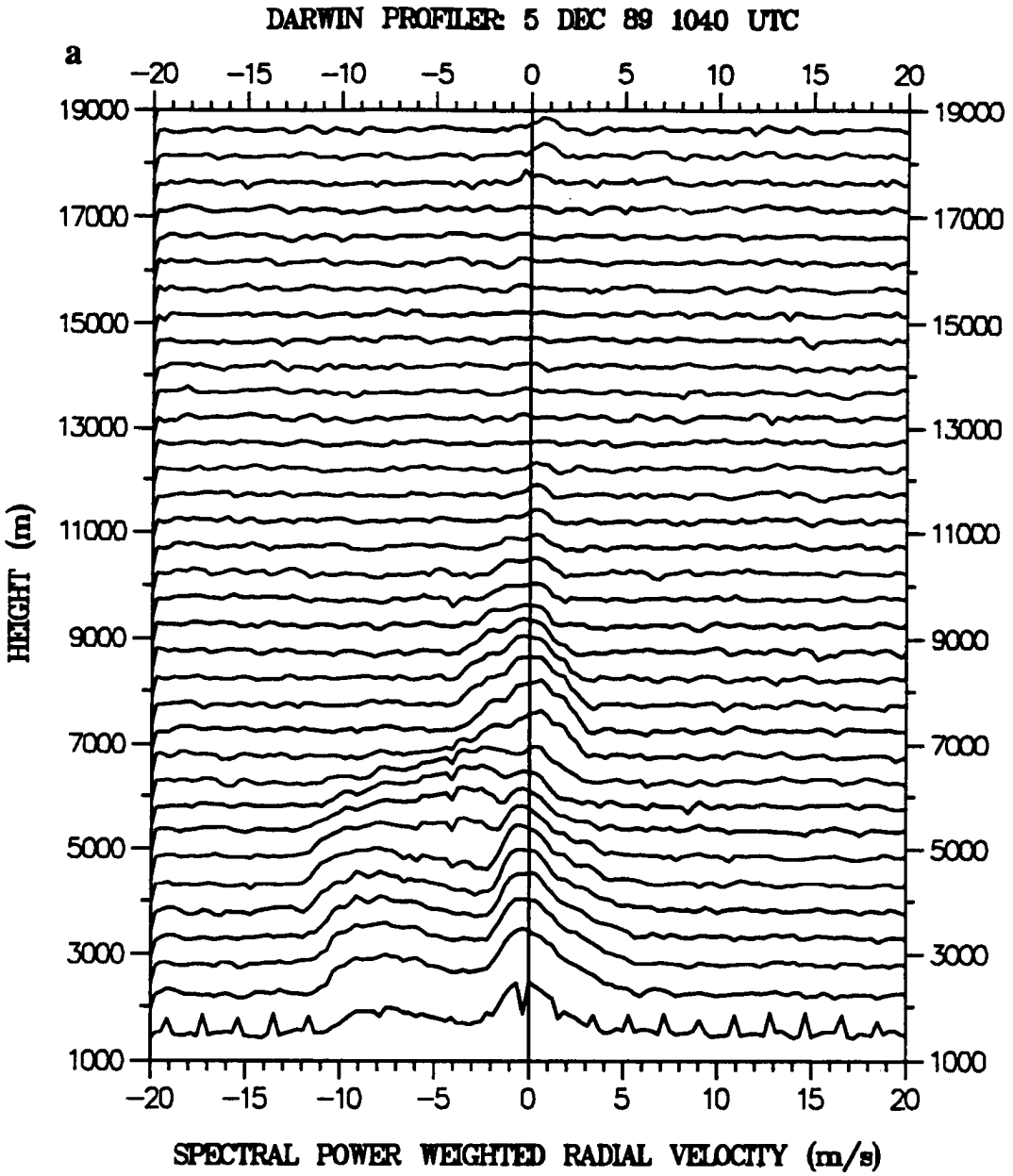


Figure 5.26 Wind profiler vertical velocity spectra for 5 December 1989 at (a) 1040 UTC.

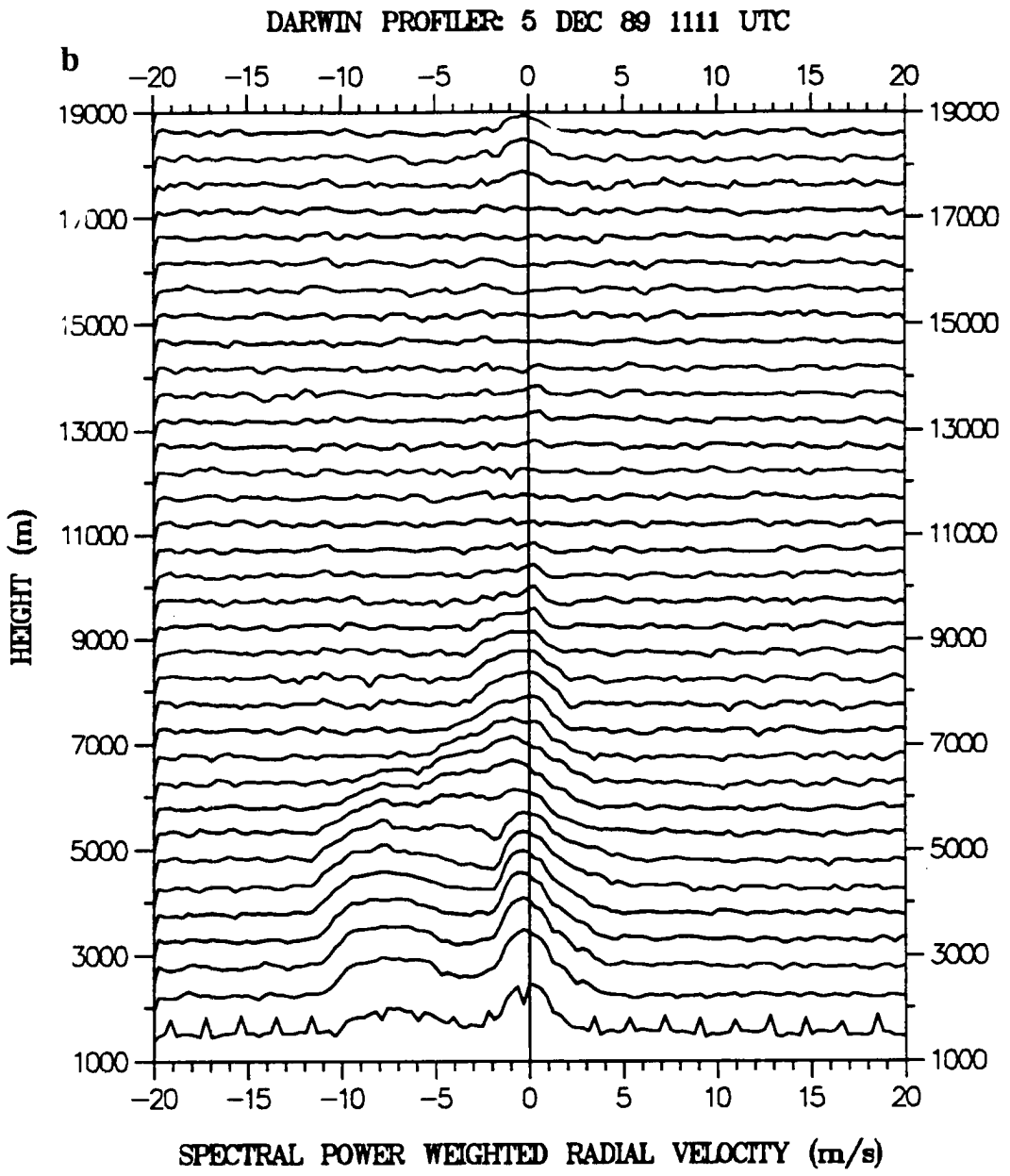


Figure 5.26 (b) 1111 UTC

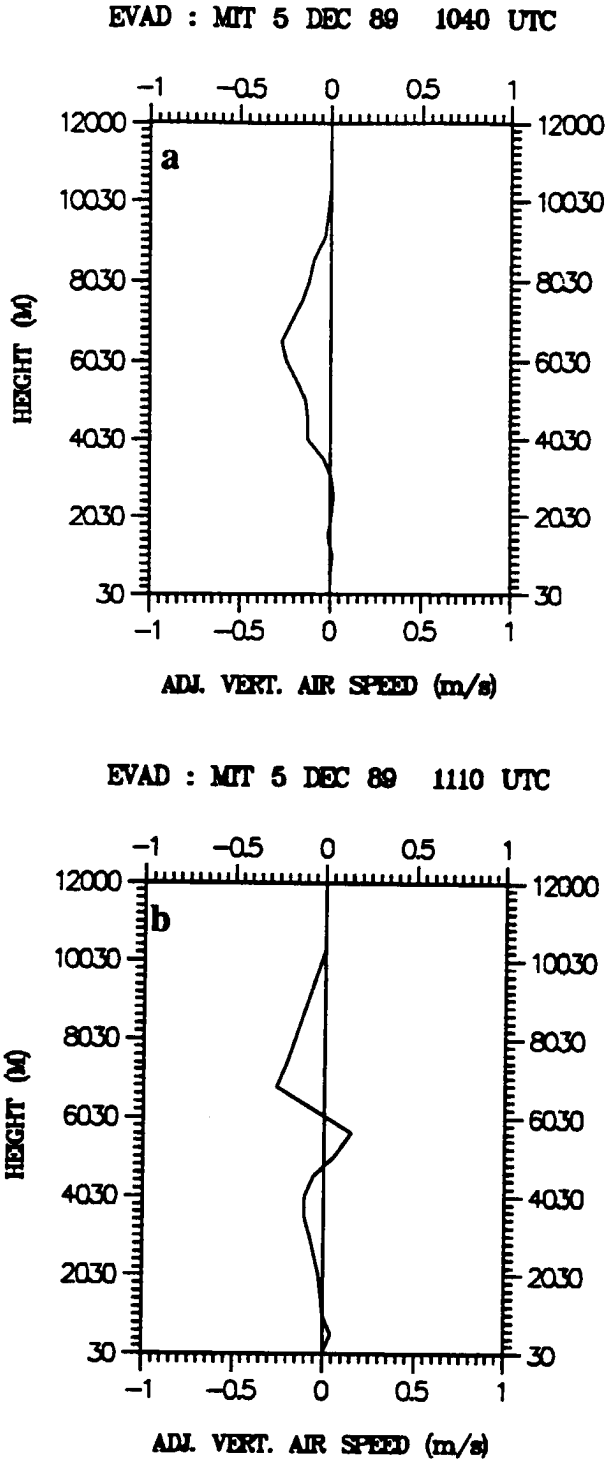


Figure 5.27 EVAD vertical velocities for 5 December 1989 (diagnosed from MIT radar data) at (a) 1040 UTC and (b) 1110 UTC.

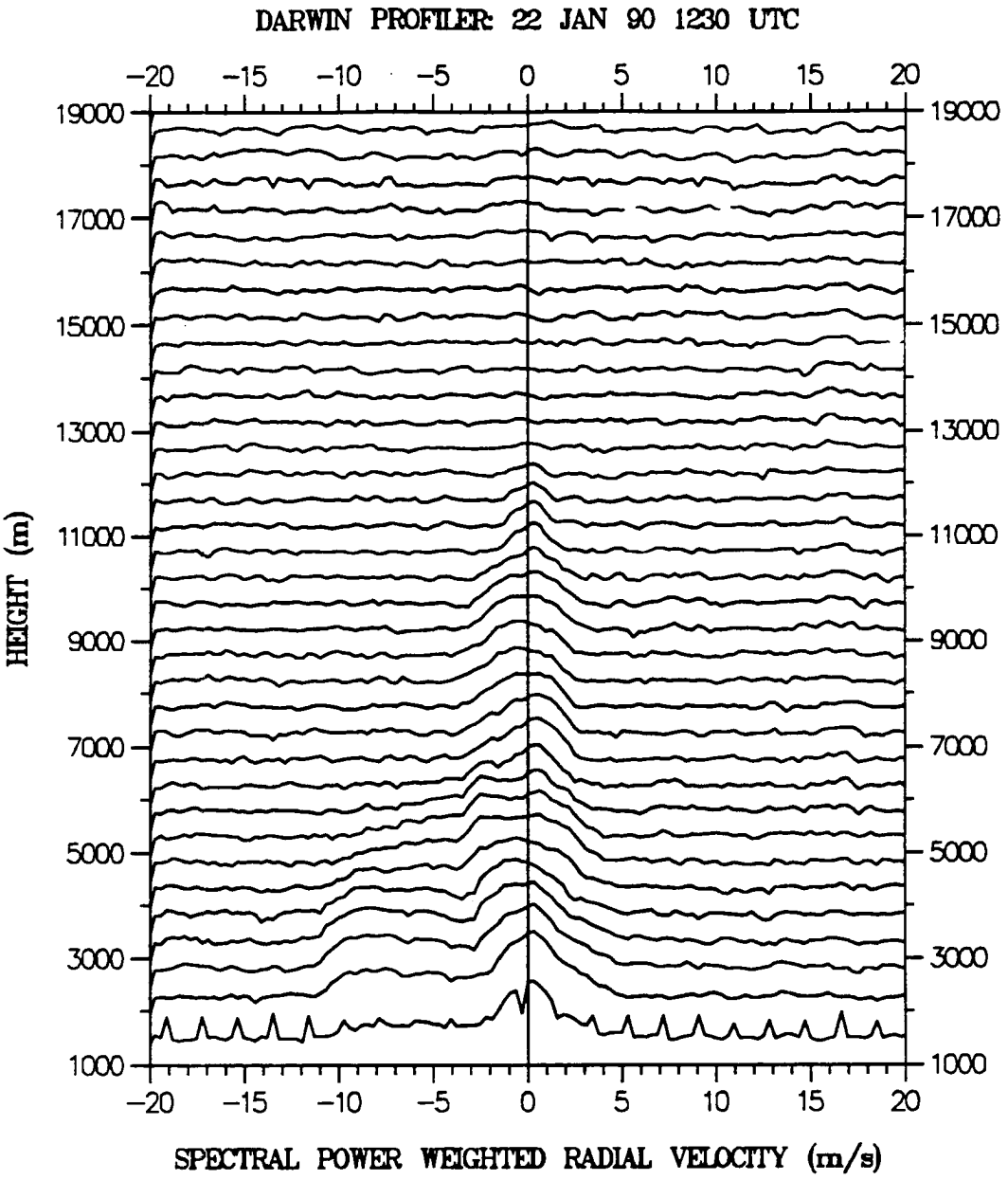


Figure 5.28 Same as Figure 5.26 except for 22 January 1990 at 1230 UTC.

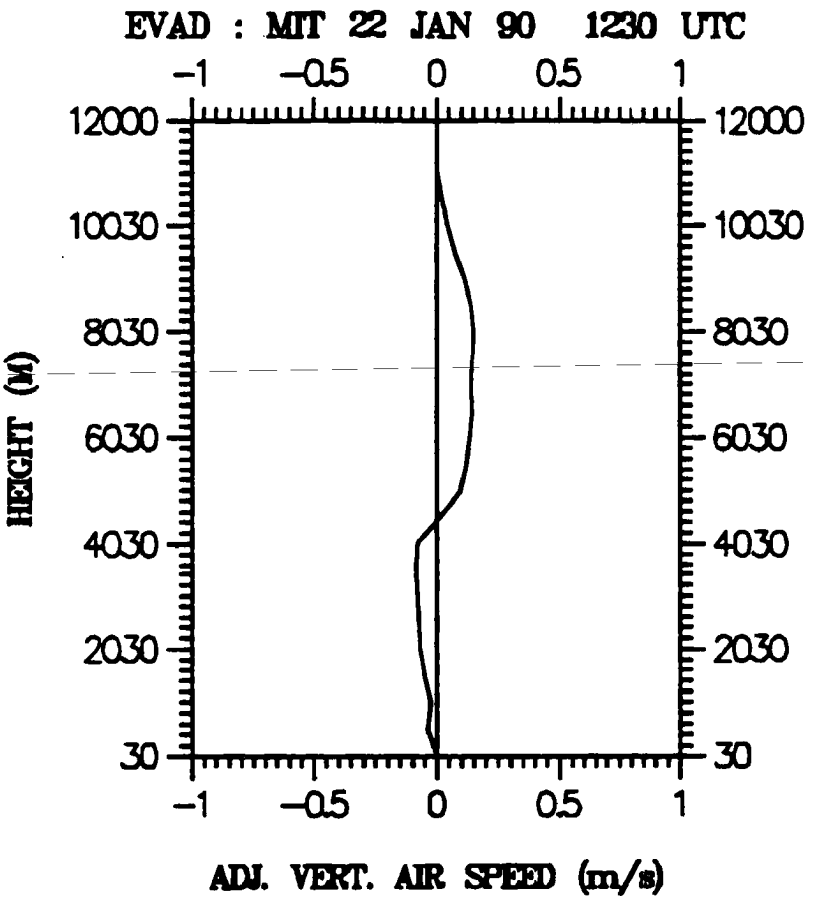


Figure 5.29 Same as Figure 5.27 except for 22 January 1990 at 1230 UTC.

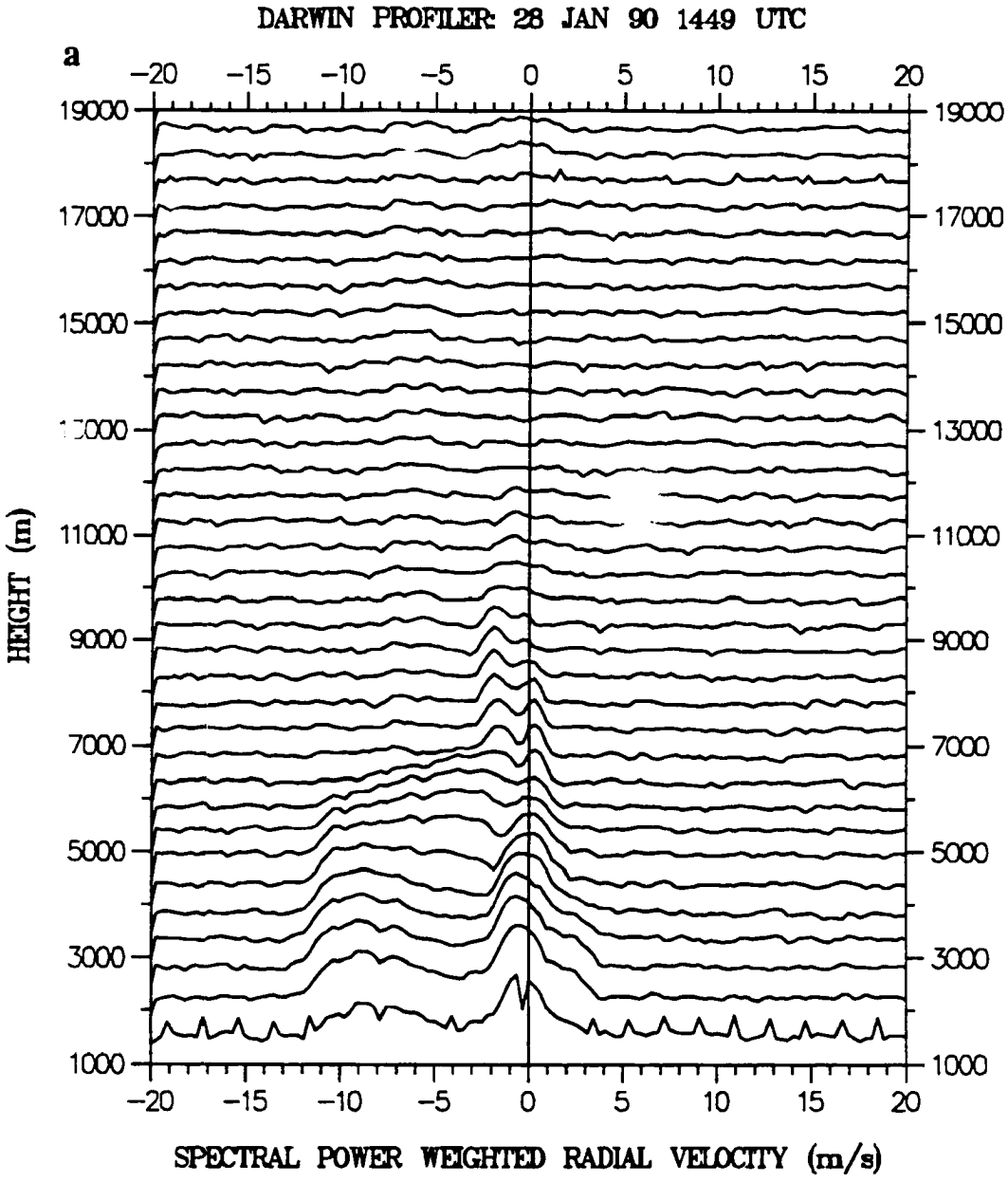


Figure 5.30 Same as Figure 5.26 except for 28 January 1990 at (a) 1449 UTC.

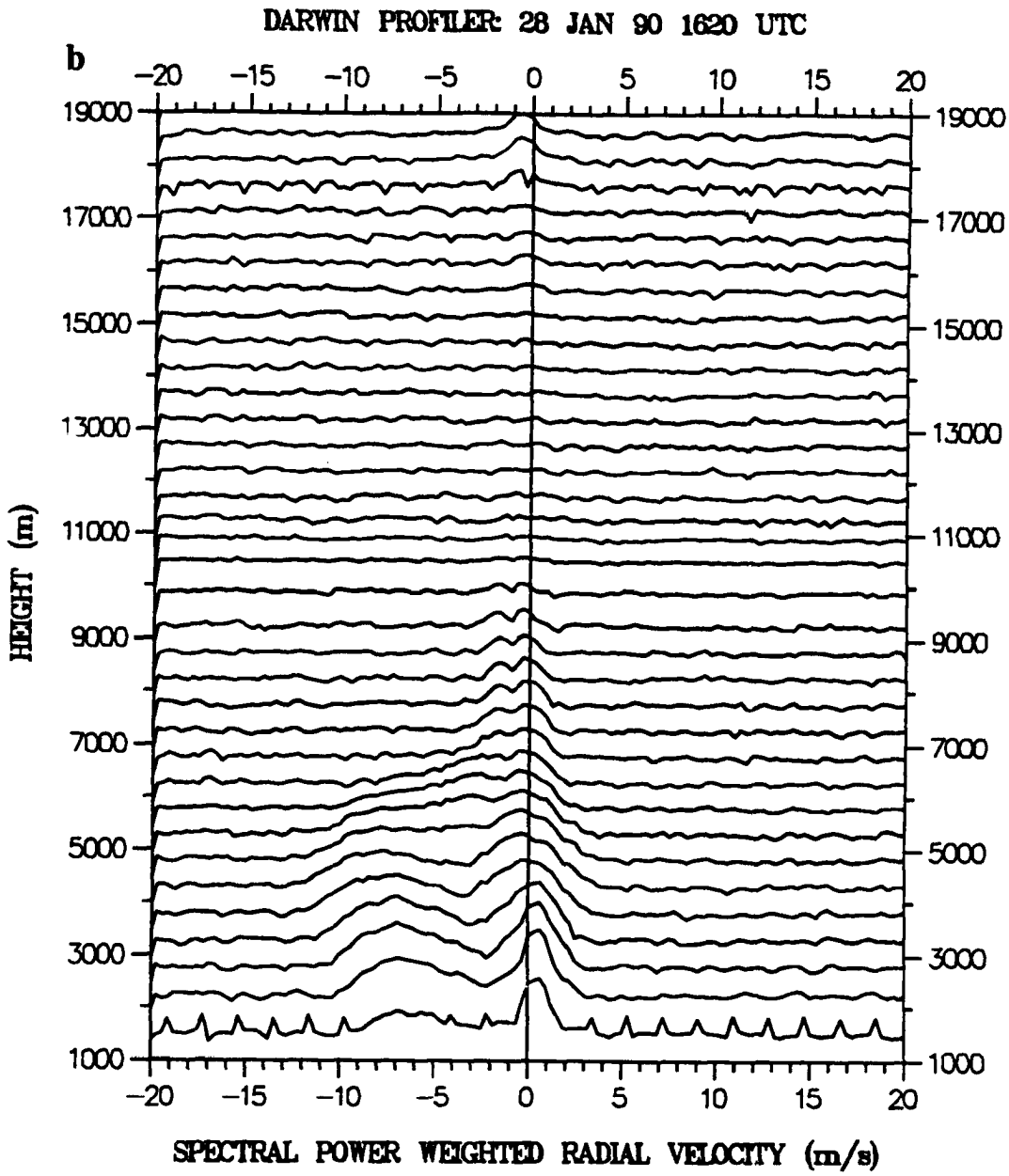


Figure 5.30 (b) 1620 UTC.

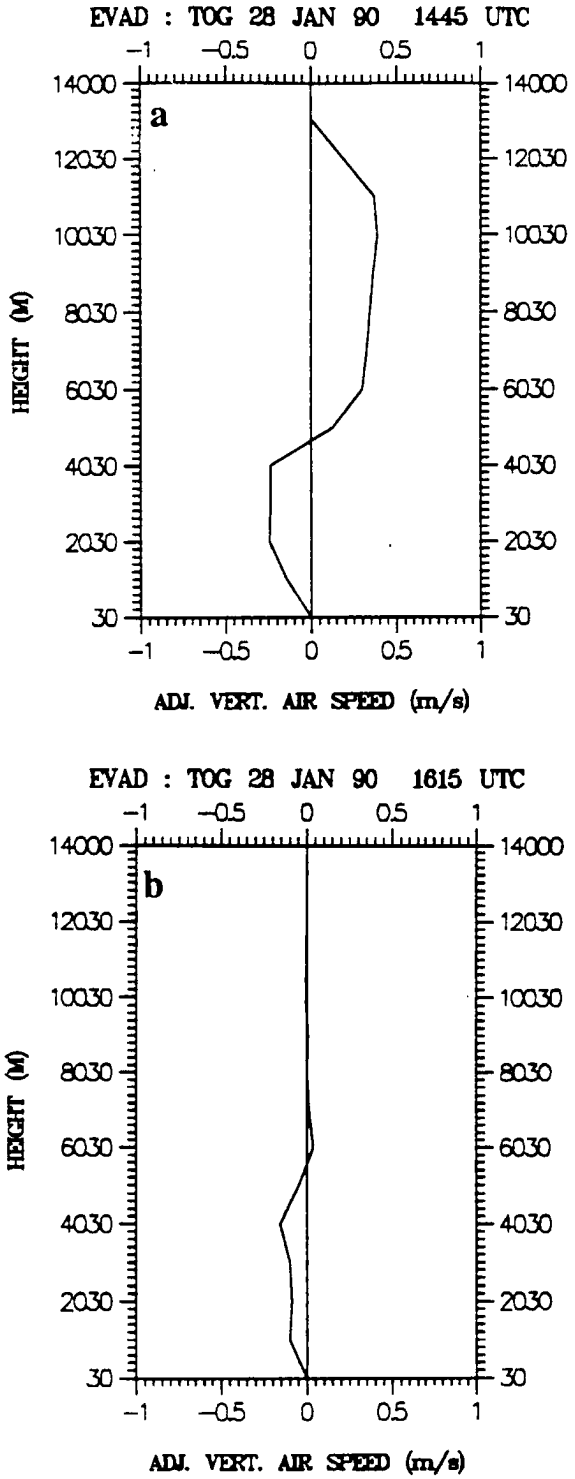


Figure 5.31 Same as Figure 5.27 except for 28 January 1990 (velocities diagnosed from TOGA radar data) at (a) 1445 UTC and (b) 1615 UTC.

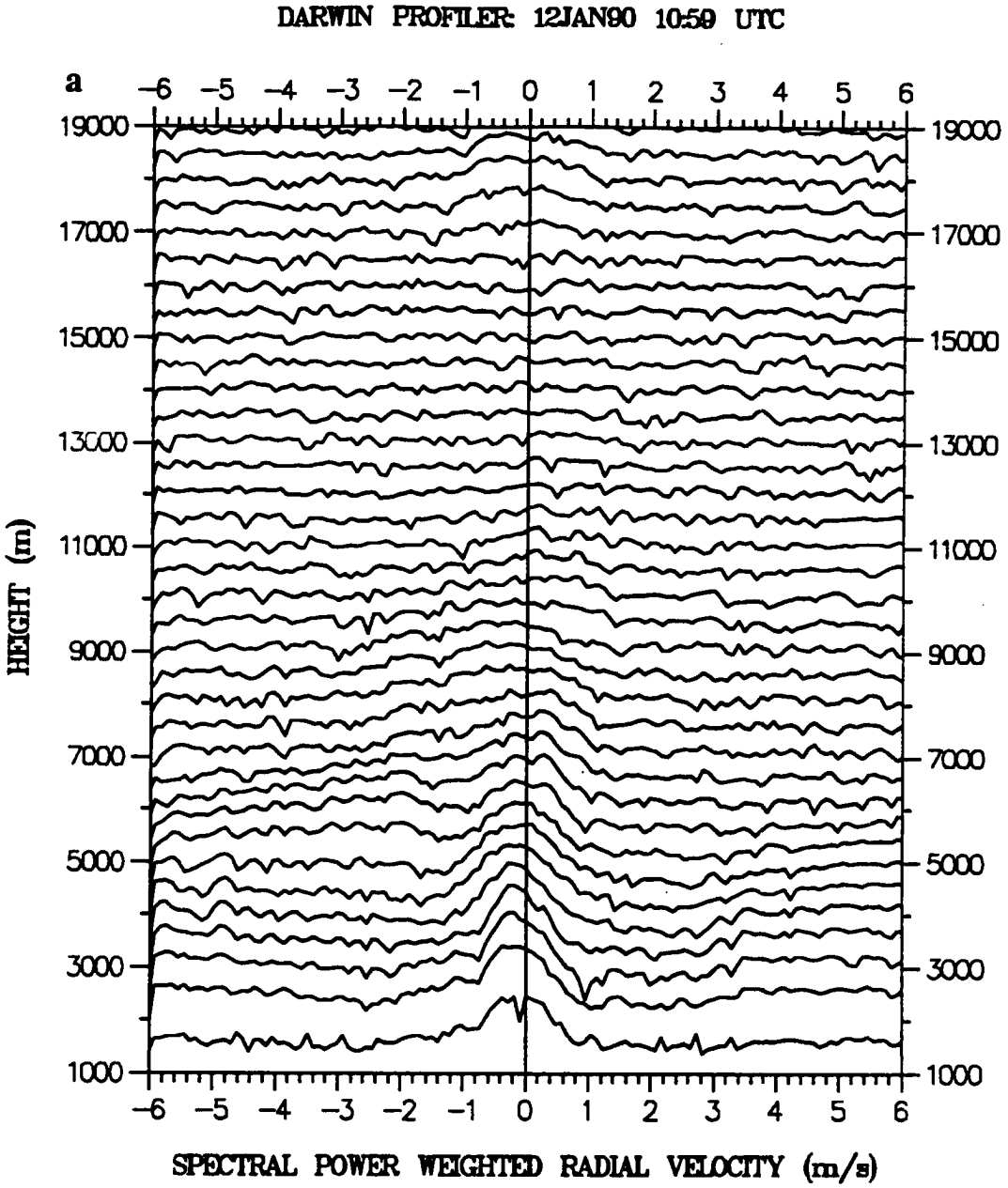


Figure 5.32 Same as Figure 5.26 except for 12 January 1990 at (a) 1059 UTC.

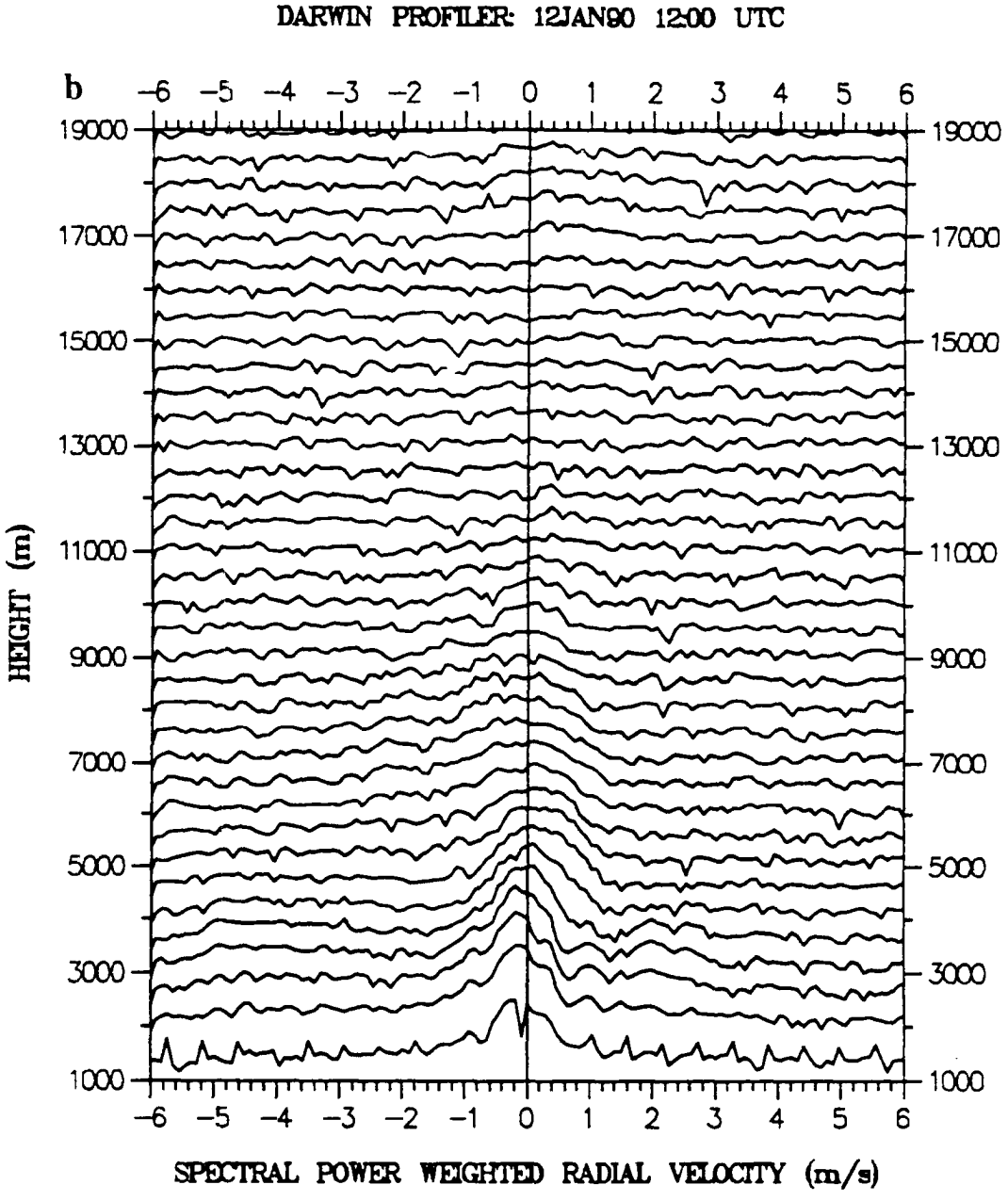


Figure 5.32 (b) 1200 UTC.

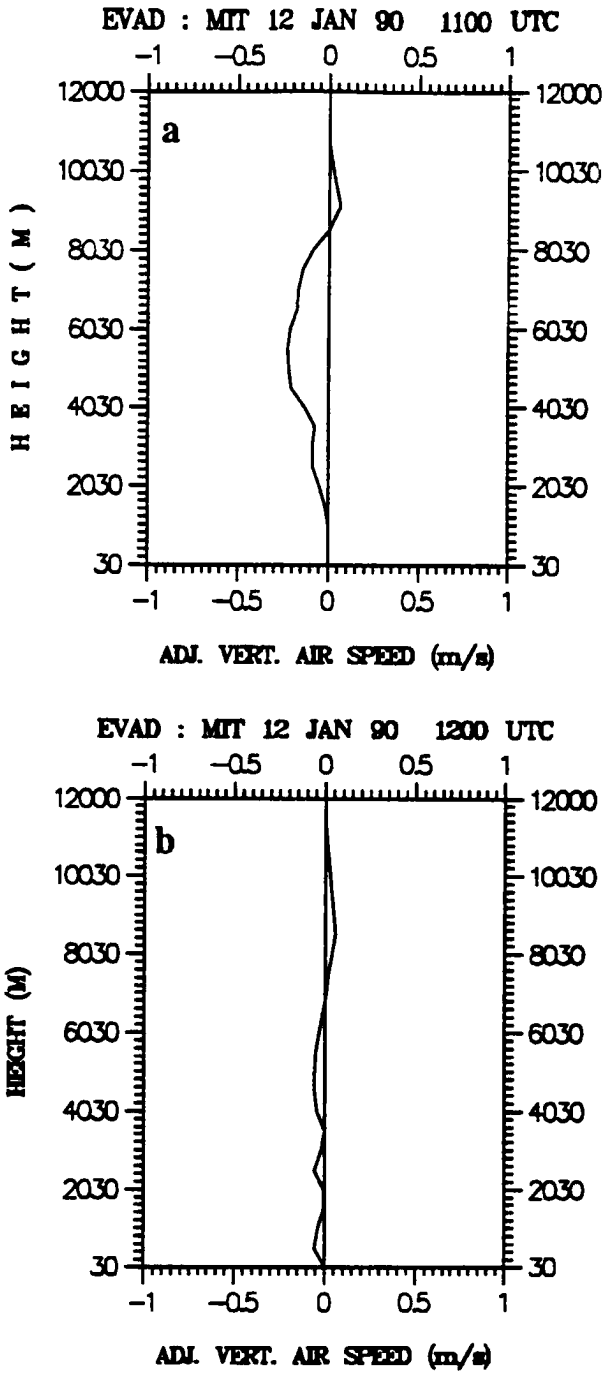


Figure 5.33 Same as Figure 5.27 except for 12 January 1990 at (a) 1100 UTC and (b) 1200 UTC.

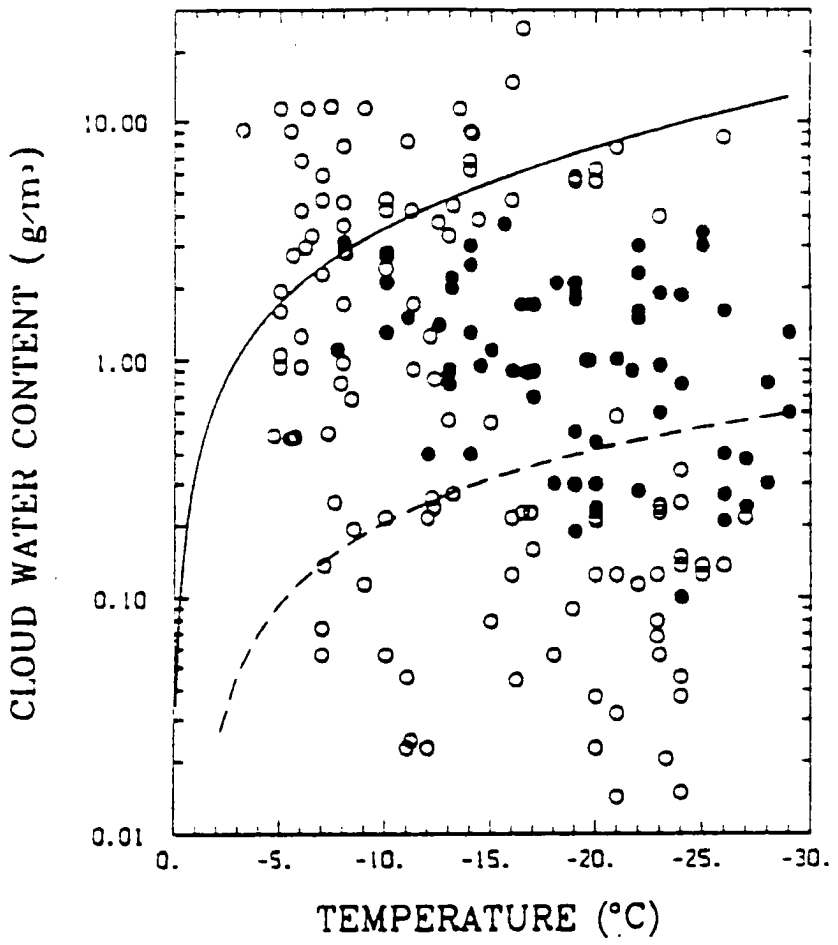


Figure 5.34 Non-inductive charging diagram from Williams et al .(1991). The theoretical results of Williams et al. (1991) are overlaid on the laboratory results of Takahashi (1978). Black (white) dots represent negative (positive) charging of a riming ice surface (Takahashi, 1978). The dashed line represents a theoretical boundary between depositional (positive charging) and sublimational (negative charging) growth states of an ice surface as a function of the liquid water content and temperature of the environment (deposition below the line, sublimation above). The solid line marks the boundary between wet (positive charging) growth of the ice surface and sublimation (negative charging) of the ice surface (Williams et al. 1991).

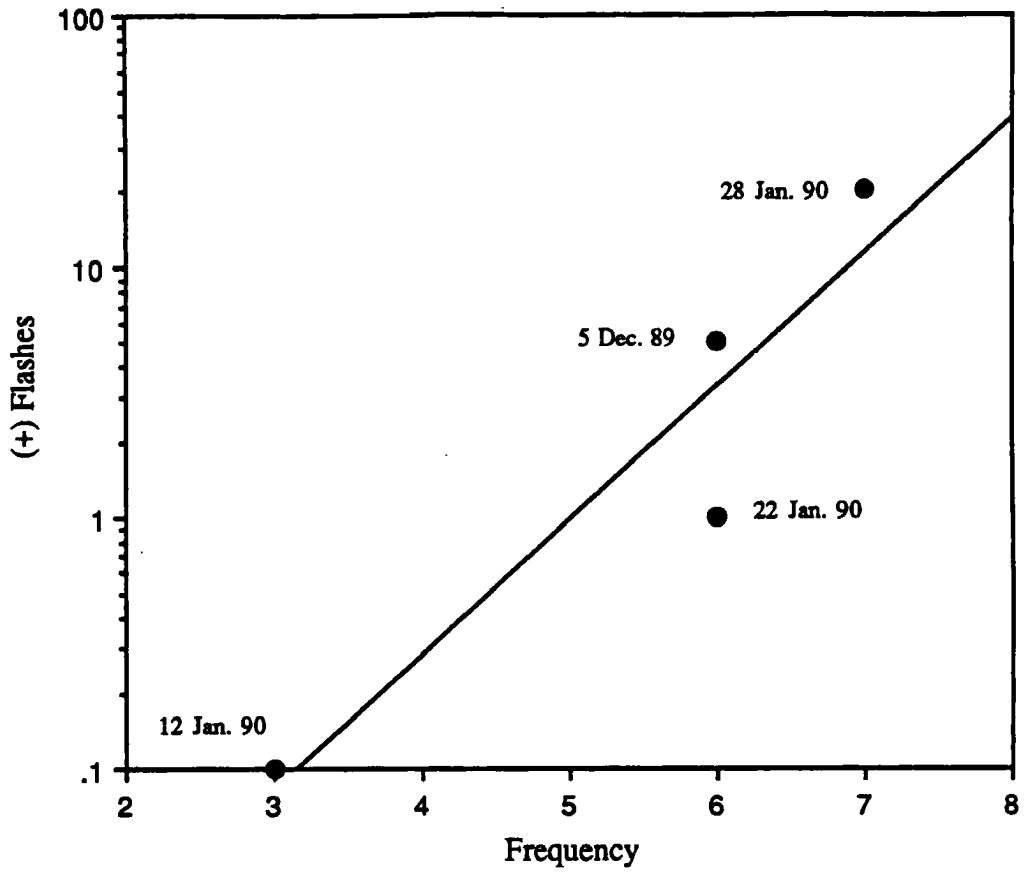


Figure 5.35 The number of positive CGs observed in the stratiform regions of four MCSs vs. the frequency of 10 minute time periods with peak updrafts ≥ 30 cm $s^{-1}$ (as determined from the wind profiler).

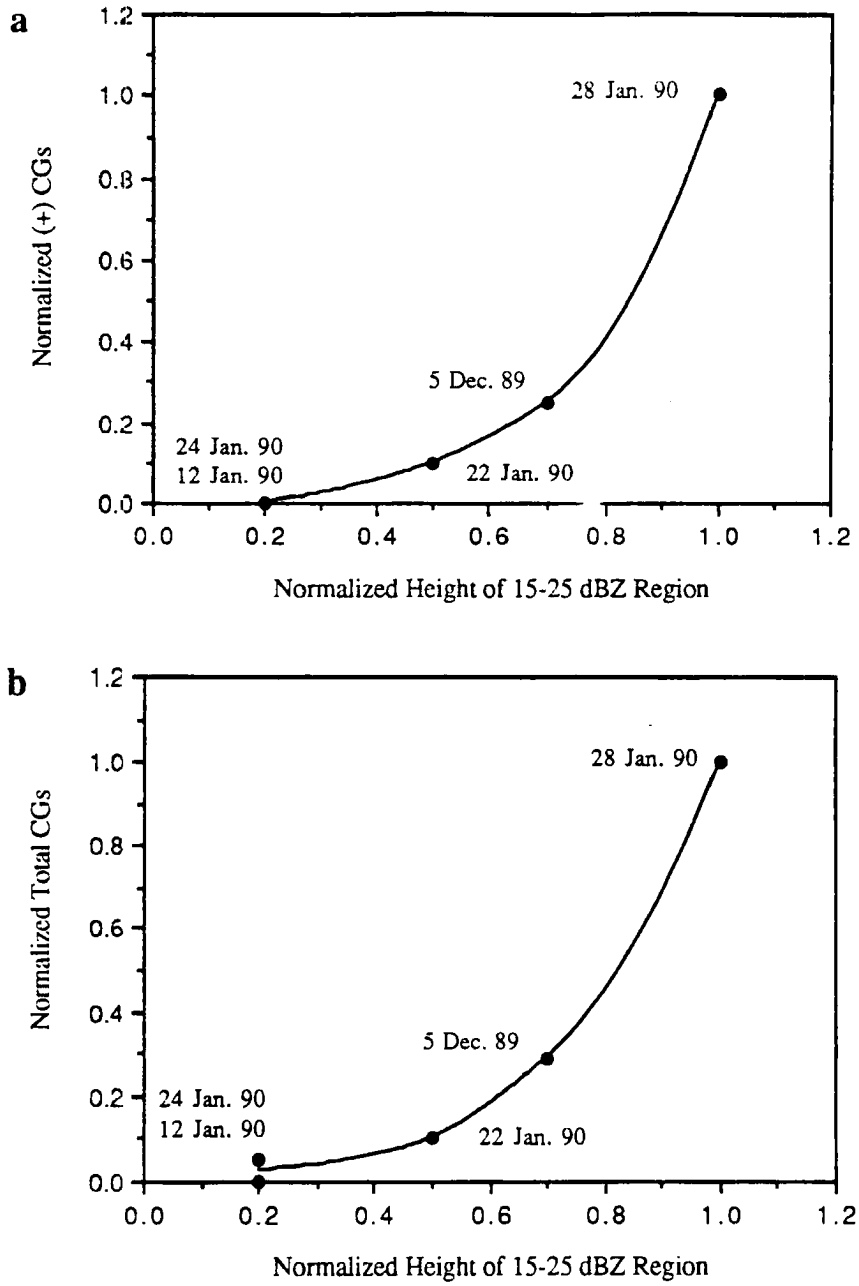


Figure 5.36 The normalized height of the 15-25 dBZ reflectivity region vs. (a) the normalized number of positive CGs that occurred in each stratiform region; and (b) the normalized number of total CGs (positives and negatives) that occurred in each stratiform region.

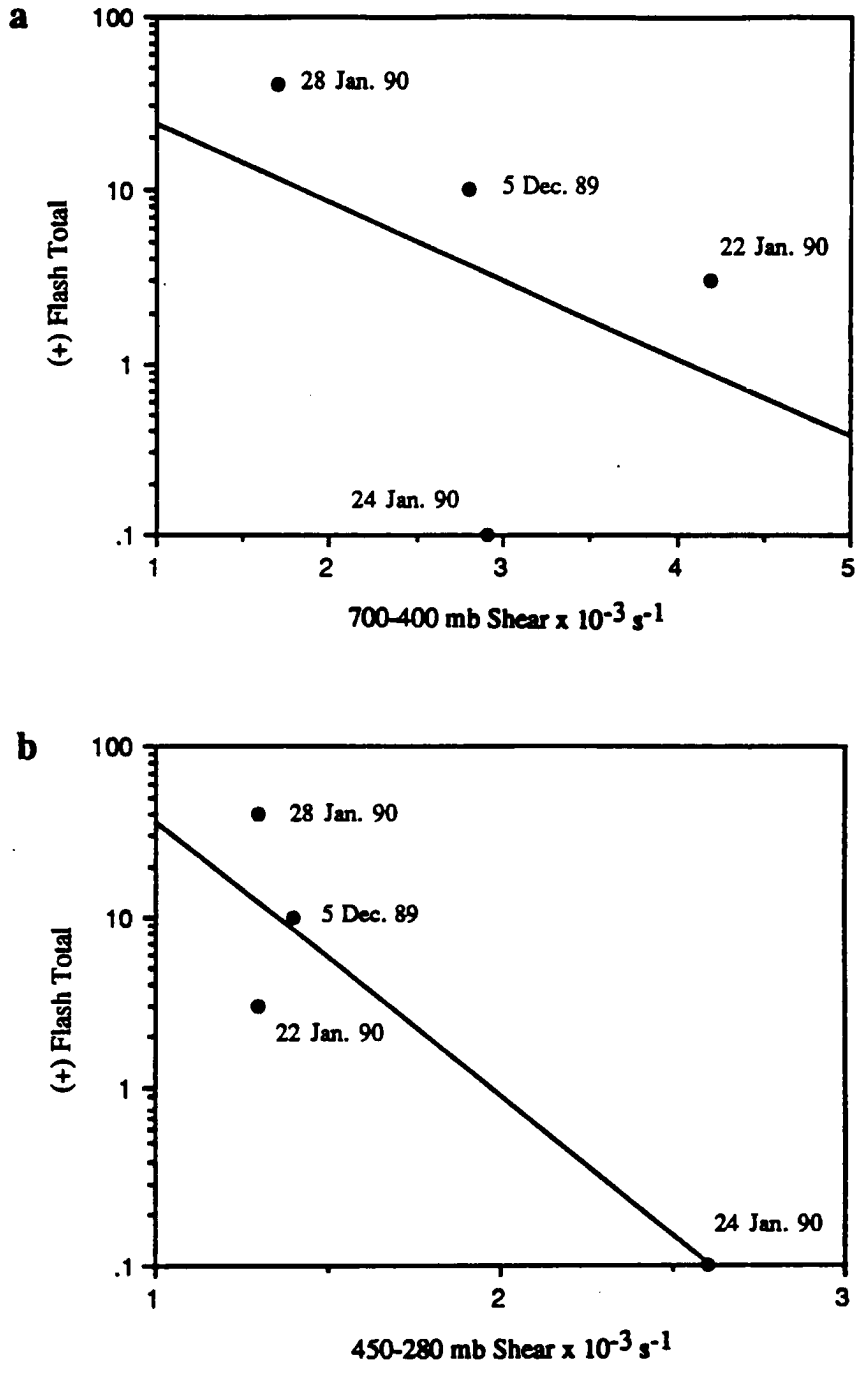


Figure 5.37 The number of positive CGs that occurred in each of four break period stratiform regions vs (a) the storm relative 700-400 mb shear; and (b) the storm relative 450-280 mb (7-10 km) shear.

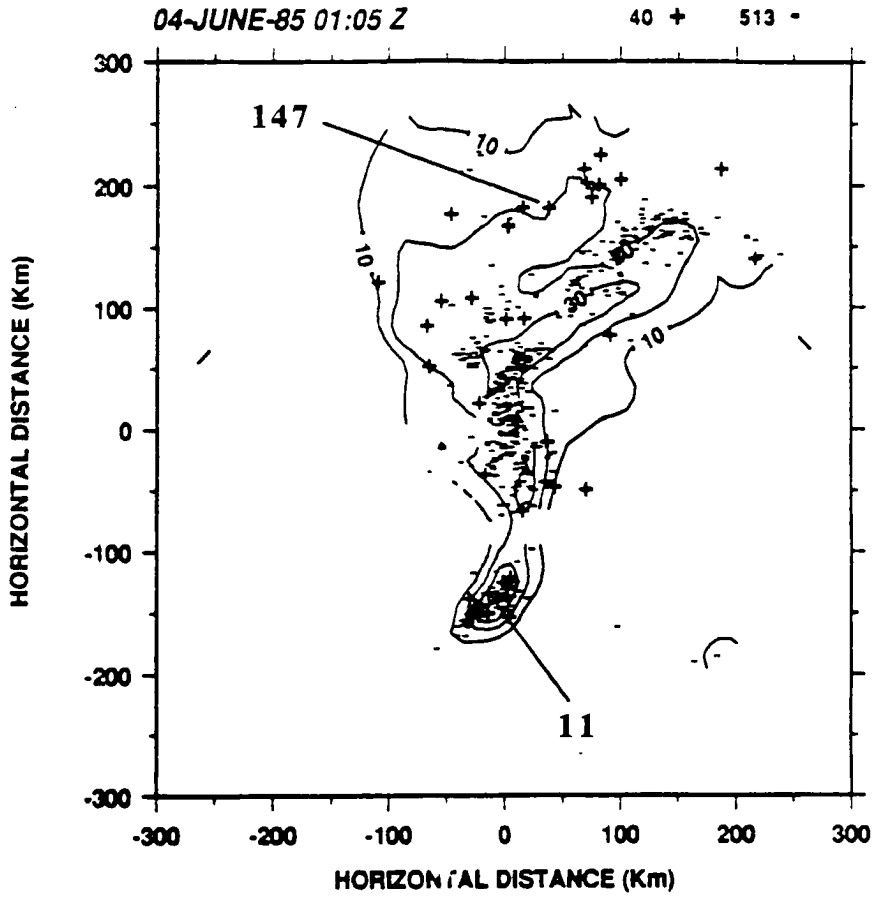


Figure 5.38 WSR-57 low level PPI of radar reflectivity (indicated by solid contours), cloud-to-ground lightning, and positive peak current extrema for the 3-4 June 1985 MCS at 0105 UTC (adapted from Rutledge et al. 1990). The location and polarity of cloud-to-ground flashes which occurred during a 30 minute interval centered on the time of the radar are indicated by a (+) for positive flashes and a (-) for negative flashes. The maximum (minimum) positive peak current is 147 (11) kA.

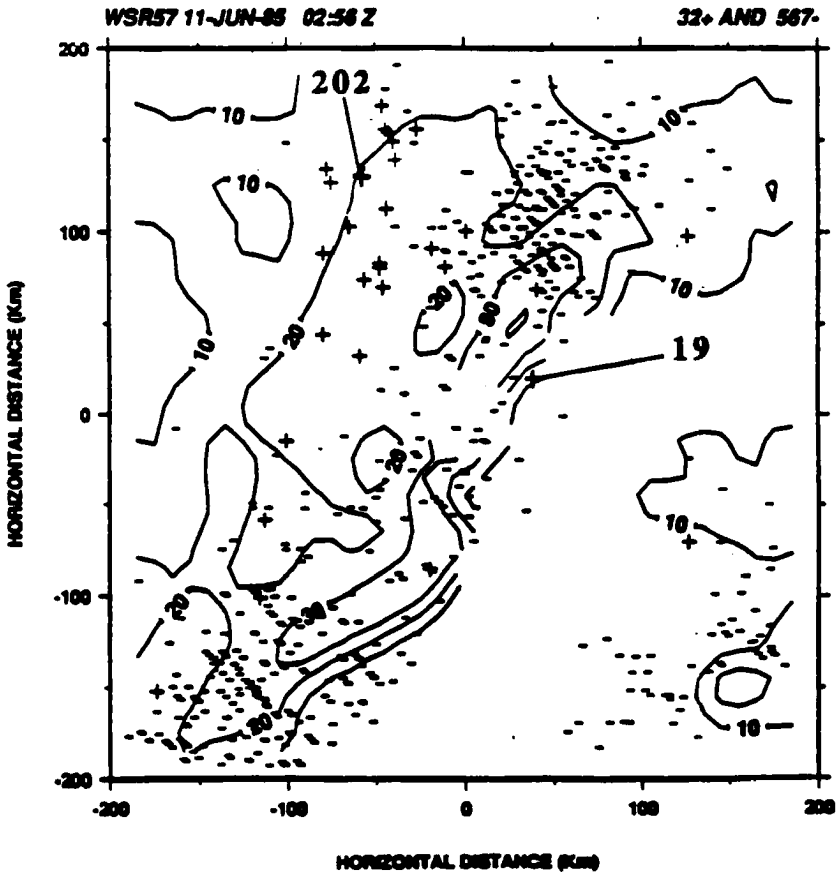


Figure 5.39 Same as Figure 5.38 except for 0256 UTC, 10-11 June 1985 (adapted from Rutledge and MacGorman, 1988). The maximum (minimum) positive peak current is 202 (19) kA.

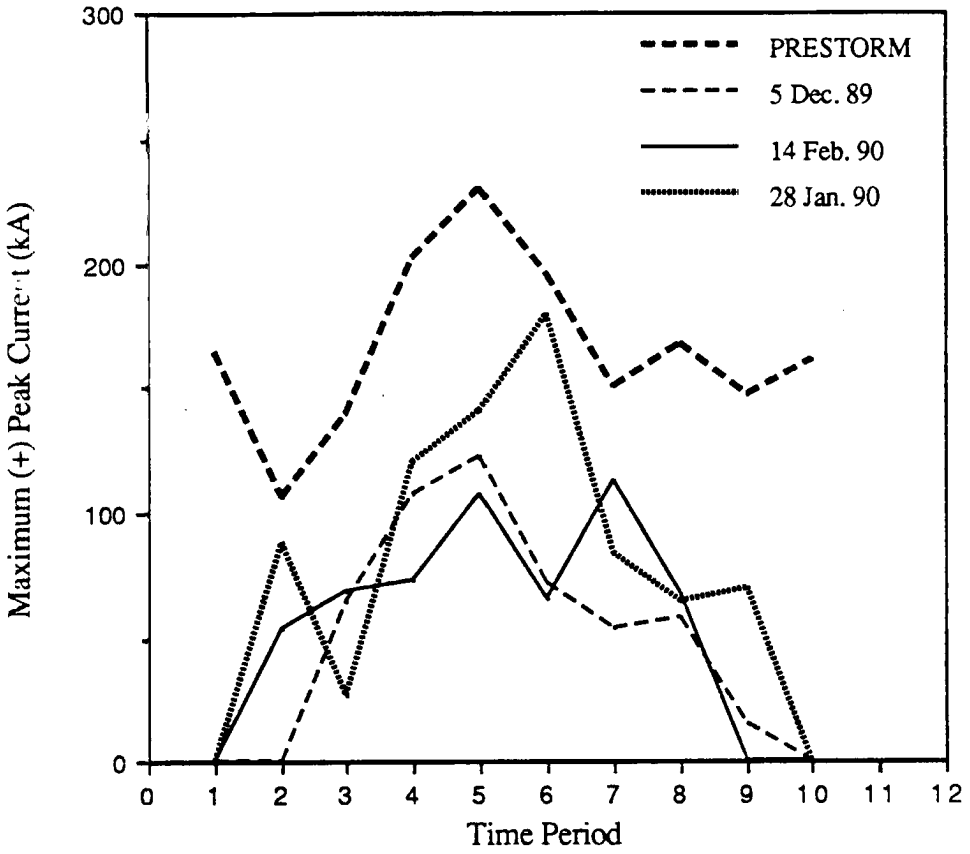


Figure 5.40 Time series of maximum positive peak current (units of kA, plotted on ordinate) observed in each 30 minute period (plotted on abscissa) of an MCS lifecycle. Time 1 indicates growth of the convective line, times 4-7 the growth of the trailing stratiform region, and times 10-12 dissipation of the MCS.

# CHAPTER 6

# CONCLUSIONS AND RECOMMENDATIONS FOR FUTURE RESEARCH

This thesis presents a description of the cloud-to-ground lightning flashes associated with the trailing stratiform regions of seven tropical MCSs observed during the second field phase (1989-90) of the DUNDEE. Through observational analyses of radar, wind profiler, and electric field data combined with a simple one-dimensional model an effort was made to determine the charging mechanism responsible for the CGs observed in the stratiform regions- particularly positive CGs. To complete the description, general statistics for a small sample of the cloud-to-ground lightning observed during the DUNDEE were also presented and compared to similar statistics in other geographical regions.

## 6.1 Observations and a possible mechanism for cloud-to-ground lightning in the trailing stratiform regions of tropical MCSs

The seven MCSs examined in Chapter 5 were comprised of six "break" period tropical squall lines and one "monsoon" period tropical squall line. Each system was characterized as having a leading convective line and a trailing region of stratiform precipitation. Compared to middle-latitude MCSs such as the 3-4 June 1985 MCS (Fig. 38) and the 10-11 June 1985 MCS (Fig. 39), the tropical systems produced fewer

numbers of cloud-to-ground flashes. The break period systems were generally more intense and exhibited a higher degree of electrification than the monsoon MCS. Cloud-to-ground flash rates were variable, with the break period 28 January 1990 MCS (Fig. 5.16) producing the largest number of CGs in a single 30 minute period (300) and the 12 January 1990 MCS (monsoon; Fig. 5.22a-c) producing the lowest number of CGs (no cloud-to-ground flashes were detected during the observational period of some 3 hours). Similar to observations made in middle-latitude MCSs (e.g., Orville et al. 1987; Rutledge and MacGorman, 1988; Engholm et al. 1990; Rutledge et al. 1990), bipolar CG patterns were found in several of the tropical MCSs examined herein (i.e., 5 December 1989; 28 January 1990, 14 February 1990, 15 February 1990). Importantly, the bipolar patterns were not true CG "bipoles" since a few negative CGs were also detected in the stratiform regions.

When vertical cross-sections of reflectivity were examined in five of the MCSs, it was found that those squall lines associated with bipolar CG patterns (i.e., those which produced relatively larger numbers of positive CGs in the stratiform region) exhibited regions of 15-25 dBZ radar reflectivity which extended well above the 0 °C level within stratiform cloud. Further, the locations of positive CGs (and a few negative CGs) were identified with these enhanced reflectivity regions above the 0 °C level (e.g., 5 December 1989; 28 January 1990). Indeed, in the 28 January 1990 case it appeared that the locations of positive CGs (and several negative CGs) in the developing region of stratiform precipitation were collocated with discrete enhancements in the reflectivity field (e.g., Fig. 5.18a) which may have been associated with weak embedded convection in the developing stratiform region. Discrete enhancements in the reflectivity field located in close proximity to positive CGs were also noted in the 5 December 1989 case (e.g., Figs 5.5a-c). The cases which exhibited stronger reflectivities above the 0 °C

level also possessed stronger, longer lived mesoscale updrafts (though the updrafts in all the cases examined appeared to vary in magnitude over time and space).

MCSs which produced little or no cloud-to-ground lighting in the stratiform regions (i.e., 12 January 1990, 22 January 1990, 24 January 1990) exhibited weaker vertical reflectivities, and in the case of the 12 January 1990 *monsoon* case a weaker, highly variable mesoscale updraft (i.e., the updraft varied in depth and location over short time periods). In these MCSs only small regions of 15-25 dBZ reflectivities were located above the 0 °C level. Thus it appears that the intensity of precipitation located above the 0 °C level in the stratiform regions is related to the electrification of stratiform cloud. This relationship was previously noted by Mach et al. (1991) as existing in ordinary winter stratiform clouds located over Florida. In fact, Mach et al. (1991) inferred from surface radar and in-situ electric field data that the electrification of the winter stratiform clouds was linked to the strength of the mixed phase regions observed therein (thus linking the electrification of the stratiform clouds to non-inductive charging processes).

To evaluate the possible existence of a mixed phase region in the tropical stratiform regions (i.e., the existence of supercooled liquid water) a simple calculation using a one-dimensional model of the vertical flux of water vapor was carried out. Assumptions of water saturation (in-cloud), steady state saturated specific humidity, and horizontal homogeneity in the saturated specific humidity field were made. In addition, water vapor was assumed to be either deposited directly onto an ice surface or condensed to create supercooled liquid water. With the above assumptions, the calculation was performed for one break period MCS (5 December 1989) and one

monsoon period MCS (12 January 1990) using vertical velocities diagnosed from wind profiler data and in-situ temperature soundings.

The model results predicted that supercooled liquid water contents on the order of 0.2 g $m^{-3}$ could be realized in the 5.7-7.2 km levels of the break period case (-5 °C to -12 °C; Table 5.1) which is consistent with previous in-situ observations (e.g., Yeh et al. 1991). Supercooled liquid water was also produced in the monsoon case (Table 5.2), however the amounts were substantially lower (i.e. < 0.1 g $m^{-3}$). The model predicted water quantities were sensitive to both updraft strength and ice particle concentrations. When the modeled liquid water contents were compared with the non-inductive charging theory of Williams et al. (1991) and Takahashi (1978), it was found that positive charge would be created in the -5 °C to -12 °C layer for the break period case (even when the updraft was adjusted to lower or higher values). For the monsoon case, the diagram from Williams et al. (1991) indicated that weak positive charging would result in layers between -5 °C and -12 °C. When a weak updraft was present in the very lowest layers of the monsoon case, 0.1 g $m^{-3}$ of supercooled water was located near the 0 ° C isotherm and negative charging would occur.

The modeling results above appear to be consistent with electric field, LLP and radar observations made in the break period case (5 December 1989). On 5 December 1989 the vertical component of the electric field measured at the surface (Fig. 5.6) indicated strong positive charge overhead coincident with the time stratiform cloud was located over the field mill. The LLP network detected approximately 10 positive CGs in the trailing stratiform region of the 5 December 1989 MCS that appeared to be collocated with regions of enhanced reflectivity in the verticle (i.e., the region of 15-25 dBZ reflectivity located above the 0 °C isotherm; Figs. 5.3d, 5.5a-c). The enhanced

reflectivities may be the result of a stronger mixed phase region according to the model predicted liquid water contents. The above are also consistent with recent in-situ observations of the vertical electric field in middle-latitude stratiform regions where layers of substantial positive charge were located in the -5 °C to -12 °C temperature range (e.g., Schuur et al. 1991; personal communication Mr. Terry Schuur).

In the 22 January 1990 break period case the electric field mill (Fig. 5.10) also indicated positive charge overhead (though quite weak) coincident with the time stratiform cloud was located over the field mill. Further, positive CGs that occurred in the northeastern portion of the 22 January 1990 (Fig. 5.7d) stratiform region may have been associated with a more intense area of stratiform precipitation (as indicated by the height of the 15-25 dBZ reflectivity region; Figs. 5.8d-e). The 24 January 1990 break period MCS also exhibited weak electrification (Fig. 5.15) coincident with time periods in the stratiform region where the 15-25 dBZ reflectivity region appeared to extend just above the 0 °C level over the field mill (Fig. 5.13d).

For the monsoon case of 12 January 1990, the model calculations indicated that only small amounts of liquid water (i.e., $< 0.1$ g $m^{-3}$) would be produced above the 0 °C level. Note that this particular monsoon case exhibited generally weaker reflectivities above the 0 °C isotherm and produced no cloud-to-ground lightning during the observational period. Electric field data for this case indicated that very weak negative charge was located overhead at first (coincident with the time that stratiform cloud was located over the field mill), with a reversal to very weak positive charge overhead at later time periods (Fig. 5.25). This observation coupled with those above seems to indicated that the strength of the mixed phase region in the stratiform clouds is related to the electrification therein, and hence a non-inductive charging mechanism may

respectively), and the relative frequencies of peak currents for each polarity of flash. We also compared the middle latitude peak current distributions of Orville et al. (1987) and López et al. (1991) to our peak current distributions from the tropics. The middle latitude flash distributions presented by Orville et al. (1987) demonstrated a marked difference in the median peak current between flashes of different polarity and a tendency for flashes with peak currents greater than 100 kA to be positive. The tropical ground flash median peak currents (by polarity) differed by only 2 kA (similar to López et al. 1991) and there was no clear tendency for flashes with large peak currents to be positive (e.g., Brook et al. 1982).

While the 5000 flashes we examined are considerably less than the 5 million flashes examined in the Orville (1990) study, we did find comparable results with regard to the mean peak currents, *independent of polarity*. The flashes we examined from the DUNDEE had an average peak current of approximately 39 kA while those flashes examined by Orville (1990) for Florida thunderstorms had an average peak current of approximately 45 kA. This result, coupled with the similarity in storm top heights between the MCSs we examined from the DUNDEE and those reported by Orville (1990) for Florida thunderstorms, lead us to suggest that Orville's (1990) hypothesis of peak current variation with latitude is reasonable if average storm top height is included.

## 6.3 Recommendations for future research

The DUNDEE was undertaken to study the electrification of tropical MCSs, however several key observations needed to completely solve the problem of MCS electrification were not available. For example, it is important to know where the cloud-to-ground lightning flashes are originating within the clouds. As mentioned at the end

be the process responsible for generation of cloud-to-ground lightning in the stratiform regions of MCSs.

The existence of an in-situ, non-inductive charging mechanism in the stratiform regions was further supported by the finding that a tendency existed for positive peak current maxima to occur primarily in the trailing stratiform regions of MCSs (two middle-latitude MCSs, and six tropical MCSs). Conversely, the positive peak current minima tended to occur in the convective regions of the MCSs studied. Neither tendency was found for negative CG peak currents. In many cases the magnitude of the positive peak current maximum in the stratiform region was an order of magnitude greater than the minimum positive peak current in the convective region. Further, maximum positive peak currents were found to occur at large distances (i.e., $\geq$ 30 km) from the convective line, and during the time of maximum growth and intensification of the stratiform regions (implying that microphysical processes in a developing mesoscale updraft may have been involved in the charging of the stratiform regions). The above observations are therefore consistent with the hypothesis that an in-situ, non-inductive charging process is the *primary* mechanism responsible for creating cloud-to-ground lightning in the trailing stratiform regions of MCSs.

## 6.2 Statistical summary

Basic statistics (see Appendix A) for approximately 5000 cloud-to-ground flashes observed during the DUNDEE were presented. These included the average peak current of the first return stroke (39 kA), the median positive (32 kA) and negative (34 kA) peak currents, the percent of total ground flashes with positive polarity (9%), the average flash rate (2.5 $min^{-1}$), maximum and minimum peak currents (346 kA and 4 kA

of Chapter 5, it is possible that positive CGs may originate in the convective line and propagate rearward over large distances through the stratiform cloud prior to reaching ground (Rust, 1986). Observations of the origin of the cloud-to-ground lightning channels in stratiform clouds (e.g., *acoustic*, MacGorman et al.1983; *interferometer*, Warwick et al. 1979; *field mill*, Krehbiel et al. 1979; or *radar* observations; Mazur et al. 1984) would help solve this problem and should be undertaken in future MCS electrification research in the tropics and the middle-latitudes.

Another key observation that needs to be made in tropical MCSs is the *in-situ* observation of the electric field (i.e., aircraft or balloon based electric field meters). Many electric field soundings have been taken in both the convective lines and stratiform regions of middle-latitude MCSs (e.g., Schuur et al. 1990; Marshall and Rust, 1991). In the stratiform regions of the middle-latitude MCSs similar electric field profiles have been obtained in different storms (personal communication, Dr. Tom Marshall and Mr. Terry Schuur). If some universal mechanism for the electrification of stratiform regions does exist, then the same *general* profiles should also be observed in the trailing stratiform regions of tropical MCSs.

Perhaps the most important type of data needed for tropical and middle-latitude MCS stratiform regions is microphysical information. This would include datasets containing not only hydrometeor and liquid water concentrations and size distributions in stratiform clouds, but also observations of the amount and sign of the charge residing on the particles (e.g., Weinheimer et al. 1991). Further, the data should not be limited to only the bright band and middle-levels of the stratiform cloud. The microphysical data should also be collected in the upper regions of the stratiform cloud (admittedly not

an easy task at present). This type of data could provide direct evidence to support or refute non-inductive charging hypotheses.

For the statistical data base and for research exploring cloud-to-ground lightning and the global electric circuit, a much larger network of lightning location and detection equipment should be established in the tropics (e.g., similar to the National Lightning Detection Network in the United States; see Orville 1986). This would also enable further investigation of latitudinal variation in the peak currents of cloud-to-ground flashes (e.g., Orville, 1990).

## REFERENCES


Baker, B., Baker, M.B., Jayaratne, E.R., Latham, J., and Saunders, C.P.R., 1987: The influence of diffusional growth rates on the charge transfer accompanying rebounding collisions between ice crystals and soft-hailstones. *Q.J.R., Meteorol. Soc.*, **113**, 1193-1215.

Bataan, L. J., 1973: Radar observation of the atmosphere. Univ. of Chicago Press, pp. 319.

Berger, K., R.B. Anderson, and H. Kroninger, 1975: Parameters of lightning flashes. *Electra.*, **80**, 23-37.

Biggerstaff, M.I., and R.A. Houze, Jr., 1991: Kinematic structure of the transition-zone downdraft in the 10-11 June 1985 squall line observed over Kansas and Oklahoma. *25th International Conference on Radar Meteorology*, June 24-28, 1991, Paris, France.

Bourdeau, C., and S. Chauzy, 1989: Maximum electric charge of a hydrometeor in the field of a thundercloud. *J. Geophys. Res.*, **94**, 13121-13126.

Breed, D.W., and J.E. Dye, 1989: The association of negative charge with precipitation in New Mexico thunderstorms. *AMS Preprint, 24th International Conference on Radar Meteorology*, Tallahassee, Florida.

Brook, M., M. Nakano, P. Krehbiel, and T. Takeuti, 1982: The electrical structure of the Hokuriku winter thunderstorms. *J. Geophys. Res.*, **87**, 1207-1215.

------, R.W. Henderson, and R.B. Pyle, 1989: Positive lightning strokes to ground. *J. Geophys. Res.*, **94**, 13295-13304.

Bruce, C.E.R., and R.H. Golde, 1941: The lightning discharge. *J. Inst. Elect. Eng.* (London), **88** (Pt. 2),487-524.

Caranti, G.M., E.E. Avila, and M.A. Re, 1991: Charge transfer during individual collisions in ice growing from vapor deposition. *J. Geophys. Res.*, **96**, 15365-15375.

Chauzy, S., M. Chong, A. Delannoy, and S. Despiau, 1985: The June 22 tropical squall line observed during COPT 81 experiment: Electrical signature associated with dynamical structure and precipitation. *J. Geophys. Res.*, **90**, 6091-6098.

Cunning, J.B., 1986: The Oklahoma-Kansas preliminary regional experiment for STORM-Central. *Bull. Amer. Meteor. Soc.*, **67**, 1478-1486

Dye, J.E., J.J. Jones, A.J. Weinheimer, and W.P.Winn: Observations within two regions of charge during initial thunderstorm electrification. Q.J.R. Meteorol. Soc., **114**, 1271-1290.

Elliot, W.P., and D.J. Gaffen, 1991: On the utility of radiosonde humidity archives for climate studies. *Bull. Amer. Meteor. Soc.*, **72**, 1507-1520.

Elster, J., and H. Geital, 1913: Zur Influenztheorie der Niederschlagselek-trizitat. *Phys. Z.*, **14**, 1287.

Engholm C.D., E.R. Williams and R.M. Dole, 1990: Meteorological and electrical conditions associated with positive cloud-to-ground lightning. *Mon. Wea. Rev.*, **118**, 470-487.

Fritsch J.M, and R.A. Maddox, 1981: Convectively driven mesoscale weather systems aloft. *J. Appl. Meteor.*, **20**, 9-19.

Gamache, J.F., and R.A. Houze, Jr., 1982: Mesoscale air motions associated with a tropical squall line. *Mon. Wea. Rev.*, **110**, 118-135.

------, 1990: Microphysical observations in summer MONEX convective and stratiform clouds. *Mon. Wea. Rev.*, **118**, 1239-1249.

Gaskell, W., 1979: Field and laboratory studies of precipitation charge. Ph.D. Thesis, Univ. of Manchester.

Heymsfield, A.J., and M.R. Hjelmfelt, 1984: Processes of Hydrometeor development in Oklahoma convective clouds. *J. Atmos. Sci.*, **41**, 2811-2835.

Hill, R.D., 1988: Interpretation of bipole patterns in a mesoscale storm. *Geophys. Res. Lett.*, **23**, 643-645.

Houze, R.A., Jr., and D.D. Churchill, 1984: Microphysical structure of winter monsoon cloud clusters. *J. Atmos. Sci.*, **41**, 3405-3411.

Illingworth, A.J., and J. Latham, 1977: Calculations of electric field structure and charge distributions in thunderstorms. *Q.J.R. Meteorol. Soc.*, **103**, 281-295.

Jacobson, E.A., and E.P. Krider, 1976: Electrostatic field changes produced by Florida lightning. *J. Atmos. Sci.*, **33**, 103-117.

Johnson, R.H., 1984: Partitioning tropical heat and moisture budgets into cumulus and mesoscale components: Implications for cumulus parameterization. *Mon. Wea. Rev.*, **112**, 1590-1601.

Kasemir, H.W., 1979: The atmospheric electric global circuit. *Proceedings: Workshop on the need for lightning observations from space.* National Aeronautics and Space Administration, Tullahoma, TN, 136-147.

Keenan T., and S.A. Rutledge, 1992: Mesoscale characteristics of monsoonal convection and associated stratiform precipitation. (Submitted) *Mon. Wea. Rev.*

Keith, W.D., and C.P.R. Saunders, 1989: Charge transfer during multiple large ice crystal interactions with a riming target. *J. Geophys. Res.*, **94**, 13103-13106.

Krehbiel, P.R., M. Brooks, and R.A. McCrory, 1979: An analysis of the charge structure of lightning discharges to ground. *J. Geophys. Res.*, **84**, 2432-2456.

Krehbiel, P.R., 1986: The electrical structure of thunderstorms. *The Earth's Electrical Environment*. National Academy Press, pp. 90-113.

Krider, E.P., R.C. Noggle, and M.A. Uman, 1976: A gated wideband magnetic direction finder for lightning return strokes. *J. Appl. Meteor.*, **15**, 301-306.

Jayaratne, E.R., C.P.R. Saunders, and J. Hallet, 1983: Laboratory studies of the charging of soft hail during ice crystal interactions. *Quart. J. Roy. Met. Soc.*, **109**, 609-630.

Jorgensen D.P., and M.A. Lemone, 1989: Vertical velocity characteristics of oceanic convection. *J. Atmos. Sci.*, **46**, 621-640.

Leary, C.A., and R.A. Houze, Jr., 1979: Melting and evaporation of hydrometeors in precipitation from anvil clouds of deep tropical convection. *J. Atmos. Sci.*, 36, 669-679.

Lewis, W.W., and C.M. Foust, 1945: Lightning investigations on transmission lines, Pt. 7. *Trans. AIEE*, **64**, 107-115.

MacGorman D.R., W.L. Taylor, and A.A. Few, 1983: Lightning location from acoustic and VHF techniques relative to storm structure from 10 cm radar. *Proceedings in Atmospheric Electricity*, A. Deepak Publishing, Hampton, Va., 377-380.

Mackerras, D., 1968: A comparison of discharge processes in cloud and ground lightning flashes. *J. Geophys. Res.*, **73**:4, 1175-1183.

Mach, D.M., D.R. MacGorman, W.D. Rust and R.T. Arnold, 1986: Site errors and detection efficiency in a lightning strike locating system. *J. Atmos. Oceanic Technol.*, **3**, 67-74.

Mach, D.M., J.C. Bailey, and H.J. Christian, 1991: Electrification of stratiform winter clouds near the Kennedy Space Center, Florida. EOS, Transactions of the AGU, Fall Meeting, San Francisco, California, December 9-13, 1991.

Marshall, T.C., and W.D. Rust, 1991: Electric field soundings through thunderstorms. *J. Geophys. Res.*, **96**, 22297-22306.

Matejka, T., and R.C. Srivastava, 1991: An improved version of the extended velocity-azimuth display analysis of single Doppler radar. *J. Atmos. Oceanic Technol.*, 8, 453-466.

Mazur, V., B.D. Fisher, and W.D. Rust, 1984: Lightning flash density versus altitude and storm structure from observations with UHF- and S-band radars. *Geophys. Res. Ltrs.*, **11**, 61-64.

Mohr, C.G., L.J. Miller, R. Vaughan, and H. Frank, 1986: The merger of mesoscale datasets into a common Cartesian format for efficient and systematic analysis. *J. Atmos. Oceanic. Technol.*, **3**, 143-161.

Murray, F.W., 1967: On the computation of saturation vapor pressure. *J. Appl. Meteor.*, **6**, 203-204.

Orville, R.E., and R.W. Henderson, 1986: Global distribution of midnight lightning: September 1977 to August 1978. *Mon. Wea. Rev.*, **114**. 2640-2653.

------, R.A. Weisman, R.B. Pyle, R.W. Henderson and R.E. Orville Jr., 1987: Cloud-to-ground lightning flash characteristics from June 1984 through May 1985: *J. Geophys. Res.*, **92**, 5640-5644.

------, R.W. Henderson and L.F. Bosart, 1988: Bipole patterns revealed by lightning locations in mesoscale storm systems. *Geophys. Res. Lett.*, **15**, 129-132.

------, 1990: Peak-current variations of lightning return strokes as a function of latitude. *Nature*, **342**:6254, 149-151.

------,1991: Calibration of a magnetic direction finding network using measured triggered lightning return stroke peak currents. *J. Geophys. Res.*, **96**, 17135-17142.

Panofsky, H. A., and J. A. Dutton, 1984: Atmospheric turbulence, models and methods for engineering applications. John Wiley and Sons, Inc., New York, NY, 397 pp.

Peckham, D.M., M.A. Uman and C.E. Wilcox Jr., 1984: Lightning phenomenology in the Tampa Bay area. *J. Geophys. Res.*, **89**:11, 11789-11805.

Petersen, W.A., and S.A. Rutledge, 1992: Some characteristics of cloud-to-ground lightning in tropical northern Australia. (Accepted) *J. Geophys. Res.*

Prentice, S.A., and D. Mackerras, 1977: The ratio of cloud-to-ground lightning flashes in thunderstorms. *J. Appl. Meteorol.*, **16**, 545-550.

Rasmussen, E.N., and S.A. Rutledge, 1992: Squall line evolution. Part 1: Kinematic and reflectivity structure. *J. Atmos. Sci.*, (Submitted).

Rawlins, F., 1982: A numerical study of thunderstorm electrification using a three-dimensional model incorporating the ice phase. *Q.J.R. Roy. Meteorol. Soc.*, **108**, 779-800.

Rogers, R.R., 1979: A short course in cloud physics. Pergamon Press, pp. 233.

Rust, W. D. and C. B. Moore, 1974: Electrical conditions near the bases of thunderclouds over New Mexico. *Quart J. Roy. Meteor. Soc.*, **100**, 450-468.

Rust, W.D., 1986: Positive cloud-to-ground lightning. *The Earths Electrical Environment*. National Academy Press, pp. 41-45.

Rutledge, S.A., and R.A. Houze, Jr., 1987: A diagnostic modeling study of the trailing stratiform region of a mid-latitude squall line. *J. Atmos. Sci.*, **44**, 2640-2656.

------, and D.R. MacGorman, 1988: Cloud-to-ground lightning activity in the 10-11 June 1985 mesoscale convective system observed during the Oklahoma-Kansas PRE-STORM project. *Mon. Wea. Rev.*, **116**, 1393-1408.

------, R.A. Houze, Jr., M.I. Biggerstaff, and T. Matejka, 1988: The Oklahoma-Kansas squall line of 10-11 June 1985 observed in PRE-STORM: Precipitation structure and single-Doppler radar analysis. *Mon. Wea. Rev.*, **116**, 1409-1430.

------, C. Lu and D.R. MacGorman, 1990: Positive cloud-to-ground lightning in mesoscale convective systems. *J. Atmos. Sci.*, **47**, 2085-2100.

------, E.W. Williams, W.A. Petersen, and E.N. Rasmussen, 1991: Radar and electrical study of a tropical squall line near Darwin, Australia during DUNDEE. *Preprints, 25 International Conference on Radar Meteorology*, Amer. Meteorol. Soc., Paris, France, June 1991.

------, E.W. Williams and T.D. Keenan, 1992a: The Down Under Doppler and Electricity Experiment (DUNDEE): Overview and preliminary results. *Bull. Am. Meteor. Soc.*, **73**, 3-15.

------, E.W. Williams and W.A. Petersen, 1992b: Lightning and electrical structure of mesoscale convective systems. (Accepted) *Atmos. Res.*

Saunders, C. P. R., and E. R. Jayaratne, 1986: Thunderstorm charge transfer values. *Preprint volume, 23rd Conf. on Radar Meteorology and Conf. on Cloud Physics*, American Meteorological Society, Snowmass, CO, 260-263.

Saunders, C.P.R., W.D. Keith, and R.P. Mitzeva, 1991: The effect of liquid water on thunderstorm charging. *J. Geophys. Res.*, **96**, 11007-11017.

Schuur, T.J., B.F. Smull, W.D. Rust, and T.C. Marshall, 1990: An electrical and kinimatic study of the stratiform precipitation region trailing an Oklahoma squall line. *J. Atmos. Sci.*, **48**, 825-842.

Seinfeld, John H., 1986: Atmospheric chemistry and physics of air pollution. John Wiley and Sons, New York, NY, 738 pp.

Selvam, A.M., R. Vijayakumar, G.K., Manohar, and A.S.R. Murty, 1991: Electrical, microphysical and dynamical observations in summer monsoon clouds. *Atmos. Res.*, **26**, 19-32.

Smull, B.F., and R.A. Houze, Jr., 1985: A mid-latitude squall line with a trailing region of stratiform rain: Radar and satellite observations. *Mon. Wea. Rev.*, **113**, 117-133.

Smull, B.F., and R.A. Houze, Jr., 1987: Rear inflow in squall lines with trailing stratiform precipitation. *Mon. Wea. Rev.*, **115**, 2869-2889.

Srivastava, R.C., T.J. Matejka, and T.J. Lorello, 1986: Doppler radar study of the trailing anvil region associated with a squall line. *J. Atmos. Sci.*, **43**, 356-377.

Stolzenburg, M, 1990: Characteristics of the bipolar pattern of lightning locations observed in 1988 thunderstorms. *Bull. Amer. Meteor. Soc.*, **71**, 1331-1338.

Takahashi, T., 1978: Riming electrification as a charge generation mechanism in thunderstorms. *J. Atmos. Sci.*, **35**, 1536-1548.

Taylor, G. I., 1921: Diffusion by continuous movement. *Proc. London Math. Soc. Ser. 2*, **20**, 196-212.

Turner, D. Bruce, 1969: Workbook of atmospheric dispersion estimates. *Public Health Service Publication No. 999-AP-26*, 84 pp.

Uman, M.A., 1987: The lightning discharge. *Academic Press Inc.*, Orlando, FL, 377 pp.

Warwick, J.W., C.O. Hayenga, and J.W. Brosnahan, 1979: Interferometric directions of lightning sources at 34 MHz. *J. Geophys. Res.*, **84**, 2457-2463.

Weinheimer, A.J., J.E. Dye, D.W. Breed, M.P. Spowart, J.L. Parrish, and T.L. Hoglin, 1991: Simultaneous measurements of the charge, size, and shape of hydrometeors in an electrified cloud. *J. Geophys. Res.*, **96**, 20809-20829.

Williams E.R., 1985: Large-scale charge separation in thunderclouds. *J. Geophys. Res.*, **90**, 6013-6025.

------, 1989: The tripole structure of thunderstorms. *J. Geophys. Res.*, **94**, 13151-13167.

------, R. Zhang, and J. Rydock, 1991: Mixed-phase microphysics and cloud electrification. *J. Atmos. Sci.*, **48**, 2195-2203.

Willis, P.T., and A.J. Heymsfield, 1989: Structure of the melting layer in mesoscale convective system stratiform precipitation. *J. Atmos. Sci.*, **46**, 2008-2025.

Wilson, C.T.R., 1920: Investigations on lightning discharges and on the electric fields of thunderstorms. *Trans. R. Soc.*, **221A**, 73-115.

Winn, W.P., C.B. Moore, C.R. Holmes, and L.G. Beyerly III, 1978: A thunderstorm on July 16, 1975, over Langmuir Laboratory: A case study. *J. Geophys. Res.*, **83**, 3080-3092.

Yeh, J., F. Beifen, W.R. Cotton, and M.A. Fortune, 1991: Observational study of microphysics in the stratiform region and transition region of a mid-latitude mesoscale convective complex. *ACTA Meteorologica Sinica*, **5**, 527-540.

# APPENDIX A

## CLOUD-TO-GROUND LIGHTNING STATISTICS FROM THE DUNDEE

Several studies describing cloud-to-ground lightning (CG) characteristics in the middle-latitudes present the opportunity for comparison to equivalent data collected cloud-to-ground flashes in the tropics. For example, Orville (1990) computed the average peak current magnitude of the first return stroke for approximately five million cloud-to-ground flashes associated with thunderstorms occurring in the the eastern United States, and found a dependence of peak current magnitude on latitude. For example, peak currents in New England storms were 20-25 kA vs. 40-45 kA for storms in Florida. Based on these data, Orville (1990) suggested that peak currents in the tropics might be considerably larger than those in the middle-latitudes. Unfortunately, no conclusions could be drawn since similar data on the cloud-to-ground peak currents in the tropics were not available.

Uman (1987) provided information on cloud-to-ground flash statistics such as flash rates and polarity percentages (percent of total number of flashes lowering either negative or positive charge to ground). Uman, quoting Bruce and Golde (1941), reported that cloud-to-ground flashes with positive polarity (those lowering positive charge to ground) generally comprise 0-30 percent of the total number of CG flashes from a storm system. However, this percentage seems to vary with latitude (Orville,

1990), season (Orville et al., 1987), and geography (Lewis and Foust, 1945). Similar information from the tropics might help to better define some of these variations.

In order to supplement the data base of parameters describing tropical flashes, we present flash statistics compiled from approximately 5000 flashes associated with tropical convection in north central Australia observed during the DUNDEE (Down Under Doppler and Electricity Experiment). More specifically, we present statistics for the average, median, and extrema of peak currents associated with the first return stroke in a flash, percentage of the total number of ground flashes that were positive, and average cloud-to-ground flash rate.

## A.1 Flash statistics

We calculated several cloud-to-ground flash statistics from the DUNDEE (Table 6.1), beginning with the average peak current of the first return stroke. The average peak current (independent of polarity) was approximately 39 kA with a mean deviation of approximately 18 kA. While the mean deviation does indicate a fair amount of variability, the average of 39 kA does compare favorably to the average of 40-45 kA computed by Orville (1990) for thunderstorms in Florida. This average value is also similar to the 30-35 kA average for thunderstorms in Switzerland (Berger, 1975). The median positive and negative peak currents were 32 kA and 34 kA respectively. The largest peak current recorded in the DUNDEE data set was 346 kA (a negative flash) while the largest positive flash was 180 kA. Several negative flashes had peak current amplitudes greater than 200 kA. This is an interesting result since it had been reported previously that flashes with peak currents on the order of 200-300 kA are primarily positive in polarity (Uman, 1987; Orville et al., 1987).

| Table A.1: DUNDEE Cloud-to-Ground Lightning Statistics | |
|---|---|
| Total number of flashes | 4976 |
| Number of negative flashes | 4523 |
| Number of positive flashes | 453 |
| Percent positive | 9 |
| Average flashes / minute | 2.5 |
| Maximum peak current (kA) | -346 |
| Minimum peak current (kA) | -4 |
| Maximum negative peak current (kA) | 346 |
| Maximum positive peak current (kA) | 180 |
| Minimum negative peak current (kA) | 4 |
| Minimum positive peak current (kA) | 6 |
| Mean positive peak current (kA) | 39 |
| Mean negative peak current (kA) | 39 |
| Median positive peak current (kA) | 32 |
| Median negative peak current (kA) | 34 |
| Mean peak current (kA) | 39 |

The minimum peak current (a negative flash) was 4 kA while the minimum positive peak current was 6 kA. The positive flashes were 9% of the total flash number which is similar to the 8% reported by Mackerras (1973) for ground flashes occurring near Brisbane, Australia and greater than the [illegible] average of less than 5

reported by Orville (1987) for ground flashes that occurred in the eastern U.S. during 1985. When the flashes were summed over the entire time of collection (eight storms observed for a duration of 2023 minutes) an average ground flash rate of 2.5 flashes $min^{-1}$ was obtained which is in the range of that reported for storm systems in Florida by Peckham et al., (1984). In comparison, the 10-11 June 1985 PRE-STORM MCS had a ground flash rate of 13.2 flashes $min^{-1}$. Approximately 8% of the ground flashes in the 10-11 June case were positive.

Fig. A.1 shows relative frequency histograms for peak currents associated with the tropical MCSs we examined from DUNDEE. The histograms show for each polarity of flash, the fraction of the total number of flashes with peak currents corresponding to a certain peak current interval (intervals are 15 kA for peak currents less than 90 kA, then increase to 45, 90, and 125 kA in width). For example, Fig. A.1 shows that approximately 20% (28%) of the positive (negative) flashes from DUNDEE had peak currents of 30-45 kA. With the exception of the 30-45 kA range, the relative frequencies for both polarities of flash are nearly equal (within 2 percent). When comparing tropical ground flash data (Fig. A.1) with data from Orville et al., (1987) for middle latitude ground flashes (Fig. A.2a-b), some differences become apparent. For example, the median peak currents (by polarity) for the middle latitude flashes displayed in Figs. A.2a-b differ by 15 kA (30 kA for negative flashes in Fig. A.2a and 45 kA for positive flashes in Fig. A.2b). In our study (Fig. A.1), the median positive and negative peak currents differed by only 2 kA (negative median 34 kA, positive median 32 kA). The approximate equality of the DUNDEE median peak currents is similar to the findings of López et al. (1991) for median peak currents associated with ground flashes occurring at a close range (within 20 - 60 km) to DFs in the northeastern Colorado LLP network.

Finally, in examining the shapes of the distributions in Fig. A.2a-b we find that the positive peak currents in Fig. A.2b are more widely distributed over larger values (i.e., >100 kA) than the negative peak currents in Fig. A.2a (also see López et al. 1991). This implies that larger peak currents (i.e., >100 kA) are more likely to be associated with positive flashes in the middle latitudes (also see Brook et al. 1982). The histograms we present for 5000 tropical flashes (Fig. A.1) do not demonstrate this trait. In fact, the distributions of negative and positive peak currents in Fig. A.1 are similar in median, mean (positive and negative mean peak currents 39 kA), and width. Also, the relative frequencies of positive and negative flashes having peak currents greater than 60 kA differ by no more than 2%.

A.2 The mean peak current and latitudinal variation

Orville (1990) hypothesized a latitudinal variation of peak current magnitude based on the existence of an apparent latitudinal gradient in the mean peak current magnitude for the eastern United States. Orville suggested that the increase in average cloud top height (12.2 km in New England, 16.2 km in Florida) would increase the total volume of the subtropical clouds (enabling them to possess larger charge volumes) and elevate the main charge centers. The increased charge volume would then make more charge available for transport to ground while the increased height of the charge center would result in a longer current channel to ground. This in turn would result in an increase in charge residing on the channel, and hence a larger peak current.

Based soley on the argument of latitudinal variation made by Orville (1990), the mean peak current for Darwin-area storms (39 kA at 12° S latitude) should be greater

than the Florida average (40-45 kA at approximately 26° N latitude). However, the average cloud tops of the storm systems in DUNDEE (based on the *maximum* height of the 0 dBZ reflectivity contour from vertical cross sections of the storms studied) were approximately 16-16.5 km. This would imply an average peak current closer to the Florida average (which is the case) if only cloud volume were considered. Therefore, Orville's suggestion may be more appropriate if the average peak currents are related to cloud top heights. While we believe this is a reasonable suggestion, it should be noted that the mean peak current (39 kA) presented from the DUNDEE flash data was calculated from a much smaller data set than that presented by Orville (1990).

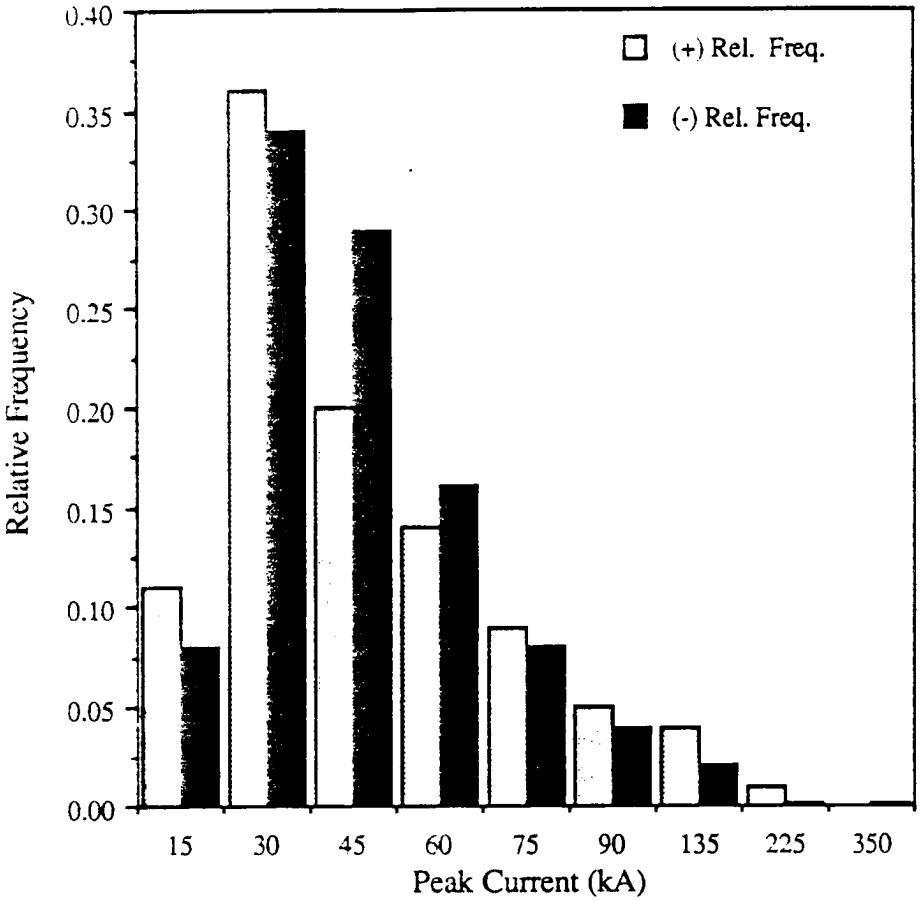


Figure A.1 Relative frequency histogram for positive and negative peak currents from DUNDEE. Numbers on the abscissa represent the upper limit of the peak current bin. Numbers on the ordinate represent the fraction of flashes in each polarity occurring in respective peak current bins.

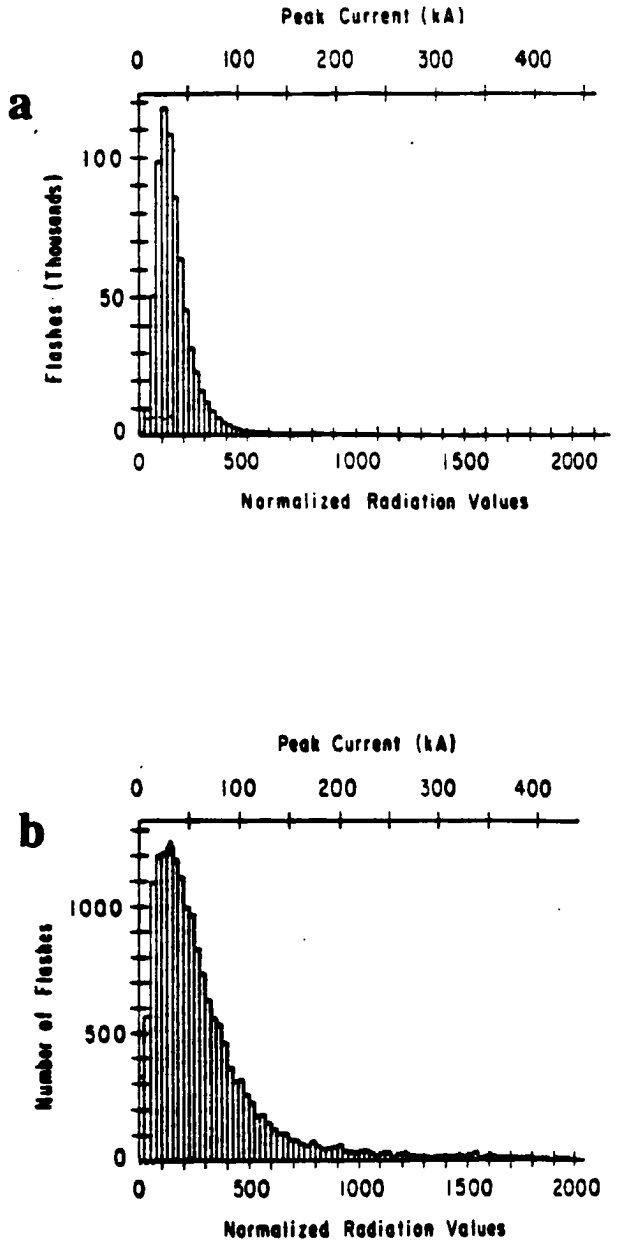


Figure A.2 Peak current frequency distributions for the eastern United States,1984-85 (adapted from Orville et al.,1987); (a) negative peak currents, and (b) positive peak currents. "Normalized radiation values" on the abscissa are LLP units, peak current values (kA) are noted above each distribution.